universität wien

DISSERTATION / DOCTORAL THESIS

Titel der Dissertation / Title of the Doctoral Thesis

„Derivatives and Advanced Applications of the Random Phase Approximation“

verfasst von / submitted by

Benjamin Ramberger, MSc BBSc

angestrebter akademischer Grad / in partial fulfilment of the requirements for the degree of

Doktor der Naturwissenschaften (Dr. rer. Nat.)

Wien / Vienna, 2020

Studienkennzahl lt. Studienblatt / degree programme code as it appears on the student record sheet:	A 796 605 411
Dissertationsgebiet lt. Studienblatt / field of study as it appears on the student record sheet:	Physik / Physics
Betreut von / Supervisor:	Univ.-Prof. Dipl.Ing. Dr. Georg Kresse

«Was siehst du?»
«Ich sehe dasselbe wie du, ich denke es nur anders.»
Im Wäldchen, Unbekannt

Acknowledgment

I want to express my sincere thanks to my supervisor Georg Kresse for his great support throughout this thesis. He always encouraged me to work independently, but also helped me with a treasure trove of experience whenever necessary. By assigning me diversified tasks, he brought me a breath of fresh air and re-ignited my motivation when it was low.

Also my colleagues with whom I had countless exciting discussions deserve my gratitude. Problems that already consumed hours of hard thinking alone, were sometimes solved within minutes by simply recapitulating them together. I am particularly grateful for the collaborations with Tobias, Menno, Zoran and José.

Thanks are also due to the administrative staff, and in particular Doris. Their professionalism and diligence have been very helpful in so many situations.

Of course I also want to thank all the people that accompanied me in my private life. First and foremost I am very grateful for the lifelong support granted by my parents, Maria and Rudolf.

Over the last few months my friend Johanna has been an incredible source of power for me, which I highly appreciated during the write-up of this thesis.

Last but not least I want to thank all my other beloved friends. They always keep my life in balance and grant me the energy to sustain my capabilities.

Abstract / Zusammenfassung

Abstract

The random phase approximation (RPA) is a method to calculate the energy of a quantum many body system. For many systems it is superior to the widely used density functional theory (DFT), especially when van der Waals interactions are important. However, the computational demand for RPA simulations of solids was far out of reach for many years. Fortunately there has been a lot of progress in the development of computer simulations employing the RPA recently, so that RPA-correlation energies became accessible for large systems. For solids, however, there has not yet been an efficient way to calculate forces in the RPA. Since the calculation of forces is crucial for the simulation of elastic and vibrational properties, as well as for structure relaxations, it presented a promising area for further investigation.

In the course of this thesis, an efficient numerical method for the calculation of forces in solids within the RPA was developed, using the Green's function formalism [1]. The new RPA forces method was developed to be compatible with the projector augmented wave method (PAW), which provides a very efficient scheme to treat orbitals numerically in electronic structure codes. Consequently the new method was implemented into the Vienna ab-initio simulation package (`VASP`) [1]. The first very successful application of the new method was presented by Bokdam, Lahnsteiner, Ramberger, Schäfer and Kresse, who developed a benchmarking tool for DFT functionals using RPA forces [2].

Additionally the RPA one particle reduced density matrix, an intermediate quantity in the force calculation, turned out to yield auspicious approximate natural orbitals. It was shown that these orbitals can decrease the computing time for post-Hartree-Fock methods significantly by providing an efficient basis [3].

Finally the RPA was used in systems where conventional DFT is of limited accuracy. The investigated systems include H_2O on hBN [4], H_2O on graphene [5] and benzene on close packed transition metal surfaces [6]. It was shown that these systems were well described with the RPA and that the deficiencies of DFT could be overcome, once again underlining the capabilities of the method.

Zusammenfassung

Die Random-Phase-Approximation (RPA) ist eine Methode zur Berechnung der Energie eines Quantenvielteilchensystems. Für viele Systeme ist sie der weit verbreiteten Dichtefunktionaltheorie (DFT) überlegen, insbesondere wenn van-der-Waals-Wechselwirkungen eine wichtige Rolle spielen. Viele Jahre lang waren RPA-Simulationen für Festkörper aufgrund der dafür benötigten Rechenleistung nicht möglich. Glücklicherweise gab es in letzter Zeit große Fortschritte bei der Entwicklung von Algorithmen für die RPA, so dass die Berechnung von RPA-Korrelationsenergien für große Systeme möglich wurde. Für Festkörper gab es jedoch noch keine effiziente Methode zur Berechnung von Kräften in der RPA. Da die Berechnung von Kräften für die Simulation von elastischen und vibrationsspezifischen Eigenschaften sowie für Strukturrelaxationen von entscheidender Bedeutung ist, stellte dieses Thema ein vielversprechendes Gebiet für weitere Untersuchungen dar.

Im Rahmen dieser Arbeit wurde unter Verwendung des Formalismus der Green'schen Funktionen eine effiziente numerische Methode zur Berechnung von Kräften in Festkörpern mittels der RPA entwickelt [1]. Die neue RPA-Kräfte-Methode ist mit der Projector-Augmented-Wave-Methode (PAW) kompatibel, welche ihrerseits eine sehr effiziente Methode zur numerischen Behandlung von Orbitalen in Elektronenstrukturprogrammen bietet. Infolge wurde die neue Methode in das Vienna ab-initio Simulation Package (`VASP`) [1] implementiert. Die erste sehr erfolgreiche Anwendung der neuen Methode wurde von Bokdam, Lahnsteiner, Ramberger, Schäfer und Kresse vorgestellt, die ein Benchmarking-Tool für DFT-Funktionale mit RPA-Kräften entwickelten [2].

Zusätzlich stellte sich heraus, dass sich aus der reduzierten Ein-Teilchen-Dichtematrix in der RPA – welche als Zwischengröße in der Kräfteberechnung auftritt – nützliche approximative natürliche Orbitale gewinnen lassen. Es wurde gezeigt, dass diese Orbitale die Rechenzeit für Post-Hartree-Fock-Methoden erheblich verkürzen können, indem sie eine effiziente Basis bereitstellen [3].

Schließlich wurde die RPA auf Systeme angewandt, in welchen herkömmliche Dichtefunktionale an die Grenzen ihrer Genauigkeit stoßen. Die untersuchten Systeme waren unter anderem H_2O auf hBN [4], H_2O auf Graphen [5] und Benzol auf dicht gepackten Übergangsmetalloberflächen [6]. Es konnte gezeigt werden, dass die RPA diese Systeme gut beschreibt und so die Mängel herkömmlicher Funktionale überwinden kann.

Contents

Chapter 1

Introduction

1.1 Context of this thesis

1.1.1 State of the art at the outset

During the last decades, density functional theory (DFT) was the predominant method in the field of computational materials physics. DFT is based on the Hohenberg-Kohn theorem [7] and Kohn-Sham theory [8]. The former basically states that the ground state energy is a unique functional of the density, while the later established the concept that a system of interacting electrons can in principle be mapped onto an equivalent system of non interacting electrons in an effective external potential. The main difficulty for DFT methods is to find a good approximation to the exchange correlation potential, which is the part of the effective potential that cannot be described classically. Currently the most widely used approximations are the local density approximation and the generalized gradient approximation (GGA). The most common GGA functionals are PBE [9], PW91[10] and BLYP[11]. DFT simulations employing LDA and GGA have proven to be very powerful for describing the electronic structure and derived quantities like bond lengths and bond energies for a wide field of applications.

However, the quality of a DFT simulation strongly depends on the validity of the approximation for the exchange correlation energy functional and there are many situations where the commonly used approximations fail to describe the properties of a system correctly. The errors have been traced down to two main sources, namely on the one hand, the delocalization error and on the other hand the static correlation error [12]. The errors are particularly large in case of long range correlation effects that, as a matter of principle, cannot be described correctly by local approximations. This is the case for van der Waals (vdW) interactions, which play an important role in many systems, including graphite inter-layer bonding, surface adsorption of molecules, or generally inter molecular binding. There exist different approaches to cure the problems that conventional DFT calculations have with vdW interactions, including semi-empirical methods pioneered by Grimme [13] or Tkatchenko [14].

Although these corrections improve the results in many cases, it is not entirely clear under which conditions it is legitimate to apply them. Hence it is desirable to have an *ab initio* alternative.

So called hybrid functionals are another popular alternative when standard GGA or LDA fails. They incorporate a portion of exact exchange from Hartree-Fock theory and thereby account for non-local quantum effects that cannot be described by local approximations. The most commonly used hybrid functionals are PBE0 [15], B3LYP [16], [17], [18] and HSE[19]. However, Stroppa and Kresse [20] conclude, that these hybrid functionals are hardly a major step forward for metals and metal surfaces. They show that the inclusion of a sizeable amount of non-local exchange alone does not capture the physics in metals properly. Furthermore, non-local exchange cannot resolve the issue of non-local vdW correlations discussed in the previous paragraph.

In this work, the focus lies on the random phase approximation (RPA), a method that attracted a lot of attention recently as it is another powerful alternative, when standard DFT reaches its limitations. The random phase approximation to the correlation energy is a method developed in the 1950s by Pines and Bohm [21, 22, 23, 24]. It can be understood from the theory of quantum many-particle systems and is well described in the textbooks of Fetter and Walecka [25] or Mattuck [26]. In the random phase approximation, the correlation part of the energy E_{RPA} is approximated by an infinite sum over the so called pair bubble ring diagrams, that are vacuum fluctuations where electron-hole pairs form spontaneously and annihilate again in the following manner:

$E_{\mathrm{RPA}} =$ 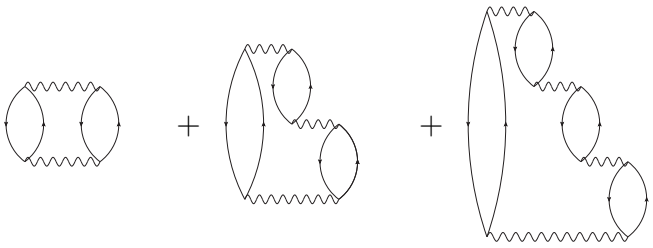 $+ \ldots$ (1.1)

In practice, the adiabatic connection dissipation fluctuation theorem allows to evaluate the RPA correlation energy E_{RPA} from the independent particle polarizability χ_0 [27], see Eq. (1.2) where v is the Coulomb kernel and Tr the trace operation:

$$E_{\mathrm{RPA}} = \frac{1}{4\pi} \int_{-\infty}^{\infty} d\nu \, \mathrm{Tr}\{\ln(1 - \chi_0(\mathrm{i}\,\nu)\,\mathrm{v}) + \chi_0(\mathrm{i}\,\nu)\,\mathrm{v}\}. \tag{1.2}$$

Moreover, χ_0 can be calculated from the KS orbitals of a standard DFT simulation carried out beforehand, e.g. with PBE. In that sense, the RPA is a post-processing method to enhance DFT calculations. The RPA may be applied to problems that cannot be solved sufficiently accurately using the LDA or GGA alone and it is particularly interesting as it does not depend on empirical presumptions, in contrast to

other post-processing methods. It is especially useful to describe weakly correlated systems like vdW interactions. In a review paper of Ren *et al.* [28], the authors illustrate the large variety of systems in which the RPA performs significantly better than common DFT functionals like PBE. Different benchmarks concerning molecular systems indicate that the RPA improves the accuracy of binding energies of weakly bonded molecular complexes and chemical reaction barrier heights, however dissociation energy curves for covalent bonds and atomization energies are usually not better than those from semi-local DFT functionals.

For periodic systems the quantum chemical hierarchy of benchmark approaches cannot be applied easily. Therefore, the RPA is an important approach in the domain of crystalline solids. Harl, Schmika, and Kresse [29, 30, 31] have shown that in solids, the RPA predicts accurate lattice constants, bulk moduli and heats of formation for insulators and semiconductors, as well as, metals, while the accuracy for atomization energies is unfortunately again somewhat disappointing. The superiority of the RPA over common functionals is especially evident for lattice constants and cohesive energies of vdW-bound solids. The inter layer interaction in graphite is a prominent example in solids that local, semi-local as well as hybrid functionals fail to describe accurately. The RPA is capable of overcoming this problem and gives the correct $1/d^3$ asymptotics [32] between the layers, as shown by Lebegue *et al.* [33].

In surface physics and chemistry, the RPA might be particularly useful. This is due to the fact that at the interface between solids and molecules many other approaches struggle. Often one method is good at describing solids while it is poor in the description of isolated molecules or vice versa. Furthermore surface science is tremendously important in industry. One technically relevant example would be the study of reactions which are catalysed at metallic surfaces. These two factors, the lack of methods and the high significance on the application side, strongly encourage the research on methods that might accurately describe the interaction at surfaces between the substrate and other atoms, molecules or clusters. One famous example is the "CO adsorption puzzle" [34]. It addresses the problem common functionals have with the absorption of CO on different metal surfaces, e.g. Pt(111). Results from low temperature experiments cannot be reproduced correctly by any kind of LDA or GGA calculation. For example at low coverage, they predict that the hollow-site should be preferred over the atop-site with respect to the underlying lattice, however experimental results clearly indicate that the CO adsorbs on the atop-site. In their work [30], Harl and Kresse state that RPA not only predicts adsorption energies in good agreement with experiment but also recovers the correct site order.

Despite the great advantages that are offered by the RPA, it is still far from being used as frequently as the LDA, GGA and hybrid functionals. One major aspect about the usability of the method is the high computational cost that comes along with the RPA. However, with increasing hardware power and recent developments in algorithms, RPA is on the best way of becoming a standard method for electronic structure studies. For example, in a recent publication by Kaltak *et al.* [35], an efficient method to calculate the RPA correlation energy was presented, which scales

only cubically in system size.

At the outset of this thesis, another aspect that prevented the widespread use of the RPA was the lack of an efficient method to calculate atomic forces in solids. The ability to conduct relaxations is crucial for a first principles method. Otherwise, one has to rely on other methods to obtain the geometry of the atoms under investigation and therefore cannot simulate systems entirely within the framework of the desired method. During relaxations, as well as in molecular dynamics simulations, usually the forces acting on the different atoms are calculated and the atoms are moved or accelerated into the direction of the force. Therefore it is very important to have an efficient way of calculating the forces within the RPA.

Different approaches using the Lagrangian technique had already been used to calculate atomic forces in molecular systems. For example Rekkedal *et al.* [36] had calculated analytic gradients for RPA implementations that are based on the ring approximation to coupled cluster doubles theory. They use Hartree-Fock reference orbitals and their method scales as $\mathcal{O}(N^6)$ with the system size N. Burow *et al.* [37] had taken a different approach, using the resolution-of-identity method for the RPA and combining it with imaginary frequency integration to achieve a more favourable scaling $\mathcal{O}(N^4)$. In contrast to the method of Rekkedal *et al.*, the implementation of Burow *et al.* is based on a semi-local KS reference determinant, not on Hartree-Fock.

Although the work on forces in the RPA for molecular systems had already been an important step forward, an efficient implementation for periodic systems was not available. In the author's master thesis [38], a different approach to calculate the forces within the RPA had been developed, using pen and paper only. The main idea is to calculate the forces variationally from the Green's functions. The gradient of the RPA correlation energy with respect to the atomic positions is calculated via the variation of the independent particle polarizability which is related to the imaginary time Green's function in Hedin's equation. Hence, the forces in the RPA are, in principle, related to the variation of the Green's function with respect to atomic positions. This approach to RPA forces in solids seemed promising as the imaginary time Green's functions were already accessible with cubic scaling in system size in the `VASP` code [35].

While in the mentioned master thesis it was pointed out that atomic forces in the RPA can in principle be calculated from Green's functions in a practicable manner, so far no work had been done on a concrete implementation. In order to obtain a feasible implementation, there were still several issues to be overcome. On the one hand, the programming necessary for embedding the method into existing routines was expected to be challenging. On the other hand conceptual difficulties had to be solved, including problems that arise from the use of an overlap operator in the projector augmented wave (PAW) method, as well as from the treatment of systems with partial occupancies in the RPA implementations at that time. The requirement for an efficient implementation of RPA forces in solids and the open problems related to it presented the starting point for this doctoral thesis.

1.1.2 Initially expected outcome

The main goal of this thesis was to adapt the method that had been described in the author's master thesis [38] for the calculation of forces in the RPA for solids and to implement it into the Vienna ab-initio simulation package (VASP). VASP is a plane-wave code that employs the projector augmented wave method (PAW). In this method, the Schrödinger equation is extended by an overlap operator $\hat{S}$, which leads to a generalized eigenvalue equation

$$\hat{H}\,|\phi_i\rangle = \epsilon_i \hat{S}\,|\phi_i\rangle \tag{1.3}$$

under the constraint

$$\langle\phi_i|\hat{S}|\phi_j\rangle = \delta_{i,j}. \tag{1.4}$$

In the preceding master thesis, however, this had not been considered and hence it was necessary to extend the method accordingly. Another difficulty related to the concrete implementation was that VASP uses pseudo potentials that contain non-local contributions. Again we needed to modify the method in order to accommodate these complications.

We also expected some issues concerning systems with partial occupancies (metals). Partial occupancies give rise to singularities in the calculation of the correlation energy and at the time, the implementation of the RPA in the VASP code used a workaround that could not be easily transferred to the method for calculating forces. One sub goal of the doctoral thesis was therefore to solve this problem. We supposed that a possible approach would be a change from the continuous description to Matsubara frequencies. However this would have required major changes to the code and we were skeptical whether an efficient implementation could be achieved.

As soon as an implementation was ready to use, and be it only for gapped materials, we planned to test it on different systems. Preferentially we would have liked to examine systems where one can expect the RPA to improve the results from local and semi local functionals. Under this perspective, we decided that van der Waals interactions are particularly interesting, e.g. interlayer bonding properties of hexagonal structures like graphite or hBN. The proposed tests included structure optimizations as well as phonon spectra calculations.

Finally, we hoped that in the end it will be possible to obtain a feasible implementation for the calculation of exact RPA forces in solids, that is reliable for a vast variety of systems. We expected that the method will be extensively used, increasing the utility of the RPA even further and facilitating the progress of computational materials sciences.

1.2 Outline of this thesis

The subsequent sections in this chapter present the basic theoretical formalism and some fundamental concepts underlying this thesis. It is designed for physics students

with a basic understanding of quantum mechanics and aims to familiarize those readers with the notation and language used in the research area this thesis is affiliated with. Readers familiar with second quantization and a basic knowledge of solid state physics may skip these and proceed directly to the theory part I.

The first two chapters 2 and 3 of the theory part I, present two well established (textbook) mean-field methods, namely Hartree-Fock and density functional theory. They are of high relevance in the context of this thesis as they provide the starting point in a historical, theoretical but also technical sense for the more elaborated methods discussed later. These chapters are hopefully instructive and are recommended as an entry point into this thesis for senior undergraduates and junior PhD students, or for anyone else who would like to get a short but rigorous introduction to these methods.

The next chapter in the theory part, 4, gives an introduction to many-body perturbation theory (MBPT). The topic is treated in a small number of textbooks, but these are generally quite sophisticated. We expect that most readers will benefit from the brief overview, outlining the MBPT concepts most relevant for this thesis.

The last two chapters of the theory part, 5 and 6, on the RPA and the PAW respectively, are already very specialized and can be considered as the starting point of the core part of the thesis. To our knowledge, these chapters treat topics not yet fully covered in any textbook. Thus we recommend to read these chapters before advancing to parts II and III, apart from experts who are already familiar with the RPA/GW and the PAW. Besides, the interested reader will find many references to publications on the RPA for further reading.

Experts in the field may completely skip the first part of the thesis and directly enter at part II. There we present a novel state of the art method to calculate forces in the random phase approximation for solids, based on our corresponding publication [1]. Moreover, we show in detail how PAW terms are treated and give a blueprint on how to calculate the stress tensor in the RPA.

In part III, we present state of the art applications of the RPA. In chapter 9, we recap our contributions to publications on surface chemistry and adsorption processes. The investigated systems include H_2O on hBN [4], H_2O on graphene [5] and benzene on close packed transition metal surfaces [6]. The next chapter 10 gives a summary on the publication "Assessing Density Functionals Using Many Body Theory for Hybrid Perovskites" by Bokdam, Lahnsteiner, Ramberger, Schäfer and Kresse [2]. In the last chapter of this part, which is based on our recent publication [3], we introduce a new approach to calculate approximate natural orbitals and show that they represent an efficient basis for post-Hartree-Fock methods.

The main parts of the thesis close with a conclusion in chapter 12.

1.3 The Many-Body Hamiltonian

The first part of this section is very basic, and its main purpose is a reference to define the notation used throughout this thesis. We will use atomic units in this

thesis, *i.e.* a unit system in which the natural constants for speed of light c, mass of the electron m_e, charge of the electron $-e$, Planck's constant $\hbar$ and dielectric constant ϵ_0 are:

$$c = m_e = e = \hbar = \frac{1}{4\pi\epsilon_0} = 1. \tag{1.5}$$

This simplifies the notation, as constant pre-factors in many equations drop away that would otherwise interfere with the readability and compactness of the equations. Furthermore we will sometimes use the hat symbol "$\hat{}$" to emphasize that the considered quantity is an operator. However, often the hat symbol is redundant as it is clear from the context that a quantity is an operator.

1.3.1 One dimensional single particle Hamiltonian and time evolution

A quantum mechanical system containing a single particle is usually described by a state vector $|\phi\rangle$, describing the actual state of the particle, and a Hamiltonian $\hat{H}$ operator that describes the interactions that the particle experiences. The state vectors are elements of a Hilbert space with the product $\langle|\rangle$ and dual vectors $\langle\phi|$. We always assume that single particle state vectors are normalized, $\langle\phi|\phi\rangle = 1$. In analogy to the Hamiltonian of classical mechanics for a single particle system, the quantum mechanical Hamiltonian describes the energy of the quantum mechanical system, which is given by:

$$E[|\phi\rangle] = \langle\phi|\hat{H}|\phi\rangle\,. \tag{1.6}$$

For a single particle system in one spatial dimension, the state vector can be expressed in the position basis as:

$$|\phi\rangle = \int \mathrm{d}r\,|r\rangle\,\langle r|\phi\rangle = \int \mathrm{d}r\,|r\rangle\,\phi(r), \tag{1.7}$$

where $\langle r|\phi\rangle$ is the probability *amplitude* for finding the particle at position r. The probability $P_r[|\phi\rangle]$ to find it at position r is given by the absolute square of the probability amplitude:

$$P_r[|\phi\rangle] = \langle\phi|r\rangle\,\langle r|\phi\rangle = \phi(r)^*\phi(r) = |\phi(r)|^2. \tag{1.8}$$

And the expectation value $\bar{r}$ of the position is given by:

$$\bar{r} = \int r \cdot P_r[|\phi\rangle]\mathrm{d}r = \int r \cdot \langle\phi|r\rangle\,\langle r|\phi\rangle\,\mathrm{d}r = \langle\phi|\hat{R}|\phi\rangle\,. \tag{1.9}$$

The energy in Eq. (1.6) can be evaluated in the position basis as:

$$E[|\phi\rangle] = \iint \mathrm{d}r\mathrm{d}r' \, \langle\phi|r\rangle \, \langle r|\hat{H}|r'\rangle \, \langle r'|\phi\rangle \tag{1.10}$$

$$= \iint \mathrm{d}r\mathrm{d}r' \phi^*(r) H(r,r') \phi(r') \tag{1.11}$$

$$= \iint \mathrm{d}r\mathrm{d}r' \phi^*(r) \delta(r-r') [-\frac{1}{2}\frac{d^2}{dr'^2} + v(r')] \phi(r'), \tag{1.12}$$

where in the last line we used that a one dimensional single particle Hamiltonian usually consists of the kinetic energy operator $\hat{T}$ and a potential energy operator $\hat{v}$ which are given as

$$\langle r|\hat{T}|r'\rangle = -\frac{1}{2}\delta(r-r')\nabla^2_{r'} \tag{1.13}$$

$$\langle r|\hat{v}|r'\rangle = \delta(r-r')v(r') \tag{1.14}$$

in the position basis and with the nabla operator ∇.

Observable quantities in quantum mechanics are described by Hermitian operators $\hat{O}$. The expectation value $\langle\hat{O}\rangle_\phi$ for an observable of a particle in state $|\phi\rangle$ is calculated as:

$$\langle\hat{O}\rangle_\phi = \langle\phi|\hat{O}|\phi\rangle \, . \tag{1.15}$$

For example, we have seen the operator to the observable *position*, $\hat{R} = \int \mathrm{d}r \; r \cdot |r\rangle \, \langle r|$, and its expectation value $\bar{r} = \langle\phi|\hat{R}|\phi\rangle$, see Eq. (1.8) and (1.9). Another example is the observable *energy*, manifesting as the Hamilton operator Eq. (1.6).

Since Hermitian operators have a set of orthogonal eigenstates (with real eigenvalues), one can form a basis with the eigenstates of an observable operator. In quantum mechanics, the eigenstates of the Hamiltonian are especially important, since the (time dependent) Schrödinger equation that describes the time evolution of quantum mechanical system is:

$$\mathrm{i}\frac{\partial}{\partial t}|\phi(t)\rangle = \hat{H}\,|\phi(t)\rangle \tag{1.16}$$

so that in principle, given the state at time t_0, one can formally calculate the state at time t as

$$|\phi(t)\rangle = e^{-\mathrm{i}\int_{t_0}^{t}\hat{H}dt}\,|\phi(t_0)\rangle \, . \tag{1.17}$$

The so called time independent or stationary Schrödinger equation is just the eigenvalue equation for the Hamiltonian:

$$\hat{H}\,|\psi_n\rangle = \epsilon_n\,|\psi_n\rangle \, . \tag{1.18}$$

The importance of the eigenstates of $\hat{H}$ will become clear by plugging an eigenstate $|\psi_n\rangle$ into the time dependent Schrödinger equation:

$$\mathrm{i}\,\frac{\partial}{\partial t}\,|\psi_n(t)\rangle = \hat{H}\,|\psi_n(t)\rangle = \epsilon_n\,|\psi_n(t)\rangle \tag{1.19}$$

$$\Rightarrow |\psi_n(t)\rangle = e^{-\mathrm{i}\,\epsilon_n(t-t_0)}\,|\phi_n(t_0)\rangle\,. \tag{1.20}$$

Since the (properly normalized) $\{|\psi_n\rangle\}$ form a basis, *i.e.*

$$\sum_n |\psi_n\rangle\,\langle\psi_n| = \hat{\mathbb{1}} \tag{1.21}$$

the time evolution of any state is given as

$$|\phi(t)\rangle = \underbrace{\sum_n e^{-\mathrm{i}\,\epsilon_n(t-t_0)}\,|\psi_n\rangle\,\langle\psi_n|}_{\hat{U}(t,t_0)}\,\phi_0\rangle \tag{1.22}$$

with the time evolution operator $\hat{U}(t,t_0)$.

1.3.2 Fock space and second quantization

Electrons are spin 1/2 particles [39] and therefore, according to the spin-statistics relation [40], they are fermions. Since the focus in this thesis lies on the description of systems of electrons in an external potential, we will proceed with a description of fermionic many particle systems.

Let $\{|\beta_n\rangle\}$ be an orthonormal basis for a single fermion. Every single particle state can be expressed in terms of that basis:

$$|\phi\rangle = \sum_n \langle\beta_n|\phi\rangle\,|\beta_n\rangle\,. \tag{1.23}$$

The sum in the above equation goes over all basis states, so that for a continuous basis it is an integral. For electrons, that can be described by a three dimensional wave function and a spin component, the basis could be all possible tensor products $|\sigma,\mathbf{r}\rangle = |\sigma\rangle\otimes|\mathbf{r}\rangle$, with spin states $|\sigma\rangle \in \{|\uparrow\rangle\,,|\downarrow\rangle\}$ and position operator eigenstates $|\mathbf{r}\rangle$, $\mathbf{r}\in\mathbb{R}^3$ so that an arbitrary single particle electronic state $|\chi\rangle$ can be written as:

$$|\chi\rangle = \sum_{\sigma=\uparrow,\downarrow}\int \mathrm{d}^3\mathbf{r}\,\langle\sigma,\mathbf{r}|\chi\rangle\,|\sigma,\mathbf{r}\rangle\,. \tag{1.24}$$

A fermionic N-particle state $|\Psi\rangle$ can be characterized with respect to its probability amplitude with a product state of single particle basis states $\{\beta_j\}$:

$$\langle\prod_{n=1}^{N}\beta_{i_n}|\Psi\rangle \tag{1.25}$$

where

$$\langle \prod_{n=1}^{N} \beta_{i_n}| = \langle \beta_{i_1}\beta_{i_2}\ldots\beta_{i_N}| = \langle \beta_{i_1}| \otimes \langle \beta_{i_2}| \otimes \ldots \otimes \langle \beta_{i_N}| \,. \tag{1.26}$$

The anti-symmetry principle states that many particle fermionic states are anti-symmetric with respect to exchange (of the "coordinates"), *i.e.*

$$\begin{aligned} &\langle \beta_{i_1}\beta_{i_2}\ldots\beta_{i_a}\ldots\beta_{i_b}\ldots\beta_{i_N}|\Psi\rangle = \\ &-\langle \beta_{i_1}\beta_{i_2}\ldots\beta_{i_b}\ldots\beta_{i_a}\ldots\beta_{i_N}|\Psi\rangle \,. \end{aligned} \tag{1.27}$$

It follows that each single particle state can only be occupied by a single fermion (Pauli exclusion principle).

A set of N different single particle basis functions can be used to construct a properly anti-symmetric and normalized state $|\beta_{i_1}, \beta_{i_2}, \ldots, \beta_{i_N}\rangle_{\mathrm{AS}}$ with the anti-symmetrization operator $\hat{A}$

$$\begin{aligned} |\beta_{i_1}, \beta_{i_2}, \ldots, \beta_{i_N}\rangle_{\mathrm{AS}} &= \hat{A}\,|\prod_{n=1}^{N} \beta_{i_n}\rangle \\ &= \frac{1}{\sqrt{N!}} \sum_{\sigma\in S_N} \mathrm{sgn}(\sigma)\,|\prod_{n=1}^{N} \beta_{i_{\sigma_n}}\rangle \end{aligned} \tag{1.28}$$

with permutations $\sigma = (\sigma_1, \ldots, \sigma_N)$ from the set of all possible permutations of N elements, S_N (= symmetric group on N elements), and the sign function $\mathrm{sgn}(\sigma)$ which is $+1$ for even and -1 for odd permutations. These anti-symmeterized, normalized product states are usually called Slater determinants and a more detailed discussion on them is found in chapter 2. We will drop the index "AS" since for fermions it is always assumed that the state is constructed according to Eq. (1.28). Note that in this thesis, we distinguish product states from anti-symmetrized states by "comma" notation:

$$|\beta_{i_1}, \beta_{i_2}, \ldots, \beta_{i_N}\rangle = \hat{A}\,|\prod_{n=1}^{N} \beta_{i_n}\rangle = \hat{A}\,|\beta_{i_1}\beta_{i_2}\ldots\beta_{i_N}\rangle \tag{1.29}$$

This is important, since usually when we refer to a many electron state, it is anti-symmetrized, but we still need standard product states as "coordinate" basis states, e.g. for N-particle states:

$$\mathbb{1} = \sum_{n_1=1}^{\infty}\sum_{n_2=1}^{\infty}\ldots\sum_{n_N=1}^{\infty} |\beta_{n_1}\beta_{n_2}\ldots\beta_{n_N}\rangle\,\langle\beta_{n_1}\beta_{n_2}\ldots\beta_{n_N}| \tag{1.30}$$

and

$$\Psi(\mathbf{r}_1, \mathbf{r}_2, \ldots, \mathbf{r}_N) = \langle \mathbf{r}_1 \mathbf{r}_2 \ldots \mathbf{r}_N | \Psi \rangle \neq \langle \mathbf{r}_1, \mathbf{r}_2, \ldots, \mathbf{r}_N | \Psi \rangle \,. \tag{1.31}$$

The next step to a compact second quantization formalism is to rewrite the N-particle Slater determinants in *occupation number notation* so that:

$$|\beta_{i_1}, \beta_{i_2}, \ldots, \beta_{i_N}\rangle = |\ldots, \underset{i_1^{th}}{1}, \ldots, \underset{i_2^{th}}{1}, \ldots\ldots, \underset{i_N^{th}}{1}, \ldots\rangle \,, \tag{1.32}$$

i.e. if the state $|\beta_k\rangle$ is part of the Slater determinant (in the example above, $k = i_j$ for exactly one $j \in \{1, \ldots, N\}$), then the k-th position on the right hand side is 1, otherwise it is zero. For example the 3 particle Slater determinant with the single particle basis states $\{\beta_2, \beta_3, \beta_5\}$ would be:

$$|\beta_2, \beta_3, \beta_5\rangle = |0, 1, 1, 0, 1, 0, 0, 0, 0, \ldots\rangle \,. \tag{1.33}$$

For fermions, the occupation numbers n_i of a state $|n_1, n_2, n_3, \ldots\rangle$ are either 1 or 0, because if two single particle states in the Slater determinant are the same, it is 0 (anti-symmetry principle). From now on we denote the set of numbers $\{i\}$ for which $n_i = 1$ as occupied indices and the corresponding sates $\{\beta_i\}$ are occupied states "$\beta_i \in$ *occ.*". Accordingly we call states $\beta_a \in$ *uocc.* where $n_a = 0$ unoccupied states. Note that in order to uniquely define a state $|n_1, n_2, n_3, \ldots\rangle$, we need to write the constituting states $\beta_i \in$ *occ.* of the resulting Slater determinant in normal order (as we did above):

$$|n_1, n_2, n_3, \ldots\rangle = |\beta_{i_1}, \beta_{i_2}, \ldots, \beta_{i_N}\rangle \quad \text{with} \quad \beta_{i_j} \in \textit{occ.} \quad \text{and} \quad i_j < i_{j+1} \tag{1.34}$$

Otherwise there would be an ambiguity due to the anti-symmetry, e.g.

$$|1, 1, 0, 0, \ldots\rangle = |\beta_1, \beta_2\rangle = -\,|\beta_2, \beta_1\rangle \,. \tag{1.35}$$

All N-particle "occupation number" states, *i.e.* normal ordered Slater determinants that can be constructed with N single particle states from a chosen single particle basis, form a basis for the N-particle states in their Hilbert space [26].

The extended Hilbert space with variable particle number, spanned by all fermionic $N \in \mathbb{N}^0$ particle states, is referred to as Fock space. All occupation number states (based on a single particle basis and with arbitrary particle number) form an orthonormal basis of the Fock space. The second quantization formalism now defines creation/annihilation operators $\hat{b}_j^\dagger / \hat{b}_j$ that create/annihilate a particle with state $|\beta_j\rangle$.[1] The creation/annihilation operators are defined in the following

[1] This is not literally true, since the newly created/annihilated state is "shared/lost" between/from all the electrons, this can be seen by adding/removing a state in Eq. (1.28).

way for fermions:

$$\hat{b}_k^\dagger \left|n_1, n_2, \ldots, n_k, \ldots\right\rangle = (-1)^{\sum_{i<k} n_i} (1 - n_k) \left|n_1, n_2, \ldots, n_k + 1, \ldots\right\rangle$$

$$\hat{b}_k \left|n_1, n_2, \ldots, n_k, \ldots\right\rangle = (-1)^{\sum_{i<k} n_i} n_k \left|n_1, n_2, \ldots, n_k - 1, \ldots\right\rangle \tag{1.36}$$

The pre-factor $(-1)^{\sum_{i<k} n_i}$ is a matter of correct anti symmetry behavior, due to the definition of the occupation number states as normal ordered Slater determinants. The creation/annihilation operators obey the following fermionic commutation rules, which can be proved easily by inserting the definitions from above:

$$[\hat{b}_i, \hat{b}_j^\dagger]_+ = \hat{b}_i \hat{b}_j^\dagger + \hat{b}_j^\dagger \hat{b}_i = \delta_{ij} \tag{1.37}$$

$$[\hat{b}_i, \hat{b}_j]_+ = 0 \tag{1.38}$$

$$[\hat{b}_k^\dagger, \hat{b}_j^\dagger]_+ = 0 \tag{1.39}$$

All occupation number basis states can be constructed from the vacuum state $|\Omega\rangle$ (*i.e.* the 0 particle state) by successive application of creation operators, e.g.:

$$|1, 0, 1, 0, 0, 1, 0, 0, 0, \ldots\rangle = \hat{b}_1^\dagger \hat{b}_3^\dagger \hat{b}_6^\dagger \left|\Omega\right\rangle . \tag{1.40}$$

and hence every fermionic many particle state can be constructed as a linear combination of successive creation operators applied to the vacuum state. Another useful property of these operator is that they can be used to count the occupation number:

$$\hat{n}_i \left|n_1, n_2, \ldots\right\rangle = \hat{b}_i^\dagger \hat{b}_i \left|n_1, n_2, \ldots\right\rangle = n_i \left|n_1, n_2, \ldots\right\rangle \tag{1.41}$$

$$\hat{N} \left|n_1, n_2, \ldots\right\rangle = \sum_i \hat{n}_i \left|n_1, n_2, \ldots\right\rangle = N \left|n_1, n_2, \ldots\right\rangle \tag{1.42}$$

where $\hat{N}$ is the so called number operator, corresponding to the observable for the total number of electrons.

1.3.3 Non-interacting many body system and Fermi level

The usefulness of second quantization notation will become evident in the following subsection. Assume we have a system of non-interacting fermions, which are all subject to the same single-particle Hamiltonian $\hat{h}$. For example the Hamiltonian could consist of the kinetic energy operator and an external potential, so that in first quantization position basis it would read, e.g.:

$$\langle \mathbf{r} | \hat{h} | \mathbf{r}' \rangle = \delta(\mathbf{r} - \mathbf{r}') \left(\nabla_{\mathbf{r}'}^2 + v(\mathbf{r}') \right) . \tag{1.43}$$

Now this Hamiltonian has eigenstates $\{\phi_n\}$ with single particle energies $\{\epsilon_n : \epsilon_i \leq \epsilon_{i+1}, i \in \mathbb{N}^+\}$:

$$\hat{h} \left|\phi_n\right\rangle = \epsilon_n \left|\phi_n\right\rangle . \tag{1.44}$$

The many body Hamiltonian $\hat{H}_N$ for a N-particle system in first quantization notation is rather unwieldy

$$\hat{H}_N = \underbrace{\hat{h} \otimes \mathbb{1} \otimes \mathbb{1} \otimes \ldots \mathbb{1}}_{\text{product of N operators}} + \mathbb{1} \otimes \hat{h} \otimes \mathbb{1} \otimes \ldots \mathbb{1} + \ldots + \mathbb{1} \otimes \mathbb{1} \otimes \mathbb{1} \otimes \ldots \otimes \hat{h}. \tag{1.45}$$

Knowing that each of the summands affects a different, say the i-th, part of the product space, this can be written briefly as follows

$$\hat{H}_N = \sum_{i=1}^{N} \hat{h}_i. \tag{1.46}$$

The Slater determinants $\left|\Psi_i^N\right\rangle = \left|\phi_{i_1}, \ldots, \phi_{i_N}\right\rangle$, constructed from N single particle eigenstates $\{\phi_n\}$, are eigenstates of this N-particle Hamiltonian:

$$\hat{H}_N \left|\Psi_i^N\right\rangle = \sum_{n=1}^{N} \epsilon_{i_n} \left|\Psi_i^N\right\rangle = E_i^N \left|\Psi_i^N\right\rangle \tag{1.47}$$

and form a complete orthonormal basis in the N-particle space. Thus, the Hamiltonian can be expressed in terms of its eigenstates:

$$\hat{H}_N = \sum_n \epsilon_n \left|\Psi_n^N\right\rangle \left\langle\Psi_n^N\right| . \tag{1.48}$$

We will now use the eigenstates of $\hat{h}$ as a single particle basis for the second quantization formalism and show that we can rewrite the Hamiltonian in a more compact and general form. We consider the occupation number states with respect to the states $\in \{\phi_n\}$ with corresponding creation/annihilation operators $c_n^\dagger / c_n$:

$$\left|\phi_n\right\rangle = c_n^\dagger \left|\Omega\right\rangle \tag{1.49}$$

$$\left|\phi_{n_1}, \phi_{n_2}, \ldots, \phi_{n_N}\right\rangle = \prod_{i=1}^{N} c_{n_i}^\dagger \left|\Omega\right\rangle = \left|\ldots, \underset{n_1^{th}}{1}, \ldots, \underset{n_2^{th}}{1}, \ldots\ldots, \underset{n_N^{th}}{1}, \ldots\right\rangle \tag{1.50}$$

$$e.g. \quad \left|\phi_2, \phi_4, \phi_5\right\rangle = c_2^\dagger c_4^\dagger c_5^\dagger \left|\Omega\right\rangle = \left|0,1,0,0,1,1,0,0,0,0,\ldots\right\rangle \tag{1.51}$$

In second quantization, the Hamiltonian for a (non-interacting) many particle state with arbitrary particle number has the simple form:

$$\hat{H} = \sum_n \epsilon_n c_n^\dagger c_n = \sum_n \epsilon_n \hat{n}_n. \tag{1.52}$$

This is easily verified by comparing the components in the N-particle energy eigenstate basis with respect to the N-particle Hamiltonian in first quantization:

$$\langle \phi_{i_1}, \ldots, \phi_{i_N} | \hat{H} | \phi_{i'_1}, \ldots, \phi_{i'_N} \rangle = \sum_n \delta_{i_n, i'_n} \epsilon_{i'_n} = \langle \phi_{i_1}, \ldots, \phi_{i_N} | \hat{H}_N | \phi_{i'_1}, \ldots, \phi_{i'_N} \rangle \quad (1.53)$$

note that the i_n and i'_n are normal ordered, thus one obtains the δ_{i_n, i'_n}.

Obviously, all occupation number states in our chosen basis are eigenstates of the second quantization Hamiltonian, giving the correct energy eigenvalue for any number of particles N. We can order all N-particle eigenstates for a particular N by ascending total energy:

$$\hat{H} \, |\Psi_0^N\rangle = \hat{H} \, |\phi_1, \phi_2, \ldots, \phi_N\rangle = \left(\sum_{i=1}^{N} \epsilon_i \right) |\phi_1, \phi_2, \ldots, \phi_N\rangle = E_0^N \, |\Psi_0^N\rangle \quad (1.54)$$

$$\hat{H} \, |\Psi_1^N\rangle = \hat{H} \, |\phi_1, \phi_2, \ldots, \phi_{N-1}, \phi_{N+1}\rangle = \left(\sum_{i=1}^{N-1} \epsilon_i + \epsilon_{N+1} \right) = E_1^N \, |\Psi_1^N\rangle \quad (1.55)$$

$$\hat{H} \, |\Psi_j^N\rangle = E_j^N \, |\Psi_j^N\rangle \quad (1.56)$$

$$E_j^N \leq E_{j+1}^N. \quad (1.57)$$

Note that the single particle ground state is ϕ_1 and that the form of the N-particle excited states beyond the first one depend on the energy spectrum of the single particle Hamiltonian. From Eq. (1.54), we see that the N-particle ground state of an non-interacting fermionic system is obtained by "filling up" the lowest N single particle states. Adding a constant local potential $-\mu(\mathbf{r}) = const.$ to the single particle Hamiltonian $\hat{h}$ does neither change the single particle wave functions, nor the many-body states $\{\Psi_j^N\}$ and their order for a given N. However, the energies are shifted. While the single particle energies are shifted by $-\mu$, the N particle states' energies are shifted by $-N\mu$:

$$\hat{h}' \, |\phi_n\rangle = \left(\hat{h} - \mu \mathbb{1} \right) |\phi_n\rangle = (\epsilon_n - \mu) \, |\phi_n\rangle = \epsilon'_n \, |\phi_n\rangle \quad (1.58)$$

$$\hat{H}' \, |\Psi_j^N\rangle = (E_j^N - \mu N) \, |\Psi_j^N\rangle = (E'^N_j) \, |\Psi_j^N\rangle \quad (1.59)$$

Assume the potential μ is chosen to be $\mu_0 = \frac{\epsilon_{N_0} + \epsilon_{N_0+1}}{2}$, then

$$\epsilon'_n \begin{cases} \leq 0 & \text{for} \quad n \leq N_0 \\ \geq 0 & \text{for} \quad n \geq N_0 \end{cases} \quad (1.60)$$

$$\min_{N,j} \left\{ E'^N_j \right\} = E'^{N_0}_0 \quad (1.61)$$

$$E'^{N_0}_0 \leq E'^{N_0-1}_0 \Rightarrow E^{N_0}_0 - E^{N_0-1}_0 \leq \mu \tag{1.62}$$

$$E'^{N_0+1}_0 \geq E'^{N_0}_0 \Rightarrow E^{N_0+1}_0 - E^{N_0}_0 \geq \mu \tag{1.63}$$

$$\frac{E^{N_0+1}_0 - E^{N_0-1}_0}{2} = \frac{1}{2}\left(\sum_{n=1}^{N_0+1}\epsilon_n - \sum_{m=1}^{N_0-1}\epsilon_m\right) = \frac{\epsilon_{N_0} + \epsilon_{N_0+1}}{2} = \mu. \tag{1.64}$$

This potential μ is often referred to as Fermi level and it determines which single particle eigenvalues ϵ'_j are smaller than 0 and which ones are larger. To get the state with the lowest energy, we have to fill up all states with negative eigenvalue $\epsilon'_j < 0$. Often one wants to fix the particle number to N_0, but does not know the corresponding Fermi level in advance. In that case one can just calculate the single particle energies for an arbitrary μ and later fix it to the choice above, between the N_0^{th} and the $(N_0+1)^{th}$ single particle energy, so that the total energy of assumes its minimum at the N_0 particle ground state. In the following subsections, we will establish a connection between the Fermi-level, which is conceptually only relevant for independent particle Hamiltonians, and the chemical potential which generalizes the concept to interacting many particle states.

1.3.4 Many body Hamiltonian in second quantization

In second quantization the many body Hamiltonian for a system of interacting electrons has typically the following form:

$$\hat{H} = \int \mathrm{d}^3\mathbf{r}\hat{\psi}^\dagger(\mathbf{r})[-\frac{1}{2}\nabla^2_{\mathbf{r}} + v_{\mathrm{ext}}(\mathbf{r})]\hat{\psi}(\mathbf{r}) + \frac{1}{2}\iint \mathrm{d}^3\mathbf{r}\mathrm{d}^3\mathbf{r}'\frac{1}{|\mathbf{r}-\mathbf{r}'|}\hat{\psi}^\dagger(\mathbf{r}')\hat{\psi}^\dagger(\mathbf{r})\hat{\psi}(\mathbf{r})\hat{\psi}(\mathbf{r}') \tag{1.65}$$

In this subsection we will rationalize this expression and explain what the different components actually mean.

We start by including two-body interactions to the many particle Hamiltonian, as all fundamental interactions are two-body interactions. A classical two body interaction is the Coulomb potential felt between two charged particles. The energy of two point charges q_1,q_2 at distance $|\mathbf{r}_1 - \mathbf{r}_2|$ is given as:

$$E = \frac{q_1 q_2}{|\mathbf{r}_1 - \mathbf{r}_2|} = \frac{1}{2}\left(\frac{q_1 q_2}{|\mathbf{r}_1 - \mathbf{r}_2|} + \frac{q_2 q_1}{|\mathbf{r}_2 - \mathbf{r}_1|}\right) \tag{1.66}$$

and for a system of point charges with charge -1 (like "point particle electrons"$q = -e$):

$$E_{ee} = \frac{1}{2}\sum_i \sum_{\substack{ij \\ j\neq i}} \frac{1}{|\mathbf{r}_i - \mathbf{r}_j|}. \tag{1.67}$$

In first quantization, the corresponding two particle potential could have the follow-

ing form:

$$\mathrm{v} = \iint \mathrm{d}^3\mathbf{r}\mathrm{d}^3\mathbf{r}' \frac{|\mathbf{r}\rangle\langle\mathbf{r}| \otimes |\mathbf{r}'\rangle\langle\mathbf{r}'|}{|\mathbf{r}-\mathbf{r}'|}. \tag{1.68}$$

In the previous chapter, we have seen how a single particle operator, like the independent particle Hamiltonian, can be written intuitively in second quantization. One can show ([41], pp. 230, 251) that a first quantization operator $\hat{V}_{1^{st}}$ acting independently on each of N particles with the same single particle operator $\hat{v}$ translates to a second quantization operator $\hat{V}_{2^{nd}}$ as:

$$\hat{V}_{1^{st}} = \sum_{i=1}^{N} \mathbb{1} \otimes \ldots \otimes \mathbb{1} \otimes \underbrace{\hat{v}}_{i^{th}pos.} \otimes \mathbb{1} \ldots \otimes \mathbb{1} \underset{2^{nd}\text{quant.}}{\rightarrow} \hat{V}_{2^{nd}} = \sum_{mn} \langle m|\hat{v}|n\rangle\, c_m^\dagger c_n \tag{1.69}$$

for an arbitrary particle number N. This is important since the second quantization operator can act on any state of the Fock space.

Every two particle operator $\hat{w}$ with the basis representation

$$\begin{aligned}
\hat{w} &= \sum_{nmlk} |n\rangle\langle n| \otimes |m\rangle\langle m|\, \hat{w}\, |l\rangle\langle l| \otimes |k\rangle\langle k| \\
&= \sum_{nmlk} |n\rangle\langle l| \otimes |m\rangle\langle k| \underbrace{\langle n| \otimes \langle m|\, \hat{w}\, |l\rangle \otimes |k\rangle}_{w_{nmlk}} \\
&= \sum_{nmlk} w_{nmlk}\, |n\rangle\langle l| \otimes |m\rangle\langle k|\,,
\end{aligned} \tag{1.70}$$

using $|n\rangle$ as shorthand for $|\phi_n\rangle$, gives rise to the first quantization N particle operator $\hat{W}_{1^{st}}$, which translates to the particle number independent second quantization operator $\hat{W}_{2^{nd}}$

$$\hat{W}_{1^{st}} = \frac{1}{2} \sum_{\substack{ij \\ j\neq i}} \sum_{nmlk} w_{nmlk} \mathbb{1} \otimes \ldots \otimes \mathbb{1} \otimes \underbrace{|n\rangle\langle l|}_{i^{th}pos.} \otimes \mathbb{1} \ldots \otimes \mathbb{1} \otimes \underbrace{|m\rangle\langle k|}_{j^{th}pos.} \otimes \mathbb{1} \ldots \otimes \mathbb{1} \tag{1.71}$$

$$\downarrow 2^{nd}\text{quant.}$$

$$\hat{W}_{2^{nd}} = \frac{1}{2} \sum_{nmlk} w_{nmlk} c_m^\dagger c_n^\dagger c_l c_k. \tag{1.72}$$

For example the electron-electron Coulomb operator in Eq. (1.68) would give:

$$\hat{V}_{\mathrm{C}} = \frac{1}{2} \sum_{nmlk} \mathrm{v}_{nmlk}\, c_m^\dagger c_n^\dagger c_l c_k \tag{1.73}$$

where

$$\mathrm{v}_{nmlk} = \iint \langle n| \otimes \langle m| \iint \mathrm{d}^3\mathbf{r}\mathrm{d}^3\mathbf{r}' \frac{|\mathbf{r}\rangle \langle \mathbf{r}| \otimes |\mathbf{r}'\rangle \langle \mathbf{r}'|}{|\mathbf{r}-\mathbf{r}'|} |l\rangle \otimes |k\rangle$$

$$= \iint \mathrm{d}^3\mathbf{r}\mathrm{d}^3\mathbf{r}' \frac{\phi_n^*(\mathbf{r})\phi_m^*(\mathbf{r}')\phi_l(\mathbf{r})\phi_k(\mathbf{r}')}{|\mathbf{r}-\mathbf{r}'|}. \tag{1.74}$$

In second quantization, one can also define field operators $\hat{\psi}^\dagger(\mathbf{r})/\hat{\psi}(\mathbf{r})$ that create/annihilate a particle at position $\mathbf{r}$, acting on many body states. They are analogue to the creation/annihilation operators encountered so far, but as a single particle basis they use eigenstates $|\mathbf{r}\rangle$ of the position operator $\hat{\mathbf{R}}$

$$\hat{\mathbf{R}} |\mathbf{r}\rangle = \mathbf{r} |\mathbf{r}\rangle \tag{1.75}$$

$$\langle \mathbf{r}|\mathbf{r}'\rangle = \delta(\mathbf{r}-\mathbf{r}'). \tag{1.76}$$

The creation/annihilation operators (as well as the field operators) for different single particle basis states are related to each other by the same transformation that relates the single particle basis states to one another:

$$\hat{\psi}^\dagger(\mathbf{r}) = \sum_n \langle \phi_n|\mathbf{r}\rangle \hat{c}_n^\dagger = \sum_n \phi_n^*(\mathbf{r})\hat{c}_n^\dagger \tag{1.77}$$

$$\hat{\psi}(\mathbf{r}) = \sum_n \langle \mathbf{r}|\phi_n\rangle \hat{c}_n = \sum_n \phi_n(\mathbf{r})\hat{c}_n. \tag{1.78}$$

As $\hat{n}_n = c_n^\dagger c_n$ counted the electrons in state ϕ_n, the density operator $\hat{n}(\mathbf{r})$ counts the electrons at position $\mathbf{r}$:

$$\hat{n}(\mathbf{r}) = \hat{\psi}^\dagger(\mathbf{r})\hat{\psi}(\mathbf{r}). \tag{1.79}$$

And the number operator $\hat{N}$ in this basis is given as

$$\hat{N} = \int \mathrm{d}^3\mathbf{r}\hat{\psi}^\dagger(\mathbf{r})\hat{\psi}(\mathbf{r}). \tag{1.80}$$

The field operators are especially useful to describe interactions that are well described in the position basis, for example the electron-electron interaction from Eq. (1.73) can be written in terms of the field operators as:

$$\hat{V}_\mathrm{C} = \frac{1}{2}\int \mathrm{d}^3\mathbf{r}_1 \ldots \mathrm{d}^3\mathbf{r}_4 \iint \mathrm{d}^3\mathbf{r}\mathrm{d}^3\mathbf{r}' \frac{\langle \mathbf{r}_1|\mathbf{r}\rangle \langle \mathbf{r}_2|\mathbf{r}'\rangle \langle \mathbf{r}|\mathbf{r}_3\rangle \langle \mathbf{r}'|\mathbf{r}_4\rangle}{|\mathbf{r}-\mathbf{r}'|} \hat{\psi}^\dagger(\mathbf{r}_2)\hat{\psi}^\dagger(\mathbf{r}_1)\hat{\psi}(\mathbf{r}_3)\hat{\psi}(\mathbf{r}_4)$$

$$= \frac{1}{2}\iint \mathrm{d}^3\mathbf{r}\mathrm{d}^3\mathbf{r}' \frac{1}{|\mathbf{r}-\mathbf{r}'|} \hat{\psi}^\dagger(\mathbf{r}')\hat{\psi}^\dagger(\mathbf{r})\hat{\psi}(\mathbf{r})\hat{\psi}(\mathbf{r}'). \tag{1.81}$$

By now it should be clear that second quantization greatly simplifies the nota-

tion. The main advantage however is that operators can be written independently of the particle number. This is especially useful for describing realistic many particle systems with a Hamiltonian that allows that the particle number can vary. For example electrons form such systems in atoms, molecules or solids, where they can be removed or added to form ions, ionic molecules, or transport charge. The prototypical many-body Hamiltonian that we consider in this thesis is given as:

$$\hat{H} = \int \mathrm{d}^3\mathbf{r}\hat{\psi}^\dagger(\mathbf{r})[-\frac{1}{2}\nabla^2_{\mathbf{r}} + v_{\mathrm{ext}}(\mathbf{r})]\hat{\psi}(\mathbf{r}) + \frac{1}{2}\iint \mathrm{d}^3\mathbf{r}\mathrm{d}^3\mathbf{r}'\hat{\psi}^\dagger(\mathbf{r}')\hat{\psi}^\dagger(\mathbf{r})v(\mathbf{r}-\mathbf{r}')\hat{\psi}(\mathbf{r})\hat{\psi}(\mathbf{r}') \tag{1.82}$$

where the two particle interaction $v(\mathbf{r}-\mathbf{r}')$ is usually the Coulomb interaction v between two electrons (cf. Eq. (1.65)):

$$v(\mathbf{r}-\mathbf{r}') = \mathrm{v} = \frac{1}{|\mathbf{r}-\mathbf{r}'|} \tag{1.83}$$

and the first term containing the kinetic energy contribution can be written heuristically as:

$$\int \mathrm{d}^3\mathbf{r}\hat{\psi}^\dagger(\mathbf{r})[-\frac{1}{2}\nabla^2_{\mathbf{r}}]\hat{\psi}(\mathbf{r}) = \int \mathrm{d}^3\mathbf{r}\hat{\psi}^\dagger(\mathbf{r})[-\frac{1}{2}\lim_{h\to 0}\sum_{i=1}^{3}\frac{\hat{\psi}(\mathbf{r}+\mathbf{h}_i) - 2\hat{\psi}(\mathbf{r}) + \hat{\psi}(\mathbf{r}-\mathbf{h}_i)}{h^2}] \tag{1.84}$$

where $\mathbf{h}_1 = (h,0,0)$; $\mathbf{h}_2 = (0,h,0)$; $\mathbf{h}_3 = (0,0,h)$. It can also easily be re-written in terms of the usual creation and annihilation operators:

$$\int \mathrm{d}^3\mathbf{r}\hat{\psi}^\dagger(\mathbf{r})[-\frac{1}{2}\nabla^2_{\mathbf{r}}]\hat{\psi}(\mathbf{r}) = \sum_{nm}(-\frac{1}{2}\int \phi^*_n(\mathbf{r})\nabla^2_{\mathbf{r}}\phi^*_m(\mathbf{r})\mathrm{d}^3\mathbf{r}\hat{c}^\dagger_n\hat{c}_m. \tag{1.85}$$

1.3.5 The chemical potential μ

Consider the N particle eigenstates of the true many-body Hamiltonian Ψ^N_i ($i \in \mathbb{N}^0$) where, analogue to the non-interacting case, we have:

$$\hat{H}\,|\Psi^N_i\rangle = E^N_i\,|\Psi^N_i\rangle \tag{1.86}$$

$$E^N_i \leq E^N_{i+1}. \tag{1.87}$$

The best way to statistically describe a system of variable particle number is the grand canonical ensemble. In the grand canonical ensemble with chemical potential

μ, the probability $p(\Psi_i^N)$ to find the system in state $|\Psi_i^N\rangle$ is given by:

$$p(\Psi_i^N) = \frac{e^{(\mu N - E_i^N)/(kT)}}{Z} \tag{1.88}$$

$$Z = \sum_{j=(N,i)} e^{(\mu N - E_i^N)/(kT)}, \tag{1.89}$$

where the grand partition function Z sums over all possible micro states j, represented as tuples (N, i) where N counts the particles and i counts the different states for a given particle number. At the limit of zero temperature $T \to 0K$, only the factor that maximizes the numerator in the exponent, $(\mu N - E_i^N)$, will have a finite probability (though the maximum value $\underset{i,N}{max}\{\mu N - E_i^N\}$ can, in principle, be assumed by more than one state, we will consider only the case were there is a unique maximum). For obvious reasons, only the ground states $|\Psi_0^N\rangle$ can in principle assume the maximum probability at $T \to 0K$. Which of all ground states assumes the maximum is determined by the chemical potential. Assume that for a chemical potential μ_0, the maximum probability is assumed for the N_0-particle ground state:

$$\max_{N,i}\{\lim_{T\to 0} p(\Psi_i^N) : \mu = \mu_0\} = \lim_{T\to 0} \frac{e^{(\mu_0 N_0 - E_0^{N_0})/(kT)}}{Z} = 1. \tag{1.90}$$

Then for the "neighboring" ground states $\Psi_0^{N_0+1}$ and $\Psi_0^{N_0-1}$ we have:

$$(\mu_0 N_0 - E_0^{N_0}) \geq (\mu_0(N_0+1) - E_0^{N_0+1}) \Rightarrow E_0^{N_0+1} - E_0^{N_0} \geq \mu_0 \tag{1.91}$$

$$(\mu_0 N_0 - E_0^{N_0}) \geq (\mu_0(N_0-1) - E_0^{N_0-1}) \Rightarrow E_0^{N_0} - E_0^{N_0-1} \leq \mu_0. \tag{1.92}$$

From the above inequalities, one also finds:

$$\frac{E_0^{N_0+1} + E_0^{N_0-1}}{2} \geq E_0^{N_0} \tag{1.93}$$

In other words, at $T \to 0$ a ground state can only be occupied if its energy is below or equal to the mean energy of its neighboring ground states (convex). Otherwise there exists no chemical potential that will favor its occupation . However, if the inequality in Eq. (1.93) holds for the N particle ground state Ψ_0^N, then the chemical potential

$$\mu_N = \frac{E^{N+1} - E^{N-1}}{2} \tag{1.94}$$

guarantees that the state Ψ_0^N is (locally) stable with respect to changes in the particle number. Changing the chemical potential by $\Delta\mu$ has the same effect as adding a constant potential $-\Delta\mu$ to the external potential in the Hamiltonian:

$$\mu \to \mu + \Delta\mu \quad \hat{=} \quad v_{\text{ext}}(\mathbf{r}) \to v_{\text{ext}}(\mathbf{r}) - \Delta\mu. \tag{1.95}$$

This is reminiscent of the Fermi level introduced in the previous subsection, see Eq. (1.60)-(1.64) and indeed, for a system of non-interacting particles, the chemical potential is equivalent to the Fermi level. Therefore both are denoted by the same variable μ. However, the chemical potential is a more general concept, since it is a well defined thermodynamic variable, suitable (along with the temperature and the volume) of characterizing a system of interacting particles in the grand canonical ensemble where the particle number is variable.

As we have seen before, changing the external potential in the second quantization Hamiltonian by $-\Delta\mu$ has the same effect as changing the chemical potential by $+\Delta\mu$. Therefore, if there exists a chemical potential μ_N that favors the N-particle ground state $|\Psi_0^N\rangle$ at $T \to 0$

$$\max_{N,i}\{\lim_{T\to 0} p(\Psi_i^N) : \mu = \mu_N\} = \lim_{T\to 0} \frac{e^{(\mu_N N - E_0^N)/(kT)}}{Z} = 1 \tag{1.96}$$

then, due to Eq. (1.94), the Hamiltonian can be changed accordingly,

$$\hat{H} \to \hat{H}' = \hat{H} - \frac{E_0^{N+1} - E_0^{N-1}}{2}\hat{N} \tag{1.97}$$

so that in the new system, the physics in the grand canonical ensemble with $\mu' = 0$ are equivalent to the physics in the old system at $\mu = (E_0^{N+1} - E_0^{N-1})/2$. Furthermore, one can add a constant (not a constant potential but just a particle independent constant) to the Hamiltonian

$$\hat{H}' \to \hat{H}'' = \hat{H}' + C, \tag{1.98}$$

so that the ground state energy eigenvalues are shifted to yield

$$E''^N_0 = 0. \tag{1.99}$$

This system with Hamiltonian $\hat{H}''$ at chemical potential $\mu'' = 0$ in the grand canonical ensemble is physically equivalent to the old system $\hat{H}$ at $\mu = (E_0^{N+1} - E_0^{N-1})/2$, while it has the following nice properties (dropping the $''$ as this system will from now on be considered as the standard system):

$$\mu = 0 \tag{1.100}$$

$$E_0^N = 0 \tag{1.101}$$

$$E_0^{N+1} = E_0^{N-1} \tag{1.102}$$

$$E_0^{N'\neq N} \geq 0 \tag{1.103}$$

and in case of a non-interacting system:

$$\epsilon_N = -\epsilon_{N+1} \Rightarrow \text{“the Fermi level is midgap”} \tag{1.104}$$

$$\epsilon_i \leq 0 \quad i \in occ. \tag{1.105}$$

$$\epsilon_a \geq 0 \quad a \in uocc. \tag{1.106}$$

Remark: Above we stated that we consider only systems where unique ground states are assumed at $T \to 0$ for a given chemical potential. This requirement can be dropped and the above equations for our standardized system still hold, though they can be valid for different particle numbers at the same time. In that case a slight (constant) change in the (chemical) potential would favor one of the otherwise degenerate states, while leaving the states per se unchanged. Also degenerate ground states with the same particle number yield a statistical mix in the grand canonical ensemble at $T \to 0$. In that case they have to be treated statistically, but again the above equations hold.

1.4 Born-Oppenheimer approximation

So far we described the electrons by a Hamiltonian with a fixed external potential, but in real molecules and solids, the nuclei are not fixed and introduce additional degrees of freedom. However, the so called Born-Oppenheimer approximation (BOA) [42] suggests that one can separate the electronic and nuclear motion so that in the end one can treat the electrons of real systems as if they were in a fixed potential. The basic idea behind the BOA is that at a given temperature, the kinetic energy of the electrons and nuclei is similar and since the mass ratio between the nuclei and the electrons is very large (for a single proton, $m_p/m_e \approx 1800$) the “movement”, *i.e.* the dynamics of the electrons is much faster.

The full (first quantization, non-relativistic) Hamiltonian of a molecular system is given by

$$\begin{aligned} H = & -\frac{1}{2}\sum_i \nabla_i^2 & +\frac{1}{2}\sum_{\substack{ij \\ i\neq j}} \frac{1}{r_{ij}} & -\sum_{Ai} \frac{Z_A}{r_{iA}} & +\frac{1}{2}\sum_{\substack{AB \\ A\neq B}} \frac{Z_A Z_B}{r_{AB}} & -\frac{1}{2}\sum_A \nabla_A^2 \\ = & \ T_e & +V_{\mathrm{C}} & +V_{\mathrm{ext}} & +V_{nn} & +T_n \end{aligned} . \tag{1.107}$$

Here, i, j and A, B are electron and nuclear indices respectively, Z is the total charge of a nucleus, $r_{iA} = |\mathbf{r}_i - \mathbf{R}_A|$, $r_{ij} = |\mathbf{r}_i - \mathbf{r}_j|$ and $r_{AB} = |\mathbf{R}_A - \mathbf{R}_B|$. Let $|\Psi^n\rangle$ be the

n-th eigenstate of the total Hamiltonian with energy $\mathcal{E}^n$

$$H\left|\Psi^n\right\rangle = \mathcal{E}^n\left|\Psi^n\right\rangle \tag{1.108}$$

$$\Psi^n(\mathbf{r}_1,\ldots,\mathbf{r}_{N_e},\mathbf{R}_1,\ldots,\mathbf{R}_{N_n}) = \langle \mathbf{r}_1,\ldots,\mathbf{r}_{N_e},\mathbf{R}_1,\ldots,.,\mathbf{R}_{N_n}|\Psi^n\rangle\,. \tag{1.109}$$

The total wave function of the system of N_e electrons and N_n nuclei is, in principle, a function of all respective coordinates simultaneously. Born and Oppenheimer showed that the eigenvalues $\mathcal{E}^n$ can be expanded in terms of the ratio $\kappa = (m_e/\bar{M}_A)^{1/4}$ where $\bar{M}_A$ is the average mass of the nuclei. The zeroth order term in κ is the energy obtained by neglecting the nuclear kinetic energy T_n. This corresponds to treating the positions of nuclei parametrically, *i.e.* they are no longer entering the wave function as dynamic degrees of freedom. Hence, one can formulate an electronic Hamiltonian

$$H_e(;\{\mathbf{R}_A\}) = T_e + V_{\mathrm{C}} + V_{\mathrm{ext}}(;\{\mathbf{R}_A\}) + V_{nn}(;\{\mathbf{R}_A\}), \tag{1.110}$$

that depends parameterically (indicated by ";") on the positions of the nuclei. If one can solve the resulting electronic Schrödinger equation

$$H_e(;\{\mathbf{R}_A\})\left|\Psi_e^m(;\{\mathbf{R}_A\})\right\rangle = E_e^m(;\{\mathbf{R}_A\})\left|\Psi_e(;\{\mathbf{R}_A\})\right\rangle, \tag{1.111}$$

a spectrum $\{E_e^m(;\{\mathbf{R}_A\})\}$ is obtained that depends parametrically on the positions $\{\mathbf{R}_A\}$ with corresponding eigenfunctions

$$\Psi_e^m(\mathbf{r}_1,\ldots,\mathbf{r}_{N_e};\{\mathbf{R}_A\}) = \langle \mathbf{r}_1,\ldots,\mathbf{r}_{N_e}|\Psi_e^m(;\{\mathbf{R}_A\})\rangle\,. \tag{1.112}$$

At ambient conditions, one can assume that the electrons are in their ground state. This approximation is justified when the Boltzmann factor for excited states is very small so that they can be disregarded in the ensemble average. For most semi conductors and for insulators, *i.e.* for materials with bands gaps well above the average thermal energy ($\approx 25meV$ at 20°C), this is the case. Also in molecules, the typical electronic excitation energies are much larger than the thermal energy. For metals, the free electron model indicates that the contribution of (electronic) excited states to materials properties are negligible [43]. In theory, this allows in a first step to assign each configuration $\{\mathbf{R}_A\}$ an electronic energy

$$V_P(\{\mathbf{R}_A\}) = E_e^0(;\{\mathbf{R}_A\}) \tag{1.113}$$

that can be viewed as an effective energy landscape (=pseudo potential) for the nuclei. The minimum of this effective energy landscape (= electronic ground state energy minimized with respect to the parametric atomic positions) is the zeroth order approximation in κ to the total ground state energy of the molecule/material:

$$\mathcal{E}^0 = \min_{\{R_A\}}[E_e^0(;\{\mathbf{R}_A\})] + O(\kappa). \tag{1.114}$$

Furthermore, one obtains an effective Hamiltonian H_n and Schrödinger equation for the nuclei

$$H_n = T_n + V_P \tag{1.115}$$

$$H_n \left|\Psi_n^l\right\rangle = E_n^l \left|\Psi_n^l\right\rangle, \tag{1.116}$$

with eigenenergies E_n^l for the material/molecule (including electronic contributions via the effective potential) and corresponding eigenfunctions $\Psi_n^l(\mathbf{R}_1, \ldots, \mathbf{R}_{N_n}) = \langle \mathbf{R}_1, \ldots, \mathbf{R}_{N_n} | \Psi_n^l \rangle$. The eigenvalues E_n^l include higher order contributions in κ: vibrations $O(\kappa^2)$ and rotations $O(\kappa^4)$ of the nuclei. The vibrational contributions are often calculated in the harmonic approximation.

The coupling between the movement of the nuclei and the electrons only enters in higher order terms $O(\kappa^6)$. The Born-Oppenheimer approximation neglects this coupling, or in other words it approximates the total wave function as a product of an electronic and a nuclear wave function:

$$\left|\Psi^n\right\rangle = \left|\Psi_e^m\right\rangle \otimes \left|\Psi_n^l\right\rangle \tag{1.117}$$

with the compound index $n = (m, l)$. This formally allows the above separation of the Hamiltonian into an electronic and a nuclear part and to calculate the electronic wave function in a first step and the nuclear wave function in a separate second step. In reality, the coupling between the electronic and the nuclei degrees of freedom leads to interesting phenomena like super conductivity, however, within the scope of this thesis we will not consider these terms and apply the Born-Oppenheimer approximation. In fact, most of the time, we will only be interested in the solution of the electronic Hamiltonian and will use the term Born-Oppenheimer approximation to indicate that the positions of the nuclei are assumed to be external parameters.

1.5 Periodic systems

In order to calculate the electronic structure of extended systems by computational/numeric means, on the one hand one needs to impose periodic boundary conditions (extended system) and on the other hand one needs to discretize (numerics) our system.

1.5.1 The model crystal and Born-von Karman boundary conditions

We will focus on extended systems that are crystalline in the mathematical sense. In three dimensions, this means they can be described by a set of basis vectors

$\{\mathbf{a}_1, \mathbf{a}_2, \mathbf{a}_3\}$ and a basis[1]. The volume that contains all points $\mathbf{v} = c_1 \cdot \mathbf{a}_1 + c_2 \cdot \mathbf{a}_3 + c_3 \cdot \mathbf{a}_3$ that can be reached by a linear combination of the basis vectors with coefficients $0 \leq c_i < 1$ is the unit cell. The lattice vectors $\{\mathbf{R}\}$ form the set of all possible linear combinations $\mathbf{R} = R_1 \cdot \mathbf{a}_1 + R_2 \cdot \mathbf{a}_2 + R_3 \cdot \mathbf{a}_3$ with integer coefficients R_i. The whole crystal structure is an infinite periodic system, generated by the translation of the basis to any possible lattice vector. The smallest unit cell from which the lattice can be constructed, *i.e.* the one with the least number of atoms in the basis, is called primitive cell. For example the face centered cubic (fcc) structure, is obtained from the basis vectors

$$\mathbf{a}_1^{\text{fcc}} = (a/2, a/2, 0) \qquad \mathbf{a}_2^{\text{fcc}} = (a/2, 0, a/2) \qquad \mathbf{a}_3^{\text{fcc}} = (0, a/2, a/2) \tag{1.118}$$

and a single atom basis, e.g. at $(0, 0, 0)$. The fcc structure, shown in Fig. 1.1 is for example found for aluminum, copper and silver.

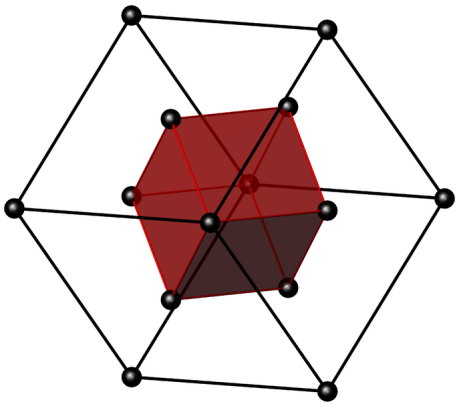

Figure 1.1: Face centered cubic (fcc) structure. The black box is the conventional unit cell, inside (red) is the primitive cell. The basis for the primitive cell is a single atom, the atoms in the other corners already belong to the next (translated) primitive cell.

A prominent example of a lattice with a two atom basis is diamond, Fig. 1.2. The basis vectors for the primitive cell are again fcc, see Eq. (1.118), but in this case the basis contains two atoms at $(0, 0, 0)$ and $1/4(\mathbf{a}_1 + \mathbf{a}_2 + \mathbf{a}_3)$.

Usually, in a piece of material the number of atoms is very large (1g of iron consists of roughly 10^{22} atoms). Therefore, for most purposes it is a reasonable assumption to approximate the conditions in the bulk by a model of an infinitely large extended crystal, neglecting surface effects. This brings considerable advantages in the mathematical description, since plane waves provide a convenient basis to describe functions in such systems and one can use Fourier transforms or the

[1]Here the term basis means a finite set of coordinates, where each coordinate corresponds to a point particle, e.g. a nucleus. The basis can be chosen such that all coordinates are within the unit cell.

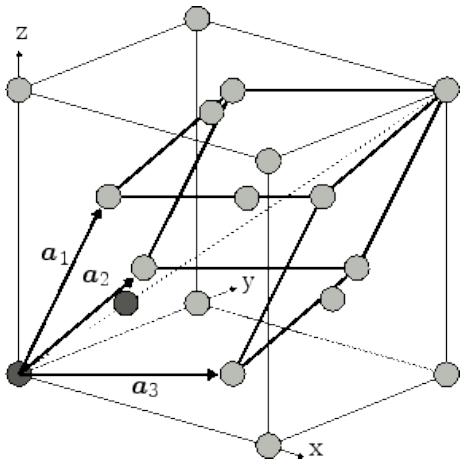

Figure 1.2: Crystal structure of diamond. The primitive cell is spanned by $\mathbf{a}_i$ and the two atom basis is indicated in dark gray. Picture taken from [44].

reciprocal space representation:

$$\tilde{f}(\mathbf{g}) = \mathcal{F}[f(\mathbf{r})](\mathbf{g}) = \int e^{-\mathrm{i}\,\mathbf{gr}} f(\mathbf{r}) \mathrm{d}^3\mathbf{r} \tag{1.119}$$

$$f(\mathbf{r}) = \mathcal{F}^{-1}[\tilde{f}(\mathbf{g})](\mathbf{r}) = \frac{1}{(2\pi)^3} \int e^{\mathrm{i}\,\mathbf{gr}} \tilde{f}(\mathbf{g}) \mathrm{d}^3\mathbf{g}, \tag{1.120}$$

where $\mathbf{g}$ is a vector in reciprocal space. Each lattice in real space has a corresponding lattice in reciprocal space and the basis vectors of the reciprocal lattice are obtained from the real space basis vectors in the following way

$$\mathbf{b}_1 = \frac{\mathbf{a}_2 \times \mathbf{a}_3}{\Omega} \qquad \mathbf{b}_2 = \frac{\mathbf{a}_3 \times \mathbf{a}_1}{\Omega} \qquad \mathbf{b}_3 = \frac{\mathbf{a}_1 \times \mathbf{a}_2}{\Omega}, \tag{1.121}$$

where $\times$ denotes the vector product and $\Omega = \mathbf{a}_1 \cdot (\mathbf{a}_2 \times \mathbf{a}_3)$ is the unit cell volume. The unit cell of the reciprocal lattice is usually called Brillouin zone.

In the above described model crystals, the total potential experienced by a test charge in the unit cell consists of contributions from all the nuclei throughout the infinitely large system. It is clear that when one uses the Born-Oppenheimer approximation for the electronic structure calculation in this model system, the total external potential experienced by the electrons is periodic, *i.e.* invariant under the translation by a lattice vector. However, the electronic wave function does not necessarily show the same periodicity. Bloch's theorem, discussed later in this section, addresses the implications of a periodic potential on the electronic wave function.

The theoretical concept for the boundary conditions to obtain a correct description of the electronic structure of a model crystal are Born-von Karman boundary conditions. They assume that the electronic wave function has the following peri-

odicity:

$$\Psi(\mathbf{r}) = \Psi(\mathbf{r} + N_i \mathbf{a}_i) \quad i \in \{1, 2, 3\}. \tag{1.122}$$

This can also be interpreted as constructing a super cell out of $N = N_1 \cdot N_2 \cdot N_3$ unit cells, with super cell basis vectors $\mathbf{a}_i^s = N_i \mathbf{a}_i$ – which is in principle just another choice for the unit cell of the same lattice – and imposing the periodicity of the super lattice on the electronic wave function. In the limit $N_i \to \infty$ one obtains the correct description since the "whole" infinitely large crystal is contained in the super cell. The super cell has in principle still periodic boundary conditions, though they are shifted to ∞. Later we will see that truncating the N_i corresponds to discretizing the Brillouin zone in the reciprocal space.

1.5.2 Discretization and discrete Fourier transforms

We will now explain the implications for the description of model crystals arising from the numerically necessary discretization of space. To explain the basic principles we will only consider a one dimensional system. The generalization to three dimensions works seamless.

We start by discretizing the real (position space) axis into intervals of length Δr.

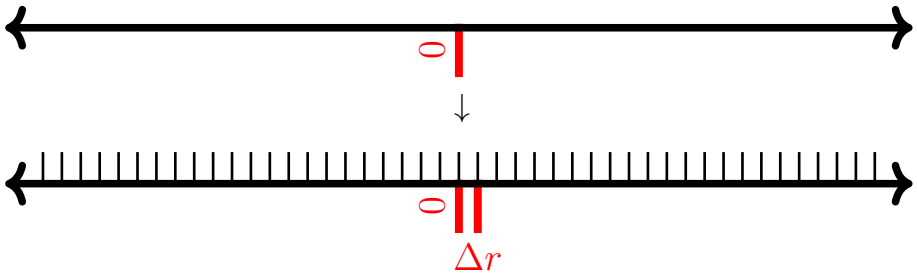

In a second step, we impose periodic boundary conditions. The interval $[-\Delta r N/2, \Delta r N/2)$ is periodically repeated in both directions ($\pm$):

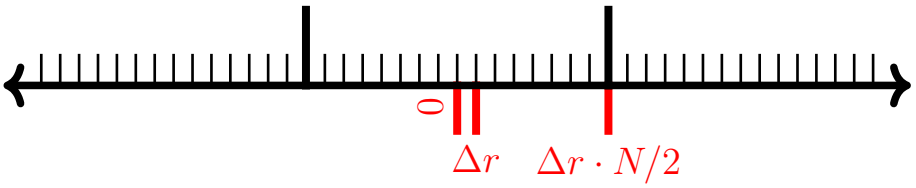

In the last step, we partition the periodic intervals into M blocks of length L, *i.e.* $N = M \cdot L$:

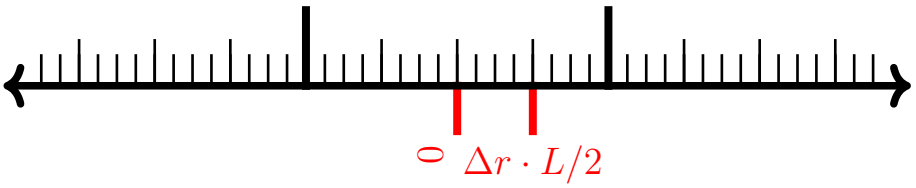

In the following, we will always assume that the distance $L \cdot \Delta r = a = const.$ and for the sake of readability, we assume M and L are even.

We may discretize any function $f : \mathbb{R} \to \mathbb{C}$ as $f_n : \mathbb{Z} \to \mathbb{C}, f_n = f(r_n)$. Since we imposed periodic boundary conditions, we can express any discretized function (=vector) through its Fourier components $\tilde{f}$ via the discrete Fourier transform:

$$f_n = \frac{1}{M} \sum_{m=-M/2}^{M/2-1} \sum_{l=-L/2}^{L/2-1} \tilde{f}_{m+l\cdot M} \exp[\mathrm{i}(k_m + g_{l\cdot M})r_n] \tag{1.123}$$

with

$$k_m = \frac{2\pi}{\Delta r} \frac{m}{ML} \tag{1.124}$$

$$g_{l\cdot M} = \frac{2\pi}{\Delta r} \frac{lM}{ML} \tag{1.125}$$

and

$$\tilde{f}_{m+l\cdot M} = \frac{1}{L} \sum_{n=-ML/2}^{ML/2-1} f_n \exp[-\mathrm{i}(k_m + g_{l\cdot M})r_n]. \tag{1.126}$$

The interval around 0 contains the points $\{r_{-ML/2}, r_{-ML/2+1}, \ldots, r_{ML/2-1}\}$, with $r_n = n \cdot \Delta r$ and any discretized function with that interval as its domain is periodically continued onto the whole discretized real axis by the above discrete Fourier transform.

Now, since the distance $L \cdot \Delta r$ is held constant, increasing the number of points per block L corresponds to making the mesh finer, *i.e.* Δr smaller. On the other hand, increasing the number of blocks per interval M corresponds to extending the length of each interval.

In the limit $M \to \infty$ at constant $a = L\Delta r$, the sum over m in the inverse discrete Fourier transform Eq. (1.123) turns into a Riemann integral:

$$\Delta k = \frac{2\pi}{\Delta r} \frac{1}{ML} \to \mathrm{d}k = \frac{2\pi}{a} \frac{1}{M} \tag{1.127}$$

$$\frac{1}{M} \sum_{m=-M/2}^{M/2-1} \tilde{h}(k_m) \to \frac{a}{2\pi} \int_{-\frac{\pi}{a}}^{\frac{\pi}{a}} \mathrm{d}k \tilde{h}(k). \tag{1.128}$$

This limit corresponds to discretizing the whole real axis, *i.e.* shifting the periodic boundaries to $\pm\infty$. From another point of view, discretizing the interval $[-\pi/a, \pi/a]$ in reciprocal (k-)space corresponds to imposing periodic boundary conditions in real (r-)space. In a 3D system, with Born-von Karman boundary conditions Eq. (1.122), truncating the limit $N_i \to \infty$ and hence imposing periodic boundary conditions at finite distances is equivalent to discretizing the first Brillouin zone in reciprocal space.

If one considers the continuum limit $\Delta r \to 0$ while keeping $a = L\Delta r$ constant,

then $L \to \infty$ and the sum over n in the discrete Fourier transform Eq. (1.126) turns into a Riemann integral:

$$\frac{1}{L} = \frac{\Delta r}{a} \to \frac{1}{L} = \frac{\mathrm{d}r}{a} \tag{1.129}$$

$$\frac{1}{L} \sum_{n=-L/2}^{L/2-1} h(r_n) \to \frac{1}{a} \int_{-\frac{a}{2}}^{a/2} \mathrm{d}r h(r). \tag{1.130}$$

Discretizing the interval $[-a/2, a/2]$ in real space corresponds to truncating the reciprocal space interval to finite boundaries. In a 3D system, this means that discretizing the real space is equivalent to imposing a cut-off on the considered reciprocal lattice vectors.

If we take both limits $L \to \infty$ and $M \to \infty$, we reproduce the continuous Fourier transform and its inverse in 1D, cf. Eq. (1.119) and (1.120):

$$\tilde{f}_{m+l\cdot M} \to \tilde{f}(k+G) = \sum_{\{R\}} \frac{1}{a} \int_{-\frac{a}{2}}^{\frac{a}{2}} \mathrm{d}r \exp[-\mathrm{i}(k+G)(r+R)] f(r+R) \tag{1.131}$$

$$f_n \to f(r+R) = \sum_{\{G\}} \frac{a}{2\pi} \int_{-\frac{\pi}{a}}^{\frac{\pi}{a}} \mathrm{d}k \exp[\mathrm{i}(k+G)(r+R)] \tilde{f}(k+G) \tag{1.132}$$

where $\{R\}$ and $\{G\}$ is the set of all 1D lattice vectors and reciprocal lattice vectors respectively:

$$\{R\} = \{R : R = n \cdot a, n \in \mathbb{Z}\} \tag{1.133}$$

$$\{G\} = \{G : G = n \cdot \frac{2\pi}{a}, n \in \mathbb{Z}\} \tag{1.134}$$

$$\exp(\mathrm{i}\, GR) = 1. \tag{1.135}$$

In summary, transferring the above observations to integrals in 3D systems, one finds that discretizing the primitive cell corresponds to truncating the sum over reciprocal lattice vectors while using truncated Born-von Karman boundary conditions corresponds to discretizing the first Brillouin zone (BZ) in reciprocal space. Note that the truncation of the reciprocal lattice vectors $\mathbf{G}$ in 3D is often associated to a basis set truncation of a plane wave basis. Hence the cut-off condition is often determined by a cut-off energy, *i.e.* only plane waves with energies ϵ_{PW} below the cut-off energy E_{cut} are considered. This leads to the following truncation of the reciprocal lattice vectors:

$$\epsilon_{\mathrm{PW}}(\mathbf{k}+\mathbf{G}) = \frac{(\mathbf{k}+\mathbf{G})^2}{2} < E_{\mathrm{cut}} \Rightarrow |\mathbf{k}+\mathbf{G}| < \sqrt{2E_{\mathrm{cut}}}, \quad \mathbf{k} \in \mathrm{BZ}. \tag{1.136}$$

It is important to keep the relation between real space and reciprocal space discretization in mind, as switching from one to the other by means of fast Fourier transforms (FFT) often increases the performance of simulations significantly, e.g. convolutions turn to simple multiplications.

1.5.3 Bloch's theorem

We already mentioned that the wave function of electrons in a lattice periodic potential does not necessarily show the same periodicity as the lattice. However, Bloch's theorem [45] states that the energy eigenstates $\{\phi_{n\mathbf{k}}(\mathbf{r})\}$ of independent particles in a perfect crystal, *i.e.* in a lattice periodic external potential, can be written as a product

$$\phi_{n\mathbf{k}}(\mathbf{r}) = \exp(\mathrm{i}\,\mathbf{k}\mathbf{r})u_{n\mathbf{k}}(\mathbf{r}), \tag{1.137}$$

where the function $u_{n\mathbf{k}}(\mathbf{r})$ observes the same periodicity as the potential, with basis vectors $\mathbf{a}_i, i \in \{1,2,3\}$ and lattice vectors $\mathbf{R} \in \{\mathbf{R} : \mathbf{R} = m_1\mathbf{a}_1 + m_2\mathbf{a}_2 + m_3\mathbf{a}_3, m_i \in \mathbb{Z}\}$:

$$u_{n\mathbf{k}}(\mathbf{r}+\mathbf{R}) = u_{n\mathbf{k}}(\mathbf{r}) \quad \forall\mathbf{R}. \tag{1.138}$$

Here, the wave vector $\mathbf{k}$ is, in principle, an arbitrary vector in reciprocal space and the band index n is a good quantum number (*i.e.* a discrete index) that orders the eigenstates of the independent particle Hamiltonian according to their energy. For a fixed n (=*within a band*), $\phi_{n\mathbf{k}}$ and its energy eigenvalue $\epsilon_{n\mathbf{k}}$ vary continuously with $\mathbf{k}$. A comprehensible proof of Bloch's theorem can be found in refernce [46] by Ashcroft and Mermin. The proof uses that the lattice translation operator $\hat{T}_{\mathbf{R}}\phi(\mathbf{r}) = \phi(\mathbf{r}+\mathbf{R})$ commutes with the Hamiltonian, hence they have a simultaneous eigenbasis. One can show that the eigenvalues of $\hat{T}_{\mathbf{R}}$ are $c(\mathbf{R}) = \exp(i\mathbf{k}\mathbf{R})$ and conclude that the energy eigenfunctions have the form proposed in Eq. (1.137). Bloch's theorem is particularly useful as the Bloch waves $\{\phi_{n\mathbf{k}}\}$ can be used as a single particle basis and in turn they can be used for the construction of Slater determinants in many particle calculations. Consider now a Bloch wave $\phi_{n(\mathbf{k}+\mathbf{G})}$:

$$\phi_{n(\mathbf{k}+\mathbf{G})} = \exp[\mathrm{i}(\mathbf{k}+\mathbf{G})\mathbf{r}]u_{n(\mathbf{k}+\mathbf{G})}(\mathbf{r}) = \exp(\mathrm{i}\,\mathbf{k}\mathbf{r})\bar{u}_{n(\mathbf{k}+\mathbf{G})}(\mathbf{r}). \tag{1.139}$$

For any reciprocal lattice vector $\mathbf{G} \in \{\mathbf{G} : \mathbf{G} = 2\pi(n_1\mathbf{b}_1 + n_2\mathbf{b}_2 + n_3\mathbf{b}_3), n_i \in \mathbb{Z}\}$, cf. Eq. 1.121), one obtains

$$\exp(\mathrm{i}\,\mathbf{R}\mathbf{G}) = 1. \tag{1.140}$$

Hence, one can conclude that $\bar{u}_{n(\mathbf{k}+\mathbf{G})}(\mathbf{r})$ is a lattice periodic function and therefore, according to Bloch's theorem, $|\phi_{n(\mathbf{k}+\mathbf{G})}\rangle$ is also a Bloch wave. As a consequence, one can equate

$$|\phi_{n(\mathbf{k}+\mathbf{G})}\rangle = |\phi_{n\mathbf{k}}\rangle\,. \tag{1.141}$$

This allows to restrict the reciprocal vectors $\mathbf{k}$ in the basis set $\{\phi_{n\mathbf{k}}\}$ to the first Brillouin zone. Therefore in periodic systems, a sum over all states, becomes a sum over the band indices and an integral over the first Brillouin zone. For example the trace of an arbitrary one particle operator $\hat{O}$ is given as

$$\mathrm{Tr}[\hat{O}] = \int_{\mathrm{BZ}} \mathrm{d}^3\mathbf{k} \sum_n \langle\phi_{n\mathbf{k}}|\hat{O}|\phi_{n\mathbf{k}}\rangle\,. \tag{1.142}$$

Of course, if one treats periodic systems numerically, the integral is replaced by an appropriate quadrature with weights w_i:

$$\int_{\mathrm{BZ}} \mathrm{d}^3\mathbf{k} \to \sum_{\mathbf{k}_i \in \mathrm{BZ}} w_i. \tag{1.143}$$

In later chapters we will implicitly make use of Bloch's theorem, and assume that for periodic systems, a sum over basis states is actually a sum over Bloch waves in the first Brillouin zone, with compound index $(n, \mathbf{k}) \to n$:

$$\sum_{\mathbf{k}_i \in \mathrm{BZ}} w_i \sum_n \to \sum_n. \tag{1.144}$$

Note that while Blochs theorem in its original formulation is only valid for non-interacting particles, it can be extended to many electron wave functions [47]. Also, even in its original formulation, one can apply Bloch's theorem directly to mean-field theories like Hartree-Fock (chapter 2) or density functional theory (chapter 3), since these widely used methods model electronic systems as non-interacting particles in an effective external potential.

1.6 Spin

The electronic spin is fundamental in the quantum mechanical description of electrons. It emerges naturally from the Dirac equation in the (special) relativistic description of quantum mechanics [48]. However, in this thesis we choose a non-relativistic approach to quantum theory and therefore the spin is just considered as an additional degree of freedom. Historically, Pauli introduced a new quantum number that allowed to describe the anomalous Zeeman effect in 1924 [39]. In this way, he could impose his exclusion principle to describe spectral properties of atoms accurately. The concept was developed further to the theory of electronic spin and to describe electrons within this theory, the spatial orbitals that yielded the original three quantum numbers (n,l,m) where extended with spin states $|\alpha\rangle$ to form a spatial-spin product state:

$$|\chi\rangle = |\phi\rangle \otimes |\alpha\rangle \tag{1.145}$$

The resulting spin orbitals $|\chi\rangle$ yield a complete description of an electronic state in non relativistic quantum mechanics. For the sake of completeness, we note that in order to explain the fine structure of spectral lines in non-relativistic quantum mechanics, the Hamiltonian needs to contain a term that couples the spatial and spin Hilbert space, *i.e.* spin-orbit coupling.

In this thesis we do not consider spin orbit coupling or external magnetic fields, *i.e.* the Hamiltonians we discuss are purely spatial and do not act in the spin Hilbert space. However, it is still important to consider single particle states as spin orbitals, because of the implications it has on symmetry properties in quantum many body theory. This important fact can already be shown for the simple model system of

the hydrogen molecule [49].

Unfortunately, including spin explicitly often makes the notation more cumbersome and can sometimes worsen readability by obscuring the relevant insights. Therefore, we will generally adopt a spin free notation throughout this thesis as commonly observed in publications in this research area. In the literature one often encounters similar sentences like "this can be easily generalized to include spin". Since this is usually true and often simplifies the task of pinning down the important details we adopt the same strategy in this thesis. However one needs to be aware that in principle, spin has to be considered always in many body fermionic theories and in some cases it may not be trivial to extend a problem, approach, algorithm, model, or theory to contain spin. Whenever this is the case, we will explicitly bring it to the reader's attention and will try to give a proper description. But most of the time, the generalization to include spin is straight forward and will not be discussed explicitly. It is implied that making the following changes is usually sufficient to achieve the desired generalization:

- replace spatial orbitals $|\phi\rangle$ with spin orbitals $|\chi\rangle = |\phi\rangle \otimes |\alpha\rangle$
- replace spatial degrees of freedom $\mathbf{r}$ with space-spin degrees of freedom $\mathbf{x} = (\mathbf{r}, \sigma)$
- replace the integration over spatial degrees of freedom with a sum over all spin degrees of freedom and spatial degrees of freedom
- if necessary, adjust occupancies f_n

$$\int \mathrm{d}^3\mathbf{r}\, \langle \mathbf{r}|\phi\rangle \longrightarrow \int \mathrm{d}\mathbf{x}\, \langle \mathbf{x}|\chi\rangle = \sum_\sigma \int \mathrm{d}^3\mathbf{r}\, \langle \mathbf{r}|\phi\rangle\, \langle \sigma|\alpha\rangle \tag{1.146}$$

$$\sum_{i\in occ.} \longrightarrow \sum_n f_n \tag{1.147}$$

$$\sum_{a\in uocc.} \longrightarrow \sum_n (1 - f_n) \tag{1.148}$$

Part I

Theory

Chapter 2

The Hartree and Hartree-Fock method

The Hartree-Fock method is one of the most prominent examples for approximations to solve the many electron Schrödinger equation. In the following chapter we will try to give a detailed description of the Hartree-Fock method, because it is not only one of the most widely used methods in computational materials science but also theoretically interesting and pedagogically valuable. It is often used as a starting point for the more sophisticated methods presented in this thesis and it introduces concepts that are highly relevant for the theoretical description of those methods.

The method originates from the work of Douglas Rayner Hartree [50] and Wladimir Alexandrowitsch Fock [51] first published in 1928 and 1930 respectively. The method was simplified two decades later by John Clarke Slatter, introducing Slatter determinants. It is nowadays a standard method in computational quantum chemistry and materials physics. Due to its high relevance for this work and because it poses a very good introduction into the electronic many body problem, a brief overview of the method is given in this chapter. This chapter is also useful for establishing the notation and terminology used throughout this thesis.

To find a solution of the N-electron Schrödinger equation in the Born-Oppenheimer approximation, one is in search for a feasible approximation as the exact solution for more than one electron, in general, cannot be solved analytically and is numerically an exponentially hard problem with respect to the number of electrons.

In a first attempt, one might consider that the electronic interaction can be described by a self consistent mean-field approach. The basic idea is to solve the single particle Schrödinger equation for one electron, in an effective field that arises from the other electrons and a given positive charge distribution (e.g. point charges for atomic nuclei). The resulting wave functions (orbitals) in turn contribute to the effective field in the Hamiltonian for the other electrons. Ultimately in a reasonable mean-field theory, it is necessary that the effective field of the electrons and the electron orbitals are self consistent. We will first ignore spin degrees of freedom in

order to establish the concept in the simplest possible way. In the last section of this chapter we will repair this simplification and provide the correct description including spin.

2.1 The Hartree product

With this approach in mind, a straight forward ansatz for the N-electron wave function would be a simple product of one electron orbitals, the so called Hartree product:

$$\Psi_{\mathrm{HP}}(\mathbf{r}_1, \mathbf{r}_2, \cdots, \mathbf{r}_N) = \phi(\mathbf{r}_1) \cdot \phi(\mathbf{r}_2) \cdots \phi(\mathbf{r}_N) \tag{2.1}$$

The contribution from the other $(N-1)$ electrons to the effective field for the i-th electron would be intuitively constructed as the classic Coulomb potential of the charge density of the $(N-1)$ electrons:

$$n^i(\mathbf{r}) = \sum_{\substack{j=1 \\ j \neq i}}^{N} |\phi_j(\mathbf{r})|^2 \tag{2.2}$$

$$v_{\mathrm{ee}}^i(\mathbf{r}) = \int d\mathbf{r}' n^i(\mathbf{r}') \frac{1}{|\mathbf{r} - \mathbf{r}'|} \tag{2.3}$$

The corresponding single particle Hamiltonians and orbitals can be calculated self consistently to obtain the Hartree approximation to the many body wave function. However, this is obviously a crude approximation, because it not only assumes that the electrons interact only via their mean-field with each other, but also the resulting wave function does not generally satisfy the anti-symmetry principle. This can be seen easily in the case for two electrons, where the anti-symmetry principle would require that

$$\Psi_{\mathrm{HP}}(\mathbf{r}_1, \mathbf{r}_2) = -\Psi_{\mathrm{HP}}(\mathbf{r}_2, \mathbf{r}_1) \tag{2.4}$$

$$\phi_1(\mathbf{r}_1) \cdot \phi_2(\mathbf{r}_2) = -\phi_1(\mathbf{r}_2) \cdot \phi_2(\mathbf{r}_1) \tag{2.5}$$

which is generally not the case.

2.2 Slater determinants

For a two electron system, one can easily construct an anti-symmetric two electron state Ψ_{AS} out of two one particle states in the following way:

$$\Psi_{\mathrm{AS}}(\mathbf{r}_1, \mathbf{r}_2) = \frac{1}{\sqrt{2}} \left[\phi_1(\mathbf{r}_1)\phi_2(\mathbf{r}_2) - \phi_1(\mathbf{r}_2)\phi_2(\mathbf{r}_1)\right] \tag{2.6}$$

This constructions fulfills the required anti-symmetry principle of fermions for every choice of one electron orbitals ϕ_1 and ϕ_2.

This approach can be generalized for N electrons with so called Slater determinants. In the above case for two electrons, one can write the expression as the determinant of a 2×2 matrix

$$\Psi_{\mathrm{AS}}(\mathbf{r}_1, \mathbf{r}_2) = \frac{1}{\sqrt{2}} \begin{vmatrix} \phi_1(\mathbf{r}_1) & \phi_2(\mathbf{r}_1) \\ \phi_1(\mathbf{r}_2) & \phi_2(\mathbf{r}_2) \end{vmatrix} \tag{2.7}$$

A N-particle fermionic state can be constructed from an arbitrary set of N single particle states analogously, cf. Eq. (1.28):

$$\begin{aligned} \Psi_{\mathrm{AS}}(\mathbf{r}_1, \mathbf{r}_2, ..., \mathbf{r}_N) &= \frac{1}{\sqrt{N!}} \begin{vmatrix} \phi_1(\mathbf{r}_1) & \phi_2(\mathbf{r}_1) & \dots & \phi_N(\mathbf{r}_1) \\ \phi_1(\mathbf{r}_2) & \phi_2(\mathbf{r}_2) & \dots & \phi_N(\mathbf{r}_2) \\ \vdots & \vdots & \ddots & \vdots \\ \phi_1(\mathbf{r}_N) & \phi_2(\mathbf{r}_N) & \dots & \phi_N(\mathbf{r}_N) \end{vmatrix} \\ &= \frac{1}{\sqrt{N!}} \sum_{\sigma \in S_N} \left(\mathrm{sgn}(\sigma) \prod_{i=1}^{N} \phi_{\sigma_i}(\mathbf{r}_i) \right) \\ &= \langle \mathbf{r}_1 \mathbf{r}_2 \dots \mathbf{r}_N | \phi_1, \phi_2, \dots, \phi_N \rangle \,, \end{aligned} \tag{2.8}$$

with permutations $\sigma = (\sigma_1, \dots, \sigma_N)$ from the set of all possible permutations of N elements S_N (= symmetric group on N elements) and the sign function $\mathrm{sgn}(\sigma)$ which is $+1$ for even and -1 for odd permutations. As can be seen above, from now on we denote a Slater determinant constructed from the orbital set $\{\phi_j, \phi_k, \dots, \phi_Z\}$ as $|\phi_j, \phi_k, \dots, \phi_Z\rangle$. Since the determinant changes its sign when two rows are exchanged it is obvious that this construction of the Slater determinant fulfills the anti-symmetry principle, *i.e.* exchanging the position coordinate of two electrons changes the sign of the many particle state. As a consequence it incorporates the Pauli exclusion principle that two electrons may not occupy the same orbital, since the determinant is 0 if any two orbitals are identical up to a phase factor. What can also be seen from this ansatz is that the electrons in a many particle state are indistinguishable. It would be wrong, to characterize the state by saying electron 1 occupies orbital number 1 and so on. Instead the situation can be visualized as all electrons being associated with all orbitals simultaneously (in a superposition of states in which the electrons would be distinguishable).

Note that the Slater determinant is invariant under unitary transformation between the orbitals $U : \{\phi_n\} \to \{\tilde{\phi}_n\}$ with $\tilde{\phi}_n = \sum_m U_{nm} \phi_m$.

Proof: Consider the matrix from which the determinant is taken in the first line of Eq. (2.8). Let's call this matrix A. The Slater determinant $\tilde{\Psi}_{\mathrm{AS}}$ for the transformed

orbitals $\{\tilde{\phi}_n\}$ can be obtained as:

$$\tilde{\Psi}_{\mathrm{AS}}(\mathbf{r}_1, \mathbf{r}_2, ..., \mathbf{r}_N) = \frac{1}{N!} det((UA^T)^T) = \frac{1}{N!} det(UA^T) \tag{2.9}$$

$$= \frac{1}{N!} \underbrace{det(U)}_{=1} det(A^T) = \frac{1}{N!} det(A)$$

$$= \Psi_{\mathrm{AS}}(\mathbf{r}_1, \mathbf{r}_2, ..., \mathbf{r}_N) \tag{2.10}$$

□

It turns out that restricting the many electron state to a single Slater determinant built from an orthonormal set of orbitals is equivalent to approximating the Hamiltonian as an independent particle Hamiltonian in which each electron only "feels" the mean-field Coulomb potential of the other electrons as well as a so called mean-field "exchange" interaction that has no classical analogue. This fact will become clear in the following sections.

2.3 The Hartree-Fock energy functional

In first quantization, the many body Hamiltonian for an N electron system – cf. Eqs. (1.46), (1.66), (1.68) and (1.71) – is given by:

$$H = \sum_{i=1}^{N} h_i + \frac{1}{2} \sum_{\substack{ij \\ i \neq j}} \mathrm{v}_{ij} + V_{NN} \tag{2.11}$$

with the one electron operator

$$h_i = -\frac{1}{2} \nabla_i^2 - \sum_{\alpha} \frac{Z_\alpha}{r_{i\alpha}} \tag{2.12}$$

and the interaction term

$$\mathrm{v}_{ij} = \frac{1}{r_{ij}} = \frac{1}{|\mathbf{r}_i - \mathbf{r}_j|} \tag{2.13}$$

For a fixed set of atomic positions (Born-Oppenheimer approximation) the term V_{NN}, describing the interactions between the nuclei, is just an additive constant and will be disregarded in the following considerations.

The electronic energy E_{el} of a given N electron state $|\Psi\rangle$ is the expectation value of the Hamiltonian in that state, which is larger than the ground state energy E_0 due to the variational theorem stating that the energy of an arbitrary N electron state is an upper bound for the N electron ground state energy

$$E_0 \leq E_{\mathrm{el}}[\Psi] = \langle \Psi | H | \Psi \rangle \,. \tag{2.14}$$

In the Hartree-Fock method, one wants to approximate the ground state by a single Slater determinant $|\Psi_{\mathrm{AS}}(\{\phi_n\})\rangle$ constructed from an orthonormal set of orbitals $\{\phi_n\}$. In general, due to the variational principle, the energy of the state $|\Psi_{\mathrm{AS}}(\{\phi_n\})\rangle$ will be larger than the true ground state energy E_0 and the energy difference is given by

$$\Delta E = \langle\Psi_{\mathrm{AS}}(\{\phi_n\})|H|\Psi_{\mathrm{AS}}(\{\phi_n\})\rangle - E_0 \tag{2.15}$$

The best choice of orbitals with respect to the energy, *i.e.* the orbital set that minimizes the energy difference ΔE, is obtained by minimizing the energy functional $E_{\mathrm{el}}[\Psi_{\mathrm{AS}}(\{\phi_n\})]$ with respect to the orbitals under the restriction that they remain orthonormal:

$$E_0^{\mathrm{HF}} = \min_{\{\phi_n\}} \left(E_{\mathrm{el}}[\Psi_{\mathrm{AS}}(\{\phi_n\})]\right). \tag{2.16}$$

The resulting approximation to the ground state energy is the Hartree-Fock energy E_0^{HF} and the corresponding state is the Hartree-Fock ground state $|\Psi_0^{\mathrm{HF}}\rangle$. The difference between the true ground state energy and the Hartree-Fock energy is usually referred to as correlation energy E^c:

$$E^c = E_0 - E_0^{\mathrm{HF}}. \tag{2.17}$$

We will now rewrite E_{el} explicitly in terms of the functions $\{\phi_n\}$, which will allow us to calculate E_0^{HF} in a systematic way.

$$E_{\mathrm{el}}[\Psi_{\mathrm{AS}}(\{\phi_n\})] = \langle\Psi_{\mathrm{AS}}(\{\phi_n\})|H|\Psi_{\mathrm{AS}}(\{\phi_n\})\rangle \tag{2.18}$$

$$= \frac{1}{N!}\int \ldots \int \mathrm{d}^3\mathbf{r}_1 \ldots \mathrm{d}^3\mathbf{r}_N$$

$$\sum_{\sigma\in S_N}\left(\mathrm{sgn}(\sigma)\prod_{n=1}^{N}\phi^*_{\sigma_n}(\mathbf{r}_n)\right)\hat{\mathrm{H}}\sum_{\sigma'\in S_N}\left(\mathrm{sgn}(\sigma')\prod_{m=1}^{N}\phi_{\sigma'_m}(\mathbf{r}_m)\right) \tag{2.19}$$

We now evaluate the one particle and the two particle part of the Hamiltonian separately. The one particle part can be simplified in the following way:

$$\langle\Psi_{\mathrm{AS}}(\{\phi_n\})|\sum_{i=1}^{N}\hat{\mathrm{h}}_i|\Psi_{\mathrm{AS}}(\{\phi_n\})\rangle = \sum_{n=1}^{N}\langle\phi_n|\hat{\mathrm{h}}|\phi_n\rangle \tag{2.20}$$

Proof:

$$\int \dots \int \mathrm{d}^3\mathbf{r}_1 \dots \mathrm{d}^3\mathbf{r}_N \sum_{\sigma \in S_N} \left(\mathrm{sgn}(\sigma) \prod_{n=1}^{N} \phi^*_{\sigma_n}(\mathbf{r}_n) \right) \hat{\mathrm{h}}_i \sum_{\sigma' \in S_N} \left(\mathrm{sgn}(\sigma') \prod_{m=1}^{N} \phi_{\sigma'_m}(\mathbf{r}_m) \right)$$

$$= \sum_{\sigma,\sigma' \in S_N} \mathrm{sgn}(\sigma)\,\mathrm{sgn}(\sigma') \underbrace{\prod_{n \neq i} \int \phi^*_{\sigma_n}(\mathbf{r}_n)\phi_{\sigma'_n}(\mathbf{r}_n)\mathrm{d}^3\mathbf{r}_n}_{=\delta_{\sigma,\sigma'}} \int \phi^*_{\sigma_i}(\mathbf{r}_i)\hat{\mathrm{h}}_i\phi_{\sigma'_i}(\mathbf{r}_i)\mathrm{d}^3\mathbf{r}_i$$

$$= \sum_{\sigma \in S_N} \int \phi^*_{\sigma_i}(\mathbf{r}_i)\hat{\mathrm{h}}_i\phi_{\sigma_i}(\mathbf{r}_i)\mathrm{d}^3\mathbf{r}_i$$

$$= (N-1)! \sum_{n=1}^{N} \int \phi^*_n(\mathbf{r}_i)\hat{\mathrm{h}}_i\phi_n(\mathbf{r}_i)\mathrm{d}^3\mathbf{r}_i \qquad \text{(note: equal for each choice of } i\text{)} \quad (2.21)$$

$$\Rightarrow \langle \Psi_{\mathrm{AS}}(\{\phi_n\})| \sum_{i=1}^{N} \hat{\mathrm{h}}_i |\Psi_{\mathrm{AS}}(\{\phi_n\})\rangle = \sum_{n=1}^{N} \int \phi^*_n(\mathbf{r})\hat{\mathrm{h}}\phi_n(\mathbf{r})\mathrm{d}^3\mathbf{r} = \sum_{n=1}^{N} \langle \phi_n|\hat{\mathrm{h}}|\phi_n\rangle \quad (2.22)$$

In the second line of Eq. (2.21), we have used that the orbitals form an orthonormal set. The normalization factor $1/N!$ that stems from Ψ_{AS} cancels with the factor $(N-1)!$ and the factor N from the sum $\sum_i$ as the summands are independent of i. □

The two particle part is a bit more complicated and yields:

$$\langle \Psi_{\mathrm{AS}}(\{\phi_n\})| \frac{1}{2} \sum_{\substack{ij \\ i \neq j}} \hat{\mathrm{v}}_{ij} |\Psi_{\mathrm{AS}}(\{\phi_n\})\rangle =$$

$$\frac{1}{2} \sum_{\substack{nm \\ n \neq m}}^{N} \langle \phi_n| \langle \phi_m| \hat{\mathrm{v}} |\phi_n\rangle |\phi_m\rangle - \langle \phi_n| \langle \phi_m| \hat{\mathrm{v}} |\phi_m\rangle |\phi_n\rangle$$

$$= \frac{1}{2} \sum_{\substack{nm \\ n \neq m}}^{N} \langle nm|nm\rangle - \langle nm|mn\rangle\,, \quad (2.23)$$

where in the last line we used the physicists' notation for the two electron integrals:

$$\langle ij|kl\rangle = \int \mathrm{d}^3\mathbf{r}_1\mathrm{d}^3\mathbf{r}_2 \phi^*_i(\mathbf{r}_1)\phi^*_j(\mathbf{r}_2)\frac{1}{r_{12}}\phi_k(\mathbf{r}_1)\phi_l(\mathbf{r}_2). \quad (2.24)$$

Proof of Eq. (2.23):

$$\int \dots \int \mathrm{d}^3\mathbf{r}_1 \dots \mathrm{d}^3\mathbf{r}_N \sum_{\sigma \in S_N} \left(\mathrm{sgn}(\sigma) \prod_{n=1}^{N} \phi^*_{\sigma_n}(\mathbf{r}_n) \right) \hat{\mathrm{v}}_{ij} \sum_{\sigma' \in S_N} \left(\mathrm{sgn}(\sigma') \prod_{m=1}^{N} \phi_{\sigma'_m}(\mathbf{r}_m) \right) =$$

$$\sum_{\sigma,\sigma' \in S_N} \underbrace{\mathrm{sgn}(\sigma)\,\mathrm{sgn}(\sigma') \prod_{n \neq i,j} \int \phi^*_{\sigma_n}(\mathbf{r}_n)\phi_{\sigma'_n}(\mathbf{r}_n)\mathrm{d}^3\mathbf{r}_n}_{=(\delta_{\sigma,\sigma'} - \delta_{\sigma,\sigma'_{i\leftrightarrow j}})} \times \tag{2.25}$$

$$\iint \phi^*_{\sigma_i}(\mathbf{r}_i)\phi^*_{\sigma_j}(\mathbf{r}_j)\hat{\mathrm{v}}_{ij}\phi_{\sigma'_i}(\mathbf{r}_i)\phi_{\sigma'_j}(\mathbf{r}_j)\mathrm{d}^3\mathbf{r}_i\mathrm{d}^3\mathbf{r}_j$$

$$= \sum_{\sigma \in S_N} \iint \phi^*_{\sigma_i}(\mathbf{r}_i)\phi^*_{\sigma_j}(\mathbf{r}_j)\hat{\mathrm{v}}_{ij}\phi_{\sigma_i}(\mathbf{r}_i)\phi_{\sigma_j}(\mathbf{r}_j) - \phi^*_{\sigma_i}(\mathbf{r}_i)\phi^*_{\sigma_j}(\mathbf{r}_j)\hat{\mathrm{v}}_{ij}\phi_{\sigma_j}(\mathbf{r}_i)\phi_{\sigma_i}(\mathbf{r}_j)\mathrm{d}^3\mathbf{r}_i\mathrm{d}^3\mathbf{r}_j$$

$$= (N-2)! \sum_{\substack{nm \\ n\neq m}}^{N} \iint \mathrm{d}^3\mathbf{r}_i\mathrm{d}^3\mathbf{r}_j \Big[\phi^*_n(\mathbf{r}_i)\phi^*_m(\mathbf{r}_j)\hat{\mathrm{v}}_{ij}\phi_n(\mathbf{r}_i)\phi_m(\mathbf{r}_j)$$

$$- \phi^*_n(\mathbf{r}_i)\phi^*_m(\mathbf{r}_j)\hat{\mathrm{v}}_{ij}\phi_m(\mathbf{r}_i)\phi_n(\mathbf{r}_j) \Big] \tag{2.26}$$

(note: equal for each choice of i and j)

$$\Rightarrow \langle \Psi_{\mathrm{AS}}(\{\phi_n\}) | \frac{1}{2} \sum_{\substack{ij \\ i\neq j}}^{N} \hat{\mathrm{v}}_{ij} | \Psi_{\mathrm{AS}}(\{\phi_n\}) \rangle =$$

$$= \frac{1}{2} \sum_{\substack{nm \\ n\neq m}}^{N} \iint \phi^*_n(\mathbf{r})\phi^*_m(\mathbf{r}')\hat{\mathrm{v}}\phi_n(\mathbf{r})\phi_m(\mathbf{r}') - \phi^*_n(\mathbf{r})\phi^*_m(\mathbf{r}')\hat{\mathrm{v}}\phi_m(\mathbf{r})\phi_n(\mathbf{r}')\mathrm{d}^3\mathbf{r}\mathrm{d}^3\mathbf{r}'$$

$$= \frac{1}{2} \sum_{\substack{nm \\ n\neq m}}^{N} \langle \phi_n | \langle \phi_m | \hat{\mathrm{v}} | \phi_n \rangle | \phi_m \rangle - \langle \phi_n | \langle \phi_m | \hat{\mathrm{v}} | \phi_m \rangle | \phi_n \rangle . \tag{2.27}$$

In the second line of Eq. (2.25), $\sigma'_{i\leftrightarrow j}$ corresponds to the permutation that is obtained by swapping σ'_j with σ'_i in σ'. In other words, the expression underbraced is 1 if $\sigma = \sigma'$ and it is -1 if σ and σ' are equal except for the entries i, j for which $\sigma_i = \sigma'_j$ and $\sigma_j = \sigma'_i$. We used again the orthonormality of the orbitals to achieve this simplification. The normalization factor $1/N!$ that stems from Ψ_{AS} cancels with the factor $(N-2)!$ in Eq. (2.25) and the factor $N(N-1)$ from the sum $\sum_{ij;i\neq j}$ as

the summands are independent of i and j. □

We can summarize the results of this section and write the Hartree-Fock energy functional $E_{\mathrm{HF}}[\{\phi_n\}]$ as a functional that depends on the orthonormal set of orbitals used to construct a many particle state $|\Psi_{\mathrm{AS}}(\{\phi_n\})\rangle$:

$$\begin{aligned} E_{\mathrm{HF}}[\{\phi_n\}] =& E_{\mathrm{el}}[\Psi_{\mathrm{AS}}(\{\phi_n\})] \\ =& \sum_{n=1}^{N} \langle\phi_n|\hat{\mathrm{h}}|\phi_n\rangle + \frac{1}{2}\sum_{\substack{nm \\ n\neq m}}^{N} \langle\phi_n|\langle\phi_m|\,\hat{\mathrm{v}}\,|\phi_n\rangle\,|\phi_m\rangle - \langle\phi_n|\langle\phi_m|\,\hat{\mathrm{v}}\,|\phi_m\rangle\,|\phi_n\rangle\,. \end{aligned} \tag{2.28}$$

2.4 The Hartree-Fock equations

The Hartree-Fock energy is obtained by minimizing the energy functional in Eq. (2.28) under the constraint that the $\{\phi_i\}$ stay orthonormal, compare Eq. (2.16). This constrained minimization can be achieved with Lagrange's method of undetermined multipliers. The functional we need to minimize is

$$\mathcal{L}[\{\phi_n\}] = E_{\mathrm{HF}}[\{\phi_n\}] + G[\{\phi_n\}] \tag{2.29}$$

which contains the constraint

$$G[\{\phi_n\}] = \sum_{nm} \lambda_{nm}(\delta_{nm} - \langle\phi_n|\phi_m\rangle) \tag{2.30}$$

with Lagrange multipliers λ_{ij}. We find the minimum by the variational method:

$$\delta\mathcal{L}[\{\phi_n\}] = 0 \tag{2.31}$$

First we calculate the variation of $E_{\mathrm{HF}}[\{\phi_n\}]$:

$$\begin{aligned}
\delta E_{\mathrm{HF}}[\{\phi_n\}] =& E_{\mathrm{HF}}[\{\phi_n + \delta\phi_n\}] - E_{\mathrm{HF}}[\{\phi_n + \delta\phi_n\}] \\
=& \sum_{n=1}^{N} \langle \delta\phi_n | \hat{\mathrm{h}} | \phi_n \rangle + \langle \phi_n | \hat{\mathrm{h}} | \delta\phi_n \rangle \\
&+ \frac{1}{2} \sum_{\substack{nm \\ m\neq n}}^{N} \langle \delta\phi_n | \langle \phi_m | \hat{\mathrm{v}} | \phi_n \rangle | \phi_m \rangle - \langle \delta\phi_n | \langle \phi_m | \hat{\mathrm{v}} | \phi_m \rangle | \phi_n \rangle \\
&\quad + \langle \phi_n | \langle \delta\phi_m | \hat{\mathrm{v}} | \phi_n \rangle | \phi_m \rangle - \langle \phi_n | \langle \delta\phi_m | \hat{\mathrm{v}} | \phi_m \rangle | \phi_n \rangle \\
&\quad + \langle \phi_n | \langle \phi_m | \hat{\mathrm{v}} | \delta\phi_n \rangle | \phi_m \rangle - \langle \phi_n | \langle \phi_m | \hat{\mathrm{v}} | \delta\phi_m \rangle | \phi_n \rangle \\
&\quad + \langle \phi_n | \langle \phi_m | \hat{\mathrm{v}} | \phi_n \rangle | \delta\phi_m \rangle - \langle \phi_n | \langle \phi_m | \hat{\mathrm{v}} | \phi_m \rangle | \delta\phi_n \rangle \\
&+ \mathcal{O}(\delta^2)
\end{aligned} \tag{2.32}$$

Since n, m are dummy indices and

$$\langle kl | \mathrm{v} | mn \rangle = \langle lk | \mathrm{v} | nm \rangle \tag{2.33}$$

we can find a more compact form for the first order (in $\delta\phi_n$) variation:

$$\begin{aligned}
\delta^{(1)} E_{\mathrm{HF}}[\{\phi_n\}] =& \sum_{n=1}^{N} \langle \delta\phi_n | \hat{\mathrm{h}} | \phi_n \rangle + \langle \phi_n | \hat{\mathrm{h}} | \delta\phi_n \rangle \\
&+ \sum_{\substack{nm \\ n\neq m}}^{N} \langle \delta\phi_n | \langle \phi_m | \hat{\mathrm{v}} | \phi_n \rangle | \phi_m \rangle - \langle \delta\phi_n | \langle \phi_m | \hat{\mathrm{v}} | \phi_m \rangle | \phi_n \rangle \\
&+ \langle \phi_m | \langle \phi_n | \hat{\mathrm{v}} | \phi_m \rangle | \delta\phi_n \rangle - \langle \phi_n | \langle \phi_m | \hat{\mathrm{v}} | \phi_m \rangle | \delta\phi_n \rangle \\
=& \sum_{n=1}^{N} \langle \delta\phi_n | \hat{\mathrm{h}} | \phi_n \rangle + \sum_{m=1}^{N} \langle \delta\phi_n | \langle \phi_m | \hat{\mathrm{v}} | \phi_n \rangle | \phi_m \rangle - \langle \delta\phi_n | \langle \phi_m | \hat{\mathrm{v}} | \phi_m \rangle | \phi_n \rangle \\
&+ \mathbf{cc}.
\end{aligned} \tag{2.34}$$

We also used that the $m = n$ term in the sum is always 0 in order to lift the restriction that we should not sum over $m = n$.

The first order variation of the constraint $G[\{\phi_n\}]$ yields:

$$\delta G^{(1)}[\{\phi_n\}] = -\sum_{nm} \lambda_{nm}(\langle\delta\phi_n|\phi_m\rangle + \langle\phi_n|\delta\phi_m\rangle) = -\sum_{nm} \lambda_{nm}\langle\delta\phi_n|\phi_m\rangle + \lambda_{mn}\langle\phi_m|\delta\phi_n\rangle\,. \tag{2.35}$$

Combining the results from Eqs. (2.34) & (2.35) and using it in Eq. (2.31) we obtain:

$$\begin{aligned}
&\delta^{(1)}\mathcal{L}[\{\phi_n\}] = \qquad\qquad (2.36)\\
&\sum_{n=1}^{N} \langle\delta\phi_n| \left(\hat{\mathrm{h}}\,|\phi_n\rangle + \sum_{m=1}^{N} \langle\phi_m|\,\hat{\mathrm{v}}\,|\phi_n\rangle\,|\phi_m\rangle - \langle\phi_m|\,\hat{\mathrm{v}}\,|\phi_m\rangle\,|\phi_n\rangle - \lambda_{nm}\,|\phi_m\rangle\right)\\
&+ \left[\sum_{n=1}^{N} \langle\delta\phi_n| \left(\hat{\mathrm{h}}\,|\phi_n\rangle + \sum_{m=1}^{N} \langle\phi_m|\,\hat{\mathrm{v}}\,|\phi_n\rangle\,|\phi_m\rangle - \langle\phi_m|\,\hat{\mathrm{v}}\,|\phi_m\rangle\,|\phi_n\rangle - \lambda^*_{mn}\,|\phi_m\rangle\right)\right]^*\\
&= 0.
\end{aligned}$$

The variational method requires the above Eq. (2.36) to be true for arbitrary small variations $\langle\delta\phi_n|$, hence we deduce that

$$\hat{\mathrm{h}}\,|\phi_n\rangle + \sum_{m=1}^{N} \langle\phi_m|\,\hat{\mathrm{v}}\,|\phi_n\rangle\,|\phi_m\rangle - \langle\phi_m|\,\hat{\mathrm{v}}\,|\phi_m\rangle\,|\phi_n\rangle - \lambda_{nm}\,|\phi_m\rangle = 0 \tag{2.37}$$

and

$$\hat{\mathrm{h}}\,|\phi_n\rangle + \sum_{m=1}^{N} \langle\phi_m|\,\hat{\mathrm{v}}\,|\phi_n\rangle\,|\phi_m\rangle - \langle\phi_m|\,\hat{\mathrm{v}}\,|\phi_m\rangle\,|\phi_n\rangle - \lambda^*_{mn}\,|\phi_m\rangle = 0. \tag{2.38}$$

It can be easily checked that Eqs. (2.37) & (2.38) individually follow from Eq. (2.36) by using first an arbitrary real variation $\mathrm{Im}(\langle\mathbf{r}|\delta\phi_n\rangle) = 0\ \forall n$ and second an arbitrary purely imaginary variation $\mathrm{Re}(\langle\mathbf{r}|\delta\phi_n\rangle) = 0\ \forall n$. In the first case, the left side of Eq. (2.37) would need to be the negative of Eq. (2.38), in the second case they would need to be equal, hence both need to be 0 individually.

By subtracting Eq.(2.37) from Eq.(2.38) we further find that λ is Hermitian. Hence Eqs.(2.37) & (2.38) are equivalent and in what follows we consider only Eq. (2.37).

The functional in Eq. (2.29) is invariant under unitary transformations between the orbitals $U : \{\phi_n\} \to \{\tilde{\phi}_n\}$ with $\tilde{\phi}_n = \sum_m U_{nm}\phi_m$. For the constraint $G[\{\phi_n\}]$ this is obvious. For $E_{\mathrm{HF}}[\{\phi_n\}]$ this follows from the fact that the Slater determinant is invariant under unitary transformations of the constituting orbitals – see also Eq.

(2.10):

$$E_{\mathrm{HF}}[\{\tilde{\phi}_n\}] = E_{\mathrm{el}}[\Psi_{\mathrm{AS}}(\{\tilde{\phi}_n\})] = E_{\mathrm{el}}[\Psi_{\mathrm{AS}}(U\{\phi_n\})] = E_{\mathrm{el}}[\Psi_{\mathrm{AS}}(\{\phi_n\})] = E_{\mathrm{HF}}[\{\phi_n\}]. \tag{2.39}$$

This means that if a set of orbitals $\{\phi_n\}$ and Lagrange multipliers λ_{nm} solve Eq. (2.37) and therefore this set minimizes the Hartree-Fock energy functional under the orthonormality constraint, so does the unitarily transformed set $\{\tilde{\phi}_n\} : \tilde{\phi}_n = \sum_m U_{nm}\phi_m$. Rewriting Eq. (2.37) in terms of $\{\tilde{\phi}_n\}$ we have:

$$\begin{aligned}
&\hat{\mathrm{h}} \sum_l U^\dagger_{nl} \left|\tilde{\phi}_l\right\rangle + \sum_{jklm} \left\langle\tilde{\phi}_j\right| U_{jm}\hat{\mathrm{v}}U^\dagger_{nl} \left|\tilde{\phi}_l\right\rangle U^\dagger_{mk} \left|\tilde{\phi}_k\right\rangle \\
&- \sum_{jklm} \left\langle\tilde{\phi}_j\right| U_{jm}\hat{\mathrm{v}}U^\dagger_{mk} \left|\tilde{\phi}_k\right\rangle U^\dagger_{nl} \left|\tilde{\phi}_l\right\rangle - \sum_{jm} \lambda_{nm} U^\dagger_{mj} \left|\tilde{\phi}_j\right\rangle = 0
\end{aligned} \tag{2.40}$$

$$\hat{\mathrm{h}} \left|\tilde{\phi}_i\right\rangle + \sum_j \left\langle\tilde{\phi}_j\right| \hat{\mathrm{v}} \left|\tilde{\phi}_i\right\rangle \left|\tilde{\phi}_j\right\rangle - \sum_j \left\langle\tilde{\phi}_j\right| \hat{\mathrm{v}} \left|\tilde{\phi}_j\right\rangle \left|\tilde{\phi}_i\right\rangle - \sum_{nmj} U_{in}\lambda_{nm}U^\dagger_{mj} \left|\tilde{\phi}_j\right\rangle = 0 \tag{2.41}$$

From Eq. (2.40) to Eq. (2.41) we multiplied both sides with with U_{in}, carried out the sum over the indices m, n, k, l in the first three terms and used the property of the unitary matrix $\sum_m U^\dagger_{jm}U_{mk} = \delta_{jk}$. Now the Lagrange multiplier matrix λ in the last term is subject to the same unitary transformation as the $\{\tilde{\phi}_n\}$ are with respect to the $\{\phi_n\}$. Since an arbitrary unitary transformation on the orbital set leaves the functional in Eq. (2.29) invariant and λ is Hermitian, we may choose U such that it diagonalizes λ:

$$\sum_{nm} U_{in}\lambda_{nm}U^\dagger_{mj} = \epsilon_i\delta_{ij} \tag{2.42}$$

Omitting the tilde this leaves us finally with the canonical Hartree-Fock equation which also defines the Fock operator $\hat{F}$:

$$\hat{\mathrm{h}} \left|\phi_i\right\rangle + \sum_j \left\langle\phi_j\right| \hat{\mathrm{v}} \left|\phi_i\right\rangle \left|\phi_j\right\rangle - \sum_j \left\langle\phi_j\right| \hat{\mathrm{v}} \left|\phi_j\right\rangle \left|\phi_i\right\rangle = \epsilon_i \left|\phi_i\right\rangle \tag{2.43}$$

$$\hat{F}(\{\phi_j\}) \left|\phi_i\right\rangle = \epsilon_i \left|\phi_i\right\rangle . \tag{2.44}$$

We have shown that we can use the eigenvalue problem in Eq. (2.43) to find a solution to the variational problem in Eq. (2.31) and hence to find the Hartree-Fock ground state and its corresponding energy as the best approximation with a single Slater determinant to the true ground state energy. In practice, since the Fock operator depends on the orbitals, Eq. (2.43) has to be solved iteratively: the Fock operator is constructed from a set of trial orbitals, the resulting eigenfunctions are used as the next trial orbitals to construct a new Fock operator and the process is repeated until the required convergence is achieved.

2.5 Including spin

We now include spin in the description in order to give a proper physical interpretation of the Hartree-Fock method and to give a correct description how it can be used to solve real world problems. All of the above derivations with orbitals $\phi(\mathbf{r})$ in position space hold for spin orbitals $|\chi_i\rangle = |\phi_i\rangle \otimes |\alpha_i\rangle$ if one just uses the substitutions shown in Sec. 1.6. Especially the basis-independent bracket notation allows to switch directly from purely spatial to spin orbitals. Most importantly, the canonical Hartree-Fock equation Eq. (2.43) has exactly the same form:

$$\hat{\mathrm{h}}\,|\chi_i\rangle + \sum_j \langle\chi_j|\,\hat{\mathrm{v}}\,|\chi_i\rangle\,|\chi_j\rangle - \sum_j \langle\chi_j|\,\hat{\mathrm{v}}\,|\chi_j\rangle\,|\chi_i\rangle = \epsilon_i\,|\chi_i\rangle \tag{2.45}$$

$$\hat{F}(\{\chi_j\})\,|\chi_i\rangle = \epsilon_i\,|\chi_i\rangle\,. \tag{2.46}$$

The set of spin orbitals that solves Eq. (2.45) self consistently are the (occupied) Hartree-Fock orbitals (of course there are more than N eigenfunctions for the self-consistent Fock operator, however only N are used for the construction of the Slater determinant and required for the self consistency, they are the occupied states, the others are called unoccupied or virtual states).

We first have a closer look at the Fock operator. It contains three terms, the one electron term $\hat{h}$, the Hartree potential v_H and the non-local exchange potential v_x. The term $\hat{h}$ is just the external potential, e.g. from the nuclei, and the kinetic energy operator that acts on all electrons in the same way. The Hartree potential v_H can be described as the Coulomb potential of all electrons:

$$\langle\mathbf{x}_1|v_\mathrm{H}|\mathbf{x}_2\rangle = \langle\mathbf{x_1}|\iint \mathrm{d}\mathbf{x}\mathrm{d}\mathbf{x}'\frac{|\mathbf{x}\rangle\,\langle\mathbf{x}|\sum_{j=1}^N\langle\chi_j|\mathbf{x}'\rangle\,\langle\mathbf{x}'|\chi_j\rangle}{|\mathbf{r}-\mathbf{r}'|}\,|\mathbf{x}_2\rangle \tag{2.47}$$

$$= \sum_{\sigma,\sigma'}\iint \mathrm{d}^3\mathbf{r}\mathrm{d}^3\mathbf{r}'\,\langle\mathbf{r}_1|\mathbf{r}\rangle\,\langle\sigma_1|\sigma\rangle\,\langle\mathbf{r}|\mathbf{r}_2\rangle\,\langle\sigma|\sigma_2\rangle\,\frac{\sum_{j=1}^N\phi_j^*(\mathbf{r}')\,\langle\alpha_j|\sigma'\rangle\,\phi_j(\mathbf{r}')\,\langle\sigma'|\alpha_j\rangle}{|\mathbf{r}-\mathbf{r}'|}$$

$$= \delta_{\sigma_1\sigma_2}\delta(\mathbf{r}_1-\mathbf{r}_2)\int \mathrm{d}^3\mathbf{r}'\frac{\sum_{j=1}^N\phi_j^*(\mathbf{r}')\phi_j(\mathbf{r}')}{|\mathbf{r}_1-\mathbf{r}'|}$$

$$= \delta_{\sigma_1\sigma_2}\delta(\mathbf{r}_1-\mathbf{r}_2)\int \mathrm{d}^3\mathbf{r}'\frac{n(\mathbf{r}')}{|\mathbf{r}_1-\mathbf{r}'|}. \tag{2.48}$$

The non-local exchange potential has no classical analogue and is a consequence of

the anti-symmetrization. It can be written as:

$$-\langle \mathbf{x}_1|v_{\mathrm{x}}|\mathbf{x}_2\rangle = \langle \mathbf{x_1}| \iint \mathrm{d}\mathbf{x}\mathrm{d}\mathbf{x}' \frac{|\mathbf{x}'\rangle \langle \mathbf{x}| \sum_{j=1}^{N} \langle \chi_j|\mathbf{x}\rangle \langle \mathbf{x}'|\chi_j\rangle}{|\mathbf{r}-\mathbf{r}'|} |\mathbf{x}_2\rangle \tag{2.49}$$

$$= \sum_{\sigma,\sigma'} \iint \mathrm{d}^3\mathbf{r}\mathrm{d}^3\mathbf{r}' \langle \mathbf{r}_1|\mathbf{r}'\rangle \langle \sigma_1|\sigma'\rangle \langle \mathbf{r}|\mathbf{r}_2\rangle \langle \sigma|\sigma_2\rangle \frac{\sum_{j=1}^{N} \phi_j^*(\mathbf{r}) \langle \alpha_j|\sigma\rangle \phi_j(\mathbf{r}') \langle \sigma'|\alpha_j\rangle}{|\mathbf{r}-\mathbf{r}'|}$$

$$= \iint \mathrm{d}^3\mathbf{r}\mathrm{d}^3\mathbf{r}' \frac{\sum_{j=1}^{N} \phi_j^*(\mathbf{r})\phi_j(\mathbf{r}')\delta_{\sigma_1\alpha_j}\delta_{\alpha_j\sigma_2}}{|\mathbf{r}-\mathbf{r}'|}\delta(\mathbf{r}_1-\mathbf{r}')\delta(\mathbf{r}-\mathbf{r}_2)$$

$$= \iint \mathrm{d}^3\mathbf{r}\mathrm{d}^3\mathbf{r}' \frac{n_\downarrow(\mathbf{r}',\mathbf{r})\delta_{\sigma_1,\downarrow}\delta_{\downarrow,\sigma_2} + n_\uparrow(\mathbf{r}',\mathbf{r})\delta_{\sigma_1,\uparrow}\delta_{\uparrow,\sigma_2}}{|\mathbf{r}-\mathbf{r}'|}\delta(\mathbf{r}_1-\mathbf{r}')\delta(\mathbf{r}-\mathbf{r}_2)$$

$$= \frac{n_\downarrow(\mathbf{r}_1,\mathbf{r}_2)\delta_{\sigma_1,\downarrow}\delta_{\downarrow,\sigma_2} + n_\uparrow(\mathbf{r}_1,\mathbf{r}_2)\delta_{\sigma_1,\uparrow}\delta_{\uparrow,\sigma_2}}{|\mathbf{r}_2-\mathbf{r}_1|}. \tag{2.50}$$

In Eq. 2.50, $n_\downarrow(\mathbf{r}',\mathbf{r})$ and $n_\uparrow(\mathbf{r}',\mathbf{r})$ are the down-spin and up-spin 1-particle reduced density matrix of the Slater determinant $\langle \mathbf{x}_1,\ldots,\mathbf{x}_N|\chi_1,\ldots,\chi_N\rangle$. From this notation it is clear that the exchange interaction is only between orbitals with same spin orientation. Also, the exchange potential cancels the self interaction in the Hartree potential exactly. The exchange interaction is often referred to as Pauli repulsion, since it is a consequence of the anti-symmetrization and consequently the Pauli principle.

From the statements above, one can conclude that each electron that is described by an eigenfunction of the Fock operator can be viewed as an independent particle that moves in the external potential of the ions, the mean Hartree-potential of the other electrons and the mean exchange potential of the other electrons with equal spin. For this reason the Hartree-Fock method is often described as a mean-field method and the procedure to obtain the Hartree-Fock orbitals is often called self-consistent field procedure.

2.5.1 Restricted Hartree-Fock

In the restricted Hartree-Fock method it is assumed that all electrons are spin paired, *i.e.* the spin orbitals occur pairwise as combinations of spatial orbitals ϕ_i and single particle spin eigenstates:

$$|\chi_{2i}\rangle = |\phi_i\rangle \otimes |\downarrow\rangle = |\phi_i,\downarrow\rangle \quad |\chi_{2i-1}\rangle = |\phi_i\rangle \otimes |\uparrow\rangle = |\phi_i,\uparrow\rangle \quad i \in \{1,\ldots,N/2\}. \tag{2.51}$$

Of course this requires that the total number of electrons is even. Looking at the Hartree-Fock equation Eq. (2.45) for one particular spin orbital $|\chi_n\rangle$ with an odd

index $n = 2i - 1$, we get:

$$\epsilon_i \left|\phi_i,\uparrow\right\rangle = \hat{\mathrm{h}} \left|\phi_i,\uparrow\right\rangle + \sum_{j=1}^{N/2} \left(\left\langle\phi_j,\uparrow\right| \hat{\mathrm{v}} \left|\phi_i,\uparrow\right\rangle \left|\phi_j,\uparrow\right\rangle + \left\langle\phi_j,\downarrow\right| \hat{\mathrm{v}} \left|\phi_i,\uparrow\right\rangle \left|\phi_j,\downarrow\right\rangle\right) \tag{2.52}$$

$$- \sum_{j=1}^{N/2} \left(\left\langle\phi_j,\uparrow\right| \hat{\mathrm{v}} \left|\phi_j,\uparrow\right\rangle \left|\phi_i,\uparrow\right\rangle + \left\langle\phi_j,\downarrow\right| \hat{\mathrm{v}} \left|\phi_j,\downarrow\right\rangle \left|\phi_i,\uparrow\right\rangle\right)$$

$$= \left(\hat{\mathrm{h}} \left|\phi_i\right\rangle + 2\sum_{j=1}^{N/2} \left\langle\phi_j\right| \hat{\mathrm{v}} \left|\phi_i\right\rangle \left|\phi_j\right\rangle - \sum_{j=1}^{N/2} \left\langle\phi_j\right| \hat{\mathrm{v}} \left|\phi_j\right\rangle \left|\phi_i\right\rangle\right) \otimes \left|\uparrow\right\rangle$$

$$\Rightarrow \qquad \hat{F}_{\mathrm{RHF}} \left|\phi_i\right\rangle = \hat{\mathrm{h}} \left|\phi_i\right\rangle + 2\sum_{j=1}^{N/2} \left\langle\phi_j\right| \hat{\mathrm{v}} \left|\phi_i\right\rangle \left|\phi_j\right\rangle - \sum_{j=1}^{N/2} \left\langle\phi_j\right| \hat{\mathrm{v}} \left|\phi_j\right\rangle \left|\phi_i\right\rangle = \epsilon_i \left|\phi_i\right\rangle . \tag{2.53}$$

In Eq. (2.52) the two terms in the Hartree part (first sum) are identical as the spins are aligned in both cases. In the exchange part (second sum) the spins are only aligned in the first term, so the second term vanishes. Clarification:

$$\left\langle\phi_j,\beta\right| \hat{\mathrm{v}} \left|\phi_k,\gamma\right\rangle \left|\phi_l,\delta\right\rangle = \iint \mathrm{d}^3\mathbf{r}\mathrm{d}^3\mathbf{r}' \sum_{\sigma,\sigma'} \left|\mathbf{r},\sigma\right\rangle \frac{\phi_j^*(\mathbf{r}') \left\langle\beta|\sigma'\right\rangle \phi_k(\mathbf{r}) \left\langle\sigma|\gamma\right\rangle \phi_l(\mathbf{r}') \left\langle\sigma'|\delta\right\rangle}{|\mathbf{r} - \mathbf{r}'|}$$

$$= \left\langle\beta|\delta\right\rangle \iint \mathrm{d}^3\mathbf{r}\mathrm{d}^3\mathbf{r}' \frac{\phi_j^*(\mathbf{r}')\phi_k(\mathbf{r})\phi_l(\mathbf{r}')}{|\mathbf{r} - \mathbf{r}'|} \left|\mathbf{r}\right\rangle \otimes \left|\gamma\right\rangle$$

$$= \left\langle\beta|\delta\right\rangle \left(\left\langle\phi_j\right| \hat{\mathrm{v}} \left|\phi_k\right\rangle \left|\phi_l\right\rangle\right) \otimes \left|\gamma\right\rangle \tag{2.54}$$

Eq. (2.53) is obtained in the same way for spin orbitals with down spin (in our notation even index n for $|\chi_n\rangle$). This means that one needs to solve the restricted Hartree-Fock equation Eq. (2.53) only for $N/2$ (purely spatial) orbitals and can construct the N spin orbitals afterwards by assigning each spatial Hartree-Fock orbital pairwise spin up and spin down.

2.5.2 Unrestricted Hartree-Fock

In the unrestricted Hartree-Fock method [52], the restriction that the number of spin-up orbitals and the number of spin-down orbitals has to be equal is dropped. The number of spin orbitals with spin up and down is $N_\uparrow$ and $N_\downarrow$ respectively, the sum $N_\uparrow + N_\downarrow = N$, the total number of electrons. The Fock operator is therefore spin dependent and the Hartree-Fock equations are two sets of coupled equations

that are not symmetric (as they were in the restricted case), the spin orbitals are

$$|\chi_n\rangle = |\phi_n^{\uparrow}, \uparrow\rangle \qquad \text{for } n \leq N_{\uparrow} \tag{2.55}$$

$$|\chi_n\rangle = |\phi_n^{\downarrow}, \downarrow\rangle \qquad \text{for } N_{\uparrow} < n \leq N \tag{2.56}$$

and the Hartree-Fock equations for the up spin space are

$$\epsilon_i \, |\phi_i^{\uparrow}\rangle = \hat{\mathrm{h}} \, |\phi_i^{\uparrow}\rangle + \sum_{j=1}^{N_{\uparrow}} \langle \phi_j^{\uparrow}| \, \hat{\mathrm{v}} \, |\phi_i^{\uparrow}\rangle \, |\phi_j^{\uparrow}\rangle - \langle \phi_j^{\uparrow}| \, \hat{\mathrm{v}} \, |\phi_j^{\uparrow}\rangle \, |\phi_i^{\uparrow}\rangle + \sum_{j=1}^{N_{\downarrow}} \langle \phi_j^{\downarrow}| \, \hat{\mathrm{v}} \, |\phi_i^{\uparrow}\rangle \, |\phi_j^{\downarrow}\rangle \tag{2.57}$$

The equation for the spin down space is obtained by exchanging $\uparrow$ with $\downarrow$ and vice versa in the above Eq. (2.57). The second Hund's rule that states that electrons arrange themselves with parallel spins if the energy levels are otherwise degenerate can be explained within the unrestricted Hartree-Fock method and is a consequence of the fact that the exchange contribution is always negative.

Note that in general the spatial orbitals of the different spin spaces differ from each other, *i.e.* $|\phi_n^{\uparrow}\rangle \neq |\phi_n^{\downarrow}\rangle$. This leads to a many particle state that is not an eigenstate of the total spin operator S^2 and the problem of spin contamination, *i.e.* the ground state is contaminated by excited states[53].

2.6 Summary and limitations of the Hartree-Fock method

The Hartree-Fock method tries to find a good approximation to the ground state (and its properties) of a many electron system. This is done by restricting the ground state to a single Slater-determinant and finding the minimum energy to a given Hamiltonian under this constraint. In theory the minimum energy can be found by minimizing the Hartree-Fock energy functional. In practice, it is found by self-consistently solving the Hartree-Fock equations, which represent an eigenvalue problem that stems from the variational method. The Hartree-Fock equations can be interpreted as a system of non-interacting electrons that move in the mean-field of all electrons, therefore the Hartree-Fock method is also referred to as a self-consistent field or mean-field method. The resulting approximate ground state energy is the Hartree-Fock energy, which includes the classical Coulomb interaction of each electron in the mean-field of the others and additionally takes into account the so called exchange interaction (or Pauli repulsion) which stems from the anti-symmetry principle for fermions and has no classical analogue. Since the true ground state energy has to be always lower or equal, the Hartree-Fock energy is an upper bound for the true ground state energy. The difference between the true ground state energy and the Hartree-Fock energy is usually referred to as correlation energy. The correlation energy is a quantum mechanical concept with no classical analogue and it is attributed to the correlations between electrons that naturally cannot be

described by a mean-field method.

The approximations used in the Hartree-Fock method give rise to considerable limitations. The neglect of dynamic correlations due to its mean-field character as well as static correlations due to the use of a single Slater determinant can lead to significant, often qualitative differences between experiments and the theoretical predictions of the Hartree-Fock method. A typical issue is that Hartree-Fock underbinds molecules and solids by 30-50%, which is related to the neglect of dynamic correlation. The dissociation of the hydrogen molecule is a particularly prominent example where Hartree-Fock fails. While restricted Hartree-Fock yields a H^+ and a H^- ion due to the electron pairing, unrestricted Hartree-Fock yields a spin contaminated state. In reality, the dissociation yields naturally two separate hydrogen atoms. Methods that try to improve on these deficiencies, are often referred to as post-Hartree-Fock methods.

Chapter 3

Density functional theory

In the previous chapter 2, with the Hartree-Fock method we showed an example of a mean-field method for treating the quantum many body problem and introduced some crucial concepts like the Slater-determinant and the exchange energy. Density functional theory (DFT) is another example of a widely used mean-field theory. Although the method's theoretical foundation is well established and extensively treated in the literature, we deem it necessary to dedicate a chapter of this thesis to it. This is for the sake of completeness, so that this thesis can stand alone, providing a complete overview of the most fundamental concepts that eventually led to the research presented in parts II and III. Ultimately, the work conducted for this thesis aims to enhance the capabilities of the RPA in order to outperform DFT. However, it is important to say that DFT remains highly important for the field of computational materials physics and quantum chemistry in general, and especially for the work presented here. For this reason, the master thesis [38] that preceded this thesis, already included a chapter on DFT. That chapter was partially reformulated and extended to provide a compact but hopefully instructive chapter on DFT in this thesis.

In the 1920's Llewellyn Thomas and Enrico Fermi developed independently a semi-classical statistical model to describe the electron density in atoms. In contrast to the quantum mechanical approach to describe the electron distribution in atoms with a wave function formalism and the Schrödinger equation at its center, the Thomas-Fermi model tried to make predictions based on a description that uses the electron density as the central object. The general idea is to assume that even for a system with an inhomogeneous electron density, the density can be treated as if it were locally uniformly distributed (*i.e.* in each volume element δV) so that in turn the kinetic and potential energy of the whole system can be modelled by statistical means. Unfortunately, this approach was an over-simplification and it turned out that for realistic systems, it did not even achieve a qualitatively correct description with bound atoms. Despite the discouraging results, the method was refined to include exchange interactions and the resulting Slater Xα method provided a simple tool that could be used to roughly describe inhomogeneous systems like atoms. This

way, the idea that the electron density alone could be sufficient to describe atoms, molecules and solids quantum mechanically correctly was introduced and it turned out that this approach would be fruitful.

3.1 The Hohenberg-Kohn theorems

In 1964 a paper by Hohenberg and Kohn on the inhomogeneous electron gas [7] was published and laid the foundation for one of the most used methods in electronic structure theory, namely DFT. They showed that the kinetic and the electronic interaction energy of a many electron system in an external potential is a universal functional of the density, $F[n(\mathbf{r})]$. Furthermore they showed the total energy functional $E_v[n(\mathbf{r})]$ for a given external potential $v(\mathbf{r})$,

$$E_v[n(\mathbf{r})] = \int v(\mathbf{r})n(\mathbf{r})\mathrm{d}^3\mathbf{r} + F[n(\mathbf{r})], \tag{3.1}$$

attains (under the constraint of a fixed particle number N) a minimum at the correct ground state density $n_{N,v}$ and yields the ground state energy $E^0_{v,N}$ (second Hohenberg-Kohn theorem):

$$\min_{n_N(\mathbf{r})}\{E_v[n_N(\mathbf{r})]\} = E_v[n_{N,v}(\mathbf{r})] = E^0_{v,N}. \tag{3.2}$$

3.1.1 Original proofs of the HK theorems

We will now present the proofs to these theorems along the lines of the original publication of Hohenberg and Kohn [7]. A system of interacting electrons in an external potential $v(\mathbf{r})$ can be described by a Hamiltonian H

$$H = T + V_{\mathrm{ext}} + V_{\mathrm{C}} \tag{3.3}$$

where V_{C} is the operator representing the Coulomb interaction between the interacting electrons, V_{ext} is the operator representing the external potential, and T represents the kinetic energy operator. With the field operators $\psi(\mathbf{r})$ and $\psi^\dagger(\mathbf{r})$ in second quantization notation, these operators can be written in the following way, cf. Eq. (1.65):

$$T \equiv \frac{1}{2}\int \nabla\psi^\dagger(\mathbf{r})\nabla\psi(\mathbf{r})\mathrm{d}^3\mathbf{r} \quad \left(= -\frac{1}{2}\int \psi^\dagger(\mathbf{r})\nabla^2\psi(\mathbf{r})\mathrm{d}^3\mathbf{r}\right) \tag{3.4}$$

$$V_{\mathrm{ext}} \equiv \int v(\mathbf{r})\psi^\dagger(\mathbf{r})\psi(\mathbf{r})\mathrm{d}^3\mathbf{r} \tag{3.5}$$

$$V_{\mathrm{C}} \equiv \frac{1}{2}\int \frac{1}{|\mathbf{r}-\mathbf{r}'|}\psi^\dagger(\mathbf{r})\psi^\dagger(\mathbf{r}')\psi(\mathbf{r}')\psi(\mathbf{r})\mathrm{d}^3\mathbf{r}\mathrm{d}^3\mathbf{r}'. \tag{3.6}$$

In the same notation the electronic density of the ground state Ψ becomes

$$n(\mathbf{r}) \equiv \langle \Psi | \underbrace{\psi^\dagger(\mathbf{r})\psi(r)}_{\hat{n}(\mathbf{r})} | \Psi \rangle \,. \tag{3.7}$$

The electronic density $n(\mathbf{r})$ associated with the ground state Ψ is uniquely determined by the external potential $v(\mathbf{r})$ as the ground state Ψ is uniquely determined by $v(\mathbf{r})$. As in the original publication of Hohenberg and Kohn, we will first prove this statement under the assumption of a non-degenerate ground state, and show later that this requirement can be droped. A different profound way to generalize the universality of the kinetic+interaction energy functional can be found in the work of Lieb and Levy, and the associated literature [54, 55, 56, 57]. They extend the theory to densities that are not pure state V-representable[1] and inherently resolve the issues with degenerate states.

If a Hamiltonian like the one in Eq. (3.3) with potential $v(\mathbf{r})$ yields a non-degenerate ground state $H|\Psi\rangle = E|\Psi\rangle$, than clearly the density is a unique functional of the potential as the ground state is uniquely determined by $v(\mathbf{r})$. We will now show that vice versa, the potential $v(\mathbf{r})$ is uniquely (up to a constant) determined by the ground state density, *i.e.* there exists a bijective mapping between potentials $v(\mathbf{r})$ and densities $n(\mathbf{r})$. We will prove this by *reductio ad absurdum*.

If there were two different potentials $v(\mathbf{r})$ and $v'(\mathbf{r})$ associated with two Hamiltonians H and H' and corresponding ground states $|\Psi\rangle$ and $|\Psi'\rangle$ respectively that yield the same ground state density $n(\mathbf{r})$, we would get the following set of equations:

$$H|\Psi\rangle = E|\Psi\rangle \qquad E = \langle\Psi|H|\Psi\rangle \qquad n(r) = \langle\Psi|\hat{n}(\mathbf{r})|\Psi\rangle \tag{3.8}$$

$$H'|\Psi'\rangle = E'|\Psi'\rangle \qquad E' = \langle\Psi'|H'|\Psi'\rangle \qquad n(r) = \langle\Psi'|\hat{n}(\mathbf{r})|\Psi'\rangle \tag{3.9}$$

Also since we assumed that the ground states are non-degenerate and the potentials differ (not only by a constant), the two ground states will be different and will not be ground states of the respective other Hamiltonian. Therefore we find that on the one hand

$$E = \langle\Psi|H|\Psi\rangle < \langle\Psi'|H|\Psi'\rangle = \langle\Psi'|H' - V'_{\text{ext}} + V_{\text{ext}}|\Psi'\rangle = E' + \int [v(\mathbf{r}) - v'(\mathbf{r})]n(\mathbf{r})d\mathbf{r} \tag{3.10}$$

and on the other hand

$$E' = \langle\Psi'|H'|\Psi'\rangle < \langle\Psi|H'|\Psi\rangle = \langle\Psi|H - V_{\text{ext}} + V'_{\text{ext}}|\Psi\rangle = E + \int [v'(\mathbf{r}) - v(\mathbf{r})]n(\mathbf{r})d\mathbf{r}. \tag{3.11}$$

This leads to the following inconsistency if we add the to inequalities together:

$$E' + E < E + E'. \tag{3.12}$$

[1] A pure state V representable density is one for which there exists a potential V^n_{ext}, so that the Hamiltonian $H = T + V^n_{\text{ext}} + V_{\text{C}}$ yields a pure ground state with that density

We have proven that for each density, there exists only one potential (up to a constant) that gives rise to a Hamiltonian with that ground state density. Together with the statement from above, that the ground state density is uniquely determined by the potential we have shown that for non-degenerate ground states there exists a one-to-one mapping between ground state densities and potentials (first Hohnberg-Kohn theorem).

Since the density uniquely determines the potential, which in turn determines the ground state $|\Psi[n]\rangle$, the kinetic+interaction energy is also determined by the density. Hence there exists a universal functional for the ground state kinetic+interaction energy

$$F[n(\mathbf{r})] \equiv \langle \Psi[n]|T + V_{\mathrm{C}}|\Psi[n]\rangle \,. \tag{3.13}$$

We now denote the correct ground state density for an N-electron system in a given potential $v(\mathbf{r})$ with $n_{N,v}(\mathbf{r})$ and the corresponding ground state with $\Psi_{N,v}$. For each potential $v(\mathbf{r})$, we define an energy functional that maps densities to energies

$$E_v[n] \equiv \int v(\mathbf{r}) n(\mathbf{r}) \mathrm{d}^3\mathbf{r} + F[n] \tag{3.14}$$

where $F[n]$ is the functional from Eq. (3.13). For the correct ground state density of an N-electron system, this functional yields the ground state energy $E^0_{N,v}$

$$\begin{aligned} E_v[n_{N,v}] &= \int v(\mathbf{r}) n_{N,v}(\mathbf{r}) \mathrm{d}^3\mathbf{r} + F[n_{N,v}] \\ &= \langle \Psi_{N,v}|V_{\mathrm{ext}}|\Psi_{N,v}\rangle + \langle \Psi_{N,v}|T + V_{\mathrm{C}}|\Psi_{N,v}\rangle = E^0_{N,v}. \end{aligned} \tag{3.15}$$

Furthermore, the functional $E_v[n]$ assumes its minimum for the correct ground state density $n_{N,v}$ under the constraint that only densities that integrate to N electrons are admissible. This is because in an N-electron system with external potential $v(\mathbf{r})$ and ground state $|\Psi_{N,v}\rangle$, the ground state energy is the minimum energy that can be assumed by any properly symmetric and normalized N-particle state $|\Psi_N\rangle$:

$$E^0_{N,v} = \langle \Psi_{N,v}|V_{\mathrm{ext}} + T + V_{\mathrm{C}}|\Psi_{N,v}\rangle < \langle \Psi_N|V_{\mathrm{ext}} + T + V_{\mathrm{C}}|\Psi_N\rangle \,. \tag{3.16}$$

Particularly for any N-particle ground state $\Psi_{N,v'}$ with density $n_{v'}$ corresponding to another potential $v'(\mathbf{r})$ we get due to Eq. (3.13) and (3.14)

$$\begin{aligned} \langle \Psi_{N,v'}|V_{\mathrm{ext}} + T + V_{\mathrm{C}}|\Psi_{N,v'}\rangle &= \int v(\mathbf{r}) n_{N,v'}(\mathbf{r}) \mathrm{d}^3\mathbf{r} + \langle \Psi_{N,v'}|T + V_{\mathrm{C}}|\Psi_{N,v'}\rangle \\ &= \int v(\mathbf{r}) n_{N,v'}(\mathbf{r}) \mathrm{d}^3\mathbf{r} + F[n_{v'}] = E_v[n_{N,v'}] \end{aligned} \tag{3.17}$$

and therefore due to Eq. (3.15) and (3.16) we obtain the minimization property of

the Hohenberg Kohn functional:

$$E_v[n_{N,v}] < E_v[n_{N,v'}]. \tag{3.18}$$

We have shown that for all pure state V-representable N-particle densities (from non-degenerate ground states), the functional (3.1) assumes its minimum at the correct ground state density $n_{N,v}$ where it yields the ground state energy (second Hohenberg-Kohn theorem):

$$\min_{n_N(\mathbf{r})} \{E_v[n_N(\mathbf{r})]\} = E_v[n_{N,v}(\mathbf{r})] = E^0_{v,N}. \tag{3.19}$$

If $F[n]$ was a known and sufficiently simple functional, one could in principle find the ground state density and energy to a given potential by a variational method, minimizing the functional $E_v[n]$ of the three-dimensional density. This is a promising approach to circumvent solving the exact N-electron Schrödinger equation and as it turned out it is also a very successful approach. The major drawback is that the functional $F[n]$ is not known and the challenging part of DFT is to find good approximations.

3.1.2 Extending the Hohenberg-Kohn theorems to degenerate ground states

We now want to show that we can drop the requirement of non-degenerate ground states while still using only pure state V-representable densities. We will not proof the first Hohenberg-Kohn theorem for degenerate states, so in principle we allow that there is not necessarily a one-to-one mapping between ground state densities and potentials. However, there exists a universal functional $F[n]$ that maps every ground state density to a specific kinetic+interaction energy. We will prove this by showing that the kinetic+interaction energy is still uniquely determined by the ground-state density, even if degenerate ground states are permitted. Provided that a universal functional $F[n]$ exists that maps every ground state density to a specific ground state kinetic+interaction energy, the proofs in the previous subsection for the second Hohenberg-Kohn theorem still hold and do not require additional modifications for degenerate ground states.

We start the proof of the existence of the universal functional $F[n]$ with some definitions. The domain of $F[n]$ is the set of all (pure state) ground state densities S_{GSD} and for each $n \in S_{GSD}$ there exists at least one Hamiltonian H with a ground state Ψ so that $|\langle\Psi|\mathbf{r}\rangle|^2 = n(\mathbf{r})$. In this subsection we denote the set of ground states for Hamiltonian H with density n as S^H_n.

Assertion: If for a single Hamiltonian H there exists more than one ground state that gives rise to the same density $n(\mathbf{r})$, then all these ground states yield the same kinetic+interaction energy.

Proof: Given are there are two ground states Ψ_1,$\Psi_2 \in S^H_n$ for Hamiltonian $H = T + V_\mathrm{C} + V_\mathrm{ext}$ (cf. Eq. (3.3)) and density $n(\mathbf{r})$. Then $|\langle\Psi_1|\mathbf{r}\rangle|^2 = |\langle\Psi_2|\mathbf{r}\rangle|^2 = n(\mathbf{r})$

and since they are both ground states, they yield the same energy $E = \langle\Psi_1|H|\Psi_1\rangle = \langle\Psi_2|H|\Psi_2\rangle$. Therefore, for both the kinetic+interaction energy is:

$$\langle\Psi_{1/2}|T + V_\mathrm{C}|\Psi_{1/2}\rangle = \langle\Psi_{1/2}|H - V_\mathrm{ext}|\Psi_{1/2}\rangle = E - \int \mathrm{d}^3\mathbf{r} v(\mathbf{r}) n\mathbf{r} = F^H[n(\mathbf{r})] \quad (3.20)$$

Since this is true for all pairs of ground states with the same density, all ground states of a single Hamiltonian H with the same density n have the same kinetic+interaction energy $F^H[n(\mathbf{r})]$. □

We have proven, that for a single Hamiltonian, the kinetic+interaction energy is uniquely determined by the ground state density, even if there are degenerate ground states. Consequently, if for a density n there exists only one Hamiltonian (up to a constant potential) that has at least one ground state with that density, the kinetic+interaction energy is uniquely determined for that density. What remains to be proved is that ground states from different Hamiltonians that give rise to the same density also have the same kinetic+interaction energy. Hence from now on we only need to look at densities, for which there exist at least two distinct (not only by a constant potential) Hamiltonians that have at least one ground state with that density.

Assume that for two Hamiltonians $H^1 = T + V_\mathrm{C} + V^1_\mathrm{ext}$ and $H^2 = T + V_\mathrm{C} + V^2_\mathrm{ext}$ there exists a density $\tilde{n}(\mathbf{r})$ so that for both Hamiltonians there is at least one ground state that gives rise to that density. Let $S^{H^1}_{\tilde{n}}/S^{H^2}_{\tilde{n}}$ be the (non-empty) set of ground states $\{\Psi^1_{\tilde{n},j}\}/\{\Psi^2_{\tilde{n},j}\}$ of H^1/H^2 with density $\tilde{n}(\mathbf{r})$. According to Eq. (3.20) we have

$$\langle\Psi^1_{\tilde{n},j}|T + V_\mathrm{C}|\Psi^1_{\tilde{n},j}\rangle = F^{H_1}[\tilde{n}(\mathbf{r})] \quad \forall\ \Psi^1_{\tilde{n},j} \in S^{H^1}_{\tilde{n}} \quad (3.21)$$

$$\langle\Psi^2_{\tilde{n},j}|T + V_\mathrm{C}|\Psi^2_{\tilde{n},j}\rangle = F^{H_2}[\tilde{n}(\mathbf{r})] \quad \forall\ \Psi^2_{\tilde{n},j} \in S^{H^2}_{\tilde{n}} \quad (3.22)$$

Assertion: There exists a state $|\tilde{\Psi}_{\tilde{n}}\rangle$ that belongs to $S^{H^1}_{\tilde{n}}$ and $S^{H^2}_{\tilde{n}}$, or in other words the intersection $S^{H^1}_{\tilde{n}} \cap S^{H^2}_{\tilde{n}}$ is non-empty.

Proof: We can proof the above assertion by *reductio ad absurdum* in the same way the first Hohenberg-Kohn theorem was proven for non-degenerate ground states. If the intersection $S^{H^1}_{\tilde{n}} \cap S^{H^2}_{\tilde{n}}$ was the empty set, then none of the states $\Psi^1_{\tilde{n},j} \in S^{H^1}_{\tilde{n}}$ would be ground states for H^2 (and none of the states $\Psi^2_{\tilde{n},j} \in S^{H^2}_{\tilde{n}}$ would be ground states for H^1). Therefore

$$E^1 = \langle\Psi^1_{\tilde{n},j}|H^1|\Psi^1_{\tilde{n},j}\rangle < \langle\Psi^2_{\tilde{n},j}|H^1|\Psi^2_{\tilde{n},j}\rangle = \langle\Psi^2_{\tilde{n},j}|H^2 - V^2_\mathrm{ext} + V^1_\mathrm{ext}|\Psi^2_{\tilde{n},j}\rangle$$

$$\Rightarrow \qquad E^1 < E^2 + \int \tilde{n}(\mathbf{r})(v^1(\mathbf{r}) - v^2(\mathbf{r}))\mathrm{d}^3\mathbf{r} \quad (3.23)$$

$$E^2 = \langle\Psi^2_{\tilde{n},j}|H^2|\Psi^2_{\tilde{n},j}\rangle < \langle\Psi^1_{\tilde{n},j}|H^2|\Psi^1_{\tilde{n},j}\rangle = \langle\Psi^1_{\tilde{n},j}|H^1 - V^1_\mathrm{ext} + V^2_\mathrm{ext}|\Psi^1_{\tilde{n},j}\rangle$$

$$\Rightarrow \qquad E^2 < E^1 + \int \tilde{n}(\mathbf{r})(v^2(\mathbf{r}) - v^1(\mathbf{r}))\mathrm{d}^3\mathbf{r} \quad (3.24)$$

Adding together each side of Eq. (3.23) and (3.24) arrive at the contradiction

$$E^1 + E^2 < E^1 + E^2 \tag{3.25}$$

$$\Rightarrow \; S_{\tilde{n}}^{H^1} \cap S_{\tilde{n}}^{H^2} \neq \{\} \tag{3.26}$$

□

Since $\exists\, |\tilde{\Psi}_{\tilde{n}}\rangle \in S_{\tilde{n}}^{H^1} \cap S_{\tilde{n}}^{H^2}$, we get according to Eq. (3.21) and (3.22) that

$$F^{H^1}[\tilde{n}(\mathbf{r})] = F^{H^2}[\tilde{n}(\mathbf{r})] = \langle \tilde{\Psi}_{\tilde{n}} | T + V_{\mathrm{C}} | \tilde{\Psi}_{\tilde{n}} \rangle \,. \tag{3.27}$$

Now we have shown that if there are any two Hamiltonians that have at least one ground state with the same density, all ground states with that density of both Hamiltonians have the same interaction+kinetic energy. Thus, all ground states with that density have the same interaction+kinetic energy.

We can summarize the results of this subsection with the following statement: All (pure) ground states with density n (of any Hamiltonian) have the same kinetic+interaction energy. Therefore, there exists a universal functional $F[n]$ that maps every (pure state) ground state density to a specific ground state kinetic+interaction energy. Hence the second Hohenberg-Kohn theorem is also valid for degenerate ground states.

3.2 The Kohn-Sham system of non-interacting electrons

In 1965, one year after the Hohenberg-Kohn paper [7], Kohn and Sham published a theory on a practical way to approximate the energy functional postulated earlier [8]. Their approach is to map a system of interacting electrons to a system of non-interaction electrons that move in an effective potential. By choosing the effective potential such that the non-interacting system has the same ground state density as the original interacting system, one can use the second Hohenberg-Kohn theorem to find the true ground state energy. The Hohenberg-Kohn theorems allow us to write the total energy of a non-uniform electron gas in a static external potential $v(\mathbf{r})$ as

$$E = \underbrace{\int v(\mathbf{r}) n(\mathbf{r}) \mathrm{d}^3\mathbf{r}}_{E_{\mathrm{ext}}} + \underbrace{\frac{1}{2} \int \frac{n(\mathbf{r}) n(\mathbf{r}')}{|\mathbf{r} - \mathbf{r}'|} \mathrm{d}^3\mathbf{r} \mathrm{d}^3\mathbf{r}'}_{E_{\mathrm{H}}[n]} + G[n]. \tag{3.28}$$

In the above Eq. (3.28), the Hartree energy $E_{\mathrm{H}}[n]$ (*i.e.* the classical Coulomb interaction between the electrons) occurs explicitly. Therefore the remaining interaction energy of the electrons $G[n]$ is related to the universal functional $F[n]$ through the

following equation:

$$G[n] \equiv F[n] - \frac{1}{2}\int \frac{n(\mathbf{r})n(\mathbf{r}')}{|\mathbf{r}-\mathbf{r}'|}\mathrm{d}^3\mathbf{r}\mathrm{d}^3\mathbf{r}'. \tag{3.29}$$

In analogy to Hartree-Fock theory (chapter 2), the Hartree term E_H can be interpreted as the classical electrostatic energy of the electrons due to their own mean-field. The energy functional $G[n]$ itself can be decomposed further into two terms

$$G[n] = T_s[n] + E_\mathrm{xc}[n], \tag{3.30}$$

where $T_s[n]$ is the kinetic energy of a system of non-interacting electrons with density n. $T_s[n]$ is a universal functional of the electron density, which follows from the first Hohenberg-Kohn theorem in analogy to the universal functional $F[n]$. In the second term, the functional $E_\mathrm{xc}[n]$ contains all contributions to the energy due to exchange and correlation effects, *i.e.* effects that have no classical analogue. Note that in general, there is a difference between the true kinetic energy of a many electron state $T[n]$, and the kinetic energy of a non-interacting system with the same density $T_s[n]$. This difference also enters $E_\mathrm{xc}[n]$. Unfortunately, a sufficiently simple and exact expression for $E_\mathrm{xc}[n]$ does not exist for arbitrary densities n. However, the so called local density approximation (LDA) provides a simple method that yields remarkably accurate results in the limiting case of slowly (with respect to position coordinates) varying densities. In this method, the following approximation is used for the exchange and correlation functional $E_\mathrm{xc}[n]$:

$$E_\mathrm{xc} \approx E_\mathrm{xc}^\mathrm{LDA} = \int n(\mathbf{r})\epsilon_\mathrm{xc}^\mathrm{LDA}(n(\mathbf{r}))\mathrm{d}^3\mathbf{r}. \tag{3.31}$$

The term $\epsilon_\mathrm{xc}^\mathrm{LDA}(n)$ describes the local exchange correlation energy per particle. While in reality, the exchange correlation energy density $\tilde{\epsilon}_\mathrm{xc}(\mathbf{r})$ at each point $\mathbf{r}$ is a functional of the density n (at every point $\mathbf{r}'$)

$$\tilde{\epsilon}_\mathrm{xc}(\mathbf{r}) = \epsilon_\mathrm{xc}[n](\mathbf{r}), \tag{3.32}$$

in the LDA $\tilde{\epsilon}_\mathrm{xc}(\mathbf{r})$ is approximated only locally, *i.e.* it is only a function of the density at the specific point:

$$\tilde{\epsilon}_\mathrm{xc}^\mathrm{LDA}(\mathbf{r}) = \epsilon_\mathrm{xc}^\mathrm{LDA}(n(\mathbf{r})). \tag{3.33}$$

The most common approximation for $\epsilon_\mathrm{xc}^\mathrm{LDA}(n(\mathbf{r}))$ is to use the exchange-correlation energy per particle of the uniform electron gas with density $\epsilon_\mathrm{xc}^\mathrm{UEG}(n(\mathbf{r}))$. For this reason, in the following we will also use this approximation for $\epsilon_\mathrm{xc}^\mathrm{LDA}(n(\mathbf{r}))$. The uniform electron gas is a theoretical toy model for a system of electrons with constant density. It is a charge neutral system with N interacting electrons placed inside a volume V along with a uniform positive compensation charge, taken to the thermodynamic limit $V, N \to \infty$ at constant density $n = N/V = const.$. In the uniform

electron gas, the Hartree energy cancels exactly against the potential energy due to the positive background charge. As a consequence, only the kinetic, exchange and correlation energy contribute to the total electronic energy. It is a very useful and successful model, thus it is still used extensively in theoretical solid state physics.

Using the variational property of the total energy functional, see Eq. (3.2), we get from the variation of Eq. (3.28) the variational equation

$$\int \delta n(\mathbf{r}) \Big(\underbrace{v(\mathbf{r}) + \int \frac{n(\mathbf{r}')}{|\mathbf{r}-\mathbf{r}'|} \mathrm{d}^3\mathbf{r}' + \mu_{\mathrm{xc}}(n(\mathbf{r}))}_{v_{\mathrm{eff}}^{\mathrm{KS}}} + \frac{\delta T_s[n]}{\delta n(\mathbf{r})} \Big) \mathrm{d}^3\mathbf{r} = 0. \tag{3.34}$$

In the local density approximation the so called exchange-correlation potential $\mu_{\mathrm{xc}}^{\mathrm{LDA}}(n)$ is given by

$$\mu_{\mathrm{xc}}^{\mathrm{LDA}}(n(\mathbf{r})) = \left. \frac{d(n\epsilon_{\mathrm{xc}}^{\mathrm{LDA}}(n))}{dn} \right|_{n(\mathbf{r})}. \tag{3.35}$$

A more general definition would define the variational derivative of E_{xc} with respect to the density as the exchange correlation potential $\mu_{\mathrm{xc}}[n](\mathbf{r})$:

$$\mu_{\mathrm{xc}}[n](\mathbf{r}) = \frac{\delta E_{\mathrm{xc}}[n]}{\delta n(\mathbf{r})}. \tag{3.36}$$

Eq. (3.34) can be interpreted as the variational equation that is obtained from applying the second Hohenberg-Kohn theorem to the following Hamiltonian

$$H^{\mathrm{KS}} = V_{\mathrm{eff}}^{\mathrm{KS}} + T = \int v_{\mathrm{eff}}^{\mathrm{KS}}(\mathbf{r}) \psi^\dagger(\mathbf{r}) \psi(\mathbf{r}) d\mathbf{r} - \frac{1}{2} \int \psi^\dagger(\mathbf{r}) \Delta \psi(\mathbf{r}) d\mathbf{r}. \tag{3.37}$$

The Kohn-Sham Hamiltonian H^{KS} describes a system of non-interacting particles effected by an external potential $v_{\mathrm{eff}}^{\mathrm{KS}}(\mathbf{r})$. For a system of N non-interacting particles with the Hamiltonian H^{KS} the fermionic ground state Ψ is obtained by an anti-symmetrization (Slater determinant) of the N lowest one-particle eigenstates ϕ_i^{KS} to the one particle Schrödinger equation

$$H^{\mathrm{KS}} |\phi_m^{\mathrm{KS}}\rangle = \epsilon_m |\phi_m^{\mathrm{KS}}\rangle \quad \text{with } m \in \mathbb{N}\ ,\ \epsilon_m \leq \epsilon_{m+1}, \tag{3.38}$$

so that

$$f_m = \langle \Psi | \hat{n}_m | \Psi \rangle = \begin{cases} 2 & \text{for } m < N/2 \\ 2 & \text{for } m = N/2\ ,\ N \text{ even} \\ 1 & \text{for } m = N/2 + 1/2\ ,\ N \text{ odd} \\ 0 & \text{else} \end{cases} \tag{3.39}$$

with the second quantization number operator $\hat{n}_m$ for the m-th one-particle eigenstate ϕ_m^{KS}. In second quantization notation, the ground state $|\Psi\rangle$ is constructed from the vacuum state $|\Omega\rangle$ with the creation operators $\{c_i^\dagger\}$, creating a particle in in the

i-th eigenstate of the one particle Schrödinger equation (3.38):

$$|\Psi\rangle = \prod_{i=1}^{N} c_i^\dagger |\Omega\rangle \,. \tag{3.40}$$

The density of $|\Psi\rangle$ is

$$n(\mathbf{r}) = \langle\Psi|\psi^\dagger(\mathbf{r})\psi(\mathbf{r})|\Psi\rangle \tag{3.41}$$

which can be calculated from the orbitals $\{\phi_i^{\mathrm{KS}}\}$ explicitly as

$$n(\mathbf{r}) = \sum_{i=1}^{\lceil N/2 \rceil} f_m \, \langle\phi_i^{\mathrm{KS}}|\mathbf{r}\rangle \, \langle\mathbf{r}|\phi_i^{\mathrm{KS}}\rangle \,. \tag{3.42}$$

The density in Eq.(3.42) obtained from solving the Kohn-Sham eigenvalue equations Eq. (3.38) is a solution to the variational problem in Eq. (3.34) supplemented by the constraint of particle number conservation

$$\int \delta n(\mathbf{r}) d\mathbf{r} = 0. \tag{3.43}$$

This is reminiscent of the Hartree-Fock method, where a constraint variational equation led to the Hartree-Fock (eigenvalue) equations. Also, similar to the Fock operator in the Hartree-Fock method, the Hamiltonian H^{KS} depends on the orbitals themselves since the effective potential depends on the density which is constructed from the orbitals $\{\phi_i^{\mathrm{KS}}\}$. This leads to the following self consistency cycle in which the orbitals and the density are calculated iteratively from the Kohn-Sham equations Eq. (3.44) until a predefined convergence criterion is reached (usually an energy difference between two cycles):

$$\begin{array}{c} \Big(-\frac{1}{2}\nabla^2 + \underbrace{v(\mathbf{r}) + \int \frac{n(\mathbf{r}')}{|\mathbf{r}-\mathbf{r}'|} \mathrm{d}^3\mathbf{r}' + \mu_{\mathrm{xc}}(\mathbf{r})}_{v_{\mathrm{eff}}^{\mathrm{KS}}} \Big) \phi_m^{\mathrm{KS}}(\mathbf{r}) = \epsilon_m \phi_m^{\mathrm{KS}}(\mathbf{r}) \\ \circlearrowright \qquad\qquad\qquad\qquad\qquad\qquad \circlearrowright \\ n(\mathbf{r}) = \textstyle\sum_{i=1}^{\lceil N/2 \rceil} f_m |\phi_i^{\mathrm{KS}}(\mathbf{r})|^2 \end{array} \tag{3.44}$$

In order to calculate the exchange correlation potential in the LDA $\mu_{\mathrm{xc}}^{\mathrm{LDA}}$, a good approximation for the energy density per particle $\epsilon_{\mathrm{xc}}^{\mathrm{LDA}}(n)$ is necessary, see Eq. (3.35). As stated above, we use the theory of the uniform electron gas and apply it in the LDA, so that $\epsilon_{\mathrm{xc}}^{\mathrm{LDA}}(n) = \epsilon_{\mathrm{xc}}^{\mathrm{UEG}}(n)$. In the uniform electron gas, the exchange energy per particle $\epsilon_{\mathrm{x}}^{\mathrm{UEG}}(n)$ in known analytically and has the following simple form [25]:

$$\epsilon_{\mathrm{x}}^{\mathrm{unif}}(n) = -\frac{3}{4}\left(\frac{3}{\pi}\right)^{1/3} n^{1/3}. \tag{3.45}$$

On the other hand, for the correlation energy density per particle of the uniform

electron gas, $\epsilon_{\mathrm{c}}^{\mathrm{UEG}}(n)$, there is no known closed analytical expression. At least in the cases of very high and very low densities an analytical limit can be expressed explicitly. In the interstitial region, very accurate quantum Monte Carlo calculations have been performed for a number of densities [58]. A common practice to obtain $\epsilon_{\mathrm{c}}^{\mathrm{UEG}}(n)$ for the LDA is to interpolate between the data points of [58], parameterizing the interpolation in a way that the analytic behavior in the limit of high and low densities is reproduced. An example of such an analytical representation is found in the work of Perdew and Wang [59]. Using the LDA as a computational electronic structure method, the exchange correlation (energy) functional $E_{\mathrm{xc}}^{\mathrm{LDA}}[n]$ is calculated by a numerical integration, using $\epsilon_{\mathrm{x}}^{\mathrm{unif}}(n)$ from Eq. (3.45) and the interpolated analytical expression $\epsilon_{\mathrm{c}}^{\mathrm{UEG\text{-}int}}(n)$ for the correlation part:

$$E_{\mathrm{xc}} \approx E_{\mathrm{xc}}^{\mathrm{LDA}}[n] = \int n(\mathbf{r})[\epsilon_{\mathrm{x}}^{\mathrm{unif}}(n(\mathbf{r})) + \epsilon_{\mathrm{c}}^{\mathrm{UEG\text{-}int}}(n(\mathbf{r}))]\mathrm{d}^3\mathbf{r}. \tag{3.46}$$

In order to improve on the LDA, so called semi local functionals which are usually referred to as generalized gradient approximations (GGA) are commonly applied. In these methods, the exchange-correlation functional is again an integration over local properties of the density, but it depends explicitly on the gradient of the density:

$$E_{\mathrm{xc}}[n] \approx E_{\mathrm{xc}}^{\mathrm{GGA}}[n] = \int f(n, \nabla n)\mathrm{d}^3\mathbf{r}. \tag{3.47}$$

The GGA implementation of Perdew, Burke and Ernzerhof (PBE) [9] is one of the most commonly used methods in electronic structure theory as of today.

3.3 Limitations of density functional theory

As should be clear by now, DFT is a powerful method extensively applied in electronic structure theory. Especially in the field of computational quantum chemistry and solid state physics, DFT simulations facilitate the research effort. As can be seen from the theoretical description in the previous subsection, a good approximation for the exchange correlation energy functional is crucial for a reasonable performance of DFT simulations. However, there are many situations, where the commonly used approximations do not grasp the properties of the material at hand, yielding inaccurate descriptions. According to Cohen, Mori-Sánchez and Yang, there are two main sources for errors: the delocalization error and the static correlation error [12].

The problem of self-interaction in the description of a single electron leads to a similar problem in many electron systems like molecules or crystals, namely the delocalization error. The self interaction causes an artificial spreading of the electronic density, if approximate exchange-correlation functionals are employed. Even in simple examples like the dissociation of the H_2^+ molecule, which in reality dissociates into a H^+ and H^0, the problem occurs and many DFT functionals wrongly predict two $H^{\frac{1}{2}}$ atoms even in the limit of very large distances. The delocalization

error stems from the problem that approximate exchange correlation functionals (in this case the exchange part is crucial) do not exactly cancel the Hartree potential. The electrons therefore feel their own Hartree potential, so that the functional often favors the delocalized over the localized solution.

The static correlation error, also occurring in Hartree-Fock theory, occurs whenever the ground state cannot be described by a single Slater determinant. DFT uses per construction a single Slater determinant as an approximation for the ground state, which may result in serious errors for systems where this is not appropriate. The closed shell H_2 molecule at the dissociation limit is an example of such a system.

Another problem deserving attention arises from inter molecular interactions like van der Waals bonds. They are naturally correlating electrons at two points in space and hence van der Waals interactions can never be described correctly by a local functional.

Recapitulating the above mentioned, problems in DFT arise for strongly correlated systems or systems with large delocalization errors. Delocalization errors lead to an underestimation of band gaps, reaction barriers, dissociation energies for molecular ions and charge transfer excitation energies. The breaking of chemical bonds, the description of transition metal systems, as well as intermolecular interactions like van der Waals forces are particularly problematic.

Despite some drawbacks, including the problems mentioned above in this subsection, DFT turned out to be the dominant method for *ab-initio* simulations of molecules and solids. The reasons are that for many systems it provides a sound theoretical description and its low computational complexity allows for simulations of many materials properties. Some of the deficiencies might be overcome with new developments within the framework of DFT, but for some it will be probably necessary to turn to other, more sophisticated methods. In the past two decades, the rise in available computer power facilitated the development of different advanced electronic structure methods, for example RPA, *GW*, Møller-Plesset perturbation theory (MPn), coupled cluster (CC) and configuration interaction (CI) methods. Methodological advances and new algorithms widen the field of applications for these methods and the development in recent years showed that many problems that arose from DFT simulations could be overcome by new advanced *ab-initio* methods. The chances offered hereby motivate research in the field and justify to further explore the possibilities of advanced electronic structure methods. The random phase approximation is one promising, but not yet fully utilized example of these methods, therefore providing an exciting research topic for this thesis.

Chapter 4

Many-body perturbation theory

So far we have seen two mean-field methods, Hartree-Fock and density functional theory, that essentially try to find the ground state (energy) of a system of interacting electrons in an external potential. They approach this problem by self-consistently solving an independent particle Schrödinger equation derived from an (approximate) many-electron energy functional in order to find a stationary solution to that functional. The approximation lies in the fact that the used functionals are not exact or that a single Slater determinant is used to approximate the many body wave function.

Another approach to describe a system of interacting electrons in an external potential is provided by many-body perturbation theory. Many-body perturbation theory (MBPT) is a more general approach to the quantum many-body problem, applied in various fields from condensed matter physics to nuclear physics and quantum chromodynamics. The basic concept is to split the Hamiltonian into a simple unperturbed part and a perturbation. The unperturbed part is chosen such that it can be treated rather easily, providing a "good starting point", and the system of the full Hamiltonian is described by a series expansion in terms of the perturbation (perturbation series). In contrast to the before mentioned mean-field methods, the approximation in perturbational methods stems from a truncation of the perturbation series.

This chapter shall give a very brief introduction into the theory of many-body perturbation theory. Unfortunately, a complete and rigorous description would go far beyond the scope of this thesis, so that the interested reader is referred to the literature [25, 26]. Instead this chapter aims to familiarize the reader with the language of many-body perturbation theory in the context of electronic structure theory, establish some of the most important quantities and provide the foundation to finally explain the concept behind the random phase approximation in the subsequent chapter 5.

4.1 The Green's function

Ideally, one would like to know the exact many-body eigenstates state $H\,|\Psi_N^i\rangle = E_N^i\,|\Psi_N^i\rangle$ to completely describe a system of N particles. However, we have seen in the previous chapter 3, that some important features of a system can be described with reduced quantities like the density in DFT. In many-body perturbation theory, the central reduced object is the Green's function which is defined in the following way:

$$\begin{aligned}\langle\phi_n|G(t-t')|\phi_m\rangle = &-\mathrm{i}\,\Theta(t-t')\,\langle\Psi_0|c_n(t)c_m^\dagger(t')|\Psi_0\rangle \\ &+\mathrm{i}\,\Theta(t'-t)\,\langle\Psi_0|c_m^\dagger(t')c_n(t)|\Psi_0\rangle\end{aligned} \tag{4.1}$$

where Ψ_0 is the zero temperature ground state and the creation/annihilation operators $c_m^\dagger(t')/c_m(t)$ are in the Heisenberg picture. For a system with a time independent Hamiltonian, the time evolution of an operator $\hat{O}(t)$ in the Heisenberg picture is determined by the Heisenberg equation[1]

$$\mathrm{i}\,\frac{\mathrm{d}}{\mathrm{d}t}\hat{O}(t) = \left[\hat{O}(t), \hat{H}\right], \tag{4.2}$$

with the commutator $[A, B] = AB - BA$. Thus the operators $c_m^\dagger(t')/c_m(t)$ are formally given as

$$c_m^\dagger(t') = e^{+\mathrm{i}\,Ht'}c_m^\dagger e^{-\mathrm{i}\,Ht'} \tag{4.3}$$

$$c_n(t) = e^{+\mathrm{i}\,Ht}c_n e^{-\mathrm{i}\,Ht}, \tag{4.4}$$

where $c_m^\dagger/c_n$ are the standard second quantization creation/annihilation operators presented earlier in Section 1.3.

Of course the Green's function can be transformed to any single particle basis, and a very common one is position basis

$$\begin{aligned}\langle\mathbf{r}|G(t-t')|\mathbf{r}'\rangle = &-\mathrm{i}\,\Theta(t-t')\,\langle\Psi_0|\hat{\psi}(\mathbf{r},t)\hat{\psi}^\dagger(\mathbf{r}',t')|\Psi_0\rangle \\ &+\mathrm{i}\,\Theta(t'-t)\,\langle\Psi_0|\hat{\psi}^\dagger(\mathbf{r}',t')\hat{\psi}(\mathbf{r},t)|\Psi_0\rangle\end{aligned} \tag{4.5}$$

with field operators $\hat{\psi}^\dagger(\mathbf{r}',t')/\hat{\psi}(\mathbf{r},t)$ in the Heisenberg picture. We will often write $G(\mathbf{r},\mathbf{r}',t-t')$ as a short form for $\langle\mathbf{r}|G(t-t')|\mathbf{r}'\rangle$. The first term in the Green's function defined in Eq. (4.1) is the probability amplitude for finding an interacting system in its ground state with an additional particle in state ϕ_n at time t if a particle in state ϕ_m was added at time t' to the system in its ground state. The

[1] The operator $\hat{O}$ in the Schrödinger picture is assumed to be time independent, otherwise there is an additional term $\mathrm{i}\left(\frac{\partial}{\partial t}\hat{O}\right)_H$ on the r.h.s.

second term is the probability amplitude for finding an interacting system with a particle in state ϕ_m removed from the ground state at time t' if a particle in state ϕ_n was removed from the ground state at time t. The Green's function is therefore often referred to as propagator, as it can be figuratively interpreted as an operator that propagates a particle (or hole) through the ground state. Its definition already adumbrates that the Green's function is suitable to describe for example spectral properties and absorption/emission processes.

4.1.1 Independent particle Green's function G^0 and perturbation series

Consider a non-interacting particle Hamiltonian in second quantization

$$\hat{H}^0 = \sum_n \epsilon_n c_n^\dagger c_n. \tag{4.6}$$

arising from a single particle Hamiltonian, $\hat{h}$, with eigenstates $\{\phi_n\}$ and eigenenergies $\{\epsilon_n\}$:

$$\hat{h} c_n^\dagger |\Omega\rangle = \hat{h} |\phi_n\rangle = \epsilon_n |\phi_n\rangle \tag{4.7}$$

where $|\Omega\rangle$ is the vacuum (0 particle) state and the one particle Hamiltonian could be for example

$$\langle \mathbf{r}|\hat{h}|\mathbf{r}'\rangle = \delta(\mathbf{r}-\mathbf{r}')h(\mathbf{r}') = \delta(\mathbf{r}-\mathbf{r}')\left[-\frac{1}{2}\nabla^2_{\mathbf{r}'} + v(\mathbf{r}')\right]. \tag{4.8}$$

The N particle ground state is a Slater determinant from the single particle states filled up to the Fermi level $\mu = (\epsilon_N + \epsilon_{N+1})/2$ (which we shift to 0 for convenience, see section 1.3.5):

$$\hat{H}^0 |\Psi_0^N\rangle = \hat{H}^0 |\phi_1, \ldots, \phi_N\rangle = \sum_{i=1}^N \epsilon_i |\Psi_0^N\rangle = E_0^N |\Psi_0^N\rangle . \tag{4.9}$$

The creation/annihilation operators in the Heisenberg picture have the following effect on the ground state:

$$c_m^\dagger(t')\,|\Psi_0^N\rangle = e^{+iH^0t'}c_m^\dagger e^{-iH^0t'}\,|\Psi_0^N\rangle = (-1)^N\Theta(\epsilon_m)e^{\mathrm{i}\,\epsilon_m t'}\,|\phi_1,\ldots,\phi_N,\phi_m\rangle \tag{4.10}$$

$$\langle\Psi_0^N|\,c_n(t) = \left(c_n^\dagger(t)\,|\Psi_0^N\rangle\right)^\dagger = (-1)^N\Theta(\epsilon_n)e^{-\,\mathrm{i}\,\epsilon_n t}\,\langle\phi_1,\ldots,\phi_N,\phi_n| \tag{4.11}$$

$$\begin{aligned} c_n(t)\,|\Psi_0^N\rangle &= e^{+\,\mathrm{i}\,H^0t}c_n e^{-\,\mathrm{i}\,H^0t}\,|\Psi_0^N\rangle \\ &= (-1)^{(n-1)}\Theta(-\epsilon_n)e^{-\,\mathrm{i}\,\epsilon_n t}\,|\phi_1,\ldots,\phi_{n-1},\phi_{n+1},\ldots,\phi_N\rangle \end{aligned} \tag{4.12}$$

$$\begin{aligned} \langle\Psi_0^N|\,c_m^\dagger(t') &= \left(c_m(t')\,|\Psi_0^N\rangle\right)^\dagger \\ &= (-1)^{(m-1)}\Theta(-\epsilon_m)e^{\mathrm{i}\,\epsilon_m t'}\,\langle\phi_1,\ldots,\phi_{m-1},\phi_{m+1},\ldots,\phi_N| \end{aligned} \tag{4.13}$$

and since

$$\langle\phi_1,\ldots,\phi_N,\phi_m|\phi_1,\ldots,\phi_N,\phi_n\rangle = \delta_{nm} \tag{4.14}$$

$$\langle\phi_1,\ldots,\phi_{n-1},\phi_{n+1},\ldots,\phi_N|\phi_1,\ldots,\phi_{m-1},\phi_{m+1},\ldots,\phi_N\rangle = \delta_{nm} \tag{4.15}$$

we get for the Green's function in Eq. (4.1):

$$\langle n|G^0(t-t')|m\rangle = -\,\mathrm{i}\,\delta_{nm}\left(\Theta(t-t')\Theta(\epsilon_n)e^{-\,\mathrm{i}\,\epsilon_n(t-t')} - \Theta(t'-t)\Theta(-\epsilon_n)e^{-\,\mathrm{i}\,\epsilon_n(t-t')}\right) \tag{4.16}$$

which can be transformed to position space:

$$\begin{aligned} \langle\mathbf{r}|G^0(t-t')|\mathbf{r}'\rangle = &-\,\mathrm{i}\,\Theta(t-t')\sum_{a\in uocc.}\phi_a(\mathbf{r})\phi_a^*(\mathbf{r}')e^{-\,\mathrm{i}\,\epsilon_a(t-t')} \\ &+\,\mathrm{i}\,\Theta(t'-t)\sum_{i\in occ.}\phi_i(\mathbf{r})\phi_i^*(\mathbf{r}')e^{-\,\mathrm{i}\,\epsilon_i(t-t')}. \end{aligned} \tag{4.17}$$

We will now show how this is related to the mathematical concept of Green's functions in the theory of partial differential equations. There, the Green's function $G_\mathcal{L}$ to a linear differential operator $\mathcal{L}[x,\partial_x,\ldots]$ is defined as:

$$\mathcal{L}[x,\partial_x,\ldots]G_\mathcal{L}(x,x^0) = \delta(x-x^0) \tag{4.18}$$

so that any inhomogeneous differential equation with inhomogeneity $I(x)$

$$\mathcal{L}[x,\partial_x,\ldots]\phi(x) = I(x) \tag{4.19}$$

can be solved by calculating the integral

$$\phi(x) = \int \mathrm{d}x_0 G_\mathcal{L}(x,x^0)I(x_0). \tag{4.20}$$

The independent particle Green's function in many body theory G^0 is a Green's function in the mathematical sense with respect to time dependent Schrödinger equation, where the linear differential operator of the homogeneous differential equation is:

$$\mathcal{L}_S = \mathrm{i}\,\frac{\partial}{\partial t} - h(r). \tag{4.21}$$

Since the functions $\phi_n(\mathbf{r})$ are eigenfunctions of the operator $h(\mathbf{r})$ with eigenvalue ϵ_n we get that:

$$[\mathrm{i}\,\frac{\partial}{\partial t} - h(r)]\left(\phi_n(\mathbf{r})\phi_n^*(\mathbf{r}')e^{-\mathrm{i}\,\epsilon_n(t-t')}\right) = 0. \tag{4.22}$$

The derivative of Θ yields

$$\frac{\partial}{\partial t}\Theta(\pm t \mp t') = \pm\delta(t-t'), \tag{4.23}$$

and the functions $\{\phi_n(\mathbf{r})\}$ are an orthonormal basis, so that:

$$\sum_n \phi_n(\mathbf{r})\phi_n^*(\mathbf{r}') = \delta(\mathbf{r}-\mathbf{r}'). \tag{4.24}$$

Therefore we get for the Green's function G^0 that:

$$\mathcal{L}_S\,\langle\mathbf{r}|G^0(t-t')|\mathbf{r}'\rangle = \delta(t-t')\delta(\mathbf{r}-\mathbf{r}'). \tag{4.25}$$

It will turn out to be useful to consider the Fourier transformed Green's function

$$G(\omega) = \mathcal{F}[G(t)](\omega) = \int \mathrm{d}t G(t)e^{\mathrm{i}\,\omega t}. \tag{4.26}$$

In order for the Fourier transform of $G^0(t)$ to converge, we use the following definition of $\Theta(t)$:

$$\Theta(t) = -\lim_{\eta\to 0^+}\frac{1}{2\pi\,\mathrm{i}}\int \mathrm{d}\omega'\frac{e^{-\mathrm{i}\,\omega' t}}{\omega' + \mathrm{i}\,\eta}. \tag{4.27}$$

That this yields the correct behavior of $\Theta(t)$ for any finite (but arbitrarily large) time t can be seen by using the residue theorem and closing the complex contour integral in the lower complex plane for $t > 0$ and in the upper complex plane for $t < 0$. Since in physical systems time differences are always finite this definition is sufficient.

Using the same technique of complex integration we get

$$\begin{aligned}\int \mathrm{d}t\Theta(\pm t)e^{-i\epsilon_n t}e^{\mathrm{i}\,\omega t} &= \int \mathrm{d}t - \lim_{\eta\to 0^+}\frac{1}{2\pi\,\mathrm{i}}\int \mathrm{d}\omega' \frac{e^{-\,\mathrm{i}\,t[\pm\omega'-(\omega-\epsilon_n)]}}{\omega'+\mathrm{i}\,\eta} \\ &= -\lim_{\eta\to 0^+}\frac{1}{\mathrm{i}}\int \mathrm{d}\omega' \frac{1}{\omega'+\mathrm{i}\,\eta}\delta(\pm\omega'-(\omega-\epsilon_n)) \\ &= \lim_{\eta\to 0^+}\mathrm{i}\,\frac{1}{\pm(\omega-\epsilon_n)+\mathrm{i}\,\eta}. \end{aligned} \tag{4.28}$$

Using Eq. (4.28) for the Fourier transform of Eq. (4.17) we get for the independent particle Green's function in frequency and position space

$$\langle \mathbf{r}|G^0(\omega)|\mathbf{r}'\rangle = \lim_{\eta\to 0^+}\sum_n \frac{\phi_n(\mathbf{r})\phi_n^*(\mathbf{r}')}{\omega-\epsilon_n+\mathrm{sgn}(\epsilon_n)\,\mathrm{i}\,\eta}, \tag{4.29}$$

were the sign before the convergence factor $(\mathrm{i}\,\eta)$ is $+$ for unoccupied and $-$ for occupied orbitals (in the ground state). From now on we will imply the convergence factor $(\mathrm{i}\,\eta)$ but not write it explicitly, or in other words we assume the single particle energies contain it: $\epsilon_n \to \epsilon_n + \mathrm{sgn}(\epsilon_n)\,\mathrm{i}\,\eta$.

In analogy to Eq. (4.21)-(4.25) and due to the properties of the Fourier transform, $\mathcal{F}[\mathrm{i}\,\partial_t f(t)](\omega) = \omega\mathcal{F}[f(t)](\omega)$, we get for the frequency domain

$$[\omega - h]G^0(\omega) = G^0(\omega)[\omega - h] = \mathbb{1}, \tag{4.30}$$

where we used a basis independent operator notation, e.g. for $G^0(\mathbf{r},\mathbf{r}',\omega)$ we get $\mathbb{1} = \delta(\mathbf{r}-\mathbf{r}')$:

$$\int \mathrm{d}^3\mathbf{r}'\,\langle \mathbf{r}|G^0(\omega)|\mathbf{r}'\rangle\,\phi_m(\mathbf{r}') = \sum_n \frac{\phi_n(\mathbf{r})\overbrace{\int \phi_n^*(\mathbf{r}')\phi_m(\mathbf{r}')\mathrm{d}^3\mathbf{r}'}^{\delta_{nm}}}{\omega-\epsilon_n} = \frac{\phi_m(\mathbf{r})}{\omega-\epsilon_m} \tag{4.31}$$

$$\Downarrow$$

$$\iint \mathrm{d}^3\mathbf{r}'\mathrm{d}^3\mathbf{r}''\,\langle \mathbf{r}|\omega-h|\mathbf{r}''\rangle\,\langle \mathbf{r}''|G^0(\omega)|\mathbf{r}'\rangle\,\phi_n(\mathbf{r}') = \phi_n(\mathbf{r}) \tag{4.32}$$

$$\iint \mathrm{d}^3\mathbf{r}'\mathrm{d}^3\mathbf{r}''\,\langle \mathbf{r}|G^0(\omega)|\mathbf{r}''\rangle\,\langle \mathbf{r}''|\omega-h|\mathbf{r}'\rangle\,\phi_n(\mathbf{r}') = \phi_n(\mathbf{r}). \tag{4.33}$$

These two equations hold for all ϕ_n and since the $\{\phi_n\}$ form an orthonormal basis, this proves Eq. (4.30).

Consider now a (local, time-independent) perturbation $\tilde{v}(\mathbf{r})$ to the one particle

Hamiltonian h, then the Hamiltonian of the perturbed system $\tilde{h}$ is

$$\tilde{h} = h + \tilde{v} \tag{4.34}$$

and the corresponding Green's $\tilde{G}^0$ function satisfies the following equation:

$$[\omega - h - \tilde{v}]\tilde{G}^0(\omega) = \mathbb{1}. \tag{4.35}$$

Applying the unperturbed Green's function on both sides we get

$$\begin{aligned} G^0(\omega)[\omega - h - \tilde{v}]\tilde{G}^0(\omega) &= G^0(\omega) \\ \left[G^0(\omega)[\omega - h] - G^0(\omega)\tilde{v}\right]\tilde{G}^0(\omega) &= G^0(\omega) \\ \left[\mathbb{1} - G^0(\omega)\tilde{v}\right]\tilde{G}^0(\omega) &= G^0(\omega) \\ \tilde{G}^0(\omega) &= G^0(\omega) + G^0(\omega)\tilde{v}\tilde{G}^0(\omega). \end{aligned} \tag{4.36}$$

The last line is the so called Dyson equation, that indicates that the perturbed Green's function $\tilde{G}^0(\omega)$ can be represented as perturbation series of the unperturbed Green's function and the perturbation $\tilde{v}$:

$$\tilde{G}^0(\omega) = G^0(\omega) + G^0(\omega)\tilde{v}G^0(\omega) + G^0(\omega)\tilde{v}G^0(\omega)\tilde{v}G^0(\omega) + \dots \tag{4.37}$$

Figuratively speaking, the propagation through the perturbed system can be described as propagating through the unperturbed system with G^0 and occasional scattering at the perturbation $\tilde{v}$. The full perturbed propagator $\tilde{G}^0$ is obtained by considering all possible scattering pathways (quantum pinball).

This process is often described diagrammatically, and indeed the diagrammatic formalism is a rigorous approach to describe quantum many body systems more conveniently than with the algebraic formulation. We will make use of the diagrammatic representation in some equations, as this is very common in the literature of the field, however we will not establish a rigorous diagrammatic frame work but rather use diagrams to provide a simple and intuitive view on the algebraically complex circumstances. A profound presentation of the diagrammatic formalism can be found in the books of Mattuck [26] or Fetter and Walecka [25].

The Dyson equation for the non interacting particle case with a perturbation $\tilde{v}$ can be written diagrammatically as:

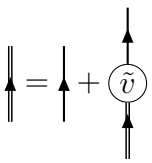

(4.38)

The double arrow represents the perturbed propagator $\tilde{G}^0$ (or generally the total propagator G), while the single arrow represents the unperturbed independent particle propagator G^0. In spatial/time coordinates, the above diagrammatic Dyson equation with the perturbation $\tilde{v}$ would translate to:

$$G(\mathbf{r},\mathbf{r}',t-t') = G^0(\mathbf{r},\mathbf{r}',t-t') + \int \mathrm{d}t'' \int \mathrm{d}^3\mathbf{r} G^0(\mathbf{r},\mathbf{r}'',t-t'')\tilde{v}(\mathbf{r}'')G(\mathbf{r}'',\mathbf{r}',t''-t') \tag{4.39}$$

4.1.2 Imaginary time propagator

In this subsection we introduce the imaginary time Green's function $\mathcal{G}(\tau)$, that has some advantages over its corresponding real time equivalent. Although the concept of imaginary time Green's functions arises from a statistical quantum many body theory at finite temperatures, the concept is also useful at T=0. The imaginary time Green's function is often used in modern electronic structure theory, especially in the literature closely related to the work in this thesis [60, 61, 35, 62, 63]. For this reason we give a very short introduction to the concept.

The Wick rotation [64], connects quantum mechanics to statistical mechanics by introducing a transformation that substitutes the real valued time variable t with an imaginary time $\mathrm{i}t \rightarrow \tau$. Although imaginary time may sound at first somehow unphysical, it is actually a very useful concept. The connection can be seen by looking at the Boltzmann factor as well as the time propagation of an energy eigenstate:

$$p(\Psi) = e^{-\tau E} \tag{4.40}$$

$$|\Psi(t)\rangle = e^{-\mathrm{i}tE}\,|\Psi(0)\rangle\,, \tag{4.41}$$

where we used the variable τ instead of the usual inverse temperature β in order to clarify the connection.

In the grand canonical ensemble the expectation value of an operator, $\langle O\rangle$, is given by

$$\langle O\rangle = \frac{\mathrm{Tr}\{O\rho\}}{\mathrm{Tr}\{\rho\}}. \tag{4.42}$$

There, the distribution operator is

$$\rho = e^{-\beta(H-\mu N)}, \tag{4.43}$$

with the inverse temperature $\beta = 1/(kT)$ and $\rho/\,\mathrm{Tr}\{\rho\}$ is usually referred to as density matrix. The trace operation is defined as

$$\mathrm{Tr}\{A\} = \sum_n \langle\Phi_n|A|\Phi_n\rangle\,, \tag{4.44}$$

where the Φ_n are any orthonormal basis in the respective Hilbert space, since $\mathrm{Tr}\{A\}$ is invariant under the choice of the orthonormal basis. The sum is a general sum over all basis states and might be an integral in the continuous case.

Now in analogy to the Green's function defined in Eq. (4.1), we can define the so called finite temperature Green's function

$$\langle n|\mathcal{G}(\tau-\tau')|m\rangle = \mathcal{G}(n,m,\tau-\tau') = -\Theta(\tau-\tau')\frac{\mathrm{Tr}\{c_n(\tau)c^\dagger(\tau')\rho\}}{\mathrm{Tr}\{\rho\}} + \Theta(\tau'-\tau)\frac{\mathrm{Tr}\{c^\dagger(\tau')c_n(\tau)\rho\}}{\mathrm{Tr}\{\rho\}}. \tag{4.45}$$

In a similar way the original Green's function in Eq. (4.1) is related to the Schrödinger equation, the finite temperature Green's function is related to the Bloch equation [25, 26, 65]:

$$\frac{\partial}{\partial\beta}\rho = -(H-\mu N)\rho. \tag{4.46}$$

Although the operators $c^\dagger(\tau')/c_n(\tau)$ are actually arising from the Bloch equation and the statistical treatment of a quantum system at finite temperature, they can be viewed as imaginary time operators $c^\dagger(\tau')/c_n(\tau)$ in the Heisenberg picture (with a modified Hamiltonian $H \to H-\mu N$, representing just a shift in single particle energies, cf. Section 1.3.5):

$$c_m^\dagger(\tau') = e^{(H-\mu N)\tau'}c_m^\dagger e^{-(H-\mu N)\tau'} \tag{4.47}$$

$$c_n(\tau) = e^{(H-\mu N)\tau}c_n e^{-(H-\mu N)\tau} \tag{4.48}$$

The imaginary time variables τ/τ' are restricted to the interval $[0,\beta]$ so that the argument of the finite temperature Green's function $(\tau-\tau') \in [-\beta,\beta]$. This leads to some algebraic differences in the treatment of the finite temperature Green's function (e.g. in the frequency domain, the Green's function has a discrete spectrum, the so called Matsubara frequencies, see [25, 26]). However there is a correspondence between the Bloch equation (4.46) and the Schrödinger equation (1.16), that becomes evident by substituting $\beta \leftrightarrow \mathrm{i}\,t$, $H-\mu N \leftrightarrow H$ and $\rho \leftrightarrow |\Psi\rangle$. This correspondence allows to apply the same diagrammatic approaches to finite temperature many body quantum mechanics that are established in the $T = 0K$ case, only the translation into algebraic forms is different.

In the limit $T \to 0$ the finite temperature formalism yields the original Green's function formalism, albeit with imaginary time. Weather the Green's function is in the real or imaginary time/frequency domain will from now on be indicated only by the argument of the Green's function: t/ω for real and (i)τ/(i)ν for imaginary time/frequency. Though in this thesis we are focusing at zero temperature properties

of solids, using the imaginary time Green's function has also some advantages in this case. The independent particle Green's function for example is ($\mu = 0$ for convenience):

$$G^0(\boldsymbol{r}, \boldsymbol{r}', \tau) = \sum_n \psi_n(\boldsymbol{r})\psi_n^*(\boldsymbol{r}')e^{-\epsilon_n \tau}[\Theta(-\tau)f(\epsilon_n) - \Theta(\tau)(1 - f(\epsilon_n))], \tag{4.49}$$

with the Fermi weights $f(\epsilon_n)$, which are in the $T = 0$ case either 1 for occupied or 0 for unoccupied orbitals. One advantage of the imaginary time Green's function is, that we do not require the convergence factor $\mathrm{i}\,\eta$ for the Fourier transformation to the frequency domain. Another advantage is that the imaginary time Green's function is Hermitian, in the following sense:

$$G(\boldsymbol{r}, \boldsymbol{r}', \tau) = G(\boldsymbol{r}', \boldsymbol{r}, \tau)^*. \tag{4.50}$$

4.2 Self energy

Consider a Hamiltonian with a non-interacting part H^0 and a weak interaction potential ΔV

$$H = H^0 + \Delta V \tag{4.51}$$

$$H^0 = \int \mathrm{d}^3\mathbf{r}\hat{\psi}^\dagger(\mathbf{r})h(\mathbf{r})\hat{\psi}(\mathbf{r}) \tag{4.52}$$

$$\Delta V = \iint \mathrm{d}^3\mathbf{r}\mathrm{d}^3\mathbf{r}'\hat{\psi}^\dagger(\mathbf{r})\hat{\psi}^\dagger(\mathbf{r}')\Delta v(\mathbf{r}, \mathbf{r}')\hat{\psi}(\mathbf{r}')\hat{\psi}(\mathbf{r}) \tag{4.53}$$

Then for the Green's function we obtain the following differential equation (equation of motion for the Green's function):

$$\begin{aligned} \mathrm{i}\,\frac{\partial}{\partial t}G(\mathbf{r}, \mathbf{r}', t - t') =& \delta(\mathbf{r} - \mathbf{r}')\delta(t - t') \\ &+ \hat{h}(\mathbf{r})G(\mathbf{r}, \mathbf{r}', t) \\ &- \mathrm{i}\,\Theta(t - t')\,\langle\Psi_0|[\hat{\psi}(\mathbf{r}), \Delta\hat{V}](t)\hat{\psi}^\dagger(\mathbf{r}', t')|\Psi_0\rangle \\ &+ \mathrm{i}\,\Theta(t' - t)\,\langle\Psi_0|\hat{\psi}^\dagger(\mathbf{r}', t')[\hat{\psi}(\mathbf{r}, \Delta\hat{V}](t)|\Psi_0\rangle\,. \end{aligned} \tag{4.54}$$

The first term is obtained by differentiating the Θ-functions in Eq. (4.5) and using the anti-commutator relations, cf. Eq. (1.37):

$$[\hat{\psi}(\mathbf{r}), \hat{\psi}^\dagger(\mathbf{r}')]_+ = \delta(\mathbf{r} - \mathbf{r}') \tag{4.55}$$

$$[\hat{\psi}^\dagger(\mathbf{r}), \hat{\psi}^\dagger(\mathbf{r}')]_+ = [\hat{\psi}(\mathbf{r}), \hat{\psi}(\mathbf{r}')]_+ = 0, \tag{4.56}$$

as well as Eq. (4.23):

$$\left(\frac{\partial}{\partial t}\Theta(t-t')\right) \langle\Psi_0|\hat{\psi}(\mathbf{r},t)\hat{\psi}^\dagger(\mathbf{r}',t')|\Psi_0\rangle - \left(\frac{\partial}{\partial t}\Theta(t'-t)\right) \langle\Psi_0|\hat{\psi}^\dagger(\mathbf{r}',t')\hat{\psi}(\mathbf{r},t)|\Psi_0\rangle =$$

$$= \delta(t-t') \langle\Psi_0|[\hat{\psi}(\mathbf{r},t), \hat{\psi}^\dagger(\mathbf{r}',t')]_+|\Psi_0\rangle$$

$$= \delta(t-t') \langle\Psi_0|[\hat{\psi}(\mathbf{r}), \hat{\psi}^\dagger(\mathbf{r}')]_+|\Psi_0\rangle$$

$$= \delta(\mathbf{r}-\mathbf{r}')\delta(t-t'). \tag{4.57}$$

To derive the last three terms in Eq. (4.54) we sketch how $\mathrm{i}\,\partial_t$ acts on the amplitude $\langle\Psi_0|\hat{\psi}(\mathbf{r},t)\hat{\psi}^\dagger(\mathbf{r}',t')|\Psi_0\rangle$, using the Heisenberg equation (4.2):

$$\mathrm{i}\,\frac{\partial}{\partial t} \langle\Psi_0|\hat{\psi}(\mathbf{r},t)\hat{\psi}^\dagger(\mathbf{r}',t')|\Psi_0\rangle = \langle\Psi_0|[\hat{\psi}(\mathbf{r},t), \hat{H}]\hat{\psi}^\dagger(\mathbf{r}',t')|\Psi_0\rangle \tag{4.58}$$

$$= \langle\Psi_0|[\hat{\psi}(\mathbf{r}), \hat{H}](t)\hat{\psi}^\dagger(\mathbf{r}',t')|\Psi_0\rangle \tag{4.59}$$

$$= \langle\Psi_0|[\hat{\psi}(\mathbf{r}), \hat{H}^0](t)\hat{\psi}^\dagger(\mathbf{r}',t')|\Psi_0\rangle$$

$$+ \langle\Psi_0|[\hat{\psi}(\mathbf{r}), \Delta\hat{V}](t)\hat{\psi}^\dagger(\mathbf{r}',t')|\Psi_0\rangle\,. \tag{4.60}$$

In the second line, we used that $[\exp(\pm\,\mathrm{i}\,Ht), H] = 0$. The commutator of the field operator with the non-interacting Hamiltonian H^0 is given by

$$\left[\hat{\psi}(\mathbf{r}), H^0\right] = \hat{\psi}(\mathbf{r}) \int \hat{\psi}^\dagger(\mathbf{r}'')h(\mathbf{r}'')\hat{\psi}(\mathbf{r}'')\mathrm{d}^3\mathbf{r}'' - H^0\hat{\psi}(\mathbf{r}) \tag{4.61}$$

$$= \int (\delta(\mathbf{r}-\mathbf{r}'')h(\mathbf{r}'')\hat{\psi}(\mathbf{r}'') + \hat{\psi}^\dagger(\mathbf{r}'')h(\mathbf{r}'')\hat{\psi}(\mathbf{r}'')\hat{\psi}(\mathbf{r})\mathrm{d}^3\mathbf{r}'' - H^0\hat{\psi}(\mathbf{r}) \tag{4.62}$$

$$= h(\mathbf{r})\hat{\psi}(\mathbf{r}) + H^0\hat{\psi}(\mathbf{r}) - H^0\hat{\psi}(\mathbf{r}) \tag{4.63}$$

$$= h(\mathbf{r})\hat{\psi}(\mathbf{r}) \tag{4.64}$$

$$\Rightarrow \left[\hat{\psi}(\mathbf{r}), H^0\right](t) = e^{\mathrm{i}\,Ht}\left[\hat{\psi}(\mathbf{r}), H^0\right]e^{\mathrm{i}\,Ht} = h(\mathbf{r})\hat{\psi}(\mathbf{r},t) \tag{4.65}$$

where we used again the anti-commutator relations in Eqs. (4.55) and (4.56). Inserting Eq. (4.65) into Eq. (4.60) we get

$$-\mathrm{i}\,\Theta(t-t')\,\mathrm{i}\,\frac{\partial}{\partial t}\,\langle\Psi_0|\hat{\psi}(\mathbf{r},t)\hat{\psi}^\dagger(\mathbf{r}',t')|\Psi_0\rangle = \tag{4.66}$$

$$-\mathrm{i}\,\Theta(t-t')\left(h(\mathbf{r})\,\langle\Psi_0|\hat{\psi}(\mathbf{r},t)\hat{\psi}^\dagger(\mathbf{r}',t')|\Psi_0\rangle + \langle\Psi_0|[\hat{\psi}(\mathbf{r}),\hat{V}](t)\hat{\psi}^\dagger(\mathbf{r}',t')|\Psi_0\rangle\right).$$

The result for $\mathrm{i}\,\Theta(t'-t)\partial_t\,\langle\Psi_0|\hat{\psi}^\dagger(\mathbf{r}',t')\hat{\psi}(\mathbf{r},t)|\Psi_0\rangle$ can be obtained analogously, so that we finally get Eq. (4.54). We can now define the self energy $\Sigma(\mathbf{r},\mathbf{r}',t-t')$ in the following way:

$$\iint \mathrm{d}^3\mathbf{r}''\mathrm{d}t''\Sigma(\mathbf{r},\mathbf{r}'',t-t'')G(\mathbf{r}'',\mathbf{r}',t''-t') = \langle\mathbf{r}|\Sigma * G|\mathbf{r}'\rangle\,(t-t') \tag{4.67}$$

$$= -\,\mathrm{i}\,\Theta(t-t')\,\langle\Psi_0|[\hat{\psi}(\mathbf{r}),\Delta\hat{V}](t)\hat{\psi}^\dagger(\mathbf{r}',t')|\Psi_0\rangle$$

$$+\,\mathrm{i}\,\Theta(t'-t)\,\langle\Psi_0|\hat{\psi}^\dagger(\mathbf{r}',t')[\hat{\psi}(\mathbf{r}),\Delta\hat{V}](t)|\Psi_0\rangle\,,$$

where $\Sigma * G$ is a convolution with respect to the time coordinate only (for the other coordinates, in this example position, we take the standard operator product). With this definition of the self energy and using a basis independent operator notation as in Eq. (4.30), we can reformulate Eq. (4.54) in the frequency domain as:

$$[\omega - h - \Sigma(\omega)]G(\omega) = \mathbb{1}. \tag{4.68}$$

At the same time we can write for the non-interacting Green's function G^0 (= independent particle Green's function corresponding to H^0)

$$[\omega - h]G^0(\omega) = \mathbb{1}. \tag{4.69}$$

This is reminiscent of Eq. (4.35) for the perturbed and Eq. (4.30) for the unperturbed independent particle Green's function, which led to the Dyson equation (4.36), but with $\Sigma(\omega)$ now taking the role of the perturbation. In analogy, we can write a Dyson equation with G^0 and Σ for the full propagator G (corresponding to the full Hamiltonian $H = H^0 + \Delta V$):

$$G(\omega) = G^0(\omega) + G^0(\omega)\Sigma(\omega)G(\omega), \tag{4.70}$$

or diagrammatically

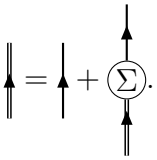

(4.71)

In order for the perturbation series that emerges from Eq. (4.70) to converge, the perturbation ΔV needs to be small. In the systems that we want to describe in the context of this thesis – electronic many body systems in the Born-Oppenheimer approximation – the interaction term ΔV is in principle the Coulomb interaction between the electrons V_{C}. Since the Coulomb interaction is a strong interaction, we cannot describe an electronic system by splitting off the Coulomb potential between the electrons from the Hamiltonian to obtain a non-interacting system and then add it as a perturbation later. However, starting from a mean-field method like Hartree-Fock or density functional theory, with the non-interacting Hamiltonian H^{MF}, we can treat the difference between the real interaction and the mean-field interaction ($H^1 = V_{\mathrm{C}} - V_{\mathrm{MF}}$) as a small perturbation. We obtain a perturbation series for the full Green's function by partitioning the full Hamiltonian H

$$\hat{H} = \int \mathrm{d}^3\mathbf{r}\hat{\psi}^\dagger(\mathbf{r})[-\frac{1}{2}\nabla^2_{\mathbf{r}} + v_{\mathrm{ext}}(\mathbf{r})]\hat{\psi}(\mathbf{r}) + \frac{1}{2}\iint \mathrm{d}^3\mathbf{r}\mathrm{d}^3\mathbf{r}'\frac{1}{|\mathbf{r}-\mathbf{r}'|}\hat{\psi}^\dagger(\mathbf{r})\hat{\psi}^\dagger(\mathbf{r}')\hat{\psi}(\mathbf{r}')\hat{\psi}(\mathbf{r}) \tag{4.72}$$

into parts

$$H = H^{\mathrm{MF}} + H^1, \tag{4.73}$$

$$H^{\mathrm{MF}} = \sum_n \epsilon_n^{\mathrm{MF}} c_n^\dagger c_n \tag{4.74}$$

$$= \int \mathrm{d}^3\mathbf{r}\hat{\psi}^\dagger(\mathbf{r})[-\frac{1}{2}\nabla^2_{\mathbf{r}} + v_{\mathrm{ext}}(\mathbf{r})]\hat{\psi}(\mathbf{r}) + \iint \mathrm{d}^3\mathbf{r}\mathrm{d}^3\mathbf{r}' v_{el}^{\mathrm{MF}}(\mathbf{r},\mathbf{r}')\hat{\psi}^\dagger(\mathbf{r})\hat{\psi}(\mathbf{r}')$$

$$H^1 = H - H^{\mathrm{MF}} \tag{4.75}$$

$$= \frac{1}{2}\iint \mathrm{d}^3\mathbf{r}\mathrm{d}^3\mathbf{r}'\frac{1}{|\mathbf{r}-\mathbf{r}'|}\hat{\psi}^\dagger(\mathbf{r})\hat{\psi}^\dagger(\mathbf{r}')\hat{\psi}(\mathbf{r}')\hat{\psi}(\mathbf{r}) - \iint \mathrm{d}^3\mathbf{r}\mathrm{d}^3\mathbf{r}' v_{el}^{\mathrm{MF}}(\mathbf{r},\mathbf{r}')\hat{\psi}^\dagger(\mathbf{r})\hat{\psi}(\mathbf{r}').$$

For example, consider we calculated an approximate Kohn-Sham effective potential, v_{eff}^{MF}, and want to use it as a starting point ($H^{\mathrm{MF}} = H^{\mathrm{KS}}$) for a particular many body perturbation method. Then in the above equations,

$$v_{el}^{\mathrm{MF}}(\mathbf{r},\mathbf{r}') = \delta(\mathbf{r}-\mathbf{r}')(v_{eff}^{\mathrm{KS}}(\mathbf{r}) - v_{\mathrm{ext}}(\mathbf{r})) \tag{4.76}$$

is the electronic part of the effective Kohn-Sham potential (as calculated by the approximation used for the DFT, e.g. LDA, PBE).

4.3 Ground state energy of many electron system

4.3.1 Formal expression in MBPT

The ground state energy of an interacting system of electrons in an external potential is formally calculated as

$$E^0 = \langle\Psi_0|H|\Psi_0\rangle = \langle\Psi_0| \iint \mathrm{d}^3\mathbf{r}\mathrm{d}^3\mathbf{r}'\delta(\mathbf{r}-\mathbf{r}')h(\mathbf{r}')\hat{\psi}^\dagger(r)\hat{\psi}(\mathbf{r}')|\Psi_0\rangle + \langle\Psi_0|\hat{V}_\mathrm{C}|\Psi_0\rangle \tag{4.77}$$

with the one particle Hamiltonian h and the Coulomb interaction $\hat{V}_\mathrm{C}$ in second quantization, as in Eq. (4.72).

Using the Green's function in position basis, Eq. (4.5), the commutator relations in Eq. (4.55) and (4.56) and the definition of the self energy in Eq. (4.67), with the Coulomb potential as the perturbation ΔV, we can write the ground state energy as [66]

$$E = \lim_{t\to 0^-} \iint \mathrm{d}^3\mathbf{r}\mathrm{d}^3\mathbf{r}'\delta(\mathbf{r}-\mathbf{r}') \left(h(\mathbf{r}')G(\mathbf{r},\mathbf{r}',t) + \frac{1}{2}(\Sigma * G)(\mathbf{r},\mathbf{r}',t) \right) \tag{4.78}$$

which can be re-written in the imaginary frequency domain as

$$E = \frac{1}{2\pi}\int \mathrm{d}\nu\, e^{\mathrm{i}\nu 0^+}\,\mathrm{Tr}\left\{ \left[h + \frac{1}{2}\Sigma(\mathrm{i}\,\nu) \right] G(\mathrm{i}\,\nu) \right\}. \tag{4.79}$$

Since we defined the Fourier transform from frequency to time with $\exp(-\mathrm{i}\,\nu\tau)$, we have a "convergence factor" $\lim_{\tau\to 0^-}\exp(-\mathrm{i}\,\nu\tau) = \exp(\mathrm{i}\,\nu 0^+)$ in the above Eq. (4.79). This equation becomes even more instructive by realizing that the Green's function at $t \to 0^-$ is the ground state density matrix, cf. Eq. (4.5):

$$n(\mathbf{r},\mathbf{r}') = \langle\Psi_0|\hat{\psi}^\dagger(\mathbf{r})\hat{\psi}(\mathbf{r}')|\Psi_0\rangle = G(\mathbf{r},\mathbf{r}',t=0^-) = \frac{1}{2\pi}\int \mathrm{d}\nu\, e^{\mathrm{i}\nu 0^+} G(\mathbf{r},\mathbf{r}',\mathrm{i}\,\nu). \tag{4.80}$$

However, as we already stated above, a perturbation series where the bare Coulomb interaction is treated as a perturbation does not converge due to its strong nature. Therefore we need to tackle the problem with another approach.

4.3.2 Adiabatic connection

A common theoretical approach to calculate the ground state energy is the so called adiabatic connection [67, 68, 27], where the full interacting Hamiltonian is connected to a mean-field Hamiltonian via an adiabatic switching. We can choose a linear switching with a switching parameter λ so that for each λ the Hamiltonian is given as:

$$H(\lambda) = H^0 + (1-\lambda)V_\mathrm{MF} + \lambda V_\mathrm{C} = H^\mathrm{MF} + \lambda H^1 \tag{4.81}$$

with

$$H^0 = \iint \mathrm{d}^3\mathbf{r}\mathrm{d}^3\mathbf{r}'\delta(\mathbf{r}-\mathbf{r}')h(\mathbf{r}')\hat{\psi}^\dagger(\mathbf{r})\hat{\psi}(\mathbf{r}') \tag{4.82}$$

$$= \iint \mathrm{d}^3\mathbf{r}\mathrm{d}^3\mathbf{r}'\delta(\mathbf{r}-\mathbf{r}')[-\frac{\nabla^2}{2} + v_{\mathrm{ext}}(\mathbf{r}')]\hat{\psi}^\dagger(\mathbf{r})\hat{\psi}(\mathbf{r}'),$$

$$V_{\mathrm{MF}} = \iint \mathrm{d}^3\mathbf{r}\mathrm{d}^3\mathbf{r}' v_{el}^{\mathrm{MF}}(\mathbf{r},\mathbf{r}')\hat{\psi}^\dagger(\mathbf{r})\hat{\psi}(\mathbf{r}'), \tag{4.83}$$

$$V_{\mathrm{C}} = \frac{1}{2}\iint \mathrm{d}^3\mathbf{r}\mathrm{d}^3\mathbf{r}'\frac{1}{|\mathbf{r}-\mathbf{r}'|}\hat{\psi}^\dagger(\mathbf{r})\hat{\psi}^\dagger(\mathbf{r}')\hat{\psi}(\mathbf{r}')\hat{\psi}(\mathbf{r}), \tag{4.84}$$

and

$$H^{\mathrm{MF}} = H^0 + V_{\mathrm{MF}}, \tag{4.85}$$

$$H^1 = V_{\mathrm{C}} - V_{\mathrm{MF}}. \tag{4.86}$$

For $\lambda = 0$ and $\lambda = 1$, we recover the mean-field and the full Hamiltonian respectively:

$$H(\lambda = 0) = H^{\mathrm{MF}} \tag{4.87}$$

$$H(\lambda = 1) = H. \tag{4.88}$$

Assume the ground states to each Hamiltonian $H(\lambda)$ are given as $|\Psi_0^\lambda\rangle$, then formally, the ground state energy of the fully interacting system is given as

$$E^0 = \langle\Psi_0|H|\Psi_0\rangle = \langle\Psi_0^{\lambda=1}|H(\lambda=1)|\Psi_0^{\lambda=1}\rangle = E^{\mathrm{MF}} + \int_0^1 \mathrm{d}\lambda\frac{d}{d\lambda}\langle\Psi_0^\lambda|H(\lambda)|\Psi_0^\lambda\rangle\,, \tag{4.89}$$

where $E^{\mathrm{MF}} = \langle\Psi_0^{\lambda=0}|H(\lambda=0)|\Psi_0^{\lambda=0}\rangle$. Using the linear adiabatic connection from Eq. (4.81) and with the aid of the Hellmann-Feynman theorem [69], we can write

$$E^0 = \langle\Psi_0|H|\Psi_0\rangle = E^{\mathrm{MF}} + \int_0^1 \mathrm{d}\lambda\,\langle\Psi_0^\lambda|H^1|\Psi_0^\lambda\rangle\,. \tag{4.90}$$

We will now re-write $\langle\Psi_0^\lambda|H(\lambda)|\Psi_0^\lambda\rangle$ in the MBPT formulation. Here we use $G(\lambda)$ for the Green's function that corresponds to $H(\lambda)$ and $\Sigma(\lambda)$ for the self-energy

corresponding to the scaled Coulomb potential $\Delta V(\lambda) = \lambda V_{\mathrm{C}}$:

$$\begin{aligned}
\langle\Psi_0^\lambda|H(\lambda)|\Psi_0^\lambda\rangle &= \langle\Psi_0^\lambda|H^0 + (1-\lambda)V_{\mathrm{MF}}|\Psi_0^\lambda\rangle + \langle\Psi_0^\lambda|\lambda V_{\mathrm{C}}|\Psi_0^\lambda\rangle \qquad (4.91)\\
&= \frac{1}{2\pi}\int \mathrm{d}\nu\, e^{\mathrm{i}\,\nu 0^+}\,\mathrm{Tr}\left\{\left[h + (1-\lambda)v_{el}^{\mathrm{MF}} + \frac{1}{2}\Sigma(\mathrm{i}\,\nu,\lambda)\right]G(\mathrm{i}\,\nu,\lambda)\right\}\\
&= \frac{1}{2\pi}\int \mathrm{d}\nu\, e^{\mathrm{i}\,\nu 0^+}\,\mathrm{Tr}\left\{\left[h + v_{el}^{\mathrm{MF}}\right]G(\mathrm{i}\,\nu,\lambda) + \frac{1}{2}\left[\Sigma(\mathrm{i}\,\nu,\lambda) - 2\lambda v_{el}^{\mathrm{MF}}\right]G(\mathrm{i}\,\nu,\lambda)\right\}\\
&= \langle\Psi_0^\lambda|H^{\mathrm{MF}}|\Psi_0^\lambda\rangle + \frac{1}{2\pi}\int \mathrm{d}\nu\, e^{\mathrm{i}\,\nu 0^+}\frac{1}{2}\,\mathrm{Tr}\left\{\left[\Sigma(\mathrm{i}\,\nu,\lambda) - 2\lambda v_{el}^{\mathrm{MF}}\right]G(\mathrm{i}\,\nu,\lambda)\right\}.
\end{aligned}$$

Note that if we consider H^{MF} as the non-interacting Hamiltonian we start from and $\lambda(V_{\mathrm{C}} - V_{\mathrm{MF}})$ as the perturbation, then the self energy as defined in Eq. (4.67) contains the mean-field potential with a factor 1, like in the case of an external perturbation (cf. section 4.1.1). However, if one wants to calculate the ground state energy from the self energy as shown in Eq. (4.79), self-energy parts from single particle operators need to be multiplied by a factor of 2. This can be seen easily by considering the non-interacting case with an external perturbing potential. This issue is related to double-counting in mean-field theories and care has to be taken which terms appear twice.

Now for $\langle\Psi_0^\lambda|H(\lambda)|\Psi_0^\lambda\rangle$ we can also write

$$\langle\Psi_0^\lambda|H(\lambda)|\Psi_0^\lambda\rangle = \langle\Psi_0^\lambda|H^{\mathrm{MF}}|\Psi_0^\lambda\rangle + \lambda\,\langle\Psi_0^\lambda|H^1|\Psi_0^\lambda\rangle\,. \qquad (4.92)$$

Comparing this with the result above for the same expression yields

$$\Rightarrow \langle\Psi_0^\lambda|H^1|\Psi_0^\lambda\rangle = \frac{1}{\lambda}\frac{1}{2\pi}\int \mathrm{d}\nu\, e^{\mathrm{i}\,\nu 0^+}\frac{1}{2}\,\mathrm{Tr}\left\{\left[\Sigma(\mathrm{i}\,\nu,\lambda) - 2\lambda v_{el}^{\mathrm{MF}}\right]G(\mathrm{i}\,\nu,\lambda)\right\}. \qquad (4.93)$$

The self-energy $\Sigma(\lambda)$ contains the Hartree potential v_{H}^λ and the exchange potential v_{x}^λ which correspond to the first order terms in λ v and are functionals of the Green's function:

$$v_{\mathrm{H}}^\lambda(\mathbf{x}_1) = \int \mathrm{d}\mathbf{x}'\frac{\lambda}{|\mathbf{r}_1 - \mathbf{r}'|}\frac{1}{2\pi}\int \mathrm{d}\nu\, e^{\mathrm{i}\,\nu 0^+}G(\mathbf{x}', \mathbf{x}', \mathrm{i}\,\nu, \lambda) \qquad (4.94)$$

$$\begin{aligned}
v_{\mathrm{x}}^\lambda(\mathbf{x}_1, \mathbf{x}_2) = -\frac{\lambda}{|\mathbf{r}_1 - \mathbf{r}_2|}\frac{1}{2\pi}\int \mathrm{d}\nu\, e^{\mathrm{i}\,\nu 0^+}\,\Big[&\delta_{\sigma_1,\uparrow}\delta_{\sigma_2,\uparrow}G(\mathbf{r}_1\otimes\uparrow, \mathbf{r}_2\otimes\uparrow, \mathrm{i}\,\nu, \lambda) \qquad (4.95)\\
&+ \delta_{\sigma_1,\downarrow}\delta_{\sigma_2,\downarrow}G(\mathbf{r}_1\otimes\downarrow, \mathbf{r}_2\otimes\downarrow, \mathrm{i}\,\nu, \lambda)\Big]
\end{aligned}$$

Note that we explicitly used spatial-spin coordinates $\mathbf{x}$ as this is important in the case of the exchange potential. That the first order terms of the self-energy correspond to these two expressions, v_{H} and v_{x}, can be seen more easily diagrammatically and will be explained in the next section.

It is useful to split the Hartree and exchange potential off from the self energy and consider the remaining correlation part of the self energy $\Sigma_c(\lambda)$ separately. This way we can write the ground state energy as

$$\begin{aligned} E^0 =& E^{\mathrm{MF}} - \mathrm{Tr}\left\{ v_{el}^{\mathrm{MF}} \int_0^1 \mathrm{d}\lambda \frac{1}{2\pi} \int \mathrm{d}\nu \; e^{\mathrm{i}\nu 0^+} G(\mathrm{i}\,\nu, \lambda) \right\} \\ &+ \frac{1}{2}\,\mathrm{Tr}\left\{ \int_0^1 \mathrm{d}\lambda \frac{v_{\mathrm{H}}^{\lambda}}{\lambda} \frac{1}{2\pi} \int \mathrm{d}\nu \; e^{\mathrm{i}\nu 0^+} G(\mathrm{i}\,\nu, \lambda) \right\} \\ &+ \frac{1}{2}\,\mathrm{Tr}\left\{ \int_0^1 \mathrm{d}\lambda \frac{v_{\mathrm{x}}^{\lambda}}{\lambda} \frac{1}{2\pi} \int \mathrm{d}\nu \; e^{\mathrm{i}\nu 0^+} G(\mathrm{i}\,\nu, \lambda) \right\} \\ &+ \frac{1}{2} \int_0^1 \mathrm{d}\lambda \frac{1}{\lambda} \left(\frac{1}{2\pi} \int \mathrm{d}\nu \; e^{\mathrm{i}\nu 0^+} \,\mathrm{Tr}\left\{ \Sigma_c(\mathrm{i}\,\nu, \lambda) G(\mathrm{i}\,\nu, \lambda) \right\} \right) \end{aligned} \tag{4.96}$$

It will turn out that this is a good starting point for a perturbative energy functional for mean-field methods and that after introducing some approximations, the RPA energy functional can be derived from this expression.

4.4 Hedin's equations and the GW-approximation

This section will give a brief introduction to how the Green's function, the self energy and other related properties of a many electron system can in principle be calculated in an iterative fashion. We will use diagrams to some extend to provide a intuitive description and to create a bridge to the literature. However, since the rigorous treatment of Feynman diagrams is rather elaborate we refer to the literature for more details [25, 26, 66, 70]. We saw already above, that the independent particle Green's function G^0 is diagrammatically represented by a single line with arrow, and the full Green's function by a double line with arrow. These type of building blocks are so called particle lines. The other building blocks we encountered so far are external potentials and the self energy, which are represented as circles. It should however be noted, that the diagrams also include a phase factor depending on the convention. In imaginary time the translations are usually direct:

$\Sigma =$  $v =$ $G^0 =$  $G =$. (4.97)

We now introduce the interaction line between two particles, which in our case is usually the Coulomb repulsion between electrons:

$-\mathrm{v} =$. (4.98)

Every interaction line has to start and end at a vertex like diagram. The bare vertex, which is just the unity operator $\mathbb{1}$ with phase factor i, is symbolized as a dot:

$$\mathrm{i}\,\mathbb{1} = \bullet. \tag{4.99}$$

In case an interaction line is not connected to any other vertex like diagram, the bare vertex is usually implied to be present on both sides of the interaction line in all diagrams, e.g.

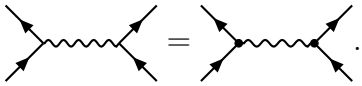

(4.100)

We will use this implicit notation wherever possible, but at times it is useful to have an explicit symbol for the bare vertex.

Whenever different building blocks in the diagrams are connected, the intermediate indices are traced over while the open indices on each term have to be the same, e.g.

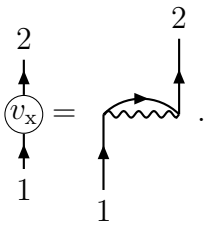

(4.101)

translates to

$$\int \mathrm{d}3\mathrm{d}4\; G^0(2,4)v_{\mathrm{x}}(4,3)G^0(3,1) = -\int \mathrm{d}3\ldots\mathrm{d}6\; G^0(2,6)G^0(5,4)\,\mathrm{v}(4,6,3,5)G^0(3,1). \tag{4.102}$$

Here the numbers are representative for positions $\{\mathbf{r}_i\}$ plus imaginary time coordinates τ_i.[1] The exact rules on how to translate diagrams into algebraic forms are designed so that they intrinsically take care of certain physical necessities such as symmetries and conservation laws.

The diagrams we consider are usually either closed or have two open indices. For the closed ones it is clear that one has to trace over all intermediate indices. The ones with two open indices like the one above, Eq. (4.102), are in any given basis a matrix. However, we will usually not write the open indices explicitly but rather treat those diagrams with open indices analogue to the basis independent operator notation, cf. Eq. (4.70) and (4.71).

The self energy we have encountered in section 4.2 is the so called proper (or irreducible) self energy and it can be shown, that it can be expressed as the sum

[1] In principle any single particle basis can be chosen instead of position coordinates, for example states of the non interacting Hamiltonian $\{\phi_k\}$, in that case however, the dressed vertex Γ (introduced later) becomes a bit more complicated [70]. The reason is that in real space coordinates, the Coulomb interaction $\mathrm{v}(1,2,3,4) \propto \delta(\mathbf{r}_1 - \mathbf{r}_2)\delta(\mathbf{r}_3 - \mathbf{r}_4)$

over all irreducible, self-energy like diagrams. These are diagrams with two open indices that can be inserted in a particle line, or in other words diagrams with an incoming and outgoing connection to a particle line. Irreducible means that in this case a diagram cannot be split in two by cutting through a single propagator line. Below are a few examples of irreducible self-energy like diagrams, arranged by the order of interactions:

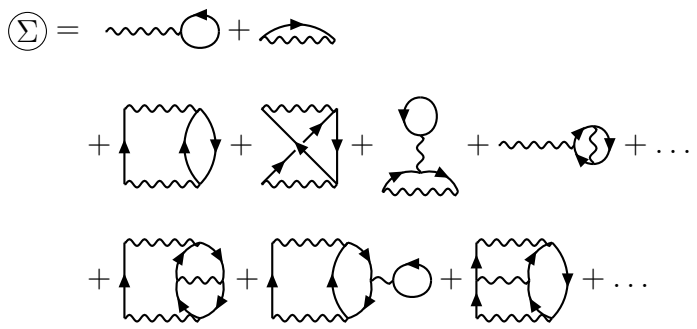

(4.103)

(4.104)

As was already mentioned, a perturbation series with a Hamiltonian where the bare Coulomb interaction V_{C} is treated as the perturbation does not converge. Therefore, often the Hartree potential of the full propagator (cf. Eq. 4.94) is separated from the rest of the self energy, while the remainder of the self energy is referred to as exchange-correlation part Σ_{xc}. This gives rise to a modified Dyson equation for the Green's function:[1]

$$G = G^0 + G^0 v_{\mathrm{H}}[G] G + G^0 \Sigma_{\mathrm{xc}} G \tag{4.105}$$

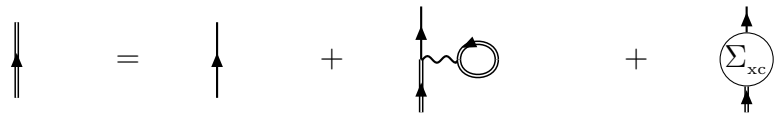

(4.106)

Also, it is possible generate an expansion of Σ_{xc} in terms of a screened potential W rather than the bare Coulomb potential v, as shown by Hedin in 1965 [66]. $W(1,2)$ essentially gives the potential at point 1 due to the presence of a test charge at point 2, including the effect of the polarization of the electrons in between. In the literature, W is usually referred to as the screened interaction, *i.e.* the interaction between two electrons, screened by the polarization effects of all the other electrons. Diagrammatically we represent the screened interaction by a double wiggly line and

[1] For every fermion loop a factor of -1 is applied in the translation of the diagrams to the algebraic form. Therefore the sign from the interaction and from the loop cancel each other and the total sign of the Hartree potential is positive as in Eq. (4.94)

it can be shown that the screened interaction obeys a Dyson like equation:

$$-W = -\mathrm{v} + -\mathrm{v}\,PW \tag{4.107}$$

(4.108)

with the proper polarization P, represented by the bubble diagram π. The proper (or irreducible) polarization is the sum of all irreducible, polarization like diagrams, i.e diagrams that cannot be split in two by cutting through a single interaction line and that have two open indices so that they can be inserted into an interaction line. For example the following diagrams are part of P:

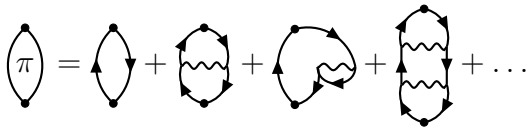

(4.109)

The full Green's function (see Dyson equation 4.106) and the screened interaction Eq. (4.108) are often referred to as dressed, or renormalized. The reason is that the full Green's function, if calculated self consistently with the self-energy, represents a quasi particle propagator and the quasi particles can be viewed as interacting via the screened interaction.

The last quantity that can be renormalized to condense the diagrammatic representation of MBPT is the vertex, Γ. Vertices represent the connection between an incoming particle line, an outgoing particle line and an interaction line. Since they connect three other building blocks, they are often represented by a triangle. The dressed vertex Γ is the sum of all irreducible vertex like diagrams, *i.e.* all diagrams that cannot be split in two by cutting neither a single particle nor a single interaction line and that have three open indices that can be connected to an incoming particle line, an outgoing particle line and an interaction line:

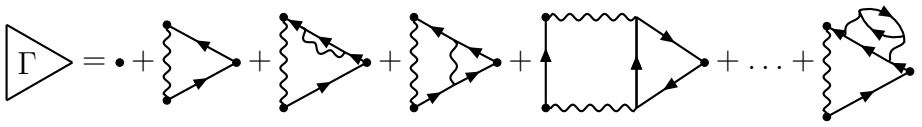

(4.110)

Using the different dressed quantities, one can show that the self energy can be expressed as [66, 70]:

$$v_{\mathrm{H}} + \Sigma_{\mathrm{xc}} = \mathrm{v}\,G - GW\Gamma \tag{4.111}$$

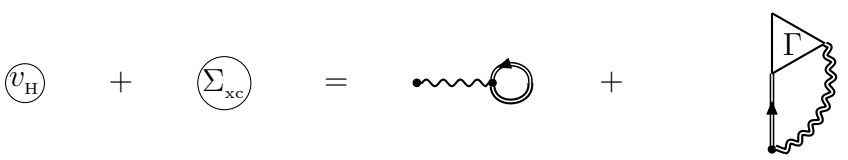

(4.112)

Similarly, the polarization P can also be expressed in terms of the Green's function and the dressed vertex:

$$P = GG\Gamma \tag{4.113}$$

. (4.114)

Finally, it can be shown that the dressed vertex also obeys a Dyson like equation:

$$\mathrm{i}\,\Gamma = \mathrm{i}\,\mathbb{1} + \frac{\delta\Sigma_{\mathrm{xc}}}{\delta G} GG\,\mathrm{i}\,\Gamma \tag{4.115}$$

. (4.116)

The Eqs. (4.105), (4.115), (4.113), (4.107) and (4.111) and their diagrammatic representation are known as the five Hedin's equations [66] and they give rise to a self-consistency cycle that in principle allows to calculate the true many body Green's function and self-energy and hence the ground state energy of the system, cf. Eq. (4.79). This cycle is often depicted in Hedin's pentagon, Fig. 4.1.

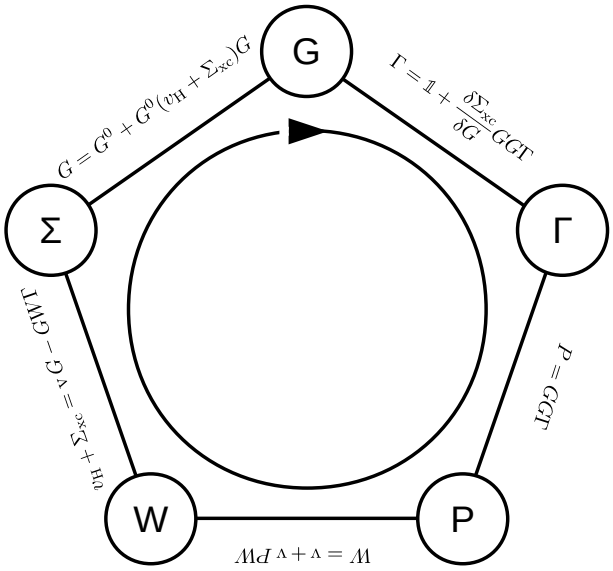

Figure 4.1: Hedin's pentagon: self consistency cycle for the iterative calculation of the Green's function, the dressed vertex, the polarization, the screened interaction and the self energy in many body perturbation theory.

In practice however, approximations are needed due to the high complexity of the equations. Starting from the Hartree-approximation, in the first self consistency cycle, the dressed vertex is just $\mathbb{1}$, since the exchange-correlation part of the self-energy is 0. As a consequence the self energy after one self consistency cycle is given as:

$$\Sigma_{\mathrm{xc}}^{GW} = -GW. \tag{4.117}$$

This gives rise to the GW approximation, where the dressed vertex is approximated by the bare one ($\mathbb{1}$). It is easily memorized by thinking of taking a short cut directly from G to P in Hedin's pentagon. Though this concept is theoretically only supported in the first cycle and starting from the Hartree reference, Hedin's GW method [66] is the most widely used approximation to the self energy in the last decades [71]. The method is regularly adopted for self consistent GW calculation and for different starting configurations such as DFT or HF reference states.

Related to the self consistent GW method is the so called G^0W^0. In this method G^0 corresponds to the independent particle Green's function from the reference mean-field Hamiltonian, while the screened interaction is still calculated in the GW approximation, *i.e.* replacing the dressed vertex with the bare one. However, the iteration is truncated after the first cycle, yielding a non-self consistent, perturbative approximation to the exchange correlation part of self energy given as

$$\Sigma_{\mathrm{xc}}^{G^0W^0} = -G^0W^0. \tag{4.118}$$

This perturbative method turned out to predict quasi particle energies and hence band gaps more accurately than the underlying mean-field methods and is widely used in computational materials physics and quantum chemistry [71]. Furthermore, we can use this approximation to derive an approximate functional for the total ground state energy, which will turn out to be the RPA energy functional.

Chapter 5

The random phase approximation

In this chapter, we introduce the random phase approximation (RPA) energy functional as an perturbative approximation to the ground state energy that can be calculated on top of an underlying mean-field calculation. We will use the adiabatic connection together with the G^0W^0 approximation introduced in the previous chapter to derive the RPA energy functional and give some references to the literature that support this ansatz. This chapter is designed to give a compact overview of the RPA, for a more detailed description we refer the reader to the review papers of Ren *et al.* [28] or Görling and Hesselmann [72, 73].

5.1 History of the RPA

During the 1950s, quantum many body theory introduced new theoretical concepts for the description of nuclei and solids. These originated from the techniques that were established in quantum electrodynamics, particularly Feynman-Dyson diagrammatic perturbation theory. In their publications between 1951 and 1953 [21, 22, 23, 24], Bohm and Pines studied the collective properties of the electron gas, describing density fluctuations by separating collective long-range (plasma) oscillations from short-range thermal or random motions of the individual electrons (or actually the dressed electrons which are quasi-particles). This can be done by characterizing the response to a wave, where collective motions produce a response in phase with the wave while the thermal motions give rise to a random phase difference. Considering systems with large numbers of electrons (high density limit), the mean value of the response for terms with a random phase, is zero. Assuming that this is also the case for large but finite densities is the original formulation of the random phase approximation.

When the many electron Hamiltonian is expressed in Fourier space by a series of momentum transfers between the electrons, the RPA amounts to neglecting the interaction between the collective and the single (quasi) particle degrees of freedom. This allows to treat the momentum transfers of the Coulomb potential in Fourier

space independently. An early application was the calculation of the dielectric function of the electron gas by Lindhard in 1954 [74].

From another point of view, in the RPA, the electrons behave like they are interacting only with a total electric potential that is composed of the external potential and a screened Coulomb potential. Figuratively, the screened potential can be viewed as the potential between two electrons, screened by the cloud of the other electrons that surround them. With this picture in mind, it appears obvious that the RPA is a good approximation if the screening (polarization effects) is large and the electrons interact via weak screened Coulomb forces. It became apparent that renormalizing the long-range Coulomb interaction into an effective screened interaction between new, effective single (quasi) particles allowed to overcome the divergences appearing in older theories of interacting many-body systems and to explain the puzzling success of the single-particle models developed earlier. Shortly afterwards in 1956, with Landaus Fermi liquid theory [75], effective theories describing many-body systems in terms of quasi particles were put on a solid theoretical foundation.

In 1957, Gell-Mann and Brueckner chose a diagrammatic approach to derive an expression for the ground-state energy of the interacting electron gas in the high-density limit [76]. They eliminated the spurious divergences of previous theories by summing the diagrams with ring structure to infinite order, yielding a geometric series and hence a convergent energy expression. Together with Goldstones paper from the same year [77], this is the earliest example in condensed-matter theory for the application of Feynman-diagrammatic methods.

Naturally, in the high density limit of the electron gas, the RPA yields exact correlation energies, but later in 1958, Nozier and Pines [78, 79] showed that under certain conditions, the RPA is also applicable to metallic densities.

In the 1970s Langreth and Perdew [67, 27] as well as Gunnarsson and Lundqvist [68], formulated the adiabatic-connection fluctuation-dissipation (ACFD) theorem in the context of exchange correlation energy functionals. They established a connection between the response function (polarizability) and the exchange correlation functional. This allowed to use the RPA as an orbital dependent energy functional.

Szabo and Oslund [80] showed that RPA yields the correct $1/R^6$ asymptotic behavior for the interaction between well-separated closed-shell subsystems. This is one of the major advantages of the RPA over LDA and GGA functionals, as those functionals do not incorporate such long-range interactions. Also in contrast to most other functionals, the self-interaction error present in the Hartree term cancels exactly with the exchange part of the RPA exchange-correlation functional [28]. Furthermore, the RPA is in principle applicable to metallic systems.

For the first time the RPA was applied to realistic systems when Furche [81], and Fuchs and Gonze [82] used RPA exchnage correlation functionals for small molecules in the early 2000s. Since then, developments on the theoretical level, significant improvements on the technical side, as well as novel and successful applications to various systems that were not well described with conventional functionals led the RPA to become an important tool in the repertoire of modern computational

quantum chemistry and materials science. An excerpt of more recent developments will be given in section 5.3 after a theoretical derivation of the RPA energy functional in the next section 5.2.

5.2 The perturbative RPA energy functional

Usually, the RPA energy functional is derived from the adiabatic connection fluctuation dissipation theorem (ACFDT). There, one starts with an energy expression from the adiabatic connection (AC) and then uses linear response theory in combination with the fluctuation dissipation theorem (FDT). The energy functional derived in this way depends on the interaction parameter λ via the λ-dependent polarizability/response function χ^λ. The RPA energy functional is then obtained by using an approximation which neglects the exchange correlation kernel $f_{\text{xc}} \approx 0$ [83]. However, instead of linear response theory, we will use a different approach by using the G^0W^0 approximation [28]. This is equivalent to using the RPA screened interaction to calculate the self energy, while leaving the Green's function unchanged. We will show that the RPA energy functional we derive in this way is equivalent to the earlier and more common ACFDT approach.[1]

Diagrammatically, the core of the random phase approximation is to approximate the proper polarization in zeroth order of the Coulomb interaction

$$P \qquad \approx \qquad P_0 \qquad = \qquad G^0 G^0 \tag{5.1}$$

(5.2)

yielding the following approximation to the screened (=effective) interaction:

$$W_{\text{RPA}} \qquad = \qquad \text{v} \qquad + \qquad \text{v}\, P_0 W_{\text{RPA}} \tag{5.3}$$

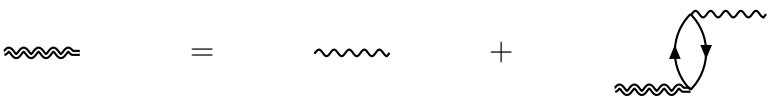

(5.4)

By summing the geometric series above, this can be re-written in terms of the RPA-dielectric constant ϵ_{RPA}:

$$W_{\text{RPA}} = \frac{\text{v}}{1 + \text{v}\, P_0} = \frac{\text{v}}{\epsilon_{\text{RPA}}}. \tag{5.5}$$

The RPA screened interaction is identical to the screened interaction W^0 in the G^0W^0 introduced in the previous chapter. We will exploit this connection between the two different diagrammatic approaches in order to formulate a Green's function

[1] In this section we use explicitly spatial-spin coordinates $\mathbf{x}$ and spin orbitals $\chi(\mathbf{x})$, cf. section 1.6.

based energy functional in the RPA. In order to do that, we recall the result of the adiabatic connection

$$\begin{aligned} E^0 =& E^{\mathrm{MF}} - \mathrm{Tr}\left\{ v_{el}^{\mathrm{MF}} \int_0^1 \mathrm{d}\lambda \frac{1}{2\pi} \int \mathrm{d}\nu \; e^{\mathrm{i}\,\nu 0^+} G(\mathrm{i}\,\nu, \lambda) \right\} \\ &+ \frac{1}{2}\,\mathrm{Tr}\left\{ \int_0^1 \mathrm{d}\lambda \frac{v_{\mathrm{H}}^{\lambda}}{\lambda} \frac{1}{2\pi} \int \mathrm{d}\nu \; e^{\mathrm{i}\,\nu 0^+} G(\mathrm{i}\,\nu, \lambda) \right\} \\ &+ \frac{1}{2}\,\mathrm{Tr}\left\{ \int_0^1 \mathrm{d}\lambda \frac{v_{\mathrm{x}}^{\lambda}}{\lambda} \frac{1}{2\pi} \int \mathrm{d}\nu \; e^{\mathrm{i}\,\nu 0^+} G(\mathrm{i}\,\nu, \lambda) \right\} \\ &+ \frac{1}{2} \int_0^1 \mathrm{d}\lambda \frac{1}{\lambda} \left(\frac{1}{2\pi} \int \mathrm{d}\nu \; e^{\mathrm{i}\,\nu 0^+} \,\mathrm{Tr}\left\{ \Sigma_c(\mathrm{i}\,\nu, \lambda) G(\mathrm{i}\,\nu, \lambda) \right\} \right). \end{aligned} \tag{5.6}$$

First, we will approximate the Green's function $G(\mathrm{i}\,\nu, \lambda)$ by it's mean-field expression $G^0(\mathrm{i}\,\nu)$

$$G(\mathrm{i}\,\nu, \lambda) \approx G(\mathrm{i}\,\nu, \lambda = 0) = G^{\mathrm{MF}}(\mathrm{i}\,\nu) = G^0(\mathrm{i}\,\nu), \tag{5.7}$$

and the screened interaction by the RPA

$$W(\lambda) \approx W^0(\lambda) = W^{\mathrm{RPA}}(\lambda) = \lambda\,\mathrm{v} + W_c^{\mathrm{RPA}}(\lambda) \tag{5.8}$$

with the correlation part

$$W_c^{\mathrm{RPA}}(\lambda) = \frac{\lambda\,\mathrm{v}}{1 + \lambda\,\mathrm{v}\,G^0 G^0} - \lambda\,\mathrm{v}\,. \tag{5.9}$$

In this approximation, the Hartree- and exchange potential are given as

$$v_{\mathrm{H}}^{\lambda}(\mathbf{x}_1, \mathbf{x}_2) \approx \delta(\mathbf{x}_1 - \mathbf{x}_2) \int \mathrm{d}\mathbf{x}' \frac{\lambda}{|\mathbf{r}_1 - \mathbf{r}'|} \frac{1}{2\pi} \int \mathrm{d}\nu \; e^{\mathrm{i}\,\nu 0^+} G^0(\mathbf{x}', \mathbf{x}', \mathrm{i}\,\nu) \tag{5.10}$$

$$\begin{aligned} v_{\mathrm{x}}^{\lambda}(\mathbf{x}_1, \mathbf{x}_2) \approx -\frac{\lambda}{|\mathbf{r}_1 - \mathbf{r}_2|} \frac{1}{2\pi} \int \mathrm{d}\nu \; e^{\mathrm{i}\,\nu 0^+} \; & \delta_{\sigma_1,\uparrow}\delta_{\sigma_2,\uparrow} G^0(\mathbf{r}_1 \otimes \uparrow, \mathbf{r}_2 \otimes \uparrow, \mathrm{i}\,\nu) \\ & + \delta_{\sigma_1,\downarrow}\delta_{\sigma_2,\downarrow} G^0(\mathbf{r}_1 \otimes \downarrow, \mathbf{r}_2 \otimes \downarrow, \mathrm{i}\,\nu), \end{aligned} \tag{5.11}$$

and the corresponding correlation part of the self-energy in the GW approximation is

$$\Sigma_c(\lambda) \approx -G^0 W_c^{\mathrm{RPA}}(\lambda). \tag{5.12}$$

Inserting the r.h.s of Eqs. (5.7), (5.10), (5.11) and (5.12) into Eq. (5.6) we find that the only λ dependence is left in the correlation part of the screened interaction $W_c^{\mathrm{RPA}}(\lambda)$ via the scaled Coulomb potential $\mathrm{v}(\lambda) = \lambda\,\mathrm{v}$, since the mean-field Green's function does not depend on the interaction parameter λ. Thus, the λ integration

of the first three terms in Eq. (5.6) is trivial and using

$$\frac{1}{2\pi}\int \mathrm{d}\nu\, e^{\mathrm{i}\,\nu 0^+} G^0(\mathbf{x},\mathbf{x}',\mathrm{i}\,\nu) = n^{\mathrm{MF}}(\mathbf{x},\mathbf{x}') = \sum_{i\in occ.} \chi_i(\mathbf{x})\chi_i^*(\mathbf{x}'), \tag{5.13}$$

with the mean-field spin orbitals $\{\chi_i\}$, we arrive at the following intermediate result for the total RPA energy functional $E_{\mathrm{tot}}^{\mathrm{RPA}}$:

$$E^0 \approx E_{\mathrm{tot}}^{\mathrm{RPA}} = E_{\mathrm{EXX}} + E_{\mathrm{RPA}}. \tag{5.14}$$

E_{EXX} is the Hartree-Fock energy functional (2.28), evaluated with the orbitals from an arbitrary mean-field method, e.g. PBE. E_{RPA} is the correlation energy in the RPA, obtained from the last term in Eq. (5.6) using (5.12).

We will show quickly how E_{EXX} emerges from the first four terms of Eq. (5.6). The first two terms yield the kinetic energy and the energy in the external potential for the mean-field orbitals:

$$E^{\mathrm{MF}} - \mathrm{Tr}\left\{v_{el}^{\mathrm{MF}} \int_0^1 \mathrm{d}\lambda \frac{1}{2\pi}\int \mathrm{d}\nu\, e^{\mathrm{i}\,\nu 0^+} G^0(\mathrm{i}\,\nu)\right\} = \tag{5.15}$$

$$\sum_{i\in occ} \langle\chi_i|\frac{-\nabla^2}{2} + v_{\mathrm{ext}} + v_{el}^{\mathrm{MF}}|\chi_i\rangle - \int \mathrm{d}\mathbf{x}_1\mathrm{d}\mathbf{x}_2\, \langle\mathbf{x}_2|v_{el}^{\mathrm{MF}}|\mathbf{x}_1\rangle \frac{1}{2\pi}\int \mathrm{d}\nu\, e^{\mathrm{i}\,\nu 0^+}\, \langle\mathbf{x}_1|G^0(\mathrm{i}\,\nu)|\mathbf{x}_2\rangle$$

$$= \sum_{i\in occ} \langle\chi_i| - \frac{\nabla^2}{2} + v_{\mathrm{ext}} + v_{el}^{\mathrm{MF}}|\chi_i\rangle - \langle\mathbf{x}'|v_{el}^{\mathrm{MF}}|\mathbf{x}\rangle \sum_{i\in occ} \langle\mathbf{x}|\chi_i\rangle\, \langle\chi_i|\mathbf{x}'\rangle$$

$$= \sum_{i\in occ} \langle\chi_i| - \frac{\nabla^2}{2}|\chi_i\rangle + \langle\chi_i|v_{\mathrm{ext}}|\chi_i\rangle$$

$$= \sum_{i\in occ} \langle\chi_i|\hat{h}|\chi_i\rangle$$

$$= E_{\mathrm{kin}}[\{\chi_i\}] + E_{\mathrm{ext}}[\{\chi_i\}]$$

corresponding to the first term in the Hartree-Fock energy functional. The third

term, containing the Hartree potential yields

$$\frac{1}{2}\,\mathrm{Tr}\left\{\int_0^1 \mathrm{d}\lambda \frac{v_{\mathrm{H}}^{\lambda}[G^0]}{\lambda}\frac{1}{2\pi}\int \mathrm{d}\nu\; e^{\mathrm{i}\,\nu 0^+} G^0(\mathrm{i}\,\nu)\right\} = \tag{5.16}$$

$$\frac{1}{2}\iint \mathrm{d}\mathbf{x}_1\mathrm{d}\mathbf{x}_2 \sum_{i,j\in occ}\int \mathrm{d}\mathbf{x}'\delta(\mathbf{x}_1-\mathbf{x}_2)\frac{\chi_i(\mathbf{x}')\chi_i^*(\mathbf{x}')}{|\mathbf{r}_1-\mathbf{r}'|}\chi_j(\mathbf{x}_2)\chi_j^*(\mathbf{x}_1) =$$

$$\frac{1}{2}\sum_{i,j\in occ}\langle\chi_i|\,\langle\chi_j|\,\mathrm{v}\,|\chi_i\rangle\,|\chi_j\rangle$$

and similarly the fourth term with the exchange potential yields

$$\frac{1}{2}\,\mathrm{Tr}\left\{\int_0^1 \mathrm{d}\lambda \frac{v_{\mathrm{x}}^{\lambda}[G^0]}{\lambda}\frac{1}{2\pi}\int \mathrm{d}\nu\; e^{\mathrm{i}\,\nu 0^+} G^0(\mathrm{i}\,\nu)\right\} = -\frac{1}{2}\sum_{i,j\in occ}\langle\chi_i|\,\langle\chi_j|\,\mathrm{v}\,|\chi_j\rangle\,|\chi_i\rangle\,. \tag{5.17}$$

The self interactions in Eq. (5.17) and (5.16) cancel each other exactly. Therefore in our approximation, the energy from the first four terms of Eq. (5.6), E_{EXX}, coincides with the Hartree-Fock energy functional (2.28) evaluated at the occupied mean-field orbitals $\{\chi_i\}$:

$$E_{\mathrm{EXX}}[\{\chi_i\}] \;=\; E_{\mathrm{kin}}[\{\chi_i\}] + E_{\mathrm{ext}}[\{\chi_i\}] \;+\; E_{\mathrm{H}}[\{\chi_i\}] \;+\; E_{\mathrm{x}}[\{\chi_i\}] \tag{5.18}$$

$$= \qquad + \qquad + \qquad . \tag{5.19}$$

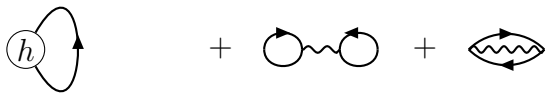

In the literature this is often referred to as *exact exchange*, hence the label "EXX".

Within the approximation (5.12), we will now evaluate the correlation part of the energy, corresponding to the remaining last term of Eq. (5.6):

$$E_{\mathrm{RPA}} = \frac{1}{2}\int_0^1 \mathrm{d}\lambda \frac{1}{\lambda}\left(\frac{1}{2\pi}\int \mathrm{d}\nu\; e^{\mathrm{i}\,\nu 0^+}\,\mathrm{Tr}\left\{-G^0(\mathrm{i}\,\nu)W_c^{\mathrm{RPA}}(\mathrm{i}\,\nu,\lambda)G^0(\mathrm{i}\,\nu)\right\}\right). \tag{5.20}$$

We will now formally perform the λ integration for W_c^{RPA}

$$\int_0^1 \mathrm{d}\lambda \frac{1}{\lambda}W_c^{\mathrm{RPA}}(\lambda) = \int_0^1 \mathrm{d}\lambda \frac{1}{\lambda}\left(\frac{\lambda\,\mathrm{v}}{1-\lambda\,\mathrm{v}\,G^0G^0} - \lambda\,\mathrm{v}\right) \tag{5.21}$$

$$= -\frac{\ln(1-\mathrm{v}\,G^0G^0)}{G^0G^0} - \mathrm{v}$$

Hence, we finally obtain

$$E_{\mathrm{RPA}} = \frac{1}{2}\left(\frac{1}{2\pi}\int \mathrm{d}\nu\, e^{\mathrm{i}\,\nu 0^+}\,\mathrm{Tr}\left\{\ln(1-\mathrm{v}\,G^0G^0) - G^0\,\mathrm{v}\,G^0\right\}\right), \tag{5.22}$$

which is equivalent to the form commonly found in the literature in terms of the mean-field polarization P_{MF} [31, 83]:

$$E_{\mathrm{RPA}} = \frac{1}{2\pi}\int_0^\infty \mathrm{d}\nu\,\mathrm{Tr}\left\{\ln(1-\mathrm{v}\,P_{\mathrm{MF}}) - \mathrm{v}\,P_{\mathrm{MF}}\right\}, \tag{5.23}$$

since $G^0 = G^{\mathrm{MF}}$ and $P_{\mathrm{MF}} = P_0 = G^0G^0$.

This result can also be obtained diagrammatically from Eq. (5.20). The integrand (apart from the negative sign) is given as:

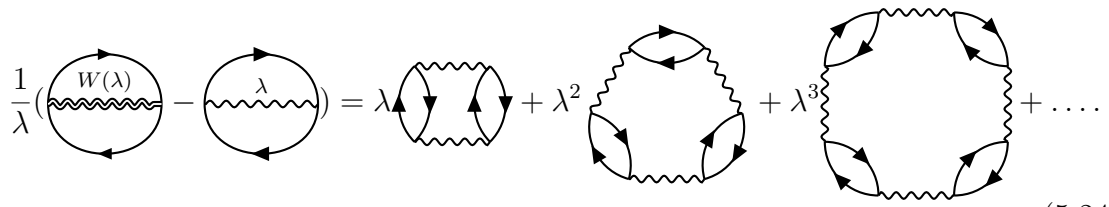

(5.24)

Thus, the λ integration yields

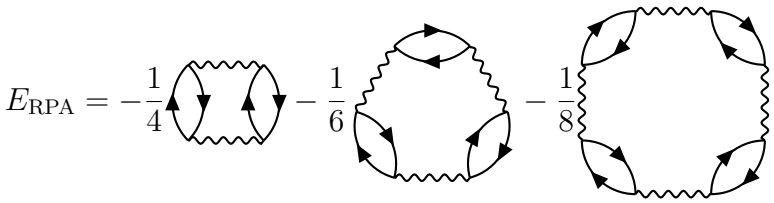

(5.25)

which is exactly the same result one obtains by formally expanding the logarithm in Eq. (5.22) around $\mathrm{v}\,G^0G^0 = 0$. This diagrammatic expansion is the reason why in the literature, the RPA is often described as summing up all "ring" or "bubble" diagrams to infinite order.

5.3 Applications and recent developments of the RPA

Today, the standard approach to use the RPA is to apply the RPA energy functional as a post processing technique on top of a DFT calculation, e.g. PBE →RPA@PBE. For most bonding types, including metallic, covalent, and ionic bonding, this approach yields a rather good and balanced description. But most importantly, due to its intrinsic non-local nature, the RPA can in principle also describe van der Waals (vdW) bonding correctly [62]. This is a major advantage over conventional density functionals, which can never truly describe non-local dynamic correlation effects (van der Waals-type bonding, dynamic dipole-dipole interactions) due to the

local or semi-local nature of those functionals.

The usefulness of the RPA was already shown over a decade ago, when several groups investigated molecular properties, in particular in the weakly bound regime, while others applied the RPA to periodic systems [28]. Extensive RPA benchmark studies for crystalline solids of all bonding types [29, 30, 31] were performed by Harl and Kresse. It became apparent that the application of the RPA to surface adsorption problems is particularly rewarding [84, 85, 86, 87, 88, 89], for example the RPA showed considerable success in resolving the "CO adsorption puzzle"[34]. Especially since the second half of the 2000s, an increasing number of publications on RPA applications was published, indicating the RPA's rising importance in the field of computational quantum chemistry and materials science.

Of course, like most methods, the RPA has also some draw backs. The first issue is the high computational cost. The original implementation of the RPA for realistic systems by Furche [81] was based on a molecular particle-hole basis and scaled with $O(N^6)$. In the beginning, this steep scaling prevented the application of the RPA to large systems (>100 atoms). However, technical advancements in recent years, especially for periodic systems by Kaltak and Kresse [35, 62], allow to calculate RPA energies with cubic scaling $O(N^3)$ in system size, so that large systems became accessible. In this context, another important publication by Liu [63] should be mentioned, where the authors describe cubic scaling GW. While these fast and parallelizable algorithms give access to new realms, the overall computational cost of an RPA energy calculation is typically still by a factor of ≈ 50 higher than with PBE. However, in comparison with other correlated methods like MP2 or coupled cluster, RPA is comparatively fast and represents a good compromise between accuracy and performance.

While in many cases the RPA is a significant improvement over conventional DFT, there are also some short comings from a theoretical point of view. It has been shown that, in the homogeneous electron gas, the RPA is not accurate for short-range correlations [90, 91]. From a MBPT point of view, among all the possible many-body diagrams that should be included, direct RPA exclusively sums the bubble-ring diagrams. This already points to one fundamental issue, namely the lack of proper anti-symmetrization. Relatedly, the GW approximation violates the crossing symmetry of the vertex, *i.e.* it violates the Pauli-principle [70]. This leads to errors in strongly correlated systems.

In the past, many different paths to improve upon standard RPA have been explored. Initially local/semi-local correlation corrections based on LDA or GGA were made [92, 93]. Later, attempts to account for other kind of diagrams, like higher-order exchange interactions [94, 95] were made. Other approaches included the contribution of single excitations [96, 97, 98], or employed approximate exchange and correlation contributions inspired by DFT [99]. Since the standard RPA is a perturbational method and is not calculated self-consistently, better starting points than standard density functionals can also enhance the method [100, 101]. [62]

With those recent developments in mind, investigating the capabilities and limits of the RPA as a post processing method on top of mean-field methods, as well

as finding potentially new fields of application within its theoretical framework, represents one main aspect of this thesis.

5.4 The challenge of RPA Forces

Upon the start of this doctoral thesis, efficient algorithms for the calculation of RPA energies for periodic systems had recently been implemented in `VASP` [35, 62]. However, a crucial feature for *ab initio* simulations was missing, namely an efficient algorithm to calculate forces in the RPA in solids. While for molecular codes, first implementations had recently been developed with $O(N^6)$ [36] and $O(N^4)$ [37] scaling, there was no equivalent approach for periodic codes.

The underlying challenge is that in mean-field *ab initio* simulations, the energy functional is stationary with respect to the mean-field orbitals, since the mean-field Hamiltonian is usually derived from the variation of the respective energy functional. Hence, the derivative of the energy with respect to the orbitals vanishes and therefore in order to calculate the force on an atom, one can ignore the terms that consider the functional derivative with respect to the orbitals:

$$\frac{\delta E^{\mathrm{MF}}}{\delta \phi_i^{\mathrm{MF}}} = 0. \tag{5.26}$$

This observation is related to the Hellmann-Feynman theorem, so that we refer to the forces in mean-field methods as Hellmann-Feynman forces. These Hellmann-Feynman forces only consider the change of the external potential with respect to atom positions, but not the change of the orbitals. For example in DFT, the energy can be considered as a functional of the external potential and the density/orbitals. When the DFT calculation reached self consistency, Eq. (5.26) holds, and the force on an atom at position $\mathbf{R} = (R_1, R_2, R_3)$ is formally calculated as

$$\begin{aligned} F_i &= -\frac{\mathrm{d}E^{\mathrm{DFT}}[v_{\mathrm{ext}}, n[\{\phi_i\}]]}{\mathrm{d}R_i} \qquad (5.27)\\ &= -\operatorname{Tr}\left\{\frac{\delta E^{\mathrm{DFT}}[v_{\mathrm{ext}}, n[\{\phi_i\}]]}{\delta v_{\mathrm{ext}}}\frac{\mathrm{d}v_{\mathrm{ext}}}{\mathrm{d}R_i}\right\} - \sum_{i\in occ}\operatorname{Tr}\left\{\underbrace{\frac{\delta E^{\mathrm{DFT}}[v_{\mathrm{ext}}, n[\{\phi_i\}]]}{\delta \phi_i}}_{=0}\frac{\mathrm{d}\phi_i}{\mathrm{d}R_i}\right\}. \end{aligned}$$

Since the second term vanishes, most available *ab initio* codes calculate only the first, Hellmann-Feynman, term. However, the RPA energy functional is calculated perturbatively and thus is not stationary with respect to the mean-field orbitals it is based on.

Therefore, in order to calculate forces in the RPA, one has to take the non-Hellmann-Feynman forces into account. Also, one would like to keep the computational cost as low as possible in order to apply the RPA force algorithm to large

periodic systems and surfaces, which is already challenging for energy calculations. These two requirements together pose a challenging problem and represent the key research topic investigated during the course of this thesis.

Chapter 6

The projector augmented wave method

The properties of materials and molecules are mainly characterized by the dynamics of the valence electrons. While the valence electrons are strongly influenced by the chemical environment and therefore shape the inter-atomic interactions dynamically, the state of electrons in the inner shells and the nucleus is very robust with respect to changes in the chemical environment. Intuitively, this can be explained by the screening from the valence electrons. In electronic structure theory, the frozen core approximation exploits this observation in order to decrease the complexity of the many electron system. In the frozen core approximation, not only the nuclei are kept at fixed positions (Born-Oppenheimer approximation) but the electron density of the inner shells (core electrons) is also kept constant and the Schrödinger equation is solved only for the valence electrons in an external pseudo potential that is constructed from the nuclei and the frozen core electrons. An example for the construction of pseudo-potentials is found in the publication of Vanderbilt [102], who introduced ultra soft pseudo potentials (USP) to reduce the necessary cut-off energy for plane-wave basis sets significantly. This is achieved by introducing a generalized orthonormality condition, allowing to divide the electron density into a soft and a hard part. The latter is strictly localized in the core regions.

Also, the efficiency of electronic structure calculations can be increased by the careful construction of basis sets, so that they can be truncated to decrease the computational costs, while still describing the system with sufficient accuracy. In the linearized augmented-plane-wave (LAPW) method this is achieved by dividing space into (non-overlapping) atomic spheres centered at the position of the nuclei and an interstitial region. In the two regions different basis sets are used: radial functions in the spheres around the nuclei and plane waves in the interstitial region [103].

The projector augmented wave method (PAW) combines the ideas of the LAPW and USP and was first proposed by Blöchl [104]. The formal relationship between USP and the PAW method has been derived by Kresse and Joubert [105]. The

PAW is implemented in the VASP code and is used there by default to achieve high efficiency. In the following, we give a brief overview on the principles behind the PAW and its implications for Green's function methods, in particular it the context of the RPA.

6.1 Introduction to the PAW formalism

Usually, the true (all electron) orbitals ψ_n show rapid oscillations around the atom centers. To describe these oscillations accurately with a plane wave basis, one would require very high cut-off energies. In order to reduce the required cut-off energy, the PAW introduces pseudo orbitals $\tilde{\psi}_n$ as auxiliary quantities. These pseudo orbitals $\tilde{\psi}_n$ are smoother than the ψ_n around the core regions so that much smaller cut-off energies are sufficient to represent them with a plane wave basis. The pseudo orbitals are constructed so that they are connected to the all electron orbitals via a linear transformation:

$$|\psi_n\rangle = \mathcal{T}\,|\tilde{\psi}_n\rangle = |\tilde{\psi}_n\rangle + \sum_\mu (|\phi_\mu\rangle + |\tilde{\phi}_\mu\rangle)\,\langle \tilde{p}_\mu|\tilde{\psi}_n\rangle\,. \tag{6.1}$$

The index μ is a compound index for the atomic site $\mathbf{R}_\mu$, the angular momentum numbers l_μ, m_μ, and the reference energy ϵ_μ. The ϕ_μ, $\tilde{\phi}_\mu$ and $\tilde{p}_\mu$ are additional auxiliary quantities that are fixed at the start of an electronic structure calculation and depend on the kind and position of the atoms. The all electron partial waves ϕ_μ are obtained for an isolated reference atom:

$$\langle \mathbf{r}|\phi_\mu\rangle = \frac{1}{\mathbf{r}-\mathbf{R}_\mu} u_{l_\mu \epsilon_\mu}(|\mathbf{r}-\mathbf{R}_\mu|) Y_{l_\mu m_\mu}(\angle[\mathbf{r}-\mathbf{R}_\mu]), \tag{6.2}$$

where $u_{l_\mu\epsilon_\mu}$ are the solution of the radial Schrödinger equation for the reference atom, $Y_{l_\mu m_\mu}$ are spherical harmonics and $\angle[\ ]$ indicates that $Y_{l_\mu m_\mu}$ depends only on the orientation, not the absolute value of the argument vector. The pseudo partial waves $\tilde{\phi}_\mu$ are equivalent to the all electron partial waves outside the augmentation sphere Ω_c – with radius r_μ^c centered at position $\mathbf{R}_\mu$ – and are constructed to continuously match the ϕ_μ at the augmentation border. Usually, the core radius r_μ^c is chosen to be approximately half the nearest-neighbor distance. The pseudo partial waves $\tilde{\phi}_\mu$ are constructed in a way that they are smoother than the all electron orbitals inside the augmentation regions by substituting the radial part $u_{l_\mu\epsilon_\mu}$ in Eq. (6.2) with a pseudized radial function $\tilde{u}_{l_\mu\epsilon_\mu}$, for details see Ref. [104, 105]. The projector functions $\tilde{p}_\mu$ are usually localized within the augmentation region and inside the augmentation spheres they need to fulfill the equation

$$\sum_\mu |\tilde{\phi}_\mu\rangle\,\langle\tilde{p}_\mu| = \mathbb{1}_{\Omega_c}, \tag{6.3}$$

so that the pseudo orbitals can be expanded in terms of the pseudo partial waves as

$$|\tilde{\psi}_n\rangle = \sum_\mu |\tilde{\phi}_\mu\rangle \langle \tilde{p}_\mu|\tilde{\psi}_n\rangle_{\Omega_c} . \tag{6.4}$$

The projector functions $\tilde{p}_\mu$ are therefore dual to the partial waves within the augmentation region:

$$\langle \tilde{p}_\mu|\tilde{\phi}_\nu\rangle_{\Omega_c} = \delta_{\mu\nu}. \tag{6.5}$$

In the theory of variational methods like DFT and HF, the all electron orbitals ψ_n are the variational quantities of an electronic structure calculation. However, in the PAW the pseudo orbitals $\tilde{\psi}_n$ take this role, while the all electron orbitals can in principle be recovered from the pseudo orbitals in retrospect by Eq. (6.1). In order to obtain a solution for the pseudo orbitals $\tilde{\psi}_n$ that is consistent with the all electron solution, operators – especially the Hamiltonian – need to be transformed accordingly. For example, it is easy to show that the expectation value of any one electron operator O for an arbitrary all electron orbital ψ_n is equal to the expectation value of the PAW operator $\tilde{O}$ for the pseudo orbital $\tilde{\psi}_n$:

$$\langle \psi_n|O|\psi_n\rangle = \langle \tilde{\psi}_n|\tilde{O}|\tilde{\psi}_n\rangle \tag{6.6}$$

$$\tilde{O} = \mathcal{T}^\dagger O \mathcal{T}. \tag{6.7}$$

This gives rise to the introduction of so called compensation charge densities $Q_{\mu\nu}$:

$$Q_{\mu\nu}(\mathbf{r}) = \langle \phi_\mu|\mathbf{r}\rangle \langle \mathbf{r}|\phi_\nu\rangle - \langle \tilde{\phi}_\mu|\mathbf{r}\rangle \langle \mathbf{r}|\tilde{\phi}_\nu\rangle = \phi^*_\mu(\mathbf{r})\phi_\nu(\mathbf{r}) - \tilde{\phi}^*_\mu(\mathbf{r})\tilde{\phi}_\nu(\mathbf{r}) \tag{6.8}$$

$$Q_{\mu\nu} = \int \mathrm{d}^3\mathbf{r}\, Q_{\mu\nu}(\mathbf{r}) = \langle \phi_\mu|\phi_\nu\rangle - \langle \tilde{\phi}_\mu|\tilde{\phi}_\nu\rangle . \tag{6.9}$$

The compensation charges can be used to write PAW operators in a more compact notation, for example, the position projector is transformed in the following way:

$$|\mathbf{r}\rangle \langle \mathbf{r}| \rightarrow |\mathbf{r}\rangle \langle \mathbf{r}| + \sum_{\mu\nu} |\tilde{p}_\mu\rangle Q_{\mu\nu}(\mathbf{r}) \langle \tilde{p}_\nu| . \tag{6.10}$$

The emerging stationary Schrödinger equation for the pseudo orbitals $\tilde{\psi}_n$ is given as the generalized eigenvalue equation

$$\tilde{H}\,|\tilde{\psi}_n\rangle = \epsilon_n S\,|\tilde{\psi}_n\rangle \tag{6.11}$$

with the overlap operator

$$S = \mathbb{1} + \sum_{\mu\nu} |\tilde{p}_\mu\rangle Q_{\mu\nu} \langle \tilde{p}_\nu| . \tag{6.12}$$

Furthermore, the pseudo orbitals are not necessarily orthogonal but rather fulfill the generalized orthogonality condition:

$$\langle\tilde{\psi}_n|S|\tilde{\psi}_m\rangle = \delta_{nm}. \tag{6.13}$$

Note that the `VASP` code (used for the applied electronic structure calculations in this thesis), uses the frozen core approximation, which is not an inherent characteristic of the PAW method. There, the core electrons are kept frozen in the configuration for which the PAW potential and auxiliary quantities like the partial waves were generated.

6.2 Implications of the PAW formalism for the RPA

Consider the formula for the RPA correlation energy

$$E_{\mathrm{RPA}} = \frac{1}{2\pi}\int_0^\infty \mathrm{d}\nu\, \mathrm{Tr}\left\{\ln(1-\mathrm{v}\,P_{\mathrm{MF}}) - \mathrm{v}\,P_0\right\}. \tag{6.14}$$

When one performs the underlying mean-field calculation in the PAW, one needs to take care of how the mean-field polarizability P_0 can be expressed in terms of the pseudo mean-field orbitals $\tilde{\psi}_n$. As we have seen in the previous chapter 5, in the RPA the polarizability can be calculated from the mean-field Green's functions as

$$P_0(\mathbf{r},\mathbf{r}',\mathrm{i}\,\tau) = G^0(\mathbf{r},\mathbf{r}',\mathrm{i}\,\tau)G^0(\mathbf{r}',\mathbf{r},-\mathrm{i}\,\tau). \tag{6.15}$$

To keep the following description as compact as possible we will only consider the case $\tau > 0$, but for negative imaginary times a similar expression can be found easily by interchanging the positions $\mathbf{r} \leftrightarrow \mathbf{r}'$ as $P_0(\mathbf{r},\mathbf{r}',\mathrm{i}\,\tau) = P_0(\mathbf{r}',\mathbf{r},-\mathrm{i}\,\tau)$.

Using Eq. (4.49) for the mean field Green's function, we obtain for the polarizability at positive imaginary times $\tau > 0$

$$\begin{aligned} P_0(\mathbf{r},\mathbf{r}',\mathrm{i}\,\tau) &= \left(-\sum_n \langle\mathbf{r}|\psi_n\rangle\langle\psi_n|\mathbf{r}'\rangle\, e^{-\tau\epsilon_n}(1-f_n)\right)\left(\sum_m \langle\mathbf{r}'|\psi_m\rangle\langle\psi_m|\mathbf{r}\rangle\, e^{\tau\epsilon_m} f_m\right) \\ &= -\sum_{nm}\langle\psi_m|\mathbf{r}\rangle\langle\mathbf{r}|\psi_n\rangle\langle\psi_n|\mathbf{r}'\rangle\langle\mathbf{r}'|\psi_m\rangle\, e^{-\tau(\epsilon_n-\epsilon_m)}(1-f_n)f_m, \end{aligned} \tag{6.16}$$

where we used f_n as short hand for the occupation number $f(\epsilon_n)$. When we substitute the orbitals ψ in the above equation with PAW pseudo orbitals $\tilde{\psi}$, we also need to apply the transformation given in Eq. (6.10) to the position projector $|\mathbf{r}\rangle\langle\mathbf{r}|$ in order to get a consistent result. Hence, the polarizability can be written in terms

of PAW pseudo orbitals as:

$$P_0(\mathbf{r},\mathbf{r}',\mathrm{i}\,\tau) = -\sum_{nm} \langle\tilde{\psi}_m| \left(|\mathbf{r}\rangle\langle\mathbf{r}| + \sum_{\mu\nu} Q_{\mu\nu}(\mathbf{r})\,|\tilde{p}_\mu\rangle\langle\tilde{p}_\nu| \right) |\tilde{\psi}_n\rangle \times \tag{6.17}$$

$$\langle\tilde{\psi}_n| \left(|\mathbf{r}'\rangle\langle\mathbf{r}'| + \sum_{\alpha\beta} Q_{\alpha\beta}(\mathbf{r}')\,|\tilde{p}_\alpha\rangle\langle\tilde{p}_\beta| \right) |\tilde{\psi}_m\rangle \times$$

$$e^{-\tau(\epsilon_n-\epsilon_m)}(1-f_n)f_m \tag{6.18}$$

$$= -\sum_{nm} \left(\langle\tilde{\psi}_m|\mathbf{r}\rangle\langle\mathbf{r}|\tilde{\psi}_n\rangle + \sum_{\mu\nu} Q_{\mu\nu}(\mathbf{r})\,\langle\tilde{\psi}_m|\tilde{p}_\mu\rangle\langle\tilde{p}_\nu|\tilde{\psi}_n\rangle \right) \times$$

$$\left(\langle\tilde{\psi}_n|\mathbf{r}'\rangle\langle\mathbf{r}'|\tilde{\psi}_m\rangle + \sum_{\alpha\beta} Q_{\alpha\beta}(\mathbf{r}')\,\langle\tilde{\psi}_n|\tilde{p}_\alpha\rangle\langle\tilde{p}_\beta|\tilde{\psi}_m\rangle \right) \times$$

$$e^{-\tau(\epsilon_n-\epsilon_m)}(1-f_n)f_m$$

$$= -\sum_{nm} \Bigg(\langle\mathbf{r}|\tilde{\psi}_n\rangle\langle\tilde{\psi}_n|\mathbf{r}'\rangle\langle\mathbf{r}'|\tilde{\psi}_m\rangle\langle\tilde{\psi}_m|\mathbf{r}\rangle \tag{6.19}$$

$$+ \sum_{\alpha\beta} Q_{\alpha\beta}(\mathbf{r}')\,\langle\mathbf{r}|\tilde{\psi}_n\rangle\langle\tilde{\psi}_n|\tilde{p}_\alpha\rangle\langle\tilde{p}_\beta|\tilde{\psi}_m\rangle\langle\tilde{\psi}_m|\mathbf{r}\rangle$$

$$+ \sum_{\mu\nu} Q_{\mu\nu}(\mathbf{r})\,\langle\tilde{p}_\nu|\tilde{\psi}_n\rangle\langle\tilde{\psi}_n|\mathbf{r}'\rangle\langle\mathbf{r}'|\tilde{\psi}_m\rangle\langle\tilde{\psi}_m|\tilde{p}_\mu\rangle$$

$$+ \sum_{\mu\nu\alpha\beta} Q_{\mu\nu}(\mathbf{r})Q_{\alpha\beta}(\mathbf{r}')\,\langle\tilde{p}_\nu|\tilde{\psi}_n\rangle\langle\tilde{\psi}_n|\tilde{p}_\alpha\rangle\langle\tilde{p}_\beta|\tilde{\psi}_m\rangle\langle\tilde{\psi}_m|\tilde{p}_\mu\rangle \Bigg) \times$$

$$e^{-\tau(\epsilon_n-\epsilon_m)}(1-f_n)f_m.$$

With the following definitions for auxiliary Green's functions:

$$\tilde{G}(\mathbf{r},\mathbf{r}',\mathrm{i}\,\tau) = \sum_n e^{-\epsilon_n \tau} \langle \mathbf{r}|\tilde{\psi}_n\rangle \langle \tilde{\psi}_n|\mathbf{r}'\rangle \left[\Theta(-\tau) f_n - \Theta(\tau)(1-f_n)\right] \tag{6.20}$$

$$\tilde{G}(\nu,\mathbf{r}',\mathrm{i}\,\tau) = \sum_n e^{-\epsilon_n \tau} \langle \tilde{p}_\nu|\tilde{\psi}_n\rangle \langle \tilde{\psi}_n|\mathbf{r}'\rangle \left[\Theta(-\tau) f_n - \Theta(\tau)(1-f_n)\right] \tag{6.21}$$

$$\tilde{G}(\mathbf{r},\alpha,\mathrm{i}\,\tau) = \sum_n e^{-\epsilon_n \tau} \langle \mathbf{r}|\tilde{\psi}_n\rangle \langle \tilde{\psi}_n|\tilde{p}_\alpha\rangle \left[\Theta(-\tau) f_n - \Theta(\tau)(1-f_n)\right] \tag{6.22}$$

$$\tilde{G}(\nu,\alpha,\mathrm{i}\,\tau) = \sum_n e^{-\epsilon_n \tau} \langle \tilde{p}_\nu|\tilde{\psi}_n\rangle \langle \tilde{\psi}_n|\tilde{p}_\alpha\rangle \left[\Theta(-\tau) f_n - \Theta(\tau)(1-f_n)\right] \tag{6.23}$$

the polarizability at $\tau > 0$ can be rewritten as (cf. Ref. [63]):

$$\begin{aligned} P_0(\mathbf{r},\mathbf{r}',\mathrm{i}\,\tau) =& \tilde{G}(\mathbf{r},\mathbf{r}',\mathrm{i}\,\tau)\tilde{G}(\mathbf{r}',\mathbf{r},-\mathrm{i}\,\tau) \\ &+ \sum_{\alpha\beta} Q_{\alpha\beta}(\mathbf{r}')\tilde{G}(\mathbf{r},\alpha,\mathrm{i}\,\tau)\tilde{G}(\beta,\mathbf{r},-\mathrm{i}\,\tau) \\ &+ \sum_{\mu\nu} Q_{\mu\nu}(\mathbf{r})\tilde{G}(\nu,\mathbf{r}',\mathrm{i}\,\tau)\tilde{G}(\mathbf{r}',\mu,-\mathrm{i}\,\tau) \\ &+ \sum_{\mu\nu\alpha\beta} Q_{\mu\nu}(\mathbf{r})Q_{\alpha\beta}(\mathbf{r}')\tilde{G}(\nu,\alpha,\mathrm{i}\,\tau)\tilde{G}(\beta,\mu,-\mathrm{i}\,\tau). \end{aligned} \tag{6.24}$$

With this result for the polarizability in the PAW, the RPA correlation can be calculated from the PAW orbitals / Green's functions by inserting Eq. (6.24) into Eq. (6.14).

When it comes to the calculation of derivatives of the RPA correlation energy in the PAW, one needs to take into account changes of the projectors $\tilde{p}$ and the augmentation charges Q_{ij}. These give rise to PAW related force terms. Also, since the pseudo orbitals are solutions to the generalized eigenvalue problem Eq. (6.11), one needs to take the overlap operator S into account when considering the Dyson equation / perturbation series for the Green's function. These issues will be examined in detail in chapter 7.

Part II

Derivatives in the RPA

Chapter 7

Forces

This chapter is dedicated to the core topic of this thesis, the calculation of (non-Hellmann-Feynman) first order derivatives of the RPA energy in solids. The first two sections 7.1 and 7.2 were already published by the author of this thesis and co-authors in a peer reviewd article [1]. These sections lay out the fundamental concepts for the calculation of RPA forces in solids and show some illustrative applications. In section 7.3, more details are given on how the additional terms arising from the PAW method are treated.

Note that in this part, we adopt a slightly different notation than in the theory part I, in order to increase the readability of the equations. We drop the label "RPA" for the screened interaction as well as the "0" for the mean-field Green's function, because in the following chapters we only consider the screened interaction in the RPA and will only use the mean-field Green's function for our calculations:

privious chapters		this chapter	
$W^{\mathrm{RPA}} = W^0$	$\rightarrow$	W	(7.1)
$G^{\mathrm{MF}} = G^0$	$\rightarrow$	G	(7.2)
$P_{\mathrm{MF}} = P_0$	$\rightarrow$	χ	(7.3)
$\Sigma_{\mathrm{RPA}} = \Sigma_c^{\mathrm{G^0W^0}}$	$\rightarrow$	Σ_{GW} .	(7.4)

Also, note that in accordance with the notation adopted in our publication [1], in this chapter we use the Greek letter ρ for the density (operator) instead of n.

7.1 Analytic interatomic forces in the random phase approximation

We discuss that in the random phase approximation (RPA) the first derivative of the energy with respect to the Green's function is the self-energy in the GW approximation. This relationship allows to derive compact equations for the RPA interatomic forces. We also show that position dependent overlap operators are elegantly incorporated in the present framework. The RPA force equations have been implemented in the projector augmented wave formalism, and we present illustrative applications, including *ab initio* molecular dynamics simulations, the calculation of phonon dispersion relations for diamond and graphite, as well as structural relaxations for water on boron nitride. The present derivation establishes a concise framework for forces within perturbative approaches and is also applicable to more involved approximations for the correlation energy.

Density functional theory (DFT) is almost ubiquitous in present day chemistry, computational and materials sciences. Compared to other methods, one of the great advantages of DFT is that forces between the atoms are readily computable, so that relaxed groundstate structures, vibrational properties, as well as finite temperature properties of any material are straightforwardly accessible. Although quantum chemists have devised ways to compute analytic forces e.g. for Møller-Plesset perturbation theory (MP) already decades ago [106, 107], in condensed matter simulations forces beyond DFT have been rarely available. This has limited the success of more involved electronic structure methods such as the random phase approximation (RPA) for solids. Only recently, this situation has improved, with first derivatives being computable for MP2 for solids [108], as well as for the RPA for molecules [37, 36]. However, to date all these implementations are limited to real valued Gaussian type orbitals and even then the algebra is often intricate.

Here we use Green's function theory, to derive compact equations for the forces in the random phase approximation. These can be recapped in two lines. One first calculates a Hermitian first order one-particle density matrix

$$\rho^{(1)} = \frac{1}{2\pi} \int_{-\infty}^{\infty} \mathrm{d}\nu \, G(\mathrm{i}\,\nu)(F + \Sigma_{\mathrm{GW}}(\mathrm{i}\,\nu))G(\mathrm{i}\,\nu), \tag{7.5}$$

involving the Fock operator F, the correlation part of the self-energy in the GW approximation Σ_{GW}, and the independent particle Green's function $G(\mathrm{i}\,\nu)$ of the Kohn-Sham (KS) Hamiltonian. Then one needs to trace this density matrix over the first derivate of the KS Hamiltonian $F_i = -\operatorname{Tr}[\rho^{(1)}\,\partial H_{\mathrm{KS}}/\partial R_i]$, where R_i are the ionic coordinates and F_i is the corresponding component of the force. We have implemented the corresponding equations in the projector augmented wave [104, 105] formalism and show the potential of this method in the present chapter.

The fundamental problem we address here is that perturbation theory (including the RPA) is non-variational, *i.e.* the kinetic, Hartree, exchange, and correlation energies are evaluated using a set of orbitals calculated using some other zero-order

Hamiltonian. For the purpose of this presentation, we assume that these one-electron orbitals are always determined using a KS Hamiltonian H. We rely on Green's function theory and establish the essentials first and then proceed to an outline of the derivation. Given the generalized eigenvalue equation

$$H\,|n\rangle = \epsilon_n S\,|n\rangle\,, \tag{7.6}$$

with a KS Hamiltonian H and an overlap operator S, the time dependent Schrödinger equation reads

$$(\mathrm{i}\,S\partial/\partial t - H)\,|n\rangle = 0. \tag{7.7}$$

Then the single particle KS Green's function G can be written as:

$$G(\mathrm{i}\,\nu) := (\mathrm{i}\,\nu S - H)^{-1}. \tag{7.8}$$

In the present paper, the Green's functions are represented in imaginary frequency $\mathrm{i}\,\nu$ and time $\mathrm{i}\,\tau$, where they are smooth functions of their arguments. The Fermi-level is placed at $\mu = 0$; occupied (unoccupied) states have all negative (positive) one-electron energies.

Green's function theory allows to write compactly the change of the Green's function upon perturbations. This is achieved by the Dyson equation, which relates the perturbed Green's function $G + \Delta G$ corresponding to $H + \Delta H$ and $S + \Delta S$ to the unperturbed Green's function G:

$$\begin{aligned} (G + \Delta G)^{-1} &= G^{-1} - (\Delta H - \mathrm{i}\,\nu \Delta S) \qquad \Leftrightarrow \\ (G + \Delta G) \quad &= G + G(\Delta H - \mathrm{i}\,\nu \Delta S)(G + \Delta G). \end{aligned} \tag{7.9}$$

Neglecting ΔG on the r.h.s. of the second line, one obtains for the change of the Green's function ΔG the first order term

$$G^{(1)}(\mathrm{i}\,\nu) = G(\mathrm{i}\,\nu)(\Delta H - \mathrm{i}\,\nu \Delta S) G(\mathrm{i}\,\nu). \tag{7.10}$$

It is noted that ΔH is the total change of the KS Hamiltonian including the self-consistent field changes.

The Green's function in imaginary time can be obtained by a Fourier transformation:

$$G(\mathrm{i}\,\tau) = \frac{1}{2\pi} \int_{-\infty}^{\infty} G(\mathrm{i}\,\nu) e^{-\mathrm{i}\,\nu\tau} \mathrm{d}\nu. \tag{7.11}$$

Using standard mathematical relations, it is easy to show that one can also write [60, 109]:

$$G(\mathrm{i}\,\tau) = \begin{cases} \sum_{j \in occ.} |j\rangle \langle j|\, e^{-\tau \epsilon_j} & \tau < 0 \\ -\sum_{a \in virt.} |a\rangle \langle a|\, e^{-\tau \epsilon_a} & \tau > 0. \end{cases} \tag{7.12}$$

Here the sums are restricted to the occupied (occ.) manifold for negative τ and to

the unoccupied or virtual (virt.) manifold for positive τ, and thus the exponents are always bound. Clearly [see Eq. (7.12)], the one-particle density operator ρ is given by the Green's function for $\tau \to 0^-$, *i.e.* for a slightly negative imaginary time

$$\rho = \lim_{\tau \to 0^-} G(\mathrm{i}\,\tau) = G(\mathrm{i}\,\eta), \tag{7.13}$$

where $\eta = 0^-$ is a small negative infinitesimal.

We now proceed to calculate first derivatives of the Hartree-Fock energy functional. This functional depends on the density matrix ρ and an external potential v_{ext}: $E = E_{\mathrm{HF}}[\rho, v_{\mathrm{ext}}]$. The total variation is

$$\delta E_{\mathrm{HF}} = \underbrace{\mathrm{Tr}\left[\frac{\delta E_{\mathrm{HF}}}{\delta v_{\mathrm{ext}}}\delta v_{\mathrm{ext}}\right]}_{\text{Hellmann-Feynman}} + \underbrace{\mathrm{Tr}\left[\frac{\delta E_{\mathrm{HF}}}{\delta \rho}\delta\rho\right]}_{\text{non-Hellmann-Feynman}} . \tag{7.14}$$

The trace operator usually involves integrals over one (for the variations of the external potential) or two spatial coordinates (for variations of the density matrix). If one calculates the HF energy derivatives at the HF density matrix ρ_{HF}, terms related to variations of the density matrix do not need to be calculated, since the Hartree-Fock density matrix fulfills the equation

$$\mathrm{Tr}\left[\frac{\delta E_{\mathrm{HF}}}{\delta \rho}\delta\rho\right]_{\rho=\rho_{\mathrm{HF}}} = \mathrm{Tr}\left[F\delta\rho\right]_{\rho=\rho_{\mathrm{HF}}} = 0, \tag{7.15}$$

where $\delta\rho$ is subject to the the orthonormality constraint of the corresponding basis functions and $\delta E_{\mathrm{HF}}/\delta\rho$ is the Fock operator F. In this case the second term in Eq. (7.14) vanishes, which is just the famous Hellmann-Feynman theorem.

If the random phase approximation is used on top of a DFT calculation (e.g. RPA@PBE), the Hartree-Fock energy functional, however, needs to be evaluated at the KS density matrix. The corresponding energy is commonly referred to as exact exchange energy (EXX) [110]. The non-Hellmann-Feynman term is then non-zero. Using Green's functions, we can write this term compactly by combining Eqs. (7.10), (7.11) and (7.13). For the non-Hellmann-Feynman term in Eq. (7.14) one then obtains

$$\frac{1}{2\pi}\int_{-\infty}^{\infty} \mathrm{d}\nu\, \mathrm{Tr}\left[F\, G(\mathrm{i}\,\nu)(\delta H - \mathrm{i}\,\nu\delta S)G(\mathrm{i}\,\nu)e^{-i\nu\eta}\right], \tag{7.16}$$

where the Fock operator F is constructed from the KS density matrix. Equation (7.16) looks expensive to evaluate, since, seemingly, for any change of the Hamiltonian $G(\mathrm{i}\,\nu)\delta H G(\mathrm{i}\,\nu)$ needs to be calculated. However, since the trace is invariant

under cyclic permutations, one can calculate two Hermitian matrices,

$$\begin{aligned}\rho^{(1)}_{\mathrm{EXX}} &= \frac{1}{2\pi}\int_{-\infty}^{\infty} \mathrm{d}\nu\, G(\mathrm{i}\,\nu) F G(\mathrm{i}\,\nu) e^{-i\nu\eta} \\ \gamma^{(1)}_{\mathrm{EXX}} &= \frac{i}{2\pi}\int_{-\infty}^{\infty} \mathrm{d}\nu\, \nu\, G(\mathrm{i}\,\nu) F G(\mathrm{i}\,\nu) e^{-i\nu\eta}\end{aligned} \tag{7.17}$$

once and then efficiently calculate the energy change for any variation of the KS Hamiltonian and overlap operator as

$$\frac{\partial E}{\partial R_i} = \mathrm{Tr}\Big[\rho^{(1)}\,\frac{\partial H}{\partial R_i} - \gamma^{(1)}\,\frac{\partial S}{\partial R_i}\Big]. \tag{7.18}$$

We note that $\rho^{(1)}$ is a density matrix, whereas $\gamma^{(1)}$ has the dimension of an energy (first moment $i\nu$). Furthermore, since F is frequency independent, the integrals in Eq. (7.17) can be calculated analytically using the residue theorem, where the term involving $\eta = 0^-$ specifies how the contours need to be closed (see section 7.2).

This equation can be straightforwardly generalized to correlation energy functionals that depend on the Green's function $E_c = E_c[G]$. Since the correlation energy usually does not depend on the external potential, the Hellmann-Feynman term is zero for this contribution. The non-Hellmann-Feynman term yields an additional contribution to the matrices,

$$\begin{aligned}\rho^{(1)}_{c} &= \frac{1}{2\pi}\int_{-\infty}^{\infty} \mathrm{d}\nu\, G(\mathrm{i}\,\nu) \Sigma_c(\mathrm{i}\,\nu) G(\mathrm{i}\,\nu), \\ \gamma^{(1)}_{c} &= \frac{i}{2\pi}\int_{-\infty}^{\infty} \mathrm{d}\nu\, \nu\, G(\mathrm{i}\,\nu) \Sigma_c(\mathrm{i}\,\nu) G(\mathrm{i}\,\nu),\end{aligned} \tag{7.19}$$

where the self-energy Σ_c is the functional derivative of the correlation energy with respect to the Green's function $\Sigma_c(\mathrm{i}\,\nu) = \delta E_c / \delta G(\mathrm{i}\,\nu)$. Eq. (7.19) is obviously analogous to Eq. (7.17), only the Fock operator F has been replaced by the self-energy. Furthermore, the exponential $e^{-i\nu\eta}$ can be dropped, since the integrand decays like $o(1/\nu^2)$, and the integral is unconditionally convergent.

For the correlation energy in the random phase approximation, E_{RPA}, the corresponding self-energy is exactly the correlation part of the GW approximation to the self-energy in Hedin's approach [66], which we rationalize now. The RPA correlation energy is defined as [79, 27, 111, 112, 113, 30, 86]:

$$E_{\mathrm{RPA}} = \frac{1}{2\pi}\int_{0}^{\infty} \mathrm{d}\nu\, \mathrm{Tr}[\ln(1 - \chi(\mathrm{i}\,\nu)\,\mathrm{v}) + \chi(\mathrm{i}\,\nu)\,\mathrm{v}], \tag{7.20}$$

where $\chi(\mathrm{i}\,\nu)$ is the independent particle polarizability calculated using KS orbitals, and v is the Coulomb kernel. The derivative with respect to $\chi(\mathrm{i}\,\nu)$ can be calculated by Taylor expanding the logarithm and taking the derivative (see also [114]). This

yields the correlation part of the screened Coulomb potential

$$-\frac{\delta E_{\mathrm{RPA}}}{\delta\chi(\mathrm{i}\,\nu)} = W_c(\mathrm{i}\,\nu) = \mathrm{v}\,\chi(\mathrm{i}\,\nu)\,\mathrm{v} + \mathrm{v}\,\chi(\mathrm{i}\,\nu)\,\mathrm{v}\,\chi(\mathrm{i}\,\nu)\,\mathrm{v} + \ldots\,. \tag{7.21}$$

Using the relation between the independent particle polarizability and the Green's function [66]

$$\chi(\mathbf{r},\mathbf{r}',\mathrm{i}\,\tau) = G(\mathbf{r},\mathbf{r}',\mathrm{i}\,\tau)G(\mathbf{r}',\mathbf{r},-\mathrm{i}\,\tau), \tag{7.22}$$

one formally obtains the desired relation (dropping the position coordinates):

$$\begin{aligned}\frac{\delta E_{\mathrm{RPA}}}{\delta G(\mathrm{i}\,\tau)} &= \frac{\delta E_{\mathrm{RPA}}}{\delta\chi(\mathrm{i}\,\tau)}\frac{\delta\chi(\mathrm{i}\,\tau)}{\delta G(\mathrm{i}\,\tau)} = -W_c(\mathrm{i}\,\tau)G(-\mathrm{i}\,\tau) \\ &= \Sigma_{\mathrm{GW}}(\mathrm{i}\,\tau).\end{aligned} \tag{7.23}$$

Details are given in the next section 7.2.

In summary, non-Hellmann-Feynman forces are simple to evaluate. One only needs to determine the one particle density matrix $\rho^{(1)}$ and its first energy moment $\gamma^{(1)}$, Eqs. (7.17) and (7.19) and then evaluate Eq. (7.18). The first derivative of the self-consistent density functional theory Hamiltonian $\partial H/\partial R_i$ and of the overlap operator $\partial S/\partial R_i$ need to be calculated for each ionic displacement, δR_i, yielding one component in the atomic forces.

Concerning the scaling, we note that we have recently implemented an algorithm that calculates the GW self-energy with linear scaling in the number of k-points and cubic scaling in the number of plane waves [63] following the work of Rojas, Godby and Needs [60, 61]. The algorithm is designed to use a minimal number of time and frequency points, with 12 points yielding μeV accuracy per atom for gapped systems [35, 62]. The scaling with the number of plane waves and k-points carries over to the calculation of the density matrices, so that the complexity of the entire calculation is, in principle, identical to standard DFT, but with much larger prefactors. In practice, the compute time required for one force calculation in the RPA is about three orders of magnitude higher than for semi-local functionals, about 10-50 times higher than for hybrid functionals (albeit scaling quadratically in the number of k-points), and about 10 times higher than for a single RPA total energy calculation. One reason for the steep computational cost is that the calculation of the GW self-energy requires about 6 times more operations than an RPA total energy calculation. Furthermore, the evaluation of $\partial H/\partial R_i$ for each ionic displacement is currently done using linear response theory and can take about the same time as the calculation of $\rho^{(1)}$ and $\gamma^{(1)}$ for systems with hundreds of atoms. On the positive side, $\mathrm{G_0W_0}$ quasiparticle energies for all orbitals are readily available and can be calculated *en passant*.

We have implemented the RPA forces in the projector augmented wave (PAW) [104, 105] based Vienna ab initio simulation package (VASP). Typically we can obtain 5 digits accuracy compared to a numerical differentiation, and the precision increases as the number of time points increases (see section 7.2). A

rigorous test for the validity of forces are first principles molecular dynamics (MD) simulations, since errors in the forces will result in a drift of the total energy. In Fig. 7.1 we show results for short simulations of crystalline diamond at 2000 K. The configurations were initially equilibrated using DFT, and then about 250 RPA-MD steps were performed. For the 64 atom supercell, one time step took 20 minutes on 40 Intel Xeon v3 cores. It is clear that the energy conservation is excellent for both the small 8 atom diamond cell, as well as the 64 atom cell.

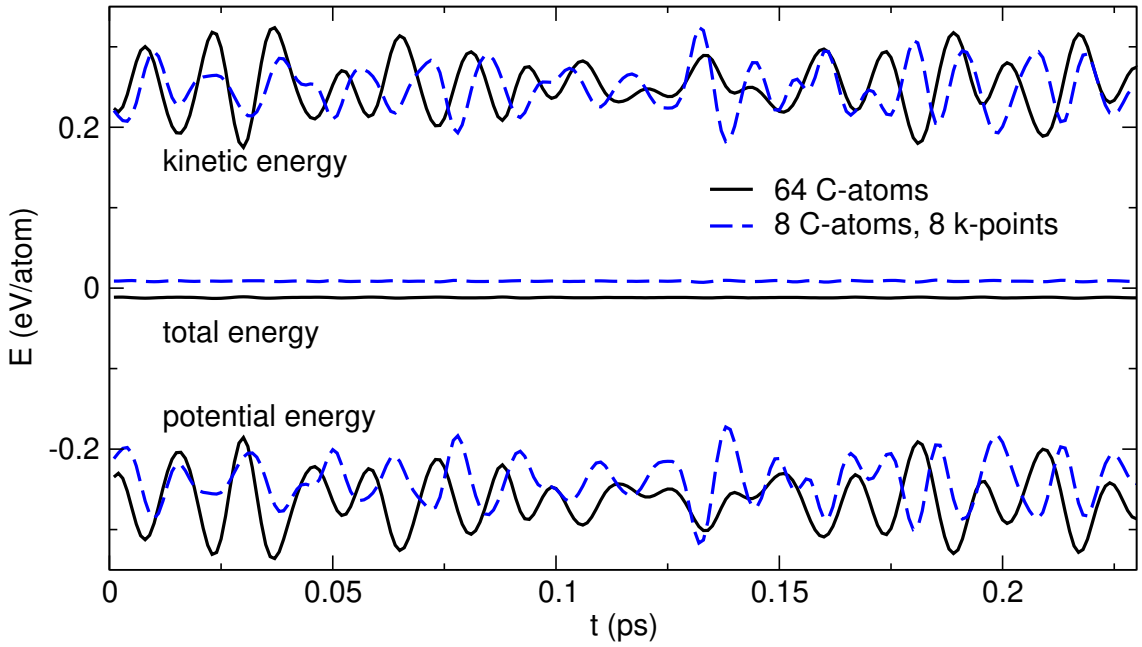

Figure 7.1: Potential and kinetic energy per atom for diamond supercells of 64 and 8 atoms, using the Γ-point and $2 \times 2 \times 2$ k-points, respectively. Energies are shifted so that the total energies approach zero. The slight fluctuations in the total energy are similar to those observed in DFT for a 1 fs time step using a Verlet algorithm.

Relaxations to the ionic groundstate structure are also feasible and fairly efficient using the present code. One advantage of the present approach is that the second ionic derivatives of the density functional E_{KS}, that is used to calculate the orbitals, are calculated when the linear response code is used. This implies that the KS Hessian matrix A is available

$$A_{ij} = \frac{\partial^2 E_{\mathrm{KS}}}{\partial R_i \partial R_j}$$

and this Hessian can be used as preconditioner for the update of the ionic positions $\mathbf{r}$

$$\mathbf{r} \leftarrow \mathbf{r} - \mathbf{A}^{-1}\mathbf{F},$$

where $\mathbf{F}$ are the RPA forces. If the RPA Hessian is close to the KS Hessian, conver-

gence to the ionic RPA groundstate is quadratic and hence, in practice, the forces often decrease by an order of magnitude in each step. Being able to relax structures adds a new important facet to the modeling of materials beyond density functional theory.

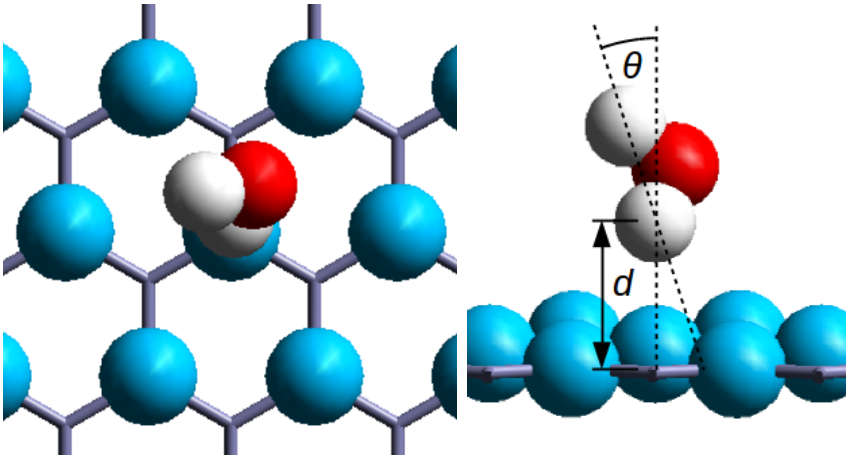

Figure 7.2: RPA relaxed geometry for H_2O adsorbed on BN. A 3×3 unit cell and $3 \times 3 \times 1$ k-points were used.

Here we have looked at one prototypical problem, H_2O adsorption on a BN layer [115, 116]. We have relaxed the H_2O molecule using the RPA and find after few steps a low symmetry configuration atop the N atom that was previously not considered. The main reason for finding this configuration was the use of the DFT Hessian as pre-conditioner which results in a rapid rotation of the molecule along a very soft mode. All used functionals confirmed that this position is lower in energy than the previously considered structures (6 meV in the RPA). In Tab. 7.1, we summarize the geometry and adsorption energy.

Table 7.1: Considered functionals with hydrogen to surface distance d and angle θ between the H-H axis and the surface normal (see Fig. 7.2) and adsorption energy E.

	d(Å)	θ(°)	E(meV)
PBE (Perdew-Burke-Ernzerhof) [9]	2.48	18	40
HSE (Heyd et al.) hybrid functional [19]	2.49	17	34
D3 (Grimme dispersion correct.) [117]	2.34	19	142
TS (Tkatchenko-Scheffler) [14]	2.33	19	152
MBD (many body dispersion) [118]	2.33	18	136
optPBE, vdW DFT functional [119]	2.31	14	132
RPA (random phase approximation)	2.39	16	92

The equilibrium distance to the surface decreases with increasing adsorption energy, with PBE and HSE yielding too small adsorption energies and too large distances. The vdW corrected functionals generally yield larger adsorption energies and shorter distances than RPA. We expect the RPA to be accurate here, since RPA parameterized force fields yield excellent contact angles for water droplets [116]. However, RPA generally overestimates the Pauli repulsion, with singles increasing the adsorption energy by 20 meV [120].

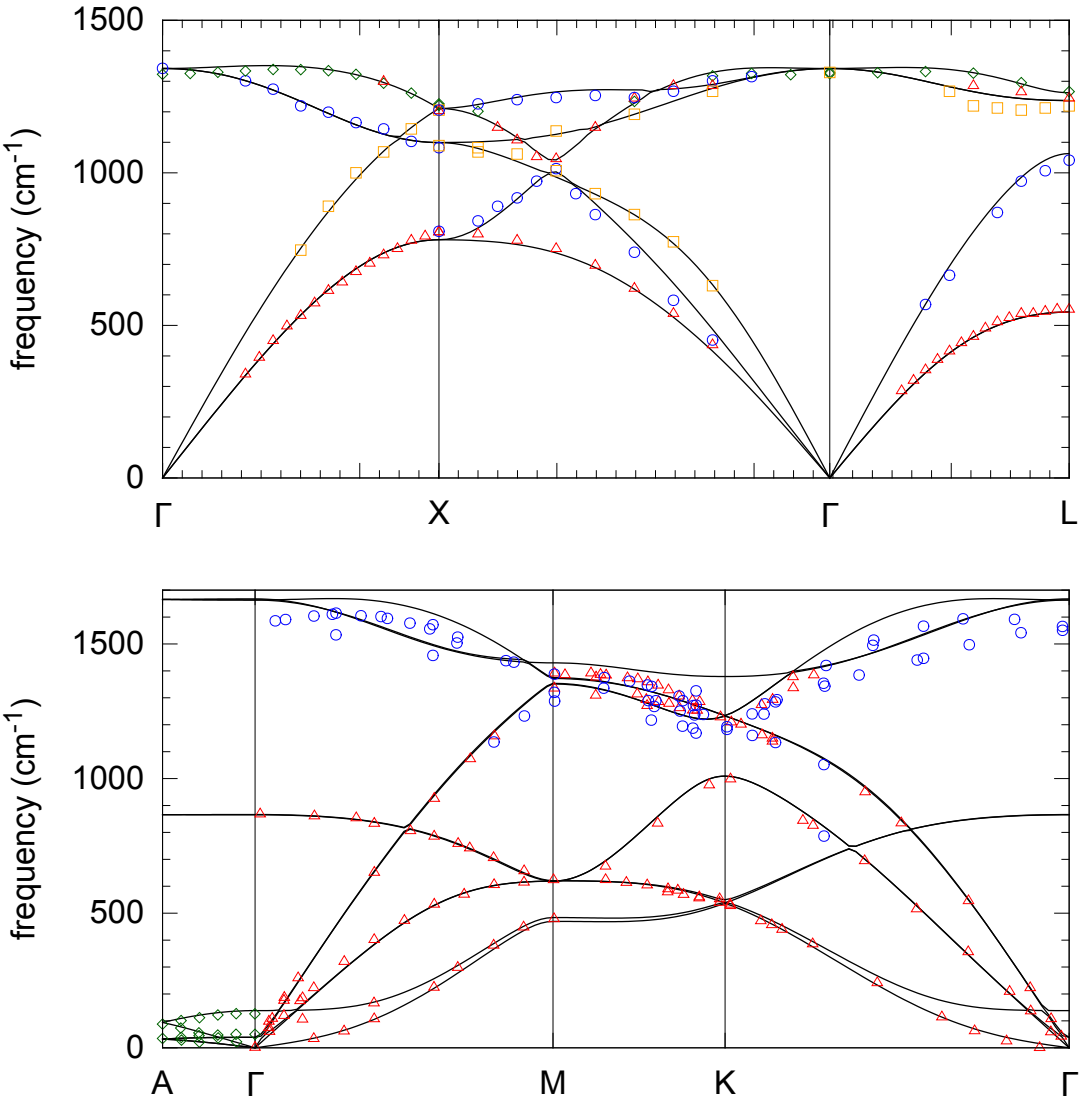

Figure 7.3: Phonon dispersion relation of diamond and graphite calculated using 128 atom supercells. RPA calculations were performed at the Γ-point, with k-point sampling errors corrected for using DFT. Experimental data and lattice constants are taken from Ref. [121, 122, 123, 124, 125].

To demonstrate that the random phase approximation yields also very good vibrational properties, we have calculated the phonon dispersion relation of diamond and graphite (see Fig. 7.3). We note that the random phase approximation yields excellent structural properties for both, diamond and graphite, with lattice constants in virtually perfect agreement with experiment [31, 33]. For the phonons, agreement between the RPA and experiment is also excellent for diamond and very good for graphite. Although phonon dispersions from DFT (not shown) can be in very good agreement with experiment, they are often under- (semi-local functionals) or overestimated (hybrid functionals) [126, 127].

In summary, we have presented an elegant scheme to calculate interatomic forces using many body perturbation theory. The derivation relies on Green's functions and the self-energy and seamlessly incorporates position dependent overlap operators. Although applied to the RPA here, analogous expressions can easily be derived for e.g. second order MP perturbation theory (MP2), with the RPA self-energy Σ_{GW} simply replaced by the self-energy in second order $\Sigma^{(2)}$. Our derivation involves a first order one-particle density matrix, and we note that seemingly related density matrices can be found in quantum chemistry literature but without reference to a self-energy [106, 107, 128, 36, 37]. We have put our equations to test by implementing them in a plane wave code, and we have demonstrated that MD simulations, relaxations and predictions of phonon frequencies are possible. We are convinced that the present work paves the way towards accurate beyond DFT modeling in condensed matter physics and materials sciences.

7.2 Methodical details for RPA forces

7.2.1 Outline and definitions for methodical details

In the subsequent sections, we will work out the equations in much greater detail than in the previous chapter. We show that the non-Hellmann-Feynman forces can be calculated as

$$\mathbf{F} = -\operatorname{Tr}\left[\rho^{(1)}\nabla_{\mathbf{R}} v^{\mathrm{KS}} - \gamma^{(1)}\nabla_{\mathbf{R}} S\right]. \tag{7.24}$$

and that the operators $\rho^{(1)}$ and $\gamma^{(1)}$ can be associated with the functional derivatives $\delta E/\delta v^{\mathrm{KS}}$ and $\delta E/\delta S$ respectively. Note that in the following, $\mathbf{F}$ is always the non-Hellmann-Feynman force. Details on the calculation of Hellmann-Feynman forces within VASP can be found e.g. in [105].

In principle, the Kohn-Sham (KS) potential v^{KS} is a purely local potential that reproduces the correct electron density of a many electron system. However in practice, there are many methods (e.g. the projector augmented wave (PAW) method) that increase the computing efficiency by using pseudo potentials which often require to include non-local terms. Therefore we will consider v^{KS} to be generally non-local, and as a result we will need to consider also the off-diagonal elements of $\rho^{(1)}$ and $\gamma^{(1)}$ in real space.

We will first calculate $\rho^{(1)}$ for the Hartree-Fock/EXX part of the energy, E_{EXX}, by

using standard perturbation theory and than show that the formulation with Green's functions is equivalent. The operator $\gamma^{(1)}$ will be also calculated for E_{EXX} and both operators will be expressed in terms of KS-orbitals by analytically performing the integration over the imaginary frequency ν. Next we will show that the functional derivative $\delta E_{\mathrm{RPA}}/\delta G$ corresponds to the correlation part of the self-energy in the GW approximation Σ_{GW}.

In order to give the reader a compact description we will first give several definitions concerning the notation. We will need functional derivatives w.r.t. to multi variate functions. For a better readability, we define

$$\frac{\delta E[X]}{\delta X(\mathbf{r}', \mathbf{r})} := \frac{\delta E[X]}{\delta X}(\mathbf{r}, \mathbf{r}'), \tag{7.25}$$

so that we may write

$$\delta E = \int \mathrm{d}\mathbf{r}\mathrm{d}\mathbf{r}' \frac{\delta E[X]}{\delta X}(\mathbf{r}, \mathbf{r}')\delta X(\mathbf{r}', \mathbf{r}) = \mathrm{Tr}\{\frac{\delta E}{\delta X}\delta X\} \tag{7.26}$$

with the trace operation Tr.

In the RPA, the total energy is given as the sum of the exact exchange energy E_{EXX} and the RPA correlation energy E_{RPA}. Here we use the terminology $E_{\mathrm{EXX}}[\rho, v_{\mathrm{ext}}]$ to indicate that the functional is evaluated at a specific density matrix ρ (obtained for example by density functional theory). The energy functional for the RPA is then:

$$E = E_{\mathrm{EXX}}[\rho, v_{\mathrm{ext}}] + E_{\mathrm{RPA}}[G]. \tag{7.27}$$

In KS theory, the one particle density operator is simply given by a sum over all projectors on occupied states

$$\rho = \sum_{i \in occ.} |i\rangle \langle i| . \tag{7.28}$$

With this, E_{EXX} can be written in terms of the density matrix $\rho(\mathbf{r}, \mathbf{r}') = \langle \mathbf{r}|\rho|\mathbf{r}'\rangle$ as

$$E_{\mathrm{EXX}} = \mathrm{Tr}\left[(T + v_{\mathrm{ext}})\rho\right] + E_{\mathrm{H}}[\rho] + E_{\mathrm{x}}[\rho] \tag{7.29}$$

with the Hartree energy

$$E_{\mathrm{H}}[\rho] = \frac{1}{2}\int \mathrm{d}\mathbf{r}\mathrm{d}\mathbf{r}' \frac{\rho(\mathbf{r}, \mathbf{r})\rho(\mathbf{r}', \mathbf{r}')}{|\mathbf{r} - \mathbf{r}'|} \tag{7.30}$$

the exchange energy

$$E_{\mathrm{x}}[\rho] = -\frac{1}{2}\int \mathrm{d}\mathbf{r}\mathrm{d}\mathbf{r}' \frac{\rho(\mathbf{r}, \mathbf{r}')\rho(\mathbf{r}', \mathbf{r})}{|\mathbf{r} - \mathbf{r}'|} \tag{7.31}$$

as well as the kinetic energy operator T and the external potential v_{ext}.

Note that in Eq. (7.30) and (7.31) we neglected the spin degrees of freedom.

Actually one would need to consider the density matrix $\rho(\mathbf{x}, \mathbf{x}') = \langle \mathbf{x}|\rho|\mathbf{x}'\rangle = \langle \mathbf{r}, \sigma|\rho|\mathbf{r}', \sigma'\rangle \propto \delta_{\sigma\sigma'}$ and sum over spin coordinates σ, σ' in addition to the integration over spatial coordinates $\mathbf{r}, \mathbf{r}'$. Therefore, the numerator in the integrand of the exchange energy in Eq. (7.31) would actually be $\rho_\downarrow(\mathbf{r}, \mathbf{r}')\rho_\downarrow(\mathbf{r}', \mathbf{r}) + \rho_\uparrow(\mathbf{r}, \mathbf{r}')\rho_\uparrow(\mathbf{r}', \mathbf{r})$, cf. Eq. (2.49) and (2.50). However, to keep the notation compact, we will disregard spin in this section. In principle the formulas can be easily extended to include spin by introducing the substitutions shown in Eq. (1.146).

The correlation energy in the RPA, E_{RPA}, can be derived from the adiabatic connection dissipation-fluctuation theorem and is given by Eq. (7.20). The independent particle polarizability χ in turn, can be expressed in terms of Green's functions using Hedin's equation (7.22) so that the E_{RPA} is in principle a functional of the Green's function.

7.2.2 Force calculation for E_{EXX} using perturbation theory

The total non-Hellmann-Feynman force $\mathbf{F}_{\mathrm{EXX}}$ originating from E_{EXX} can be formally written as

$$\mathbf{F}_{\mathrm{EXX}} = -\int \frac{\delta E_{\mathrm{EXX}}}{\delta\rho(\mathbf{r}, \mathbf{r}')} \nabla_{\mathbf{R}} \rho(\mathbf{r}, \mathbf{r}') \mathrm{d}\mathbf{r}\mathrm{d}\mathbf{r}'. \tag{7.32}$$

To calculate $\mathbf{F}_{\mathrm{EXX}}$ explicitly, one can use first order perturbation theory to calculate $\delta\rho$ or $\nabla_{\mathbf{R}}\rho(\mathbf{r}, \mathbf{r}')$ respectively:

$$\nabla_{\mathbf{R}}\rho(\mathbf{r}, \mathbf{r}') = \langle \mathbf{r}| \sum_{\substack{in \\ i\in occ. \\ n\neq i}} \frac{|i\rangle \langle i| \nabla_{\mathbf{R}} v_{\mathrm{KS}} |n\rangle \langle n|}{\epsilon_i - \epsilon_n} + h.c. \, |\mathbf{r}'\rangle \,, \tag{7.33}$$

with n going over occ. and virt. states. The other factor in the integral in Eq. (7.32) can be easily calculated as:

$$\begin{aligned} \frac{\delta E_{\mathrm{EXX}}}{\delta\rho(\mathbf{r}, \mathbf{r}')} =& \delta(\mathbf{r} - \mathbf{r}') \left(\nabla^2_{\mathbf{R}} + v_{\mathrm{ext}}(\mathbf{r})\right) + \\ &+ \int \mathrm{d}\mathbf{r}'' \frac{\rho(\mathbf{r}'', \mathbf{r}'')}{|\mathbf{r}'' - \mathbf{r}|} \delta(\mathbf{r} - \mathbf{r}') - \frac{\rho(\mathbf{r}', \mathbf{r})}{|\mathbf{r}' - \mathbf{r}|} \\ =& \langle \mathbf{r}'| \underbrace{T + v_{\mathrm{ext}} + v_{\mathrm{H}} + v_{\mathrm{x}}}_{F} |\mathbf{r}\rangle \,, \end{aligned} \tag{7.34}$$

with the Fock operator F. The same result shall in the following be obtained by means of a Green's function formalism to familiarize the idea to be used for the correlation part.

7.2.3 Force calculation with Green's functions

Assume the energy can be expressed as a functional of the Green's function G and the external potential v_{ext}, as it is the case for the total RPA energy, then the force can be calculated by

$$\begin{aligned}\mathbf{F}_{\text{total}} =& \mathbf{F}_{\text{non-Hellmann-Feynman}} + \mathbf{F}_{\text{Hellmann-Feynman}} \\ =& -\int \frac{\delta E}{\delta G(\mathbf{r}, \mathbf{r}', \mathrm{i}\,\nu)} \nabla_{\mathbf{R}} G(\mathbf{r}, \mathbf{r}', \mathrm{i}\,\nu) \mathrm{d}\mathbf{r}\mathrm{d}\mathbf{r}'\mathrm{d}\nu \\ & -\int \frac{\delta E}{\delta v_{\text{ext}}(\mathbf{r}, \mathbf{r}')} \nabla_{\mathbf{R}} v_{\text{ext}}(\mathbf{r}, \mathbf{r}') \mathrm{d}\mathbf{r}\mathrm{d}\mathbf{r}'. \end{aligned} \tag{7.35}$$

The second term in Eq. (7.35) is the Hellmann-Feynman force while the first term is an additional term that would vanish if the energy functional was stationary with respect to G. As already mentioned above, in the following, only this additional term $\mathbf{F}_{\text{non-Hellmann-Feynman}}$ shall be discussed while the Hellmann-Feynman force is no longer considered and we drop the subscript "non-Hellmann-Feynman".

The derivative of the (KS) Green's function with respect to atomic positions $\mathbf{R}$ can be derived from the Dyson equation (7.9). Concerning the KS-Hamiltonian, the perturbation caused by shifting atomic positions ultimately effects the effective potential v_{KS} only. Therefore ΔH in the Dyson equation (7.9) is simply replaced by Δv_{KS}, which is the variation of the (KS) effective potential. Since many pseudo potential implementations use non-local effective potentials, in the following the KS potential is allowed to be generally non-local. Neglecting the overlap operator in Eq. (7.9) we get

$$\begin{aligned} &(G + \Delta G)(\mathrm{i}\,\nu) = G(\mathrm{i}\,\nu) + G(\mathrm{i}\,\nu)\Delta v_{\text{KS}} G(\mathrm{i}\,\nu) + \mathcal{O}(\Delta v_{\text{KS}}^2) \\ &\Rightarrow \nabla_{\mathbf{R}} G = G(\nabla_{\mathbf{R}} v_{\text{KS}})G \\ &\nabla_{\mathbf{R}} G(\mathbf{r}, \mathbf{r}', \mathrm{i}\,\nu) = \\ &\int \mathrm{d}\mathbf{r}''\mathrm{d}\mathbf{r}''' G(\mathbf{r}, \mathbf{r}'', \mathrm{i}\,\nu)(\nabla_{\mathbf{R}} v_{\text{KS}}(\mathbf{r}'', \mathbf{r}'''))G(\mathbf{r}''', \mathbf{r}', \mathrm{i}\,\nu). \end{aligned} \tag{7.36}$$

If we insert this result in the second line of Eq. (7.35), we may rewrite $\mathbf{F}$ as

$$\mathbf{F} = -\int \mathrm{d}\nu \mathrm{d}\mathbf{r}'' \mathrm{d}\mathbf{r}''' \Bigg\{ \nabla_{\mathbf{R}} v_{\mathrm{KS}}(\mathbf{r}'', \mathbf{r}''') \times \tag{7.37}$$

$$\underbrace{\int G(\mathbf{r}''', \mathbf{r}', \mathrm{i}\,\nu) \frac{\delta E}{\delta G(\mathbf{r}, \mathbf{r}', \mathrm{i}\,\nu)} G(\mathbf{r}, \mathbf{r}'', \mathrm{i}\,\nu) \mathrm{d}\mathbf{r} \mathrm{d}\mathbf{r}'}_{\frac{\delta E}{\delta v_{\mathrm{KS}}}(\mathbf{r}''', \mathbf{r}'', \mathrm{i}\,\nu)} \Bigg\}$$

and by using the notation defined in Eq. (7.26) this can be expressed in the condensed form

$$\mathbf{F} = -\int \mathrm{d}\nu \, \mathrm{Tr} \left[\frac{\delta E}{\delta v_{\mathrm{KS}}} \nabla_{\mathbf{R}} v_{\mathrm{KS}} \right] \tag{7.38}$$

In the presence of an overlap operator S, an additional term originating from the Dyson equation (7.9) is evaluated along the same lines, but with an additional factor $-\mathrm{i}\,\nu$ under the frequency integral:

$$\mathbf{F}_S = -\int \mathrm{d}\nu \, \mathrm{Tr} \left[\frac{\delta E}{\delta S} \nabla_{\mathbf{R}} S \right] \tag{7.39}$$

where

$$\frac{\delta E}{\delta S}(\mathbf{r}''', \mathbf{r}'', \mathrm{i}\,\nu) = \tag{7.40}$$

$$-\mathrm{i}\,\nu \int G(\mathbf{r}''', \mathbf{r}', \mathrm{i}\,\nu) \frac{\delta E}{\delta G(\mathbf{r}, \mathbf{r}', \mathrm{i}\,\nu)} G(\mathbf{r}, \mathbf{r}'', \mathrm{i}\,\nu) \mathrm{d}\mathbf{r} \mathrm{d}\mathbf{r}'$$

7.2.4 $\mathbf{F_{EXX}}$ from Green's functions

In this section we will verify that the Green's functions approach, Eq. (7.38), yields the same result for the Hartree-Fock/EXX energy functional E_{EXX} as standard perturbation theory, Eqs. (7.32)-(7.34). As an intermediate result we will see that the first order density operator from Eq. (7.24), in this case $\rho^{(1)}_{\mathrm{EXX}}$, can be expressed in terms of Green's functions and is of the form proposed in Eq. (7.17). After expressing $\rho^{(1)}_{\mathrm{EXX}}$ in position space, the equivalence to perturbation theory will be manifest. Finally we will show how to calculate the operator $\gamma^{(1)}_{\mathrm{EXX}}$, see Eq. (7.24), which is necessary in the presence of an overlap operator.

The simplest way to show the equivalence between the Green's functions approach, Eq. (7.38), and standard perturbation theory, Eqs. (7.32)-(7.34), is to exploit the following relation between the Green's function and the one particle density matrix [see also Eqs. (7.11)-(7.13)]:

$$\rho(\mathbf{r}, \mathbf{r}') = \frac{1}{2\pi} \int e^{-\mathrm{i}\,\nu\eta} G(\mathbf{r}, \mathbf{r}', \mathrm{i}\,\nu) \mathrm{d}\nu \quad ; \quad \eta = 0^{-}. \tag{7.41}$$

From Eq. (7.41) it follows that

$$\frac{\delta\rho(\mathbf{r}'',\mathbf{r}''')}{\delta G(\mathbf{r},\mathbf{r}',\mathrm{i}\,\nu)} = \frac{1}{2\pi}\delta(r-r'')\delta(r'-r''')e^{-\mathrm{i}\,\nu\eta} \tag{7.42}$$

and since E_{EXX} only depends on the density matrix,

$$\begin{aligned}\frac{\delta E_{\mathrm{EXX}}}{\delta G(\mathbf{r},\mathbf{r}',\mathrm{i}\,\nu)} &= \int \frac{\delta E_{\mathrm{EXX}}}{\delta\rho(\mathbf{r}'',\mathbf{r}''')}\frac{\delta\rho(\mathbf{r}'',\mathbf{r}''')}{\delta G(\mathbf{r},\mathbf{r}',\mathrm{i}\,\nu)}\mathrm{d}\mathbf{r}''\mathrm{d}\mathbf{r}''' \\ &= \frac{1}{2\pi}\frac{\delta E_{\mathrm{EXX}}}{\delta\rho(\mathbf{r},\mathbf{r}')}e^{-\mathrm{i}\,\nu\eta}. \end{aligned} \tag{7.43}$$

In Eq. (7.37), we can move $\nabla_{\mathbf{R}} v_{\mathrm{KS}}$ out of the frequency integration, because it is usually frequency independent. The force is then given by inserting Eq. (7.43) into Eq. (7.37)

$$\mathbf{F}_{\mathrm{EXX}} = -\int \mathrm{d}\mathbf{r}''\mathrm{d}\mathbf{r}'''\Bigg\{\nabla_{\mathbf{R}} v_{\mathrm{KS}}(\mathbf{r}'',\mathbf{r}''')\times \tag{7.44}$$

$$\underbrace{\frac{1}{2\pi}\int G(\mathbf{r}''',\mathbf{r}',\mathrm{i}\,\nu)\frac{\delta E_{\mathrm{EXX}}}{\delta\rho(\mathbf{r},\mathbf{r}')}e^{-\mathrm{i}\,\nu\eta}G(\mathbf{r},\mathbf{r}'',\mathrm{i}\,\nu)\mathrm{d}\nu\mathrm{d}\mathbf{r}\mathrm{d}\mathbf{r}'}_{\langle\mathbf{r}'''|\rho^{(1)}_{\mathrm{HF}}|\mathbf{r}''\rangle}\Bigg\}$$

From this result and Eq. (7.34), one can see directly that $\rho^{(1)}_{\mathrm{EXX}}$ in Eq. (7.24) is indeed of the form proposed in Eq. (7.17).

To show the equivalence of this result with the one obtained by standard perturbation theory, we will proceed by calculating $\langle\mathbf{r}'''|\rho^{(1)}_{\mathrm{EXX}}|\mathbf{r}''\rangle$ in Eq. (7.44) explicitly in terms of KS-orbitals. The frequency integration can be carried out by a contour integration of $G(\mathbf{r},\mathbf{r}'',\mathrm{i}\,\nu)G(\mathbf{r}''',\mathbf{r}',\mathrm{i}\,\nu)e^{-\mathrm{i}\,\nu\eta}$ along a path in the upper half of the complex plane, where the outer contour vanishes because of the factor $e^{-\mathrm{i}\,\nu\eta}$. However, it will turn out that it is more comprehensible to perform the integration over the inner indices $\mathbf{r}$ and $\mathbf{r}'$ first and then proceed with the frequency integration afterwards. Although the calculation is not difficult it is a bit cumbersome and will therefore be sketched here briefly.

$$\langle\mathbf{r}'''|\rho^{(1)}_{\mathrm{EXX}}|\mathbf{r}''\rangle = \frac{1}{2\pi}\int \mathrm{d}\mathbf{r}\mathrm{d}\mathbf{r}'\mathrm{d}\nu\Bigg\{ \tag{7.45}$$

$$G(\mathbf{r}''',\mathbf{r}',\mathrm{i}\,\nu)F(\mathbf{r}',\mathbf{r})G(\mathbf{r},\mathbf{r}'',\mathrm{i}\,\nu)e^{-\mathrm{i}\,\nu\eta}\Bigg\}$$

Inserting the definition of the Green's function from Eq. (7.8) gives

$$\frac{1}{2\pi}\int \mathrm{d}\mathbf{r}\mathrm{d}\mathbf{r}'\mathrm{d}\nu e^{-\mathrm{i}\,\nu\eta}\Bigg\{ \tag{7.46}$$

$$\sum_{nm}\frac{\langle\mathbf{r}'''|n\rangle\langle n|\mathbf{r}'\rangle}{\mathrm{i}\,\nu-(\epsilon_n-\epsilon_F)}\langle\mathbf{r}'|F|\mathbf{r}\rangle\frac{\langle\mathbf{r}|m\rangle\langle m|\mathbf{r}''\rangle}{\mathrm{i}\,\nu-(\epsilon_m-\epsilon_F)}\Bigg\}.$$

After integrating over $\mathbf{r}$ and $\mathbf{r}'$ we close the contour in the upper half of the complex plane and use the residue theorem to evaluate the integral. Denoting the residue of the function $f(x)$ at $x=x_0$ as $\operatorname*{Res}_{x=x_0} f(x)$ we get

$$\mathrm{i}\sum_{\substack{im\\ i\in occ.\\ m\neq i}}\operatorname*{Res}_{\nu=\frac{(\epsilon_i-\epsilon_F)}{\mathrm{i}}}\left(\frac{\langle\mathbf{r}'''|i\rangle\langle i|}{\mathrm{i}\,\nu-(\epsilon_i-\epsilon_F)}F\frac{|m\rangle\langle m|\mathbf{r}''\rangle}{\mathrm{i}\,\nu-(\epsilon_m-\epsilon_F)}\right)$$

$$+\mathrm{i}\sum_{\substack{in\\ i\in occ.\\ n\neq i}}\operatorname*{Res}_{\nu=\frac{(\epsilon_i-\epsilon_F)}{\mathrm{i}}}\left(\frac{\langle\mathbf{r}'''|n\rangle\langle n|}{\mathrm{i}\,\nu-(\epsilon_n-\epsilon_F)}F\frac{|i\rangle\langle i|\mathbf{r}''\rangle}{\mathrm{i}\,\nu-(\epsilon_i-\epsilon_F)}\right)$$

$$+\mathrm{i}\sum_{i\in occ.}\operatorname*{Res}_{\nu=\frac{(\epsilon_i-\epsilon_F)}{\mathrm{i}}}\left(\frac{\langle\mathbf{r}'''|i\rangle\langle i|F|i\rangle\langle i|\mathbf{r}''\rangle}{[\mathrm{i}\,\nu-(\epsilon_i-\epsilon_F)]^2}\right). \tag{7.47}$$

Evaluating the residues gives

$$\langle\mathbf{r}'''|\rho^{(1)}_{\mathrm{EXX}}|\mathbf{r}''\rangle = \tag{7.48}$$

$$\sum_{\substack{in\\ i\in occ.\\ n\neq i}}\frac{\langle\mathbf{r}'''|i\rangle\langle i|F|n\rangle\langle n|\mathbf{r}''\rangle+\langle\mathbf{r}'''|n\rangle\langle n|F|i\rangle\langle i|\mathbf{r}''\rangle}{\epsilon_i-\epsilon_n}.$$

Note that the n-summation here goes over all orbitals, although in principle it can be restricted to a sum over all virtual orbitals $a\in virt.$, since the summation over $n\in occ.$ vanishes. If we now insert this result in Eq. (7.44) and rewrite it as a trace, we get

$$\mathbf{F}_{\mathrm{EXX}} = -\,\mathrm{Tr}\left[\sum_{\substack{in\\ i\in occ.\\ n\neq i}}\frac{|i\rangle\langle i|F|n\rangle\langle n|+h.c.}{\epsilon_i-\epsilon_n}\nabla_{\mathbf{R}}v_{\mathrm{KS}}\right] \tag{7.49}$$

which is consistent with the result from perturbation theory in Eqs. (7.32)-(7.34).

To obtain the operator $\gamma^{(1)}_{\mathrm{EXX}}$ which occurs in Eqs. (7.17) and (7.24), we can proceed analogously for the overlap term given in Eqs. (7.39) and (7.40) with two

differences:

1. The *occ./occ.* terms do not cancel each other but instead the pairs of Hermitian conjugates cancel with the denominator, leaving behind only $\langle \mathbf{r}|i\rangle \langle i|F|j\rangle \langle j|\mathbf{r}'\rangle$.

2. The $i = j$ of the *occ./occ.* terms do not vanish, since

$$\operatorname*{Res}_{\nu=-i(\epsilon_i-\epsilon_F)} \left(\frac{\mathrm{i}\,\nu \langle \mathbf{r}'''|i\rangle \langle i|F|i\rangle \langle i|\mathbf{r}''\rangle}{[\mathrm{i}\,\nu - (\epsilon_i - \epsilon_F)]^2} \right) =$$

$$-\,\mathrm{i} \langle \mathbf{r}'''|i\rangle \langle i|F|i\rangle \langle i|\mathbf{r}''\rangle \tag{7.50}$$

Taking this into account one obtains the operator $\gamma^{(1)}_{\mathrm{EXX}}$ in Eq. (7.24) as

$$\langle \mathbf{r}'''|\gamma^{(1)}_{\mathrm{EXX}}|\mathbf{r}''\rangle = \frac{1}{2\pi} \lim_{\tau\to 0^-} \int \mathrm{d}\mathbf{r}\mathrm{d}\mathbf{r}'\mathrm{d}\nu \Big\{$$

$$\mathrm{i}\,\nu\, G(\mathbf{r}''', \mathbf{r}', \mathrm{i}\,\nu) F(\mathbf{r}', \mathbf{r}) G(\mathbf{r}, \mathbf{r}'', \mathrm{i}\,\nu) e^{-\mathrm{i}\,\nu\tau} \Big\}$$

$$= \sum_{\substack{i\in occ.\\ a\in virt.}} \frac{\epsilon_i}{\epsilon_i - \epsilon_a} \langle \mathbf{r}'''| \left(|i\rangle \langle i|F|a\rangle \langle a| + h.c. \right) |\mathbf{r}''\rangle$$

$$+ \sum_{i,j\in occ.} \langle \mathbf{r}'''|i\rangle \langle i|F|j\rangle \langle j|\mathbf{r}''\rangle\,. \tag{7.51}$$

In the present implementation Eqs.(7.48) and (7.51) are used to determine the first order density operators $\rho^{(1)}_{\mathrm{EXX}}$ and $\gamma^{(1)}_{\mathrm{EXX}}$. They are however stored in the basis of canonical orbitals, which is more convenient for the subsequent calculations.

7.2.5 $\mathbf{F_{RPA}}$ from Green's functions

If one is able to find an expression for $\frac{\delta E_{\mathrm{RPA}}}{\delta G}$, the force can be calculated by inserting it in Eqs. (7.37) - (7.40). By applying a chain rule equivalent for functional derivatives we may write

$$\frac{\delta E_{\mathrm{RPA}}}{\delta G(\mathbf{r}, \mathbf{r}', \mathrm{i}\,\nu)} = \tag{7.52}$$

$$\int \frac{\delta E_{\mathrm{RPA}}}{\delta \chi(\mathbf{r}'', \mathbf{r}''', \mathrm{i}\,\nu')} \frac{\delta \chi(\mathbf{r}'', \mathbf{r}''', \mathrm{i}\,\nu')}{\delta G(\mathbf{r}, \mathbf{r}', \mathrm{i}\,\nu)} \mathrm{d}\mathbf{r}''\mathrm{d}\mathbf{r}'''\mathrm{d}\nu'$$

We will now show that the first factor is proportional to the correlation part of the RPA screened interaction W_c. For this purpose it is useful to consider a certain class

of functionals and their functional derivatives:

Given an operator X (or equivalently a bivariate function in a given basis) and an analytic function $f : D \to \mathbb{R}, x \to f(x)$ with a proper D that allows a series expansion around 0, we shall define

$$f(X) = \sum_{d=0}^{\infty} \frac{f^{(d)}(0)}{d!} X^d. \tag{7.53}$$

Consequently we can define a class of functionals $\{\mathrm{F}\}$ that have the simple form

$$F[X] = \mathrm{Tr}[f(X)]. \tag{7.54}$$

The spectral density of the RPA correlation energy $e_{\mathrm{RPA}}[\chi](\mathrm{i}\,\nu)$ at a given frequency can be viewed as a functional of the polarizability that belongs to this class, see Eq. (7.20). Generally, functional derivatives are calculated in the following way:

$$\delta F[X] = \mathrm{Tr}\left[\frac{\delta F[X]}{\delta X}\delta X\right] \tag{7.55}$$

$$= \lim_{\epsilon\to 0} \frac{1}{\epsilon} F[X + \epsilon\delta X] - F[X]$$

Inserting a functional from the class of functionals described above gives

$$\delta F[X] = \lim_{\epsilon\to 0} \frac{1}{\epsilon} \mathrm{Tr}\left[f(X + \epsilon\, \delta X) - f(X)\right] \tag{7.56}$$

$$= \lim_{\epsilon\to 0} \frac{1}{\epsilon} \mathrm{Tr}\left[\sum_{d=0}^{\infty} \frac{f^{(d)}(0)}{d!} \left((X + \epsilon\, \delta X)^d - X^d\right)\right] \tag{7.57}$$

$$= \lim_{\epsilon\to 0} \sum_{d=1}^{\infty} \frac{f^{(d)}(0)}{d!} \mathrm{Tr}\left[\sum_{k=0}^{d-1} X^k \delta X X^{d-1-k}\right] + \mathcal{O}(\epsilon), \tag{7.58}$$

because the linear property of the trace allows us to move the sum and pre-factors out of the trace. We can now perform the ϵ limit and rearrange the terms in the brackets by exploiting the cyclic property of the trace to get

$$\delta F[X] = \sum_{d=1}^{\infty} \frac{f^{(d)}(0)}{d!} \sum_{k=0}^{d-1} \mathrm{Tr}\left[X^{d-1}\delta X\right], \tag{7.59}$$

where the summation over k gives just a factor d that can be cancelled with the denominator.

$$\delta F[X] = \mathrm{Tr}\left[\sum_{d=1}^{\infty} \frac{f^{(d)}(0)}{(d-1)!} X^{d-1}\delta X\right] \tag{7.60}$$

One can immediately recognize that the sum over d can be just written as the ordinary derivative f' so that

$$\delta F[X] = \mathrm{Tr}\left[f'(X)\delta X\right]. \tag{7.61}$$

If we compare this with Eq. (7.55), it follows that

$$\frac{\delta F[X]}{\delta X} = f'(X). \tag{7.62}$$

After the derivation of this general result we come back to our original goal of calculating the functional derivative

$$\frac{\delta E_{\mathrm{RPA}}}{\delta\chi(r, r', \mathrm{i}\,\nu)}. \tag{7.63}$$

Again we consider $e_{\mathrm{RPA}}[\chi](\mathrm{i}\,\nu)$ as a functional of a bivariate function, in this case $\chi(\mathbf{r}, \mathbf{r}')$, but now it depends parametrically on $(\mathrm{i}\,\nu)$ via the third variable of the three point function $\chi(\mathbf{r}, \mathbf{r}', \mathrm{i}\,\nu)$:

$$e_{\mathrm{RPA}}[\chi](\mathrm{i}\,\nu) = \mathrm{Tr}\left[f_{\mathrm{RPA}}(\chi\,\mathrm{v})\right]|_{\chi=\chi(\mathrm{i}\,\nu)} \tag{7.64}$$

$$\text{with} \qquad f_{\mathrm{RPA}}(x) = \frac{1}{4\pi}(\ln(1-x)+x) \tag{7.65}$$

Now $e_{\mathrm{RPA}}[\chi](\mathrm{i}\,\nu)$ at a specific imag. frequency $\mathrm{i}\,\nu$ is of the form shown in Eq. (7.54). Hence

$$\frac{\delta e_{\mathrm{RPA}}[\chi]}{\delta\chi\,\mathrm{v}} = f'_{\mathrm{RPA}}(\chi\,\mathrm{v}) = \frac{1}{4\pi}(1-(1-\chi\,\mathrm{v})^{-1}). \tag{7.66}$$

We apply the chain rule for functional derivatives on $\frac{\delta e_{\mathrm{RPA}}}{\delta\chi}$ and get

$$\frac{\delta e_{\mathrm{RPA}}[\chi]}{\delta\chi(\mathbf{r}'', \mathbf{r}''')} = \int \mathrm{d}\mathbf{r}\mathrm{d}\mathbf{r}' \frac{\delta e_{\mathrm{RPA}}[\chi]}{\delta(\chi\,\mathrm{v})(\mathbf{r}, \mathbf{r}')} \frac{\delta(\chi\,\mathrm{v})(\mathbf{r}, \mathbf{r}')}{\delta\chi(\mathbf{r}'', \mathbf{r}''')} \tag{7.67}$$

and it follows that

$$\frac{\delta e_{\mathrm{RPA}}[\chi]}{\delta\chi(\mathbf{r}'', \mathbf{r}''')} = \int \mathrm{d}\mathbf{r}\mathrm{d}\mathbf{r}' f'_{\mathrm{RPA}}(\chi\,\mathrm{v})(\mathbf{r}', \mathbf{r})\,\mathrm{v}(\mathbf{r}''', \mathbf{r}')\delta(\mathbf{r}-\mathbf{r}'') \tag{7.68}$$

$$= \frac{1}{4\pi}\left(\mathrm{v}(1-(1-\chi\,\mathrm{v})^{-1})\right)(\mathbf{r}''', \mathbf{r}''). \tag{7.69}$$

Since e_{RPA} is the spectral density of E_{RPA} one can now easily conclude that

$$\frac{\delta E_{\mathrm{RPA}}}{\delta\chi(\mathbf{r}, \mathbf{r}', \mathrm{i}\,\nu)} = \frac{1}{4\pi}\left(\mathrm{v}(1-(1-\chi\,\mathrm{v})^{-1})\right)(\mathbf{r}', \mathbf{r}, \mathrm{i}\,\nu) \tag{7.70}$$

from which we can see in turn that the functional derivative of E_{RPA} w.r.t. χ is proportional to the correlation part of the screened Coulomb interaction W_c:

$$\frac{\delta E_{\mathrm{RPA}}}{\delta \chi(\mathbf{r}, \mathbf{r}', \mathrm{i}\,\nu)} = -\frac{1}{4\pi} W_c(\mathbf{r}', \mathbf{r}, \mathrm{i}\,\nu). \tag{7.71}$$

The second factor in Eq. (7.52) can be obtained straight forwardly from Eq. (7.22):

$$\frac{\delta \chi(\mathbf{r}, \mathbf{r}', \mathrm{i}\,\nu)}{\delta G(\mathbf{r}'', \mathbf{r}''', \mathrm{i}\,\nu')} = \tag{7.72}$$

$$\delta(\mathbf{r} - \mathbf{r}'')\delta(\mathbf{r}' - \mathbf{r}''')G(\mathbf{r}', \mathbf{r}, \mathrm{i}(\nu' - \nu)) +$$

$$\delta(\mathbf{r} - \mathbf{r}''')\delta(\mathbf{r}' - \mathbf{r}'')G(\mathbf{r}, \mathbf{r}', \mathrm{i}(\nu' + \nu)).$$

If we now just insert the results from Eqs. (7.71) and (7.72) into Eq. (7.52) and exploit the symmetric property of W_c

$$W_c(\mathbf{r}', \mathbf{r}, -\mathrm{i}\,\nu) = W_c(\mathbf{r}, \mathbf{r}', \mathrm{i}\,\nu), \tag{7.73}$$

we obtain the following convolution for $\frac{\delta E_{\mathrm{RPA}}}{\delta G}$:

$$\frac{\delta E_{\mathrm{RPA}}}{\delta G(\mathbf{r}, \mathbf{r}', \mathrm{i}\,\nu)} = -\frac{1}{2\pi} \int \mathrm{d}\nu' G(\mathbf{r}', \mathbf{r}, \mathrm{i}\,\nu') W_c(\mathbf{r}', \mathbf{r}, \mathrm{i}(\nu - \nu')). \tag{7.74}$$

Since the correlation part of the self-energy Σ_{GW} in the GW approximation is given as

$$\Sigma_{\mathrm{GW}}(\mathbf{r}, \mathbf{r}', \mathrm{i}\,\tau) = -G(\mathbf{r}, \mathbf{r}', \mathrm{i}\,\tau) W_c(\mathbf{r}, \mathbf{r}', \mathrm{i}\,\tau) \tag{7.75}$$

the convolution theorem allows us to finally write

$$\frac{\delta E_{\mathrm{RPA}}}{\delta G(\mathbf{r}, \mathbf{r}', \mathrm{i}\,\nu)} = \Sigma_{\mathrm{GW}}(\mathbf{r}', \mathbf{r}, \mathrm{i}\,\nu). \tag{7.76}$$

The force is therefore given as [see Eqs. (7.37) and (7.38)]

$$\mathbf{F} = -\operatorname{Tr}\left[\int G \Sigma_{\mathrm{GW}} G \, \mathrm{d}\nu \;\; \nabla_{\mathbf{R}} v_{\mathrm{KS}}\right], \tag{7.77}$$

and in presence of an overlap operator, we have the additional term [see Eqs. (7.39) and (7.40)]

$$\mathbf{F} = \operatorname{Tr}\left[\int \mathrm{i}\,\nu G \Sigma_{\mathrm{GW}} G \, \mathrm{d}\nu \;\; \nabla_{\mathbf{R}} S\right]. \tag{7.78}$$

7.2.6 Summary

So far we showed that the total non-Hellmann-Feynman force can be calculated by a trace over the contraction of a "functional derivative operator" $\rho^{(1)}$ or $\gamma^{(1)}$ with the change of the effective KS potential or the overlap operator S respectively, as suggested in Eq. (7.24). We also showed how the operators $\rho^{(1)}$ and $\gamma^{(1)}$ can be evaluated for E_{EXX} and E_{RPA}. In the orbital basis of the KS Hamiltonian we get for the E_{EXX} contribution the remarkably simple expressions

$$\langle n|\rho^{(1)}_{\mathrm{EXX}}|m\rangle = \frac{1}{\epsilon_n - \epsilon_m} \langle n|F|m\rangle \, (f_n - f_m) \tag{7.79}$$

$$\begin{aligned} \langle n|\gamma^{(1)}_{\mathrm{EXX}}|m\rangle = &\langle n|F|m\rangle \, f_n f_m \\ &+ \frac{f_n\epsilon_n + f_m\epsilon_m}{\epsilon_n - \epsilon_m} \langle n|F|m\rangle \, (f_n - f_m) \end{aligned} \tag{7.80}$$

with the Fermi weights

$$f_n = \begin{cases} 1 & : n \in occ. \\ 0 & : n \in virt. \end{cases} . \tag{7.81}$$

For the correlation part we have to evaluate the frequency integral numerically using the following expressions that contain the Green's function and Σ_{GW} in the KS orbital basis:

$$\langle n|\rho^{(1)}_c|m\rangle = \sum_{kl} \int G_{nk}(\mathrm{i}\,\nu)\Sigma_{\mathrm{GW},kl}(\mathrm{i}\,\nu)G_{lm}(\mathrm{i}\,\nu)\mathrm{d}\nu \tag{7.82}$$

$$\langle n|\gamma^{(1)}_c|m\rangle = \sum_{kl} \int \mathrm{i}\,\nu G_{nk}(\mathrm{i}\,\nu)\Sigma_{\mathrm{GW},kl}(\mathrm{i}\,\nu)G_{lm}(\mathrm{i}\,\nu)\mathrm{d}\nu. \tag{7.83}$$

The frequency integration is approximated using the Minimax method introduced by Kaltak [35]. Usually $N = 12$ grid points on the τ/ν axis are sufficient to achieve results with 4 to 5 significant values.

7.2.7 Testing against numerical differentiation

In order to verify the proposed method for the calculation of first derivatives of the RPA total energy, we tested it against numerical differentiation. The test system was a super cell with 8 carbon atoms in the diamond structure. Atoms were displaced by up to 0.5 Å from their equilibrium positions to generate a symmetry broken starting configuration.

In the first test, a single atom was then displaced in increments of $h = \pm 0.018$ Å in the z direction, and for each displacement the RPA energy as well as the analytic gradient in the direction of the displacement was calculated. Afterwards the first derivative of individual energy contributions (EXX, correlation, and total energy)

was estimated using central differences

$$f'(x) \approx \frac{f(x+h) - f(x-h)}{2h} \tag{7.84}$$

and compared with the analytic derivatives. The results for this test are shown in Fig. 7.4. It is clear that the EXX contribution dominates. The correlation contribution has an opposite sign and amounts to about 10 % of the EXX value. In most calculations we find a similar behavior with the EXX contribution dominating the forces. As a matter of fact, this is beneficial, since the EXX contribution can be calculated accurately without the need for a numerical integration of the frequency dependent self-energy. The latter is required for the correlation part.

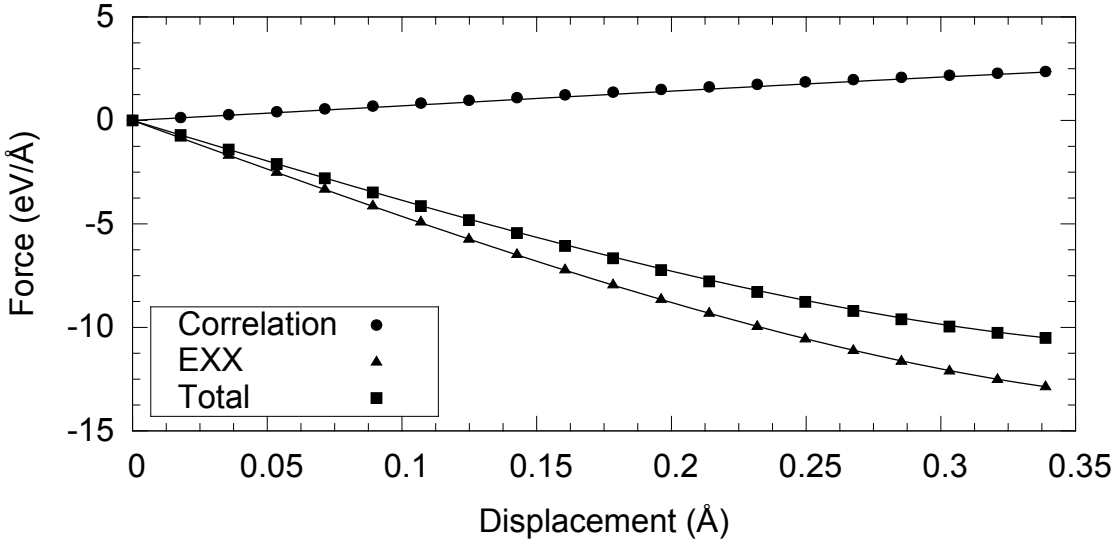

Figure 7.4: Forces from finite differences (symbols) are compared with the analytic method introduced in this work (lines). This plot shows the returning force in z-direction on a C atom which was moved along the z-direction in a 8 atom diamond super cell.

In a second test, we picked one configuration from the 8 atom diamond finite temperature simulation shown in the main text and calculated the analytic RPA forces on all atoms using the approach presented above. To compare with finite differences, each atom was then displaced in all three Cartesian directions and central differences were again used to estimate the first derivative of the total (EXX and RPA) energy. Results for the first three atoms are shown in Tab. 7.2 (results for the other atoms are similar). In this case, a small displacement of $h = 3.6 \cdot 10^{-4}$Å was used. To obtain accurate values for the finite differences a tight tolerance for the self-consistent density functional theory calculation had to be used. As alluded to in the previous section, we achieve about 5 significant digits accuracy using 12 frequency points.

Table 7.2: Analytic RPA derivatives F and numerical first derivatives of the total (EXX and RPA) energy obtained using finite differences F_{fd}. Values are reported for the first three atoms (1,2,3) of the 8 atom supercell. The forces were calculated numerically in all three Cartesian directions (x, y, z) for each atom. A Γ-centered $2 \times 2 \times 2$ k-point grid was used and the plane-wave cut-off was set to 414 eV. The break condition for the electronic SC-loop was set to $\Delta E = 10^{-8}$eV and the number of points for the imaginary time and frequency grid was set to 12. For the finite difference we used a displacement of $h = 3.6 \cdot 10^{-4}$Å

	F (eV/Å)	F_{fd} (eV/Å)	ΔF (eV/Å)
x_1	−5.658 650	−5.658 677	−0.000 027
y_1	−2.794 653	−2.794 645	0.000 008
z_1	−6.415 603	−6.415 615	−0.000 012
x_2	1.978 188	1.978 133	−0.000 055
y_2	−2.737 907	−2.738 015	−0.000 108
z_2	−6.483 599	−6.483 600	−0.000 001
x_3	−2.135 295	−2.135 128	0.000 167
y_3	−1.662 236	−1.662 181	0.000 055
z_3	4.757 047	4.757 079	0.000 032

7.3 PAW related contribuitons to forces

In the PAW method additional terms occur in the calculation of RPA forces due to the change of the projectors $|\tilde{p}\rangle$ and the augmentation charges Q_{ij}. Formally the first derivative of the RPA correlation Energy w.r.t. atomic positions can be written as follows (dropping all intermediate indices and assuming summation/integration over those):

$$\frac{\partial E_{\mathrm{RPA}}}{\partial R_A} = \sum \int \mathrm{d}... \frac{\delta E_{\mathrm{RPA}}}{\delta \chi} [\frac{\delta \chi}{\delta G} \frac{\partial G}{\partial R_A} + \frac{\delta \chi}{\delta Q} \frac{\partial Q}{\partial R_A} + \frac{\delta \chi}{\delta p} \frac{\partial p}{\partial R_A}], \tag{7.85}$$

where the A in R_A is a compound index for the atom index and the direction, e.g. $A = 1$ for the x-coordinate of atom number 1. The first part in brackets is the one we already discussed earlier. The other two parts stem from the form that is taken

by the polarizability χ in the PAW method, see chapter 6 or Ref. [63]:

$$\begin{aligned}\chi(\mathbf{r},\mathbf{r}',\tau) =& G(\mathbf{r},\mathbf{r}',\tau)G(\mathbf{r}',\mathbf{r},-\tau) \\ &+ \sum_{\mu\nu} Q_{\mu\nu}(\mathbf{r}) \iint_{\Omega_c} \mathrm{d}\mathbf{s}\mathrm{d}\mathbf{s}' \, \langle \tilde{p}_\nu|\mathbf{s}\rangle \, G(\mathbf{s},\mathbf{r}',\tau)G(\mathbf{r}',\mathbf{s}',-\tau) \, \langle \mathbf{s}'|\tilde{p}_\mu\rangle \\ &+ \sum_{\alpha\beta} Q_{\alpha\beta}(\mathbf{r}') \iint_{\Omega_c'} \mathrm{d}\mathbf{s}\mathrm{d}\mathbf{s}' \, \langle \tilde{p}_\beta|\mathbf{s}'\rangle \, G(\mathbf{s}',\mathbf{r},-\tau)G(\mathbf{r},\mathbf{s},\tau) \, \langle \mathbf{s}|\tilde{p}_\alpha\rangle \\ &+ \sum_{\alpha\beta\mu\nu} Q_{\mu\nu}(\mathbf{r})Q_{\alpha\beta}(\mathbf{r}') \iint_{\Omega_c\,\Omega_c'} \mathrm{d}\mathbf{s}\mathrm{d}\mathbf{s}' \, \langle \tilde{p}_\nu|\mathbf{s}\rangle \, G(\mathbf{s},\mathbf{s}',\tau) \, \langle \mathbf{s}'|\tilde{p}_\alpha\rangle \times \\ &\iint_{\Omega_c\,\Omega_c'} \mathrm{d}\mathbf{s}''\mathrm{d}\mathbf{s}''' \, \langle \tilde{p}_\beta|\mathbf{s}'''\rangle \, G(\mathbf{s}''',\mathbf{s}'',-\tau) \, \langle \mathbf{s}''|\tilde{p}_\mu\rangle \, .\end{aligned} \tag{7.86}$$

In the above representation of the polarizability, the second and third line describe plane wave - augmentation charge related terms, whereas the fourth and fifth line represent augmentation - augmentation charge related terms. In the terms with the projectors $\tilde{p}$, the integration can be restricted to the augmentation region Ω_c. Note that in this context the Green's function G is constructed from one-electron pseudo orbitals $\tilde{\psi}_n$ that correspond to the PAW Hamiltonian, *i.e.*

$$G(\mathbf{r},\mathbf{r}',\tau) = \Theta(-\tau) \sum_i^{\mathrm{occ}} \tilde{\psi}_i(\mathbf{r})\tilde{\psi}_i^*(\mathbf{r}')e^{-\epsilon_i\tau} - \Theta(\tau) \sum_a^{\mathrm{unocc}} \tilde{\psi}_a(\mathbf{r})\tilde{\psi}_a^*(\mathbf{r}')e^{-\epsilon_a\tau} \tag{7.87}$$

The second part in Eq. (7.85) describes the force component due to a change in the augmentation charges Q_{ij} which is treated in detail below:

$$\left.\frac{\partial E_{\mathrm{RPA}}}{\partial R_A}\right|_{G,p} = \sum_{ij} \int \mathrm{d}\mathbf{r}\mathrm{d}\mathbf{r}'\mathrm{d}\mathbf{r}''\mathrm{d}\tau \frac{\delta E_{\mathrm{RPA}}}{\delta\chi(\mathbf{r}',\mathbf{r}'',\tau)} \frac{\delta\chi(\mathbf{r}',\mathbf{r}'',\tau)}{\delta Q_{ij}(\mathbf{r})} \frac{\partial Q_{ij}(\mathbf{r})}{\partial R_A} \tag{7.88}$$

$$= \sum_{ij} \int \mathrm{d}\mathbf{r} \underbrace{\int \mathrm{d}\mathbf{r}'\mathrm{d}\mathbf{r}''\mathrm{d}\tau - \frac{1}{2} W_c(\mathbf{r}'',\mathbf{r}',-\tau) \frac{\delta\chi(\mathbf{r}',\mathbf{r}'',\tau)}{\delta Q_{ij}(\mathbf{r})}}_{=\frac{\delta E_{\mathrm{RPA}}}{\delta Q_{ij}(\mathbf{r})}} \frac{\partial Q_{ij}(\mathbf{r})}{\partial R_A} \tag{7.89}$$

Again we can calculate $\frac{\delta E_{\mathrm{RPA}}}{\delta Q_{ij}(\mathbf{r})}$ once and use it for all different atoms and directions for which we want to calculate the force. However in this case, the part $\frac{\delta\chi}{\delta Q}$ is very unwieldy as can be seen from Eq. (7.86). For the sake of completeness, we write

out all the terms that occur explicitly

$$\frac{\delta\chi(\mathbf{r}',\mathbf{r}'',\tau)}{\delta Q_{ij}(\mathbf{r})} = \iint_{\Omega_c} \mathrm{d}\mathbf{s}\mathrm{d}\mathbf{s}' \,\langle\tilde{p}_j|\mathbf{s}\rangle\, G(\mathbf{s},\mathbf{r}'',\tau)G(\mathbf{r}'',\mathbf{s}',-\tau)\,\langle\mathbf{s}'|\tilde{p}_i\rangle\,\delta(\mathbf{r}-\mathbf{r}') \tag{7.90}$$

$$+ \iint_{\Omega_c'} \mathrm{d}\mathbf{s}\mathrm{d}\mathbf{s}' \,\langle\tilde{p}_j|\mathbf{s}'\rangle\, G(\mathbf{s}',\mathbf{r}',-\tau)G(\mathbf{r}',\mathbf{s},\tau)\,\langle\mathbf{s}|\tilde{p}_i\rangle\,\delta(\mathbf{r}-\mathbf{r}'')$$

$$+ \delta(\mathbf{r}-\mathbf{r}')\sum_{\alpha\beta} Q_{\alpha\beta}(\mathbf{r}'')$$

$$\times \iint_{\Omega_c\,\Omega_c'} \mathrm{d}\mathbf{s}\mathrm{d}\mathbf{s}' \,\langle\tilde{p}_j|\mathbf{s}\rangle\, G(\mathbf{s},\mathbf{s}',\tau)\,\langle\mathbf{s}'|\tilde{p}_\alpha\rangle \iint_{\Omega_c\,\Omega_c'} \mathrm{d}\mathbf{s}''\mathrm{d}\mathbf{s}''' \,\langle\tilde{p}_\beta|\mathbf{s}'''\rangle\, G(\mathbf{s}''',\mathbf{s}'',-\tau)\,\langle\mathbf{s}''|\tilde{p}_i\rangle$$

$$+ \delta(\mathbf{r}-\mathbf{r}'')\sum_{\alpha\beta} Q_{\alpha\beta}(\mathbf{r}')$$

$$\times \iint_{\Omega_c\,\Omega_c'} \mathrm{d}\mathbf{s}\mathrm{d}\mathbf{s}' \,\langle\tilde{p}_j|\mathbf{s}\rangle\, G(\mathbf{s},\mathbf{s}',-\tau)\,\langle\mathbf{s}'|\tilde{p}_\alpha\rangle \iint_{\Omega_c\,\Omega_c'} \mathrm{d}\mathbf{s}''\mathrm{d}\mathbf{s}''' \,\langle\tilde{p}_\beta|\mathbf{s}'''\rangle\, G(\mathbf{s}''',\mathbf{s}'',\tau)\,\langle\mathbf{s}''|\tilde{p}_i\rangle$$

or more compact in an alternative notation:

$$\begin{aligned}\frac{\delta\chi(\mathbf{r}',\mathbf{r}'',\tau)}{\delta Q_{ij}(\mathbf{r})} =& G(j,\mathbf{r}'',\tau)G(\mathbf{r}'',i,-\tau)\delta(\mathbf{r}-\mathbf{r}') \\ &+ G(j,\mathbf{r}',-\tau)G(\mathbf{r}',i,\tau)\delta(\mathbf{r}-\mathbf{r}'') \\ &+ \delta(\mathbf{r}-\mathbf{r}')\sum_{\alpha\beta} Q_{\alpha\beta}(\mathbf{r}'')G(j,\alpha,\tau)G(\beta,i,-\tau) \\ &+ \delta(\mathbf{r}-\mathbf{r}'')\sum_{\alpha\beta} Q_{\alpha\beta}(\mathbf{r}')G(j,\alpha,-\tau)G(\beta,i,\tau)\end{aligned} \tag{7.91}$$

Contracting the result with the screened interaction gives the functional derivative

of the correlation energy with respect to the augmentation charges:

$$\frac{\delta E_{\mathrm{RPA}}}{\delta Q_{ij}(\mathbf{r})} = \int \mathrm{d}\mathbf{r}'\mathrm{d}\mathbf{r}''\mathrm{d}\tau - \frac{1}{2} W_c(\mathbf{r}'', \mathbf{r}', -\tau) \frac{\delta \chi(\mathbf{r}', \mathbf{r}'', \tau)}{\delta Q_{ij}(\mathbf{r})} \tag{7.92}$$

$$= -\frac{1}{2} \int \mathrm{d}\mathbf{r}'\mathrm{d}\tau [W_c(\mathbf{r}', \mathbf{r}, -\tau) G(j, \mathbf{r}', \tau) G(\mathbf{r}', i, -\tau) +$$

$$W_c(\mathbf{r}, \mathbf{r}', -\tau) G(j, \mathbf{r}', -\tau) G(\mathbf{r}', i, \tau) +$$

$$W_c(\mathbf{r}', \mathbf{r}, -\tau) \sum_{\alpha\beta} Q_{\alpha\beta}(\mathbf{r}') G(j, \alpha, \tau) G(\beta, i, -\tau) +$$

$$W_c(\mathbf{r}, \mathbf{r}', -\tau) \sum_{\alpha\beta} Q_{\alpha\beta}(\mathbf{r}') G(j, \alpha, -\tau) G(\beta, i, \tau)]$$

This can be rearranged for an efficient numerical treatment to

$$\frac{\delta E_{\mathrm{RPA}}}{\delta Q_{ij}(\mathbf{r})} = \tag{7.93}$$

$$-\frac{1}{2} \int \mathrm{d}\mathbf{r}'\mathrm{d}\tau \{ W_c(\mathbf{r}', \mathbf{r}, -\tau) [G(j, \mathbf{r}', \tau) G(\mathbf{r}', i, -\tau) + \sum_{\alpha\beta} Q_{\alpha\beta}(\mathbf{r}') G(j, \alpha, \tau) G(\beta, i, -\tau)]$$

$$+ W_c(\mathbf{r}, \mathbf{r}', -\tau) [G(j, \mathbf{r}', -\tau) G(\mathbf{r}', i, \tau) + \sum_{\alpha\beta} Q_{\alpha\beta}(\mathbf{r}') G(j, \alpha, -\tau) G(\beta, i, \tau)] \}$$

In an efficient implementation, $\frac{\delta E_{\mathrm{RPA}}}{\delta Q_{ij}(\mathbf{r})}$ is calculated once, stored and used for all atoms and directions, analogously to the matrices $\rho^{(1)}$ and $\gamma^{(1)}$ in Eq. (7.18). The individual force contributions are obtained by tracing over the contraction of the above expression with $\frac{\partial Q_{ij}(\mathbf{r})}{\partial R_A}$:

$$\left.\frac{\partial E_{\mathrm{RPA}}}{\partial R_A}\right|_{G,p} = \mathrm{Tr}\left\{ \frac{\delta E_{\mathrm{RPA}}}{\delta Q} \frac{\partial Q}{\partial R_A} \right\}. \tag{7.94}$$

Note that $\frac{\partial Q_{ij}(\mathbf{r})}{\partial R_A}$ is calculated by linear response routines.

Finally we have to treat the third part in Eq. (7.85). This part is the contribution to the energy that comes from the change of the projector functions $\tilde{p}_i$. We can proceed as before by writing the functional derivative of the RPA correlation energy

with respect to the projector function while leaving everything else fixed:

$$\left.\frac{\partial E_{\mathrm{RPA}}}{\partial R_A}\right|_{G,Q} = \sum_i \int \mathrm{d}\mathbf{r}\mathrm{d}\mathbf{r}'\mathrm{d}\tau \frac{\delta E_{\mathrm{RPA}}}{\delta\chi(\mathbf{r},\mathbf{r}',\tau)} \left(\frac{\delta\chi(\mathbf{r},\mathbf{r}',\tau)}{\delta\left|\tilde{p}_i\right\rangle} \frac{\partial\left|\tilde{p}_i\right\rangle}{\partial R_A} + \frac{\delta\chi(\mathbf{r},\mathbf{r}',\tau)}{\delta\left\langle\tilde{p}_i\right|} \frac{\partial\left\langle\tilde{p}_i\right|}{\partial R_A} \right)$$

$$= \sum_i \underbrace{\int -\frac{1}{2} W_c(\mathbf{r}',\mathbf{r},-\tau) \frac{\delta\chi(\mathbf{r},\mathbf{r}',\tau)}{\delta\left|\tilde{p}_i\right\rangle} \mathrm{d}\mathbf{r}\mathrm{d}\mathbf{r}'\mathrm{d}\tau}_{\frac{\delta E_{\mathrm{RPA}}}{\delta\left|\tilde{p}_i\right\rangle}} \frac{\partial\left|\tilde{p}_i\right\rangle}{\partial R_A} + \frac{\delta E_{\mathrm{RPA}}}{\delta\left\langle\tilde{p}_i\right|} \frac{\partial\left\langle\tilde{p}_i\right|}{\partial R_A} \tag{7.95}$$

Again we can use Eq. (7.86) to calculate this contribution. First we calculate the functional derivative of the response function χ with respect to the projector function $\tilde{p}$:

$$\begin{aligned} \frac{\delta\chi(\mathbf{r},\mathbf{r}',\tau)}{\delta\left|\tilde{p}_i\right\rangle} = & \sum_\mu Q_{i\mu}(\mathbf{r}) G(\mu,\mathbf{r}',\tau) \int \mathrm{d}\mathbf{s}\; G(\mathbf{r}',\mathbf{s},-\tau)\left\langle\mathbf{s}\right| \\ & + \sum_\mu Q_{i\mu}(\mathbf{r}') G(\mu,\mathbf{r},-\tau) \int \mathrm{d}\mathbf{s}\; G(\mathbf{r},\mathbf{s},\tau)\left\langle\mathbf{s}\right| \\ & + \sum_{\alpha\beta\mu} Q_{i\mu}(\mathbf{r}) Q_{\alpha\beta}(\mathbf{r}') G(\mu,\alpha,\tau) \int \mathrm{d}\mathbf{s} G(\beta,\mathbf{s},-\tau)\left\langle\mathbf{s}\right| \\ & + \sum_{\alpha\beta\mu} Q_{i\mu}(\mathbf{r}') Q_{\alpha\beta}(\mathbf{r}) G(\mu,\alpha,-\tau) \int \mathrm{d}\mathbf{s}\; G(\beta,\mathbf{s},\tau)\left\langle\mathbf{s}\right| \end{aligned} \tag{7.96}$$

and

$$\begin{aligned} \frac{\delta\chi(\mathbf{r},\mathbf{r}',\tau)}{\delta\left\langle\tilde{p}_i\right|} = & \sum_\mu Q_{\mu i}(\mathbf{r}) G(\mathbf{r}',\mu,-\tau) \int \mathrm{d}\mathbf{s}\left|\mathbf{s}\right\rangle G(\mathbf{s},\mathbf{r}',\tau) \\ & + \sum_\mu Q_{\mu i}(\mathbf{r}') G(\mathbf{r},\mu,\tau) \int \mathrm{d}\mathbf{s}\left|\mathbf{s}\right\rangle G(\mathbf{s},\mathbf{r},-\tau) \\ & + \sum_{\alpha\beta\mu} Q_{\mu i}(\mathbf{r}) Q_{\alpha\beta}(\mathbf{r}') G(\beta,\mu,-\tau) \int \mathrm{d}\mathbf{s}\left|\mathbf{s}\right\rangle G(\mathbf{s},\alpha,\tau) \\ & + \sum_{\alpha\beta\mu} Q_{\mu i}(\mathbf{r}') Q_{\alpha\beta}(\mathbf{r}) G(\beta,\mu,\tau) \int \mathrm{d}\mathbf{s}\left|\mathbf{s}\right\rangle G(\mathbf{s},\alpha,-\tau). \end{aligned} \tag{7.97}$$

It can be shown easily that

$$\left(\frac{\delta\chi(\mathbf{r},\mathbf{r}',\tau)}{\delta\left\langle\tilde{p}_i\right|}\right)^* = \frac{\delta\chi(\mathbf{r},\mathbf{r}',-\tau)}{\delta\left|\tilde{p}_i\right\rangle}. \tag{7.98}$$

Inserting Eq. (7.96) into the expression for $\frac{\delta E_{\mathrm{RPA}}}{\delta \langle \tilde{p}_i |}$ in Eq. (7.95) we get

$$\frac{\delta E_{\mathrm{RPA}}}{\delta \left| \tilde{p}_i \right\rangle} = \int \mathrm{d}\mathbf{s} - \frac{1}{2} \int \mathrm{d}\mathbf{r}\mathrm{d}\mathbf{r}'\mathrm{d}\tau [W(\mathbf{r}', \mathbf{r}, -\tau) + W(\mathbf{r}, \mathbf{r}', \tau)] K_i(\mathbf{r}, \mathbf{r}', \tau; \mathbf{s}) \left\langle \mathbf{s} \right| \tag{7.99}$$

where

$$K_i(\mathbf{r}, \mathbf{r}', \tau; \mathbf{s}) = \tag{7.100}$$

$$\sum_{\mu} Q_{i\mu}(\mathbf{r}) \left[G(\mu, \mathbf{r}', \tau) G(\mathbf{r}', \mathbf{s}, -\tau) + \sum_{\alpha,\beta} G(\mu, \alpha, \tau) Q_{\alpha,\beta}(\mathbf{r}') G(\beta, \mathbf{s}, -\tau) \right].$$

An analogous expression can be found for $\frac{\delta E_{\mathrm{RPA}}}{\delta \langle \tilde{p}_i |}$. Finally the contribution to the total derivative corresponding to the projector functions $\tilde{p}_i$ can be expressed similarly to Eq. (7.94) as

$$\left. \frac{\partial E_{\mathrm{RPA}}}{\partial R_A} \right|_{G,Q} = \mathrm{Tr} \left\{ \frac{\delta E_{\mathrm{RPA}}}{\delta \left| p \right\rangle} \frac{\partial \left| p \right\rangle}{\partial R_A} + \frac{\delta E_{\mathrm{RPA}}}{\delta \left\langle p \right|} \frac{\partial \left\langle p \right|}{\partial R_A} \right\}. \tag{7.101}$$

Chapter 8

Stresstensor

The stress tensor for a periodic structure with the lattice vectors $\{\mathbf{a}^{(1)}, \mathbf{a}^{(2)}, \mathbf{a}^{(3)}\}$ can be found by considering an infinitesimal transformation

$$\bar{\mathbf{a}}_i^{(k)} = (\delta_{ij} + t_{ij})\mathbf{a}_j^{(k)} \tag{8.1}$$

which is equivalent to transforming the underlying Cartesian basis with the transposed matrix:

$$\bar{\mathbf{e}}^{(i)} = \mathbf{e}^{(j)}(\delta_{ji} + t_{ji}) \Leftrightarrow \bar{\mathbf{e}}_j^{(i)} = \langle \mathbf{e}^{(j)} | \bar{\mathbf{e}}^{(i)} \rangle = (\delta_{ji} + t_{ji}). \tag{8.2}$$

The stress tensor can be generally found by calculating the energy derivative with respect to t_{ij}

$$\sigma_{ij} = -\frac{\partial E}{\partial t_{ij}}. \tag{8.3}$$

Since we calculate the total energy in the RPA as

$$E = E_{\mathrm{EXX}} + E_{\mathrm{RPA}}, \tag{8.4}$$

we can calculate the stress tensor by calculating the individual contributions to the stress and summing them up. For each energy term, there is a set of quantities which is subject to change under infinitesimal basis transformations. The following quantities have to be considered:

- Cell volume
- Coulomb kernel
- Kohn-Sham orbitals
  - basis functions
  - coefficients

However, using plane waves, the discretized basis functions $e^{\mathrm{i}\,\mathbf{k}_i\mathbf{r}_j}$ are up to first order independent of the transformation, which greatly simplifies things.

The following expressions concerning derivatives of the volume and the reciprocal lattice vectors with respect to t_{ij} occur regularly in the calculation of the stress tensor and therefore it is useful to write them down once explicitly:

$$\frac{\partial\Omega}{\partial t_{ij}} = \delta_{ij}\Omega \tag{8.5}$$

$$\frac{\partial|\mathbf{G}+\mathbf{k}|}{\partial t_{ij}} = -\frac{(\mathbf{G}+\mathbf{k})_i(\mathbf{G}+\mathbf{k})_j}{|\mathbf{G}+\mathbf{k}|} \tag{8.6}$$

8.1 Stress tensor contribution from RPA correlation energy

One contribution to the stress tensor stems from the variation of the plane wave coefficients of the KS-orbitals. This can be also regarded as the contribution due to a variation in the KS-Hamiltonian that leaves the basis unchanged. Accordingly there is an analogous expression to the one for the forces, yielding:

$$\sigma_{ij}^{\mathrm{RPA},\Sigma} = -\int_{-\infty}^{\infty} \mathrm{d}\nu\, \mathrm{Tr}\left[G\,\Sigma_{\mathrm{GW}}\,G\,\frac{\partial\,\mathrm{H}^{\mathrm{KS}}}{\partial t_{ij}}\right]. \tag{8.7}$$

Again we employed the trick that the contribution to the derivative regarding the orbitals can be expressed as a derivative with respect to the Green's function instead and rewrite it formally as:

$$\mathrm{Tr}\left[\frac{\delta E}{\delta\phi}\frac{\delta\phi}{\delta t_{ij}}\right] = \mathrm{Tr}\left[\frac{\delta E}{\delta G}\frac{\delta G}{\delta\phi}\frac{\delta\phi}{\delta t_{ij}}\right] = \mathrm{Tr}\left[\frac{\delta E}{\delta G}\frac{\delta G}{\delta t_{ij}}\right]. \tag{8.8}$$

Additional contributions arise from the change of the basis set. The simplest way to collect all contributions is to take the derivative of the RPA-correlation energy with respect to $\chi\,\mathrm{v}$ and then calculate via a chain rule all contributions by considering all dependencies of $\chi\,\mathrm{v}$ on the basis transformations t_{ij}. In case of the RPA correlation energy these additional contributions can be calculated along the following lines:

$$E_{\mathrm{RPA}} = \frac{1}{2\pi}\int_0^{\infty} \mathrm{d}\nu\, \mathrm{Tr}\left\{\ln(1-\chi(\mathrm{i}\,\nu)\,\mathrm{v}) + \chi(\mathrm{i}\,\nu)\,\mathrm{v}\right\} \tag{8.9}$$

$$\frac{\partial E}{\partial t_{ij}} = \frac{\delta E}{\delta(\chi\,\mathrm{v})}\frac{\partial(\chi\,\mathrm{v})}{\partial t_{ij}} \tag{8.10}$$

The first factor was already evaluated in the previous section 7.1 – Eq. 7.21 and section 7.2 – Eq. (7.71) – and yields essentially the correlation part of the screened

interaction in the RPA

$$\frac{\delta E_{\mathrm{RPA}}}{\delta(\chi\nu)} = -\frac{1}{4\pi}W^c. \tag{8.11}$$

Now the expression $\chi\,\mathrm{v}$ depends on the Coulomb kernel v, on the volume since

$$(\chi\,\mathrm{v}) \propto \frac{1}{\Omega}, \tag{8.12}$$

and finally on the Green's function via the response function χ, giving rise to three contributions to the stress tensor. The one concerning the Green's function is already taken care of by Eq. (8.7) – in analogy to the calculation of forces. Using Eq.(8.5) the contribution due to the volume dependency can be calculated straightforwardly since

$$\frac{\delta(\chi\,\mathrm{v})}{\delta\Omega}\frac{\partial\Omega}{\partial t_{ij}} = -(\chi\,\mathrm{v})\delta_{ij} \tag{8.13}$$

and therefore we obtain

$$\sigma_{ij}^{\mathrm{RPA},\Omega} = -\frac{1}{2\pi}\delta_{ij}\int_{-\infty}^{\infty}\mathrm{d}\nu\,\mathrm{Tr}\left\{[W^c\chi\,\mathrm{v}](\mathrm{i}\,\nu)\right\}. \tag{8.14}$$

As for the Coulomb kernel contribution, we can use Eq. (8.6) and get

$$\frac{\delta(\chi\,\mathrm{v})}{\delta\,\mathrm{v}}\frac{\partial\,\mathrm{v}}{\partial t_{ij}} = 2\chi(\mathrm{i}\,\nu)\sum_{\mathbf{G}}|\mathbf{G}+\mathbf{k}\rangle\langle\mathbf{G}+\mathbf{k}|\,\frac{(\mathbf{G}+\mathbf{k})_i(\mathbf{G}+\mathbf{k})_j}{|\mathbf{G}+\mathbf{k}|^4} \tag{8.15}$$

so that this contribution can be evaluated as

$$\sigma_{ij}^{\mathrm{RPA,v}} = \frac{1}{\pi}\int_{-\infty}^{\infty}\mathrm{d}\nu\,\mathrm{Tr}\left\{W^c(\mathrm{i}\,\nu)\chi(\mathrm{i}\,\nu)\sum_{\mathbf{G}}|\mathbf{G}+\mathbf{k}\rangle\langle\mathbf{G}+\mathbf{k}|\,\frac{(\mathbf{G}+\mathbf{k})_i(\mathbf{G}+\mathbf{k})_j}{|\mathbf{G}+\mathbf{k}|^4}\right\}. \tag{8.16}$$

The total stress due to the correlation energy is the sum of the individual components:

$$\sigma_{ij}^{\mathrm{RPA}} = \sigma_{ij}^{\mathrm{RPA},\Sigma} + \sigma_{ij}^{\mathrm{RPA},\Omega} + \sigma_{ij}^{\mathrm{RPA,v}}. \tag{8.17}$$

8.2 Stress tensor contribution from E_{EXX}

The Hartree-Fock energy functional evaluated at arbitrary one electron orbitals $\{\phi_n\}$ can be considered as a functional $E_{\mathrm{EXX}}[n]$ of the respective one particle reduced density matrix (1-RDM) n, see Eq. (7.29). However, for the calculation of the stress tensor, it is useful to have a closer look at the numerical treatment of this expression. There, the density matrix is stored in terms of its coefficients w.r.t. a certain basis, e.g. plane waves. In the following, we will denote the matrix of 1-RDM coefficients as $\bar{n}$ and the basis functions as $\{\mathbf{G}\}$. Similarly, the Hamiltonian, the kinetic energy operator, the Coulomb kernel and the external potential is stored as a matrix of coefficients $\bar{H}$, $\bar{T}$, $\bar{\mathrm{v}}$ and $\bar{v}_{\mathrm{ext}}$ respectively. Now for the derivation of

the stress tensor contribution from E_{EXX}, we will consider it as a functional

$$E_{\mathrm{EXX}} = E_{\mathrm{EXX}}[\bar{n}, \bar{T}, \bar{v}_{\mathrm{ext}}, \{\mathbf{G}\}]. \tag{8.18}$$

Thus, the stress tensor can be written formally as

$$-\frac{\partial E_{\mathrm{EXX}}}{\partial t_{ij}} = \sigma_{ij}^{\mathrm{EXX,HF}} + \underbrace{\mathrm{Tr}\left[\frac{\delta E_{\mathrm{EXX}}}{\delta \bar{n}} \frac{\partial \bar{n}}{\partial t_{ij}}\right]}_{\sigma_{ij}^{\mathrm{EXX},\bar{n}}} \tag{8.19}$$

The contributions $\sigma_{ij}^{\mathrm{EXX,HF}}$ take into account the variation w.r.t. to t_{ij} of the matrix elements $\bar{T}$ and $\bar{v}_{\mathrm{ext}}$, and of the basis functions $\{\mathbf{G}\}$ at fixed coefficients $\bar{n}$. They are the stress analogue[1] of Hellmann-Feynman and Pulay forces and are already widely implemented in common electronic structure codes. For a detailed description we refer to Ref. [105] and [129]. Therefore, in the following we will sketch how to evaluate the contribution $\sigma_{ij}^{\mathrm{EXX},\bar{n}}$ arising from the variation of $\bar{n}$ w.r.t. t_{ij}, which can be calculated along the same lines as the corresponding non-Hellmann-Feynman forces $\mathbf{F}_{\mathrm{EXX}}$.

The functional derivative $\frac{\delta E_{\mathrm{EXX}}}{\delta \bar{n}}$ is the Fock operator F constructed from the orbitals $\{\phi_n\}$ (e.g. PBE orbitals) in the respective basis (e.g. plane waves) – cf. Eq. (7.34). Using the correspondence between the Green's function G at $\tau = 0^-$ and the 1-RDM together with the Dyson equation – see Eq. (4.80) and Eq. (7.10) – the term $\frac{\partial \bar{n}}{\partial t_{ij}}$ can be obtained similarly to the analogue term in the force calculation. With the basis vectors fixed, the variation of the density matrix is given as

$$\delta n = G \delta H^{\mathrm{KS}} G + \mathcal{O}((\delta H^{\mathrm{KS}})^2). \tag{8.20}$$

Note again that changes w.r.t the basis set $\{\mathbf{G}\}$ are already included in $\sigma_{ij}^{\mathrm{EXX,HF}}$ and can therefore be neglected (in first order) at this point. Thus, one obtains for the derivative of the matrix elements $\bar{n}$ w.r.t. t_{ij}

$$\frac{\partial \bar{n}}{\partial t_{ij}} = \overline{G \frac{\partial H^{\mathrm{KS}}}{\partial t_{ij}} G}. \tag{8.21}$$

Finally, one can once again use the cyclic property of the trace operation and obtain for the E_{EXX} related non-Hellmann-Feynmann stress

$$\sigma_{ij}^{\mathrm{EXX},\bar{n}} = -\mathrm{Tr}\left[GFG \frac{\partial H^{\mathrm{KS}}}{\partial t_{ij}}\right], \tag{8.22}$$

which is analogous to Eq. (8.7).

[1] This analogy is not entirely accurate. For the stress tensor, variations with respect to changes in the basis functions must be considered. Those do not occur in force calculations.

Part III

Advanced Applications of the RPA

Chapter 9

Surface chemistry and adsorption processes

In the course of this thesis, opportunities to test the capabilities of the RPA emerged from collaborations with other groups. Studies on surface chemistry and adsorption processes turned out to be particularly fruitful and led to several publications [4, 5, 6]. In this chapter, we will briefly present our contributions to these publications and summarize the findings.

Surface science is the study of interactions of atoms and molecules with surfaces – e.g. adsorption and diffusion – and the phenomena that occur at the interface between solids and other phases like gases or liquids. These phenomena are not only ubiquitous in nature and pose fundamental research questions, but also play a significant role in countless industrial applications, including catalysis, gas storage, corrosion, desalination, and more. Therefore, experimental surface science has obviously been a very active field of research for a long time.

2D van der Waals (vdW) materials are particularly interesting substrates as they exhibit long-range correlation interactions that are usually not as pronounced in solids or molecules. One possible application for these materials is water processing and purification, as low dimensional materials such as graphene and hexagonal boronnitride (hBN) are considered as adsorbents for harmful impurities. The close connection between adsorption and vdW interactions extends the topic to different research areas. For example, vdW interactions play a fundamental role in the formation of complex molecular crystals, that are found in biological systems and applied in medicine. Consequently, an accurate knowledge of adsorption energies helps to understand and design new systems in this broad field of applications. [4]

Concerning before mentioned experimental surface science, it is difficult so obtain accurate adsorption energies on clean surfaces. On the one hand, immaculate surfaces under ultra high vacuum are hard to prepare. On the other hand, the techniques capable of reaching the required level of precision to measure weak physisorption energies are very limited. [4]

During the last decade, theoretical studies by means of electronic structure meth-

ods provided an important complement to experiments, allowing a deeper understanding of the investigated phenomena. Due to the increasing computer power and the development of sophisticated electronic structure methods (especially for periodic systems), it is now possible to calculate accurate adsorption energies.[5]

Using periodic codes, the super cells needed to model the surfaces are usually large, thus the calculations demand considerable computational resources. Sophisticated methods are therefore often computationally too expensive to be applied to surface simulations. Also, the employed electronic structure approach has to give a balanced description for both the solid and the adsorbate (e.g., atoms, molecules, or clusters), as well as the interface between the two. The problem is, that many of the computationally less complex approaches perform well for either the solid or the isolated adsorbate, but not for the combined system. Hence, the challenge is to balance the accuracy and computational cost and choose an appropriate method for a given surface problem.[28]

The RPA is known to achieve a balanced description for many different systems at feasible computational costs, and it is also capable of describing van der Waals interactions, which are often important in the description of surface phenomena. It is therefore a promising candidate for surface simulations.

9.1 Adsorption energies of benzene on close packed transition metal surfaces

In this section we summarize the results from Ref. [6], by Garrido Torres, Ramberger, Früchtl, Schaub and Kresse. The figures in this section are published in Ref. [6] and were produced by José A. Garrido Torres.

Semi local functionals generally predict trends between different metal surfaces reasonably well. However, absolute adsorption energies can be inaccurate even for prototypical molecules. Aromatic molecules are particularly difficult, since their adsorption involves a mixture of covalent and van der Waals (vdW) bonding. The former is overestimated by the PBE functional, whereas the latter is not captured at all by GGA functionals. Although these two errors may compensate each other, often this is not the case and there is no systematic way to predict the behavior. Efforts to include vdW corrections have been extensive in recent years. The most successful schemes are additive D3 dispersion corrections by Grimme and co-workers [117, 130], the similar scheme of Tkatchenko and Scheffler (TS) [14], as well as van der Waals density functionals (vdW-DF) that depend on the density at two positions in space, originally introduced by Dion et al. [131].

For the adsorption of aromatic molecules on (111) transition metal surfaces, the results using vdW corrections are overall quite promising, however, particularly on catalytic substrates, the adsorption energies for aromatic molecules tend to be overestimated. Also, problems at the DFT level in the description of covalent bonding are inherrited by the vdW corrected methods. A prominent example for this is the

CO puzzle, which describes the failure of DFT functionals to predict the correct adsorption site for CO on metal surfaces [34]. Encouraged by the systematic improvement that can be achieved with the RPA for CO on metal surfaces [86], we set out to investigate whether a similar improvement carries over to the more intricate adsorption of aromatic molecules. For this purpose, we investigated the adsorption of benzene on various transition metal (111) surfaces. We compared RPA results for adsorption energies and related properties with results from different semi local as well as van der Waals corrected functionals. The employed functionals include a standard GGA (PBE [9]), atom based vdW correction schemes (PBE-D3 [117] and PBE-TS [14]) and vdW-DFs (vdW-DF [131], vdW-DF2 [132] and optB86b-vdW [133]). We found that only the RPA yields reference quality results in excellent agreement with experiment.

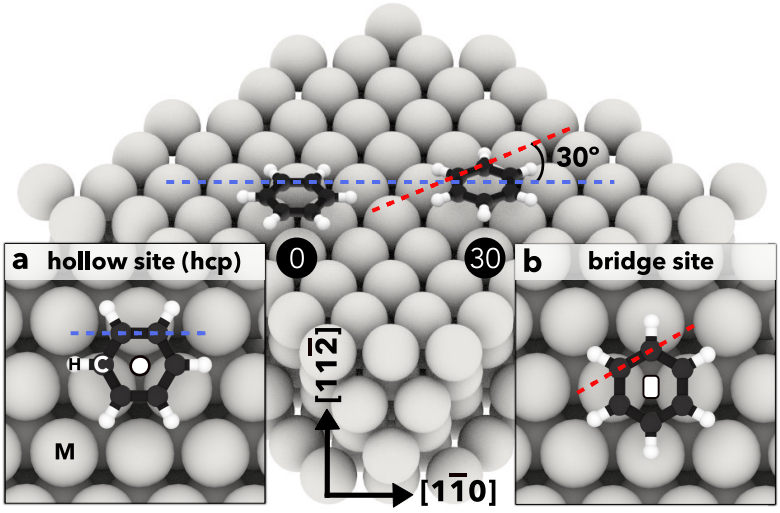

Figure 9.1: *"Representation of the two most common adsorption sites for benzene on transition metals. The blue and red dashed lines are set to emphasize the different alignment of the C-C bonds for the 0 and 30 configurations. Carbon, hydrogen, and metal atoms are represented as black, white, and gray spheres, respectively."* [6]

On (111) surfaces, the benzene molecule mainly adsorbs on two sites: the twofold (bridge) or the threefold (hollow) site with the C6 ring parallel to the surface plane (see Fig. 9.1). The preferred adsorption site depends on the nature of the substrate, the coverage, and the presence of coadsorbates. We investigated both sites for a series of transition metals, but will only present results for the respective lower energy configuration on each metal, since only the stable configuration can be compared with experiments (see Tab. 9.1).

For the investigated metals, best agreement with the experimental adsorption energies is obtained with the RPA. RPA adsorption energies fall within the experimental error bars were such data were available, whereas the other methods performed

mediocre. For PBE, this was expected as it completely neglects vdW interactions. This deficiency becomes apparent for the physisorbed cases (Cu, Ag, Au), where the PBE adsorption energy is close to zero. The vdW corrections and vdW-DFs turned out to be particularly erratic for the chemisorbed cases (Ni, Pd, Pt, Rh) where benzene is strongly bound. Concerning PBE-D3, PBE-TS, and optB86b-vdW, our results suggest that they overestimate the vdW corrections slightly for coinage metals and substantially for reactive metals as the difference between e.g PBE and PBE-D3 is up to twice as large as the difference between RPA and PBE. While for Cu, Ag, Au, and Pt, the error seems to be only about 25%, it increases to almost 100% for Pd and Rh – a non-systematic behavior that hinders conclusive interpretations. The error might be due to already inadequate descriptions in the parent DFT functional. Another source might be the neglect of the interplay between the local excitations and jelliumlike screening in metals. Finally, the vdW-DF and vdW-DF2 methods were overall disappointing, predicting adsorption energies below the PBE values, even though they should include additional contributions due to vdW interactions. This suggests that the errors in the covalent contribution are substantial for these methods.

Table 9.1: *"Calculated adsorption energies (in eV) for benzene adsorbed on different (111) metal substrates at medium coverage. Experimental values from the literature are included for comparison (in bold are the theoretical values that are within the experimental errors). Calculations were performed for a ($2\sqrt{3}$ x 4) unit cell with 4 layers. The topmost 2 layers were relaxed using DFT. 3x3x1 k-points were used for the RPA, and corrected for k-point errors using the PBE functional. The asterisk * marks those cases where the bridge configuration is energetically more favourable than hcp."* [6]

	Cu	Ag	Au	Ni	Pd	Pt	Rh
PBE	0.09*	0.05*	0.05	1.04*	1.16*	0.82*	1.46
PBE-D3	0.98	0.78	0.83	3.09	2.34*	2.09*	2.58
PBE-TS	0.87	0.77	0.80	2.85*	2.10*	1.99*	2.72*
vdW-DF	0.53	0.46*	0.53	0.56	0.83*	0.37*	1.16
vdW-DF2	0.75	0.43	0.43*	−0.07	0.63*	1.33*	0.63
optB86b-vdW	**0.69**	**0.69**	0.76*	2.25*	2.41*	2.12*	2.68
RPA	**0.66**	**0.63**	**0.64**	1.46*	**1.72***	**1.74***	2.08
Exp.	0.69[a]	0.68[a]	0.65[a]	–	1.74[b]	1.67[c]	–
Δ Exp.	±0.04	±0.05	±0.03	–	±0.30	±0.17	–

[a] Ref. [134]; recent interpretation of TPD spectra based on the Polanyi-Wigner equation [135].
[b] Ref. [136]; TPD experiments using the Redhead analysis [137].
[c] Ref. [138]; microcalorimetry measurements for benzene at θ=0.80 ML, corresponding to the $2\sqrt{3}$ x 4 unit cell.

Investigating the geometries for the different functionals, we found that PBE yields (as expected) too large benzene-substrate distances for the physisorbed systems (e.g. Ag and Au). Although including vdW interactions – either by using corrections like D3 and TS or by using a vdW functionals like optB86b-vdW – yields benzene-substrate distances closer to the experimental values, they are still somewhat too large for physisorbed systems. For chemisorbed systems like Pt, we found that all functionals, including PBE, yield benzene-substrate distances only slightly above the experimental values. These results are summarized in Fig. 9.2. Concerning the benzene-substrate distance, the RPA is again in very good agreement with experiment (Ag: 2.95 Å, Au: 3.02 Å). Furthermore, we found that the benzenes' intramolecular geometries (*i.e.* relaxation with different methods) have little influence on the RPA energies. However, an accurate benzene-substrate distance is crucial to obtain accurate RPA adsorption energies.

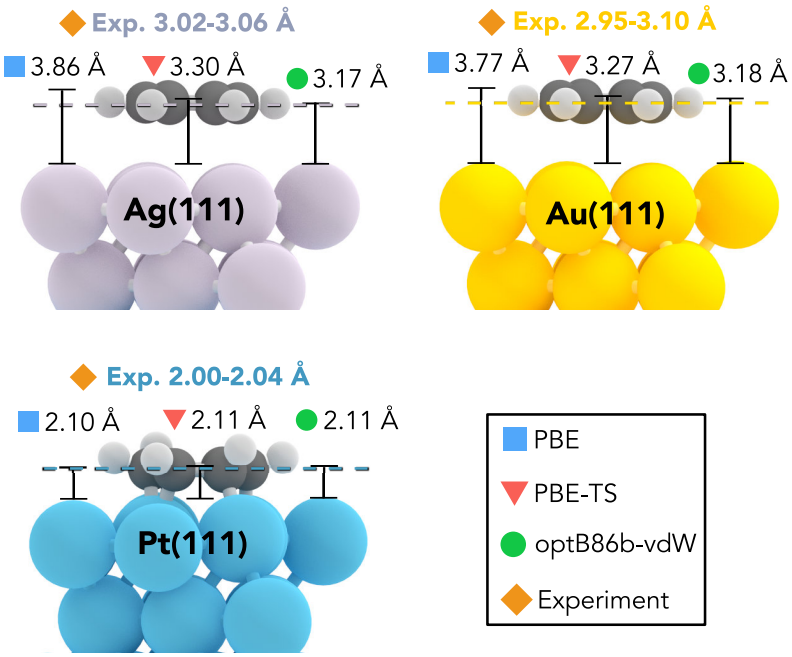

Figure 9.2: *"Averaged carbon-metal distances for benzene on Ag, Au, and Pt using the PBE, PBE-TS, and optB86b-vdW functionals. Experimental heights are included for comparison."* [6]

Finally, we investigated the coverage dependence of the adsorption energy (see Fig. 9.3). It is expected – and confirmed by experiment – that the adsorption energy decreases with increasing coverage, due to repulsions between the molecules and a progressive passivation of the substrate atoms. The results for PBE, vdW-DF, and vdW-DF2 where not satisfactory on an absolute scale and cannot even qualitatively reproduce the trend of decreasing adsorption energy. The other functionals (PBE-D3, PBE-TS and optB86b) are closer to the experimental data on an absolute scale but predict an instability at 70% coverage, that is not observed experimentally. Again, only the RPA was within the experimental error bars on an absolute scale and also reproduced the trend in the experimental data flawless.

In summary, we established that the RPA's systematic improvement, which had been observed for the adsorption of CO on metal surfaces, carries over to the much more challenging aromatic molecules.

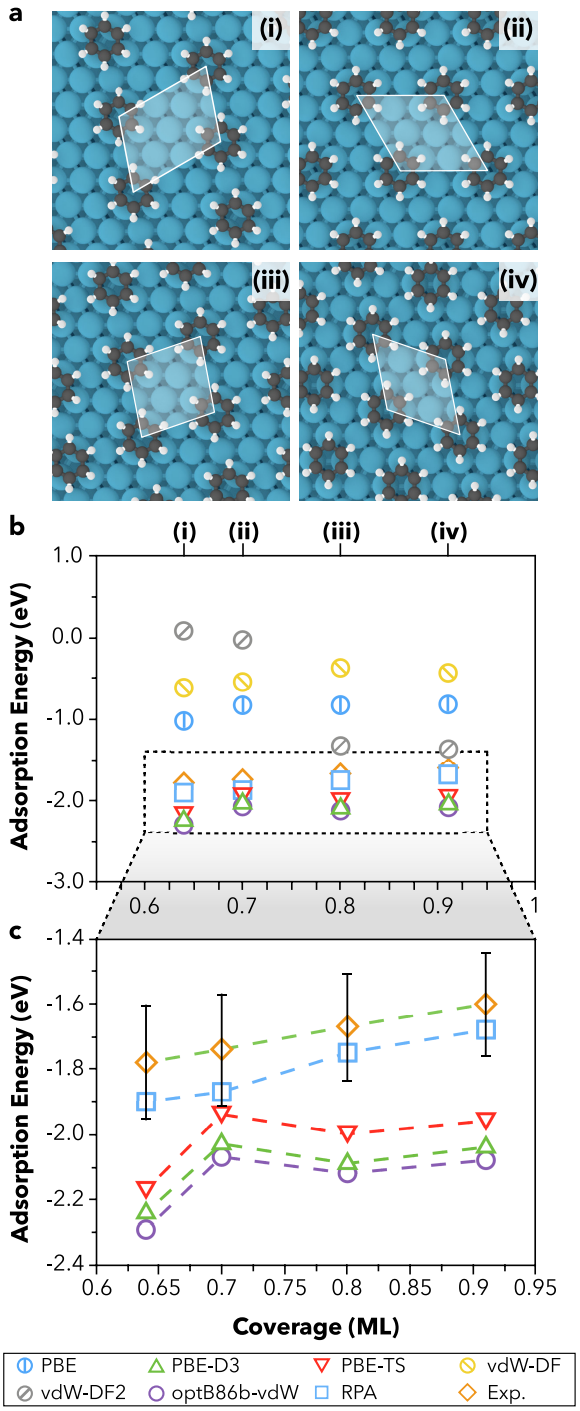

Figure 9.3: *"Adsorption energy as function of the coverage for benzene on Pt(111). (a) Considered geometries for benzene at coverages θ_i=0.64, θ_{ii}=0.71, θ_{iii}=0.80 and θ_{iv}=0.91 monolayers (ML), defined by the corresponding surface unit cells: (i)=(4 2 | -1 3), (ii)=(3 0 | 0 3), (iii)=(3 1 | 1 3) and (iv)=(2 -1 | 1 3). (b) Adsorption energy (in eV) for benzene on Pt(111) for those coverages (in ML). (c) Magnification of the previous plot in the area near the experimental energy range (dotted lines are added to underline the trends)."* [6]

9.2 Water on boron nitride

In Ref. [4], Al-Hamdani, Rossi, Alfè, Tsatsoulis, Ramberger, Brandenburg, Zen, Kresse, Grüneis, Tkatchenko, and Michaelides conducted a comprehensive benchmark study on the adsorption of water on boron nitride. In this collaboration, wave function based methods and different density functionals as well as vdW corrections were used to calculate adsorption energies for water on boron nitride substrates of varying size and dimension. Additionally many body dispersion corrections (MBD) and time-dependent DFT (TD-DFT) were used to calculate static polarizabilities and dynamic polarizabilities. The participants provided versatile contributions, including reference data from methods of their respective expertise. In this context, we performed RPA calculations for water on hexagonal boron nitride (hBN) at different cell sizes and with varying k-points. Additionally, we calculated corrections to the RPA correlation energy from GW single excitations (GWSE) [120]. In the following we will give a very brief excerpt of Ref. [4], focusing on results directly related to our contributions. For a more elaborate presentation we refer the interested reader to the original publication.

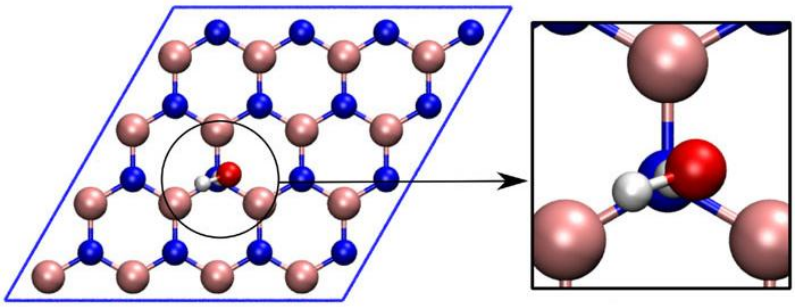

Figure 9.4: Adsorption of water at hBN N-site. Picture taken from reference [4].

In biology and surface science, the interactions between compounds often originate from a mixture of different physical effects, for example electrostatic and dispersion interactions. The adsorption of water on BN substrates is an interesting model system to examine this interplay of various interaction. BN substrates form hexagonal rings that are geometrically analogous to carbon substrates, see Fig. 9.4. Due to its 2D nature, hBN gives rise to long-range Coulomb interactions similar to graphene. However, since hBN is an insulator – unlike its carbon equivalent graphene – it is not obvious whether it gives rise to substantial non-additive dispersion interactions. By computing adsorption energies with coupled cluster theory, fixed-node quantum Monte Carlo (FNQMC), the RPA, and second order Møller-Plesset theory as well as different semi local density functionals and vdW corrections, Al-Hamdani *et al.* found that the water adsorption energy remains almost constant as the BN substrate size increases. Using TD-DFT and MBD techniques they showed that the consider-

able non-additivity in the dispersion interactions can be explained by a high degree of anisotropy in the polarizability. [4]

We used RPA@PBE to calculate the adsorption energy for water on the N-site of hBN. In this context we used a pristine hexagonal lattice with the experimental lattice constant a=2.51 Å and 16 Å vacuum between the periodic images in the direction perpendicular to the surface. We calculated energies with a 430 eV plane-wave energy cutoff for varying substrate-water distances up to 7.5 Å (details on the gemoetries can be found in the supplemental material of Ref. [4]). In a 4×4 unit cell (32 surface atoms) using the Γ-point approximation to sample the Brillouin zone we obtain a minimum RPA energy of -69 meV at 3.36 Å, when we use the RPA energy at 7.5 Å as reference zero. However, this result is not very accurate as significant finite size errors occur at the chosen cell size. Therefore we computed the RPA energy at different cell sizes up to 98 surface atoms (7×7). For this calculations we used always a oxygen/hBN distance of $d_O = 3.25$ Å. We found that the finite size correction in the RPA is 20 meV. This value is very close to the finite size corrections in MP2 or PBE+MBD, also reported in Ref. [4]. This suggests that the PBE+MBD method is a convenient choice to estimate the finite size correction of correlated methods for these kind of systems. It is expected that an improved k-point sampling has a similar effect as increasing the cell size, once the cell size is large enough that interactions between the periodic images of the water can be neglected. In confirmation of that, we found that the adsorption energy with a $4 \times 4 \times 1$ k-mesh using a (3×3) cell differs only by 2 meV from value from the Γ (7x7) calculation. Additionally we calculated GWSE as corrections to improve on the RPA results and it turned out that they account for another 19 meV. Our best estimate for the adsorption energy of water on hBN using the RPA+GWSE and finite size correction was 108 meV at $d_O = 3.25$ Å, which is very close to the MP2 result (110 meV at $d_O = 3.25$ Å) as well as the FNQMC result (107 ± 7 meV at $d_O = 3.40$ Å) also reported in Ref. [4].

Finally we conducted similar calculations for water on borazine in a 15x15x15 $Å^3$ cell at the Γ-point. There, at $d_O = 3.32$ Å, our best estimate for the adsorption energy of water using the RPA+GWSE was 112 meV, which is less than 10% lower than the MP2 result (120 meV) as well as the FNQMC result (122 ± 4 meV) also reported in Ref. [4].

Once again, the RPA turned out to yield a balanced description for a theoretically challenging model system and the results reported in Ref. [4] by Al-Hamdani *et al.* provide valuable insights into the nature of interactions in 2D-materials as well as into the capabilities of different correlated electronic structure methods.

9.3 Water on graphene

In Ref. [5], Brandenburg, Zen, Fitzner, Ramberger, Kresse, Tsatsoulis, Grüneis, Michaelides, and Alfè conducted a comprehensive benchmark study on the adsorption of water on graphene. In this collaboration, different many-body approaches were used to calculate adsorption energies for water on benzene, coronene and graphene. The participants provided versatile contributions, including reference data from methods of their respective expertise. In this context, we calculated RPA correlation energies for water on graphene at different water-substrate distances and orientations. Additionally, we calculated corrections to the RPA correlation energy from GW single excitations (GWSE) [120]. In the following, we will give a very brief excerpt of Ref. [5], focusing on results directly related to our contributions. For a more elaborate presentation we refer the interested reader to the original publication.

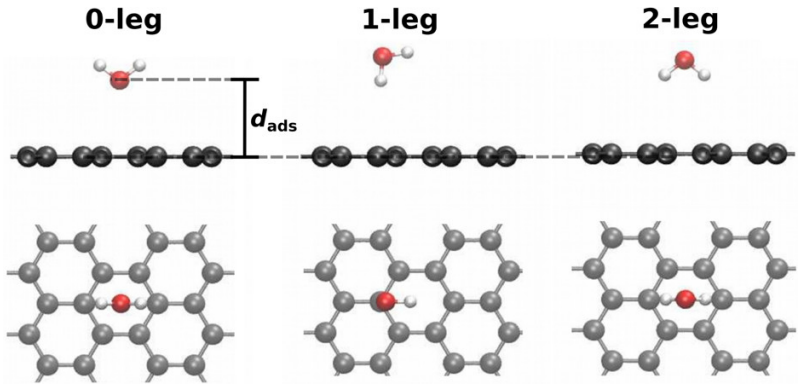

Figure 9.5: Investigated binding motifs for the adsorption of water on graphene. Picture taken from reference [5].

Within the broad field of surface science, special attention is payed to water-carbon interfaces. On the one hand, they play an integral role in the process of water purification and for desalination membranes. On the other hand, water-carbon interfaces can exhibit intriguing behaviors that arouse great scientific interest. For example, on sp2-bonded carbon surfaces – as present in carbon nano tubes or graphene – water can flow in an essentially frictionless manner. Graphene itself is of general interest, in its role as a prototype 2D van der Waals (vdW) material. To understand the fascinating properties of water-carbon interfaces, it is essential to accurately assess the interaction strength between the constituents, the relative orientation of the molecule on the surface, and the physical nature of the interaction. The fact that as little as 60 meV difference in the predicted adsorption energy of water transforms the graphene surface from hydrophobic to hydrophilic led to an intensive debate over the hydrophobicity of graphene and underpins how crucial accurate adsorption energies are for theoretical predictions. Contact angle measurements provide an experimental technique to investigate the water-graphene interface and in one of these

experiments, a support lattice independent water contact angle of 42 ±3° was found. The wide spread (0° to 90°) in contact angle predictions from computer simulations illustrates the sensitivity with respect to the water-carbon interaction parameter. However, there is hope that accurate estimates of the water-carbon interaction from advanced electronic structure methods will help to solve this hydrophobicity conundrum. To address this issue, Brandenburg *et al.* [5] used different methods to calculate adsorption energy curves of molecular water on graphene, coronene and benzene. These methods included diffusion Monte Carlo (DMC); periodic coupled cluster approach including singles, doubles, and perturbative triples [p-CCSD(T)]; and RPA with GWSE. They found that the employed methods are in good agreement with each other – see Tab. 9.2 – and demonstrated that adsorption energies on extended surfaces can now be computed with subchemical accuracy. Their study revealed that although the different water orientations on the graphene layer show quite distinct interaction behaviors, they ultimately yield very similar binding energies.

Table 9.2: Equilibrium binding distances d_{ad} (Å) and energies E_{ad} (meV) of a single water monomer on graphene from DMC, p-CCSD(T), RPA, and RPA+GWSE. The values were obtained by interpolating the binding energy curves $E_{\mathrm{b}}(d)$ with a Morse fit, yielding E_{ad}, d_{ad}, and the corresponding error. The p-CCSD(T) values were only calculated for a single point, at the DMC equilibrium positions.[5]

	DMC		p-CCSD(T)		RPA		RPA+GWSE	
	d_{ad}	E_{ad}	d_{ad}	E_{ad}	d_{ad}	E_{ad}	d_{ad}	E_{ad}
0-leg	3.10(3)	−90(6)	–	−84	3.09(1)	−81(2)	3.05(1)	−90(2)
1-leg	3.46(3)	−92(6)	–	−76	3.52(1)	−74(1)	3.45(1)	−87(1)
2-leg	3.37(2)	−99(6)	–	−87	3.41(1)	−82(1)	3.33(1)	−98(1)

We performed RPA@PBE and GWSE calculations for three different motifs of water on graphene (see. Fig. 9.5). We calculated the RPA total energy as well as GWSE corrections at different O/substrate distances d_{ad} in a $5 \times 5 \times 1$ cell (50 carbon atoms) at 14 Å vacuum distance between the periodic images of the graphene sheets. To improve our accuracy, we corrected the obtained energies with results from an increased vacuum of 20 Å at the equilibrium geometry. Using PAWs with an energy cutoff of 430 eV, we extrapolated to the basis set limit assuming that errors drop off like one over the basis set size. In these calculations we used the Γ-point approximation to sample the first Brillouin zone and justified it by testing the convergence of the k-point sampling with additional calculations using $2 \times 2 \times 1$ k-points and a $4 \times 4 \times 1$ supercell. This additional setting corresponds to 64 points in the Brillouin zone of a primitive graphene cell, whereas the original setting corresponds to 25. For each motif, the reference zero energy was set to the energy at a configuration far from the surface $E(d_{\mathrm{far}})$, or in other words, the binding

energy E_b at distance d is calculated as

$$E_\mathrm{b}(d) = E(d) - E(d_\mathrm{far}). \tag{9.1}$$

More details on the geometries are found in the supplemental material of Ref. [5].

From analyzing the binding energy curves of water on benzene, coronene and graphene, Brandenburg *et al.* concluded that the electrostatic component to the interaction is attractive for the 1-leg and 2-leg motifs, while it is repulsive for the 0-leg motif on benzene. However, they found that with increasing substrate size, this repulsive interaction decreases significantly and simultaneously the contribution from attractive vdW interactions grows. Analyzing the charge redistribution upon moving the water towards the graphene surface, they found that the 1-leg and 2-leg motifs behave in a rather similar manner, while the 0-leg motif has a quite distinct electrostatic interaction along with a more pronounced charge reorganization in the substrate. Interestingly, while on smaller substrates the orientation of the water molecule plays a significant role for the binding energy, the effects seen in graphene balance the interactions in a way that the binding energy is relatively independent of the orientation. We hope that these findings facilitate further studies on this exciting subject and that they can be used to explain the very low friction coefficient of liquid water on sp2-bonded carbon.

Chapter 10

RPA as a benchmarking tool for DFT functionals

In their publication [2], Bokdam, Lahnsteiner, Ramberger, Schäfer, and Kresse presented a novel method to assess the quality of DFT functionals, employing the RPA as benchmark tool. This scheme was the first significant application of our RPA forces algorithm beyond standard relaxations and phonon calculations. For this reason, we will outline the key features of the newly developed benchmark method in the following chapter.

DFT is extremely successful in modeling the electronic structure of most molecules and solids. Many different functionals have been developed, providing versatile tools required for investigating different systems with diverse properties. However, there is a fundamental flaw in some way directly related to the huge variety of different functionals, namely the selection of the appropriate one. While experts often have a "chemical intuition" helping to pick one of the numerous functionals for a given task, there are few systematic approaches to the selection of the "best" functional for structure simulations of a particular material. In Ref. [2], Bokdam *et al.* present a concise, first principles, approach to address this problem.

They developed a fully *ab initio* benchmark scheme for density functionals using RPA molecular dynamics (MD), designed to systematically select the best functional for finite temperature structure predictions of a certain material. To demonstrate the capabilities of the method, this approach was applied to the hybrid perovskite methyl ammonium lead iodide ($MAPbI_3$), a promising new solar cell material.

Hybrid perovskites are highly interesting due to practical considerations. While they can be produced at low cost using wet chemistry, they reach a light to electricity conversion efficiency of 20%, close to that of costly fabricated silicon based solar cells. Since experimental studies on the atomic structure of these materials are extremely challenging, they represent a particularly interesting species for *ab initio* electronic structure studies.

However, it is also very difficult to describe these systems with high precision using first principles methods. Accurate band gap related properties and lattice constants

seem important to describe instabilities in the perovskite cage while even at room temperature, the MA molecules exhibit rotations coupled to concerted movements of the surrounding PbI_3 lattice. To describe these materials accurately with an *ab inito* approach, it is crucial to use an appropriate functional.

We will now present the method Bokdam *et al.* used to judge the quality of different functionals for $MAPbI_3$, but stress that the method can be easily transferred to other materials, providing a general and systematic approach to select an appropriate functional.

The center piece of the method is to construct a well-distributed RPA canonical ensemble. We show how this can be achieved on the basis of the specific example presented in Ref. [2]. First 16 practically independent configurations were obtained from long preparatory DFT-MDs at 400K. These were then used as the starting configurations for 16 separate, independent RPA-MDs at 400K, using the RPA forces algorithm presented in chapter 7. From the finite temperature RPA-MD trajectories, 32 equally spaced (in time) configurations of the last 1.3 ps were picked. The resulting 512 partly correlated configurations obtained in this manner represent the desired RPA canonical ensemble.

Table 10.1: "*Considered functionals, and the square root of the variance (σ, in meV) of the energy difference between the RPA and the functionals in the RPA/SCAN/PBEsol-ensemble, respectively.*" [2]

SCAN	Strongly Constrained and Appropriately Normed [139]	25	53	67
HSE-D3	HSE [140] + Grimme D3 [117]	27	55	68
HSE	Heyd-Scuseria-Ernzerhof [140]	27	57	69
PBE	Perdew-Burke-Ernzerhof [9]	44	87	104
PBE-MBD	Many body dispersion [118]	47	89	109
PBE-D3	Grimme D3, vdW corrections [117]	51	88	111
PBE-TS	Tkatchenko-Scheffler, vdW corrections [14]	54	90	109
optPBE	vdW DFT functional based on PBE [141]	54	95	104
PBEsol	Revised PBE for solids [142]	55	96	106

Now, the energy difference between each functional and the RPA for all configurations in the RPA ensemble is calculated. Since a constant shift in the energy does not change the dynamics of a system, the differences are shifted by the the mean difference between the RPA and the respective functional. By construction, the thereby obtained numbers ΔE are distributed around zero for all functionals. In the specific example presented in Ref. [2], the histograms show roughly a Gaussian distribution. Finally, one can rank the quality of the examined functionals, by evaluating the variance σ^2 of the (shifted) energy differences ΔE for each functional. Per se, this is of course only a measure for the agreement of a certain functional with the RPA. However, as should be clear by now, in many cases the RPA is superior to most density functionals, so that it is justified to use the agreement with the RPA

as a benchmark.

It should be mentioned, that Bokdam *et al.* used a relatively small cell for the RPA-MDs due to the computational complexity of the calculation of RPA forces. To address this issue, they constructed ensembles from MD simulations for larger supercells using the tentatively best and worst preforming functional (SCAN and PBEsol). As before, the energy differences to the RPA and the resulting variance were calculated for the additional ensembles. The additional simulations confirmed that the results carry over to larger supercells and were not biased by the short simulation times. The results for all three ensembles are summarized in Tab. 10.1.

The study found that from the considered functionals, SCAN is the best one to describe $MAPbI_3$. Consequently, the authors used the SCAN functional to study the tetragonal distortion ($c/a > 1.0$) that is experimentally observed up to and about room temperature. That way, they found a tetragonal instability at low temperatures in agreement with experiment. To underline the predictive power of the RPA-MD benchmark we note that the intuitive choice for these kind of materials, the PBEsol functional, does not yield a similar instability. Furthermore, in contrast to previous suggestions that vdW corrections should be included for these kind of materials, the study showed that this does not seem to be the case. Bokdam *et al.* explained this by the strong screening of the PI_3 cage.

In summary, using the RPA forces algorithm for MD simulations, one can create RPA ensembles to benchmark DFT functionals, based on the variance with respect to the RPA energy surface. This avoids the usual trial and error approach, where many different functionals are tested against experimental data until the desired agreement is reached. The systematically selected functional can then be used as a cheap and viable alternative to create ensembles for large scale structure predictions, when higher level many body electronic structure methods are too expansive.

Chapter 11

RPA natural orbitals and their application to post-Hartree-Fock electronic structure methods

We present a method to approximate post-Hartree-Fock correlation energies by using approximate natural orbitals obtained by the random phase approximation (RPA). We demonstrate the method by applying it to the helium atom, the hydrogen and fluorine molecule, and to diamond as an example of a periodic system. For these benchmark systems we show that RPA natural orbitals converge the MP2 correlation energy rapidly. Additionally we calculated FCI energies for He and H_2, which are in excellent agreement with literature and experimental values. We conclude that the proposed method may serve as a compromise to reach good approximations to correlation energies at moderate computational cost, and we expect the method to be especially useful for theoretical studies on surface chemistry by providing an efficient basis for correlated wave function based methods. Note that this chapter was already published by the author of this thesis and co-authors in a peer reviewd article [3].

11.1 Introduction

In *ab initio* quantum chemistry and computational materials physics there exists a well know trade off between accuracy and computational cost. Solving the many electron Schrödinger equation is an exponentially hard problem with respect to the number of electrons and therefore solving it exactly is out of scope for most practically relevant systems. Therefore approximations with varying degrees of accuracy are employed. While mean-field methods like Hartree-Fock (HF) [50, 51, 143] and density functional theory (DFT) [7, 8] possess computationally favorable scaling of N^3 with the number of electrons, they sometimes lack accuracy and fail to describe certain processes. For example describing the dissociation of simple molecules like

H_2 already poses a challenge for such methods [12]. The properties that are not well described by the HF approximation are attributed to so called electron correlation and there exists a wide variety of electronic structure methods all of which attempt to take the correlation effects into account in an approximate manner. Most of them have in common that one can increase the accuracy systematically at the expense of computational resources, e.g. Møller-Plesset perturbation theory (MPn) [53, 144] , coupled cluster (CC) [145, 146, 147] and configuration interaction (CI) [148, 149, 150, 151, 152, 153, 154] methods.

DFT and HF calculations can provide a useful single electron basis as a starting point for correlated methods. However the correlated methods have in common that they usually involve virtual orbitals, *i.e.* eigenstates of the single-electron Hamiltonian from the underlying HF or DFT calculation that are unoccupied in the respective underlying calculation. To obtain the energy exactly (within the approximation of the respective correlated method) a complete basis set of single particle states is required. The convergence behavior with respect to the number of single particle states depends of course on the specific set of orbitals employed. Therefore one can in principle obtain results that are converged up to machine precision with a finite number of virtual states and ideally reduce the computational costs significantly by using a small number of appropriate single particle orbitals.

The essence of the above statement is that, by choosing an appropriate set of single particle orbitals, one can extract the relevant information resting in the full many body wave function from a small number of single particle wave functions. The question remains how to choose an appropriate set. One possible answer is to use natural orbitals as they turned out to capture much of the relevant information required to converge correlation energies quickly [155]. It has already been demonstrated that natural orbitals at the MP2 level can be employed to reduce the computational cost of wave function based methods [156]. Furthermore, recently Bruneval has shown that the so called linearized GW density matrix is of similar quality as the MP2 density matrix [157, 158]. This and the connection [159] between the random phase approximation (RPA) [27, 79] and GW method [66], as well as the successful applications of the RPA [28, 29, 30, 160, 161] suggests that RPA natural orbitals (RPANOs) should provide an efficient basis for higher hierarchy methods.

In this chapter, we will show how we can approximate natural orbitals by employing the RPA and how to utilize the approximate natural orbitals to obtain accurate correlation energies at moderate computational cost. We will demonstrate the method by showing the convergence behavior of the MP2 energy with respect to the number of RPANOs for the following prototypical systems: the helium atom, the hydrogen molecule at various internuclear distances, the fluorine molecule at equilibrium distance and diamond as an example for a periodic system. In the case of He and H_2 we will also show results for FCI calculations using an RPANO basis and will furthermore compare the exact natural orbitals from FCI with the RPANOs.

11.2 Theory

In second quantization notation, the one particle reduced density matrix (1-RDM) is

$$n(\mathbf{r},\mathbf{r}') = \langle\Psi|\hat{\psi}^\dagger(\mathbf{r}')\hat{\psi}(\mathbf{r})|\Psi\rangle \tag{11.1}$$

with the usual field operator $\hat{\psi}$. Natural orbitals $\{\varphi_i\}$ are just the eigenstates of the 1-RDM:

$$\int_{-\infty}^{\infty} \mathrm{d}^3\mathbf{r}'\; n(\mathbf{r},\mathbf{r}')\;\varphi_i(\mathbf{r}') = f_i\;\varphi_i(\mathbf{r}). \tag{11.2}$$

The 1-RDM is the central object of reduced density matrix functional theory (RDMFT) [162]. In comparison with conventional DFT, RDMFT has the advantage that besides the Hartree energy, also the kinetic and the exchange energy are obtained exactly. Finding an efficient way to approximate the 1-RDM as well as natural orbitals can therefore provide an interesting pathway for RDMFT [163]. Though we did not pursue it, we still want to note that the method described hereafter for approximating the 1-RDM within the RPA might also be interesting for research in the field of RDMFT.

We will now try to establish a connection between the 1-RDM and the RPA by using a Green's function formalism. The 1-RDM is obtained from the Green's function in the limit of small negative time:

$$n(\mathbf{r},\mathbf{r}') = -\,\mathrm{i}\lim_{t\to 0^-} G(\mathbf{r},\mathbf{r}',t), \tag{11.3}$$

which can be easily seen from the definition of the Green's function

$$G(\mathbf{r},\mathbf{r}',t'-t) = -\,\mathrm{i}\,\langle\Psi_0|\hat{T}\{\hat{\psi}(\mathbf{r},t)\hat{\psi}^\dagger(\mathbf{r}',t')\}|\Psi_0\rangle\,, \tag{11.4}$$

where $\hat{T}$ is the Wick time-ordering operator.

In a system with N electrons, the independent particle Green's function G^0 corresponds to a ground state with a single Slater determinant $|\phi_1\cdots\phi_N\rangle$ and the 1-RDM reduces to

$$n^0(\mathbf{r},\mathbf{r}') = -\,\mathrm{i}\lim_{t\to 0^-} G^0(\mathbf{r},\mathbf{r}',t) = \sum_{i\in occ.}\phi_i(\mathbf{r})\phi_i^*(\mathbf{r}'). \tag{11.5}$$

The natural orbitals are then just the occupied independent particle orbitals $\{\phi_i\}$. This would be the situation for a DFT or HF calculation.

To improve on the independent particle 1-RDM and to include "information" on the unoccupied virtual space, the Dyson equation for the Green's function

$$G(2,1) = G^0(2,1) + G^0(2,3)\Sigma(3,4)G(4,1) \tag{11.6}$$

can be used to write a perturbation series for the (full) 1-RDM as a functional of

the total self-energy Σ and the independent particle Green's function G^0:

$$n = n^0 - \mathrm{i} \lim_{t \to 0^-} \left\{ G^0 \Sigma G^0 + G^0 \Sigma G^0 \Sigma G^0 + ... \right\}. \tag{11.7}$$

In the imaginary time/frequency domain, the first order term (with respect to Σ), $n^{(1)}$, is explicitly obtained as [1, 120, 164, 165]

$$n^{(1)}(\mathbf{r}, \mathbf{r}') = \lim_{\tau \to 0^-} \frac{1}{2\pi} \int_{-\infty}^{\infty} \mathrm{d}\nu \; e^{-\mathrm{i}\,\nu\tau}$$

$$\int \mathrm{d}\mathbf{r}'' \mathrm{d}\mathbf{r}''' G^0(\mathbf{r}, \mathbf{r}'', \mathrm{i}\,\nu) \Sigma(\mathbf{r}'', \mathbf{r}''', \mathrm{i}\,\nu) G^0(\mathbf{r}''', \mathbf{r}', \mathrm{i}\,\nu). \tag{11.8}$$

In the method shown below we will use this first order correction to the density matrix. Furthermore, we will approximate the self-energy using the RPA so that we will ultimately obtain an approximate set of natural orbitals, the RPANOs, as eigenfunctions of the first order RPA density matrix

$$n^{\mathrm{RPA}}(\mathbf{r}, \mathbf{r}') = -\mathrm{i} \lim_{\tau \to 0^-} \left[G^0 + G^0 \Sigma_{\mathrm{RPA}} G^0 \right] (\mathbf{r}, \mathbf{r}', \mathrm{i}\,\tau). \tag{11.9}$$

We note that the RPA violates the Pauli principle since it does not include all properly anti-symmetrized diagrams (see e.g. Kosov [166] or Hummel and co-workers [167]). Here it is important to recall that the main purpose of our method is an efficient low scaling calculation of an approximate density matrix to allow one to obtain a compact set of orbitals for wave function based calculations. A highly accurate description of the density matrix is not strictly required in the present case. We will document one case where the RPA density matrix is qualitatively wrong but still yields a very compact set of orbitals (compare Fig. 11.13). More details on the RPA density matrix can be found in the references [120, 157, 158, 159, 164].

11.3 Method

Assuming that with only a few RPA natural orbitals one can span the relevant subspace of the one electron wave functions for advanced methods like MP2 or CI, we aim to accurately approximate electronic ground state energies of these methods using a small number of virtual states. Thereby we are hopefully able to reduce the computational cost in these calculations significantly. In Subsection 11.3.1, we will give a step by step recipe for obtaining RPA natural orbitals in order to calculate approximate post-Hartree-Fock ground state energies (e.g. MP2, CC and CI) with a reduced number of virtual states.

11.3.1 RPA natural orbitals

In the first step, one calculates the electronic ground state at mean-field level (HF or DFT) in order to obtain a well converged set of one electron wave functions for the occupied space. These occupied orbitals fix the respective mean-field Hamiltonian for the subsequent steps. In the second step "all" unoccupied orbitals are calculated by diagonalizing the one particle Hamiltonian in the entire underlying basis set. "All" means that the number of eigenfunctions of the Hamiltonian (*i.e.* orbitals) that are calculated is equal to the number of basis functions used. Specifically for a plane wave basis with a cut-off energy E_{cut} this means that the sum of occupied orbitals N_{occ} and virtuals N_{virt} is equal to the number of plane waves below the cut-off, or in other words equal to the size of the underlying plane-wave basis set:

$$N_{\text{occ}} + N_{\text{virt}} = \text{card}\left\{\mathbf{G} : \frac{\hbar^2}{2m_e}|\mathbf{G}+\mathbf{k}|^2 < E_{\text{cut}}\right\}, \tag{11.10}$$

where $\mathbf{k}$ is the Bloch wave vector.

In the next step, the independent particle Green's function G^0 is calculated from all orbitals to subsequently calculate the independent particle polarizability χ^0, the RPA screened interaction W^{RPA}, as well as the RPA self energy Σ_{RPA} [35, 62, 63]. Note that Σ_{RPA} is related to the GW-approximation as the self energy in the first self-consistency cycle [1, 28]

$$\Sigma_{\text{RPA}}(\mathrm{i}\,\tau) = -G^0(\mathrm{i}\,\tau)W^0(\mathrm{i}\,\tau), \tag{11.11}$$

where W^0 in the GW framework is synonymous to W^{RPA}. Having the self energy at hand, one can use Eq. (11.9) to calculate the RPA density matrix. Note that this RPA density matrix is an approximation to the fully self-consistent GW density matrix [159] in the same way as the linearized GW density matrix [157, 158]. The density matrix $n = n^0 + n^{\text{RPA}}$ is than diagonalized in the subspace of the virtual states, *i.e.* the occupied states from the mean-field calculation are retained. The occupied orbitals together with the eigenstates obtained from that subspace diagonalization form the RPANOs basis set. Keeping the occupied states has practical reasons. In this way, the RPANOs reproduce the underlying HF or DFT ground state energy exactly, while at the same time the virtual states are rearranged to yield a more compact set for higher hierarchy methods when the orbital set is truncated. RPANOs obtained by this approach therefore provide a versatile basis for different applications.

The RPANOs are sorted by descending occupation number, *i.e.* eigenvalue with respect to the density matrix, and to obtain a truncated basis with N basis functions, one simply uses the first N RPANOs according to this order. In some cases, it is now necessary to diagonalize the mean-field Hamiltonian in the subspace spanned by the truncated RPANOs basis. For example, to calculate the MP2 energy with 256 RPANOs, the HF Hamiltonian is diagonalized in the subspace spanned by the first 256 RPANOs. The subspace HF orbitals from that diagonalization span the same

space as the truncated RPANOs and allow at the same time to use the Brillouin theorem as required by most MP2 implementations.

The computational cost for all the above calculations scales cubically in system size [35, 62, 63], allowing the method to be used for relatively big systems ($\approx$ 100 atoms) with moderate computing resources ($\approx$ 100 CPUs).

11.3.2 FCI

The full configuration interaction method (FCI) solves the non-relativistic Schrödinger equation within a given basis set exactly. Therefore it provides a useful benchmark for other correlation-consistent methods. Its computational cost scales exponentially with the number of orbitals and the number of electrons, limiting its range of application. In order to obtain the FCI solution, one starts with the HF orbitals and constructs all possible Slater determinants with N_{occ} occupied orbitals. By separating each Slater determinant in its spin up and spin down part, and by using Slater-Condon rules, it is possible to efficiently evaluate contractions of the form HC, where C is the vector of Slater determinant weights in the wave function. Following the method of Handy and Knowles [149] and using a Davidson-Liu algorithm to iteratively diagonalize the matrix H [168], the FCI solution can be obtained. Using Eq. (11.1), the FCI 1-RDM can be easily calculated once the FCI wave function is known. Finally, the diagonalization of this density matrix gives the FCI natural orbitals.

11.4 Application

All calculations regarding the RPANOs were performed using `VASP` [169, 170, 171]. To obtain the RPANOs we tried two different approaches, namely (restricted) HF as well as PBE as underlying single determinant method. However, since the observations for these two approaches were very similar, we will focus on presenting the results that we obtained from using the HF orbitals as the underlying approach for the RPA calculations. For large scale applications on many atom systems, one would most likely though revert to the more efficient DFT approximation. The RPANO calculations are based on the RPA implementation described in previous work [35, 62, 63]. For the investigated systems, 8-12 points on the imaginary time/frequency axis were sufficient. For the MP2 calculations presented here, we used the standard routines available in `VASP` [172, 173]. The FCI calculations were performed with a development version, briefly described above. Details can be found in the master thesis of Sukurma [174]. Besides using RPANOs, we also performed MP2 and FCI calculations with truncated HF basis sets, for the purpose of comparison. For these truncated HF basis sets, HF orbitals were ordered by ascending HF eigenvalues and only the lowest ones were used. Where not stated otherwise, the shown figures were obtained from calculations with a plane wave cut-off of 750 eV. Note that the orbitals shown below are approximations and do not fulfil the exact cusp condition

due to the use of a finite sized plane wave basis set [compare Eq. (11.10)].

11.4.1 Helium atom

The first benchmark system that we studied is the helium atom. The helium atom is an ideal benchmark system for many body approaches for various reasons. First, unlike other model systems (e.g. Jellium) it is a real many body system that can be studied experimentally. Though it is a relatively simple system, its theoretical description faces already prototypical many-body challenges and it is not possible to write down a closed form for its exact solution. Furthermore a numerically exact solution is available, providing a perfect ground to compare to the results of approximate many body approaches [175].

The set-up was a 10 Å $\times$ 10 Å $\times$ 10 Å unit cell with periodic boundary conditions. We used a plane-wave basis with different cut-offs up to 750 eV and a $1/r$ potential for the ion.

First, we examined the convergence behavior of the MP2 correlation energy with respect to the RPANOs and compared it with that for canonical HF-orbitals. The results are shown in Fig. 11.1. While the correlation energy using canonical HF orbitals converges very slowly and would require almost the full basis set (for this set-up with a 750 eV plane-wave cut-off, these are $47 \cdot 10^3$ orbitals), with only 128 RPANOs the correlation energy converged to < 1 meV above the exact value. Note that in this case, converged results means converged for a specific fixed plane wave basis set size. To obtain accurate MP2 correlation energies one would also need to check convergence with respect to the plane wave cut-off. However to show the qualitative difference between RPANOs and HF orbitals it is sufficient to inspect the behavior at a fixed cut-off, where the error in the MP2 energy related to the cut-off is much smaller than the difference between the MP2 energy at a few hundred RPANOs and the same number of canonical HF orbitals.

We repeated the procedure for FCI correlation energies using 10 to 60 orbitals, see Fig. 11.2. As was seen for the MP2 correlation energy, canonical HF-orbitals converge the energy very slowly. Again, to reach highly accurate results, one would also need to go to higher plane wave cut-offs, but for a qualitative comparison the chosen cut-off suffices for the same reasons as at the MP2 level. As a matter of fact, the ground state energy of an FCI calculation with a specific basis is always an upper bound for the real ground state energy. One can conclude from this, that the RPANOs are much better in spanning the relevant space of correlated single particle states than the HF-orbitals.

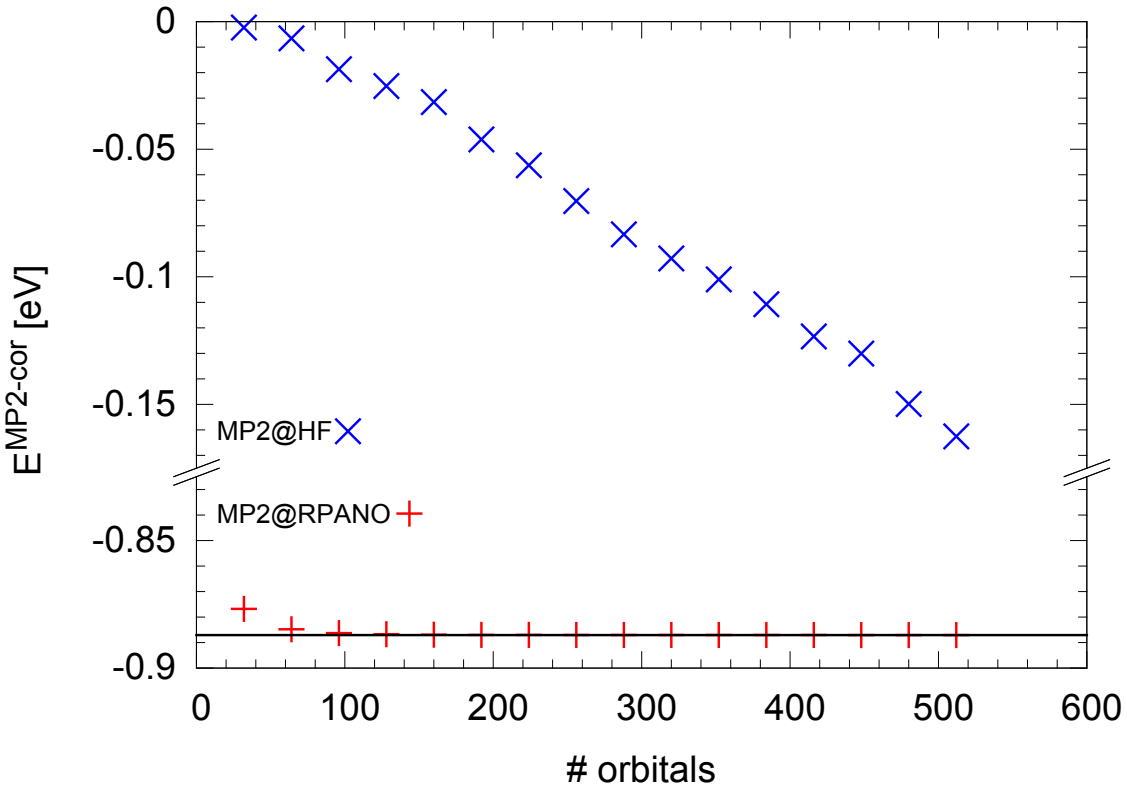

Figure 11.1: Convergence behavior of the MP2 correlation energy for the He atom. The convergence with respect to the number of RPANOs and HF-orbitals is compared. The black line shows the result for the full basis set. Note that we use two different ranges for the energy.

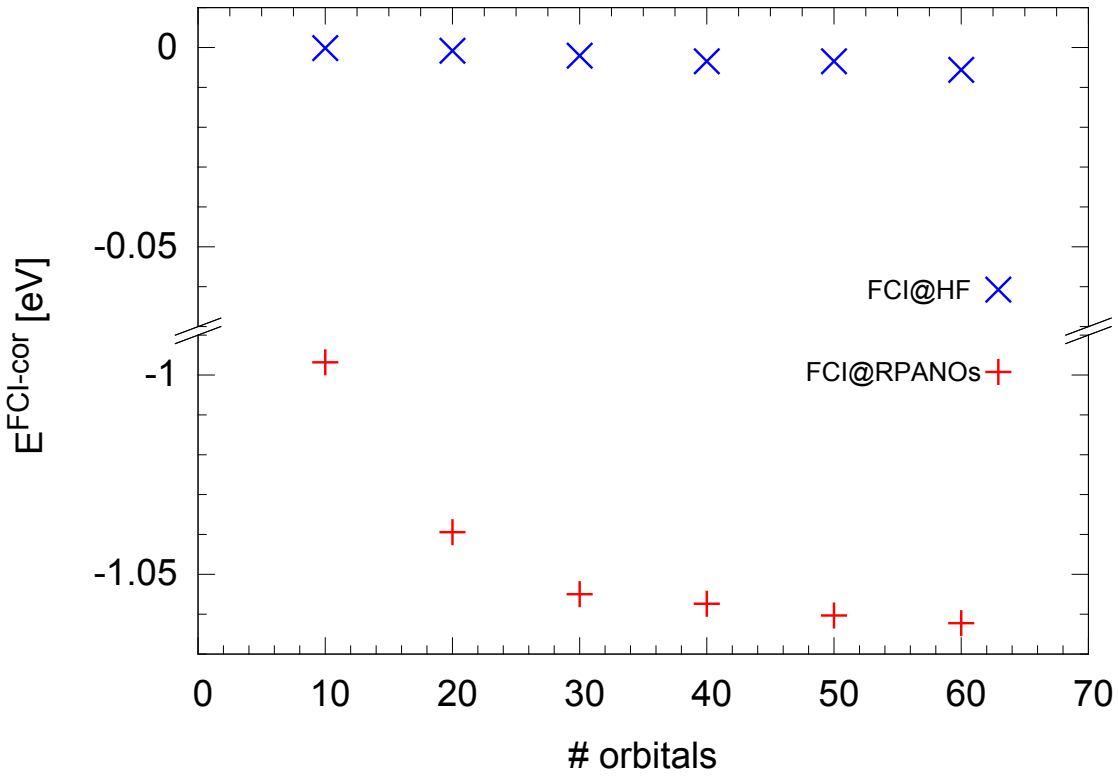

Figure 11.2: Convergence behavior of the FCI correlation energy for the He atom. The convergence with respect to the number of RPANOs and HF-orbitals is compared. The FCI energy using 10-60 HF virtual orbitals is at least 1 eV above the converged value.

In order to obtain a more accurate approximation to the total energy of the helium atom, $E^{\mathrm{tot}} = E^{\mathrm{HF}} + E^{\mathrm{cor}}$, we first used a plane wave cut-off extrapolation for the FCI correlation and the HF energy [176, 177]. The correlation energy was extrapolated from FCI values at plane wave cut-offs of 474 eV, 621 eV and 750 eV. The HF energy was extrapolated separately from plane wave cut-offs up to 6000 eV in a 16 Å × 16 Å × 16 Å unit cell in order to reach more accurate predictions. This procedure is justified, because the correlation energy is less than 1.5% of the HF energy. For the plane wave extrapolation of the energies we used a linear regression with respect to the inverse number of plane waves, N_{PW}^{-1}, which is itself proportional to $E_{\mathrm{cut}}^{-3/2}$,

$$E^{\mathrm{cor/HF}}(E_{\mathrm{cut}}) \approx E^{\mathrm{cor/HF}}(\infty) + p \cdot E_{\mathrm{cut}}^{-3/2}. \tag{11.12}$$

This value is the best approximation we can achieve for a fixed number of truncated RPANOs.

However, the value for the cut-off extrapolated correlation energy still depends on the number of RPANOs used in the FCI calculation. Therefore, to obtain a highly accurate correlation energy, we performed an orbital-set extrapolation on top of the cut-off extrapolation. To achieve this, we calculated cut-off extrapolated FCI correlation energies as described above with different numbers of RPANOs (10,20,...,60). These cut-off extrapolated values were extrapolated by another linear regression, this time with respect to the inverse number of RPANOs used in the respective FCI calculations,

$$E^{\text{FCI-cor}}(N_{\text{RPANOs}}) \approx E^{\text{FCI-cor}}(\infty) + q \cdot N_{\text{RPANOs}}^{-1}. \tag{11.13}$$

By doing so, we obtained an approximate value for the FCI total energy of −79.019 eV, which differs by less than 1 meV from the literature value from the basis set extrapolation with Gaussian cc-pVxZ basis sets [175]. The extrapolated values for the two methods are therefore well within the error bars of each other. Another "exact" value from Hylleraas-like calculations is −79.014 eV [178]; our estimation is around 5 meV bellow that. These results are summarized in Fig. 11.3.

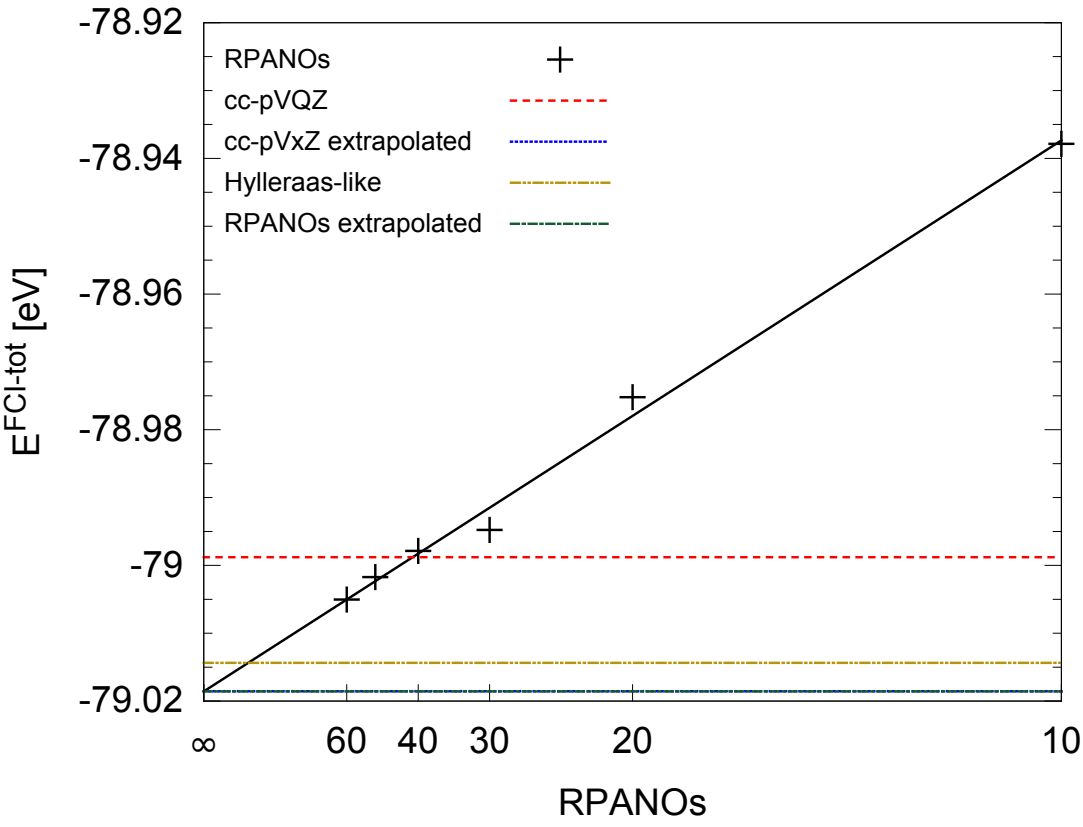

Figure 11.3: The cut-off extrapolated FCI total energies for the He atom are shown for different numbers of RPANOs. A basis set extrapolation with 1/RPANOs yields a He total energy that is 5 meV below the value from Hylleraas-like calculations. The value for extrapolated RPANOs and extrapolated cc-pVxZ are on top of each other.

Finally, we compared the shape of the natural orbitals along an axes through the nucleus of the atom. In Figs. 11.4-11.6 we show the 1s and 2s orbitals of helium for the different methods we employed. While the occupied 1s orbital is well described in the mean-field methods, the 2s orbitals for the different methods vary significantly. This is not very surprising as the HF/DFT states are not computed as eigenstates of the density matrix, but stem from a mean-field Hamiltonian. In fact, by construction, the virtual HF/DFT states are degenerate eigenstates to the HF/DFT density matrix with eigenvalue 0. This is easily seen by Eq. (11.2) and (11.5), since the mean-field single particle states are orthogonal to each other. Furthermore, from Fig. 11.6 we can deduce that the 2s FCI natural orbital is already converged with as little as 10 RPANOs, but far from converged with 60 HF orbitals. This substantiates the results from Figs. 11.1 and 11.2 that canonical HF orbitals calculated from a plane wave basis are impractical for correlated calculations, which is cured by introducing RPANOs.

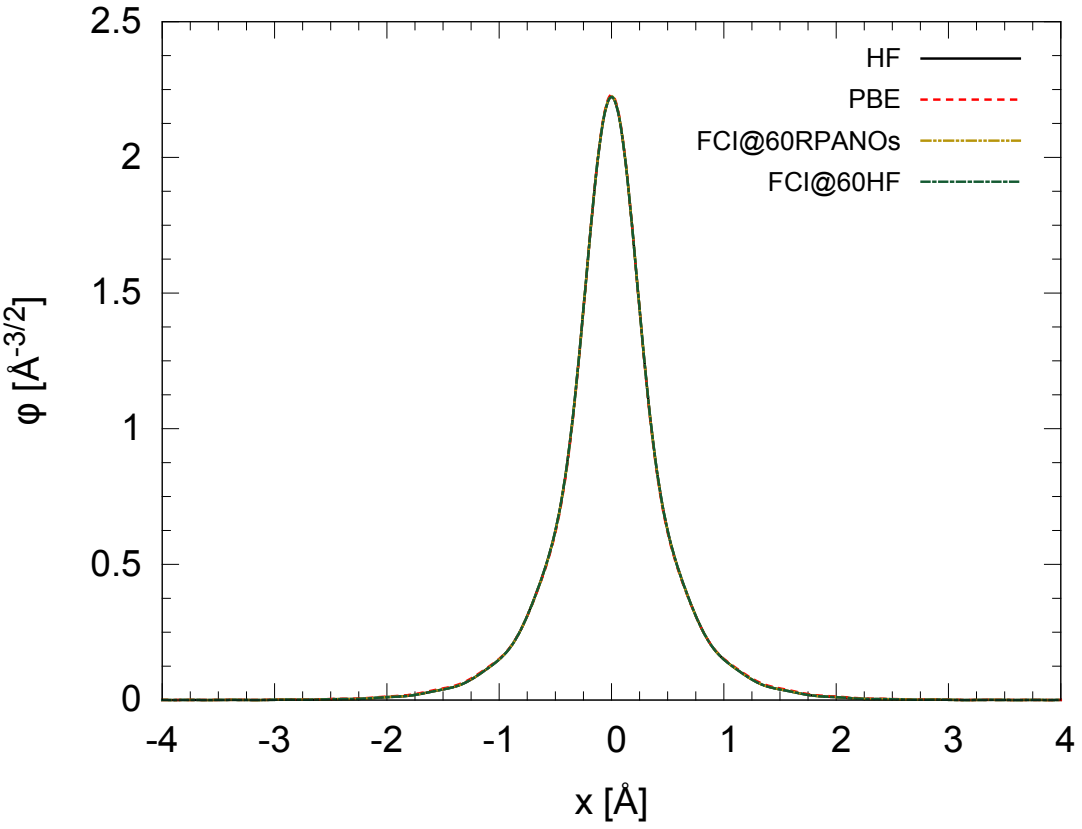

Figure 11.4: He 1s orbital. The occupied orbital is shown for PBE, HF, FCI@60RPANOs and FCI@60HF. RPANO and HF are by construction identical.

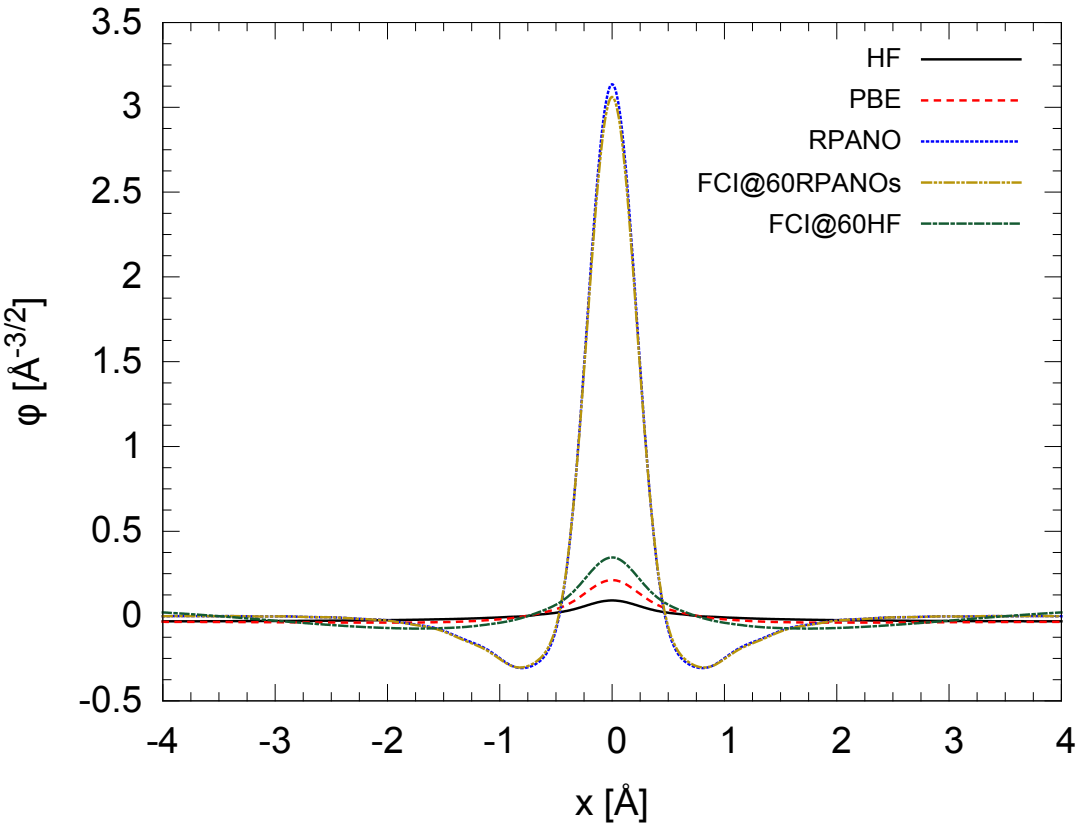

Figure 11.5: He "2s orbital". The first unoccupied mean-field or natural orbital is shown for PBE, HF, RPANO, FCI@60RPANOs and FCI@60HF.

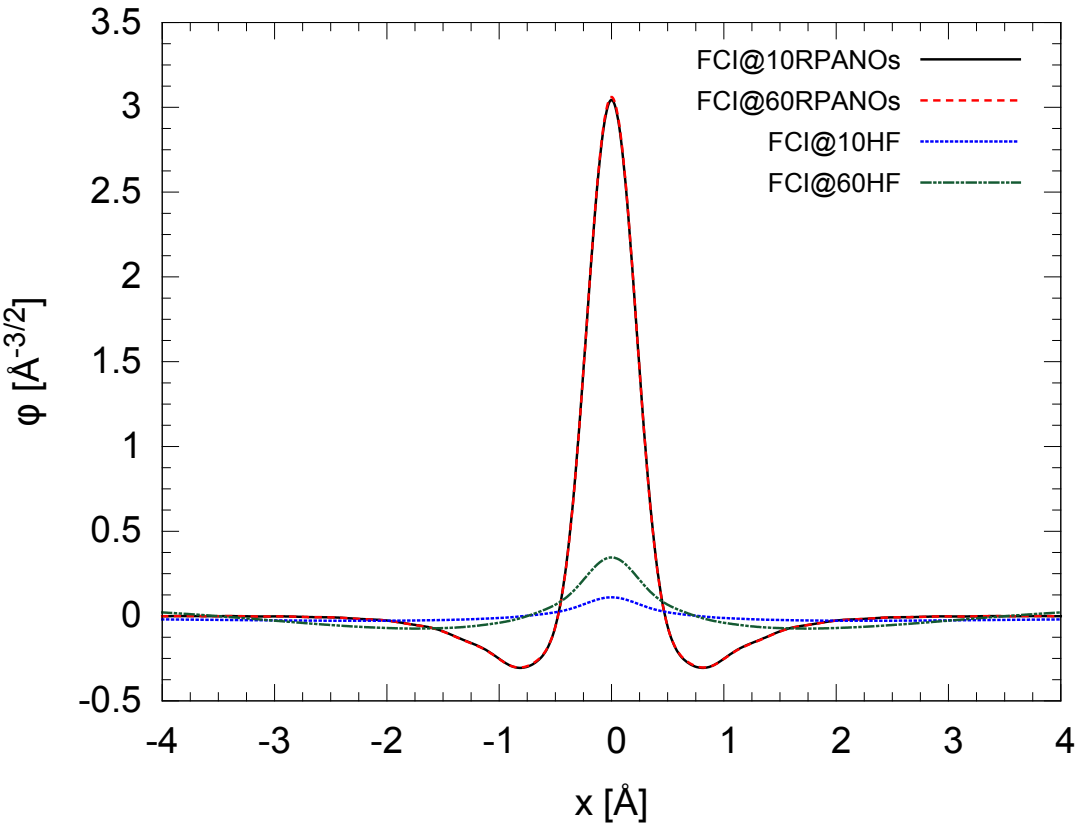

Figure 11.6: He "2s orbital". The first unoccupied FCI natural orbital is shown for 10 and 60 RPANOs as well as for 10 and 60 HF orbitals.

11.4.2 Hydrogen molecule

The second benchmark system investigated is the hydrogen molecule. Though H_2 is the simplest molecule, it's exact quantum mechanical description already shows prototypical challenges. Specifically the dissociation of the two hydrogen atoms is challenging from a theoretical point of view. In the dissociation limit an accurate wave function based method should yield a wave function corresponding to two separate hydrogen atoms. The restricted HF method, however, yields an inadequate dissociation limit with an energy substantially above the correct limit due to a flawed mixture of single electron states. Conversely, the spin-unrestricted HF (URHF) method yields a solution with an up electron on one site and a down electron on the other site, which is a spin contaminated singlet. The true singlet would have an equal expectation value for up and down electrons on both sites and is a mixture of (at least) two Slater determinants. The underlying problem is that a single determinant description is insufficient to describe the dissociation process. Similar problems exist in DFT [179]. Therefore the hydrogen molecule is, despite being seemingly simple, an interesting benchmark system for correlated electronic structure methods.

The computational set-up was again a 10 Å × 10 Å × 10 Å unit cell with periodic boundary conditions. We used a plane-wave basis with different cut-offs up to 750 eV. The internuclear distance was varied between the equilibrium distance of 0.74 Å and 5.0 Å.

As for the helium atom, we examined the convergence behaviors of the MP2 as well as the FCI correlation energy with respect to the RPANOs and compared them with convergence for HF-orbitals. The results of the calculations are shown in Figs. 11.7 and 11.8. Similarly to the helium atom, the correlation energies converge very slowly with an increasing number of HF orbitals. Using RPANOs, we only need a few hundred basis functions to obtain converged results for the MP2-energy. The statements on the cut-off convergence in Subsection 11.4.1 on the helium atom apply here as well.

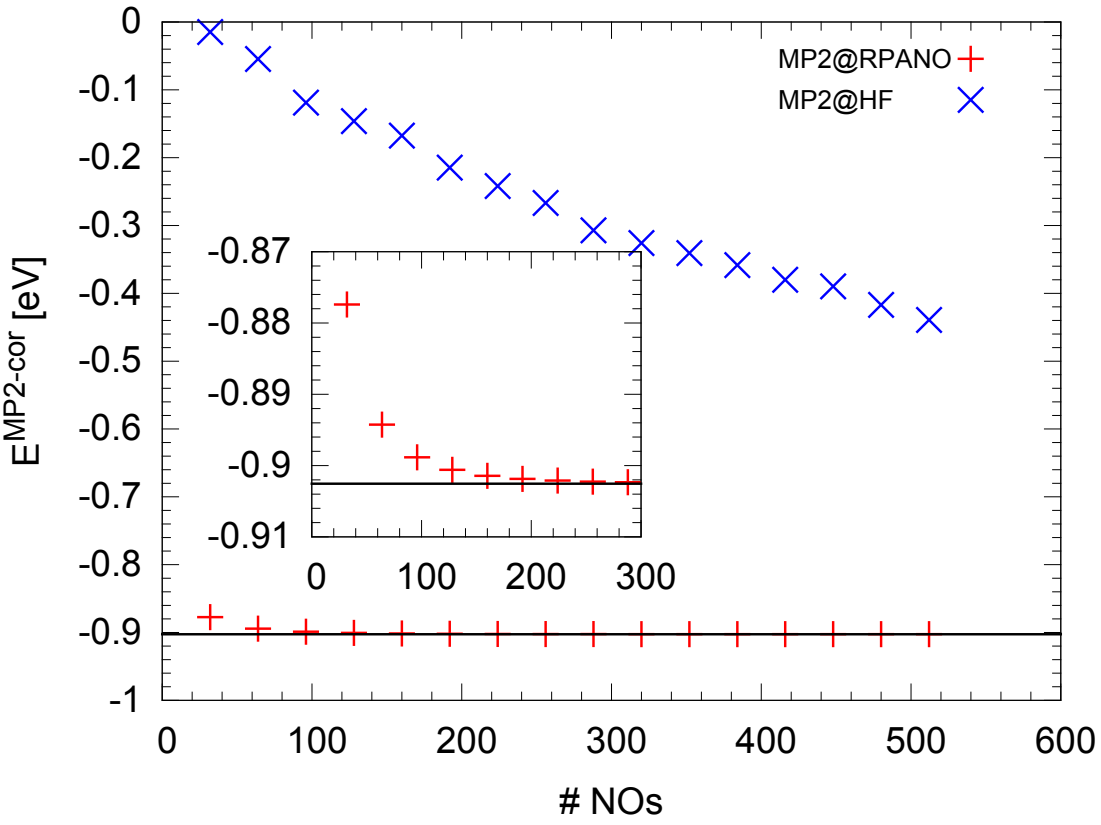

Figure 11.7: Convergence behavior of the MP2 correlation energy for the H_2 molecule at equilibrium distance. The convergence with respect to the number of RPANOs and HF-orbitals is compared. The black line shows the result for the full basis set.

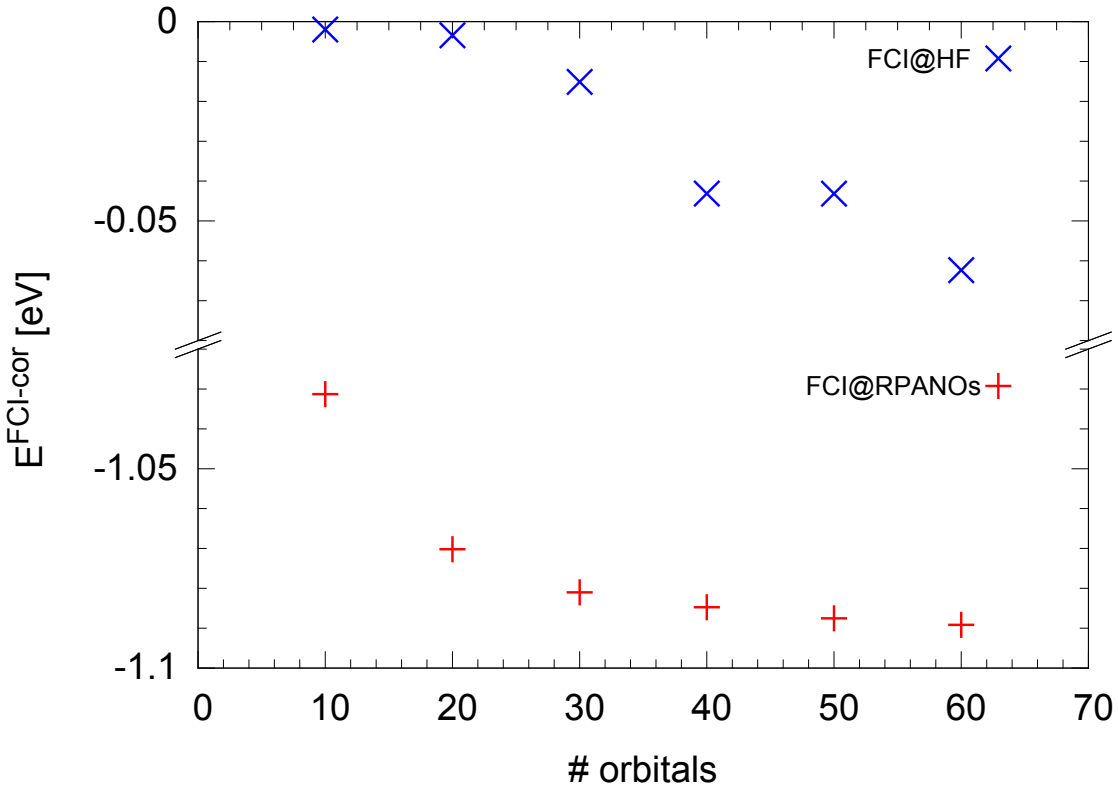

Figure 11.8: Convergence behavior of the FCI correlation energy for the H_2 molecule at equilibrium distance. The convergence with respect to the number of RPANOs and HF-orbitals is compared. The FCI energy using 10-60 HF virtual orbitals is at least 1 eV above the converged value.

For the FCI total energies, a cut-off extrapolation was done in the same fashion as for the helium atom according to Eq. (11.12) – from cut-offs up to 6000 eV for HF, and from cut-offs of 474 eV, 621 and 750 eV for the FCI correlation energy. Additionally we also performed an orbital set extrapolation with respect to the number of RPANOs, compare Eq. (11.13). In order to compare our results with experimental energies, we calculated the dissociation energy by subtracting twice the URHF energy for the isolated atom obtained with the same procedure (cut-off extrapolation), from the extrapolated FCI total energy at equilibrium distance (0.74 Å). An appropriate experimental value to compare our *ab-initio* Born-Oppenheimer approximation result with was obtained by adding the experimental vibrational zero point energy (E_{ZPE}) [180] to the experimental dissociation energy D_0 [181],

$$D_{\mathrm{e}} = D_0 + E_{\mathrm{ZPE}}. \tag{11.14}$$

Our extrapolated FCI binding energy ($-D_{\mathrm{e}}$) is -4.749 eV, which is 1 meV below the corresponding experimental value of -4.748 eV. Additionally we performed FCI calculations with the Gaussian pp-VxZ basis sets, with $x = 2, 3, 4$, and extrapolated in order to obtain an estimation for the basis set limit of the H_2 binding energy in the Born-Oppenheimer approximation. The extrapolation was done along the lines of Ref. [175], *i.e.* for the correlation energy we extrapolated according to

$$E^{\mathrm{cor}}(x) = E^{\mathrm{cor}}(\infty) + c \cdot x^{-3}, \tag{11.15}$$

while for the HF energy we fitted

$$E^{\mathrm{HF}}(x) = E^{\mathrm{HF}}(\infty) + a \cdot e^{-b \cdot x}. \tag{11.16}$$

The extrapolated energy from the pp-VxZ basis sets was -4.755 eV, 6 meV below the value for RPANOs and 7 meV below the experimental value. These results are summarized in Fig. 11.9.

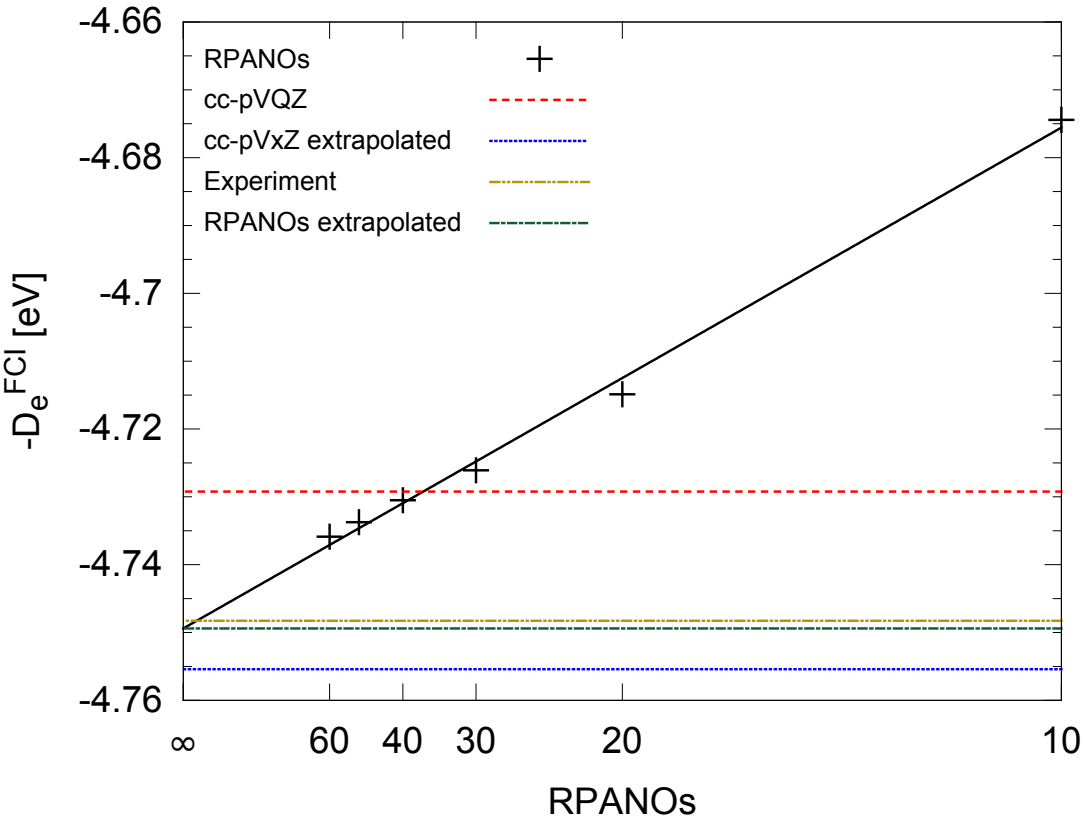

Figure 11.9: The cut-off extrapolated FCI binding energies for the H_2 molecule are shown at different numbers of RPANOs. A basis set extrapolation with 1/RPANOs yields a H_2 binding energy that is 1meV below the corresponding experimental reference value, see Eq. 11.14.

Again we also inspected the shape of the orbitals, this time along the bond-axis of the hydrogen molecule. In the equilibrium position, the first NO (*i.e.* the occupied 1σ state) is well approximated by the mean-field methods 1σ orbital, see Fig. 11.10. But the second natural orbital is already very different from DFT and even more so from the HF $1\sigma^*$, see Fig. 11.11. This has the same reasons as for the He 2s orbital. In Fig. 11.11, one can also see that the RPANO does not match the FCINO perfectly. But using just 10 RPANOs for the FCI calculation, the FCI natural orbital is already converged, see Fig. 11.12. This is a hint that, at least in this case, the RPANOs span the relevant space efficiently. In contrast, the HF orbitals are not even close to convergence with 60 orbitals.

Similar observations can be made for other cases, with varying internuclear distances and orbital levels as well as basis set sizes and underlying mean-field methods. We have investigated a variety of cases, and we have picked a few illustrative examples in an effort to summarize our findings. One of these examples is the third orbital (2σ) at an internuclear distance of 1.588 Å ($= 3a_0$). This example is interesting since in this case the RPANO noticeably differs from the FCINO, see Fig. 11.13. However, inspecting Fig. 11.14, one can see again that only very few RPANOs are necessary to describe the third FCINO correctly, even though the third RPANO does not match well with the third FCINO. Furthermore once again, the canonical HF-orbitals poorly describe the FCINO.

Finally, we show the orbitals at dissociation (5 Å). This time we compare the first two orbitals again. At this distance, the occupied orbitals vary more between the employed methods than they did at equilibrium distance, compare Fig. 11.10 and 11.15. By construction, the occupied RPANO is equal to the occupied HF orbitals. It is noteworthy that in this case, the PBE orbitals and hence the PBE electron density, is much closer to the FCINO than the HF orbital is (Figs. 11.15 and 11.16).

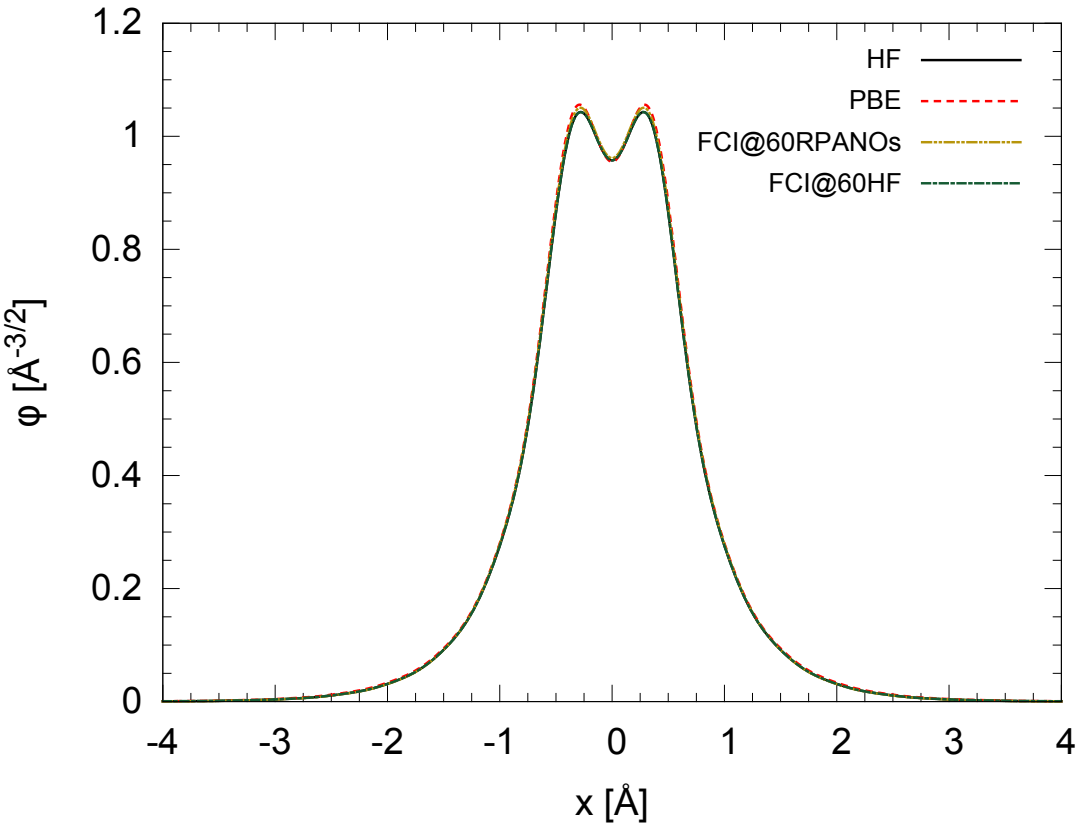

Figure 11.10: H_2 1σ orbital at equilibrium distance. The occupied orbital is shown for PBE, HF, FCI@60RPANOs and FCI@60HF. RPANO and HF are by construction identical.

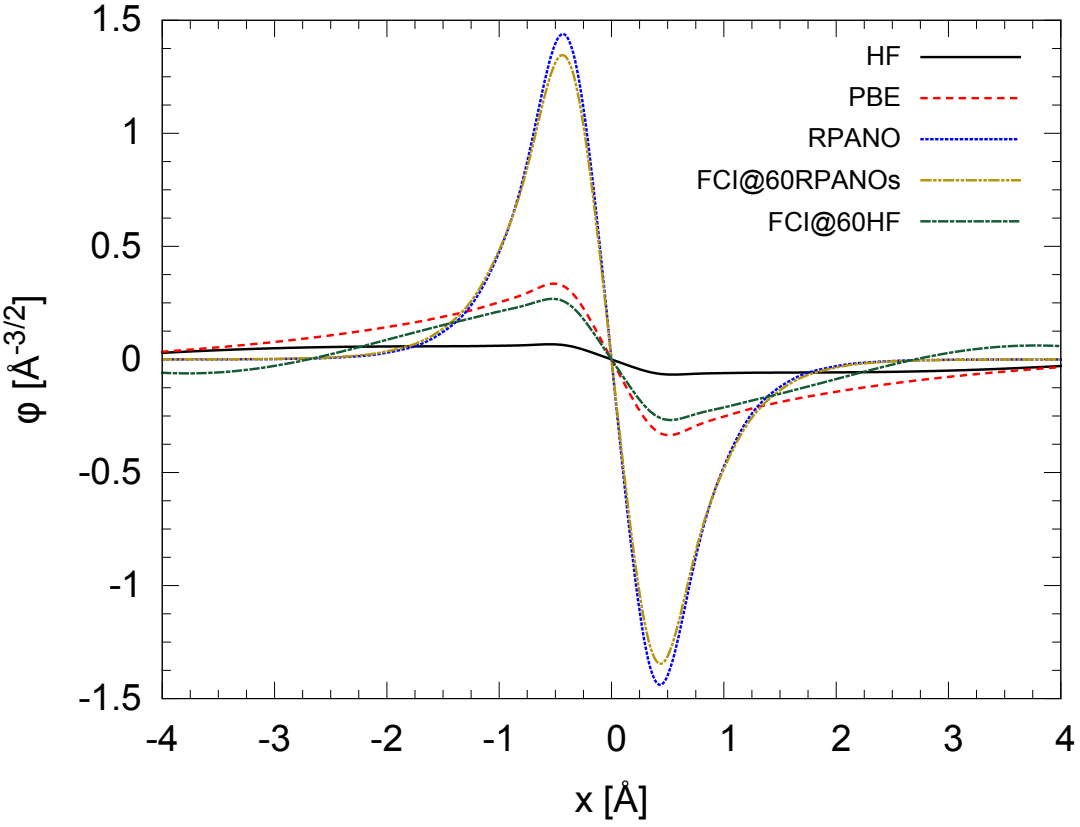

Figure 11.11: H_2 $1\sigma^*$ orbital at equilibrium distance. The first unoccupied mean-field or natural orbital is shown for PBE, HF, RPANO, FCI@60RPANOs and FCI@60HF.

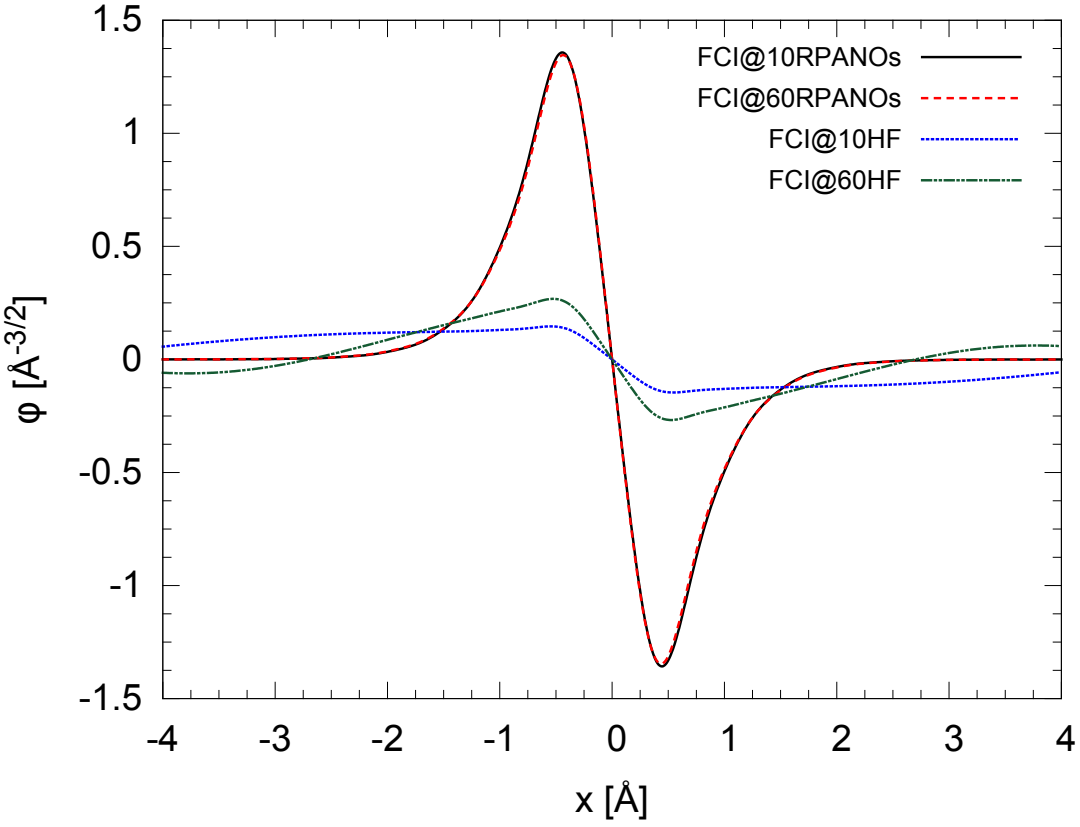

Figure 11.12: H_2 $1\sigma^*$ orbital at equilibrium distance. The first unoccupied FCI natural orbital is shown for 10 and 60 RPANOs as well as for 10 and 60 HF orbtials.

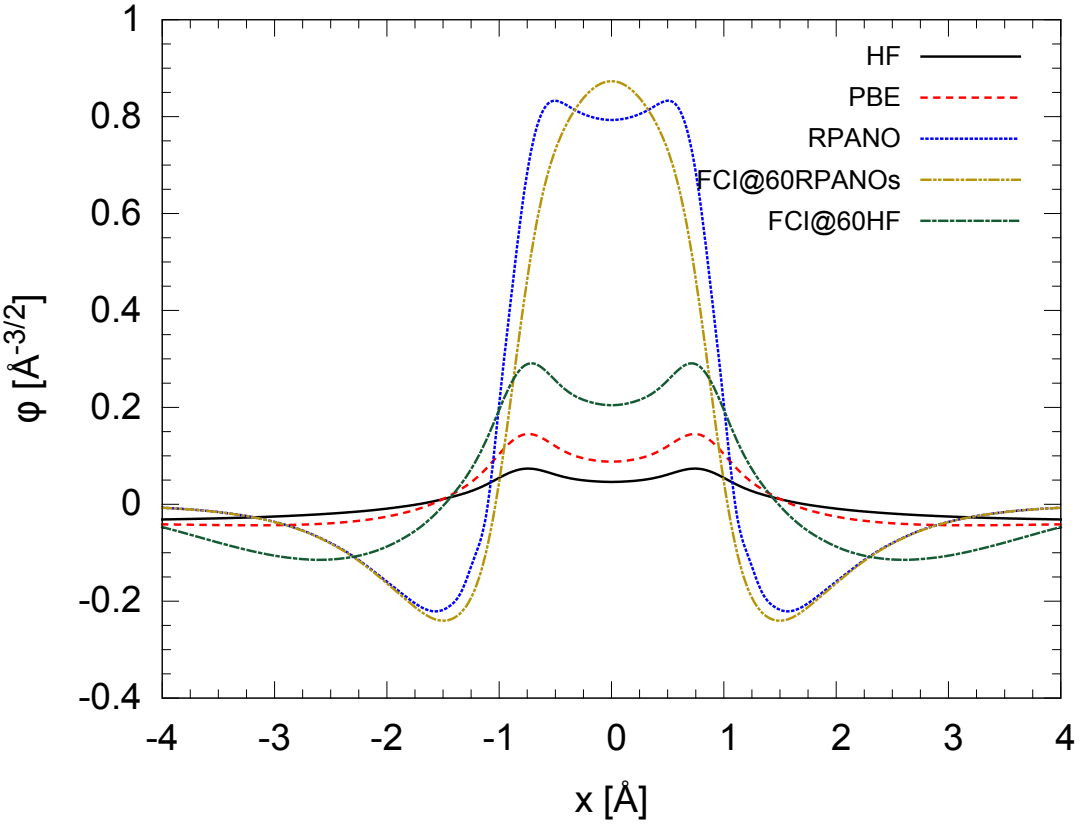

Figure 11.13: H_2 2σ orbital at an internuclear distance of 1.588 Å (=3 a_0). The second unoccupied mean-field or natural orbital ($\hat{=}2\sigma$) is shown for PBE, HF, RPANO, FCI@60RPANOs and FCI@60HF.

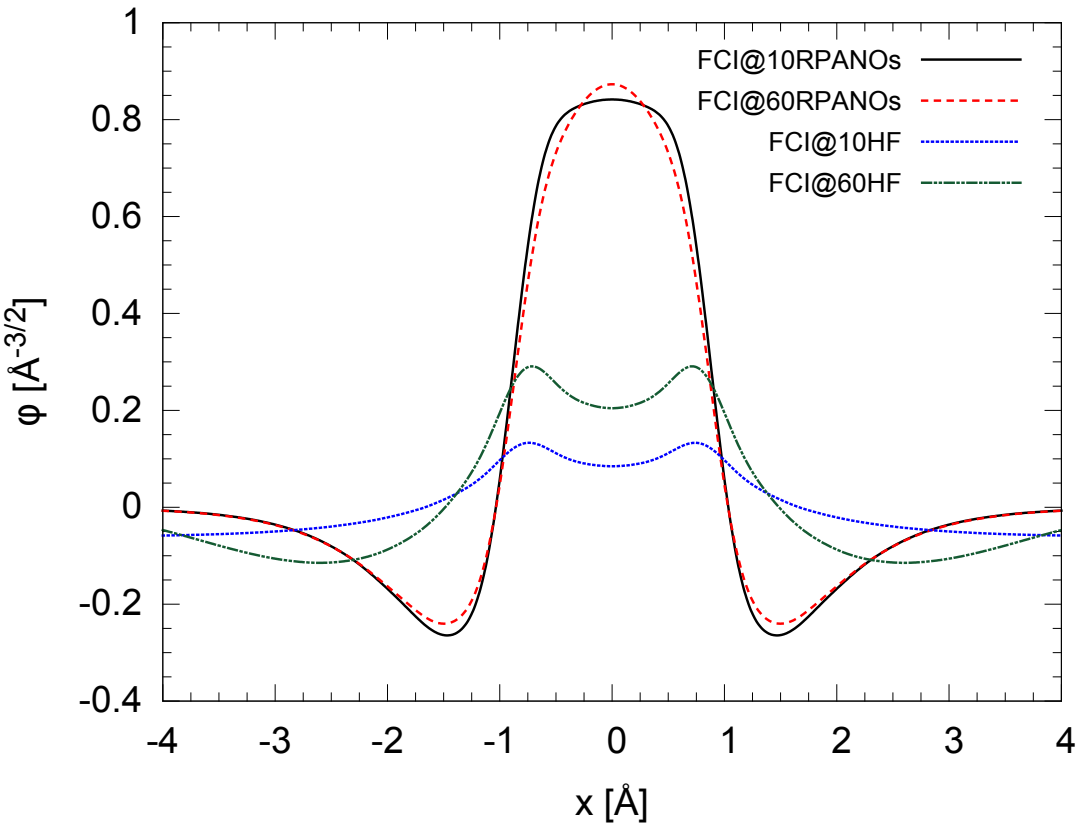

Figure 11.14: H_2 2σ orbital at an internuclear distance of 1.588 Å (=3 a_0). The second unoccupied FCI natural orbital ($\hat{=}2\sigma$) is shown for 10 and 60 RPANOs as well as for 10 and 60 HF orbtials.

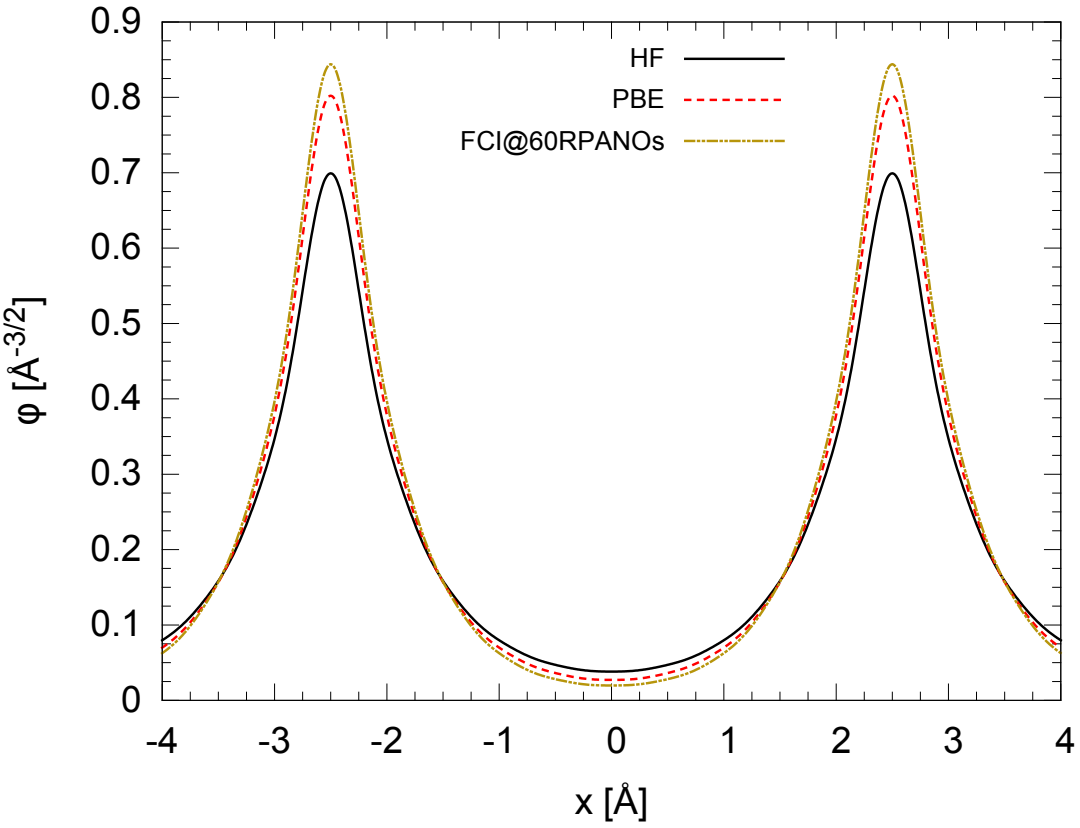

Figure 11.15: H_2 1σ orbital at an internuclear distance of 5 Å. The first occupied orbital ($\hat{=}1\sigma$) is shown for PBE, HF, and FCI@60RPANOs.

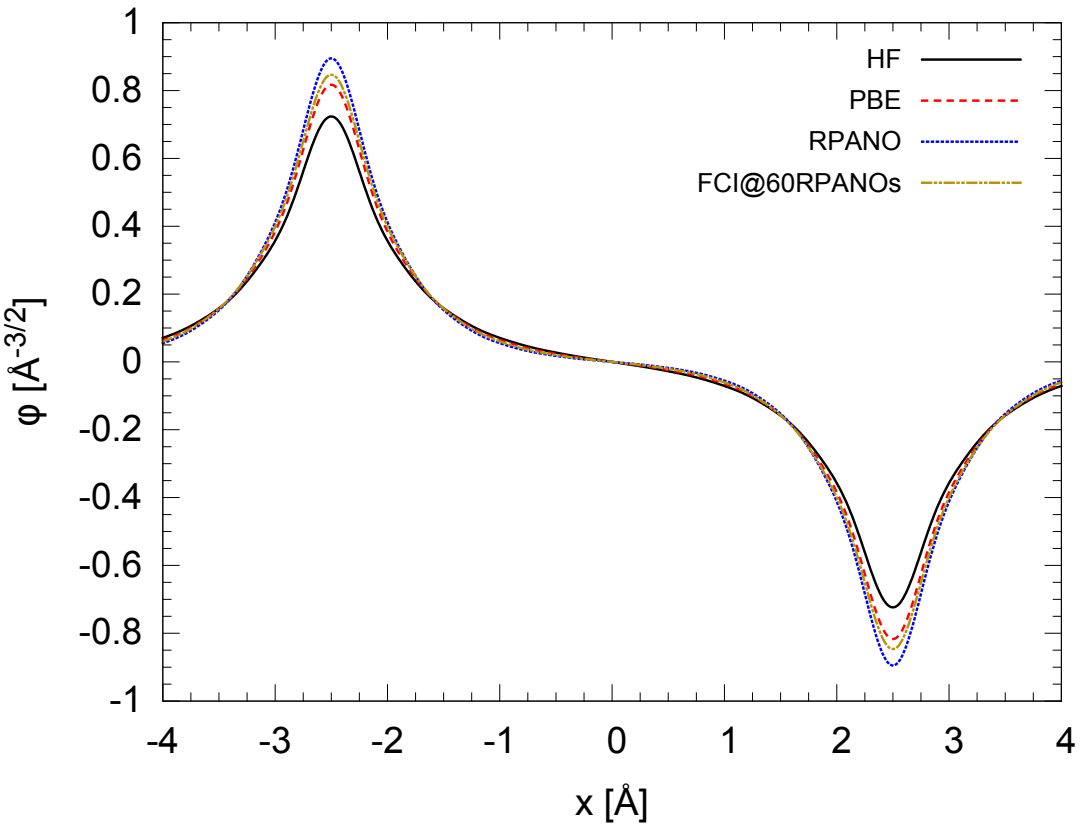

Figure 11.16: H_2 $1\sigma^*$ orbital at an internuclear distance of 5 Å. The first unoccupied mean-field or natural orbital ($\hat{=}1\sigma^*$) is shown for PBE, HF, RPANO and FCI@60RPANOs.

11.4.3 Fluorine molecule

In the two electron systems H_2 and He, the direct and exchange contribution to the MP2 correlation energy are related by a simple factor of -2, *i.e.* $E_d^{(2)} = -2E_x^{(2)}$. As Σ_{RPA} consists of an infinite series of bubble diagrams (χ^0), it intrinsically contains the direct part of the MP2 self energy $\Sigma_d^{(2)}$, but also accordingly models the exchange part $\Sigma_x^{(2)}$. For these two reasons, we expected the RPANOs to efficiently span the relevant subspace for MP2 calculations in H_2 and He. However, for a multi electron system like the fluorine molecule, the simple relation between direct and exchange part of the MP2 energy is no longer valid and it is therefore not clear from the outset that RPANOs will converge the MP2 energy quickly. Thus we investigated the convergence behavior for the direct (MP2D) and exchange (MP2X) contribution to the MP2 correlation energy with respect to RPANOs separately (Fig. 11.17). We compare again the performance of RPANOs and HF orbitals for calculating the total MP2 correlation energy (Fig. 11.18). For these calculation, we employed the PAW method [105, 182] and used again a 10 Å × 10 Å × 10 Å unit cell and a plane wave cut-off of 750 eV.

We observed that using RPANOs for fluorine, the exchange contribution to the MP2 correlation energy converges rapidly and in the same manner as the direct contribution, see Fig. 11.17. This is a strong indication that the proposed method, using RPANOs to construct orbitals for more expansive correlated methods, is straightforwardly applicable to complex, multi electron systems. As expected from the previous results, the energy convergence with respect to the number of HF orbitals is again extremely slow compared to the RPANOs, see Fig. 11.18.

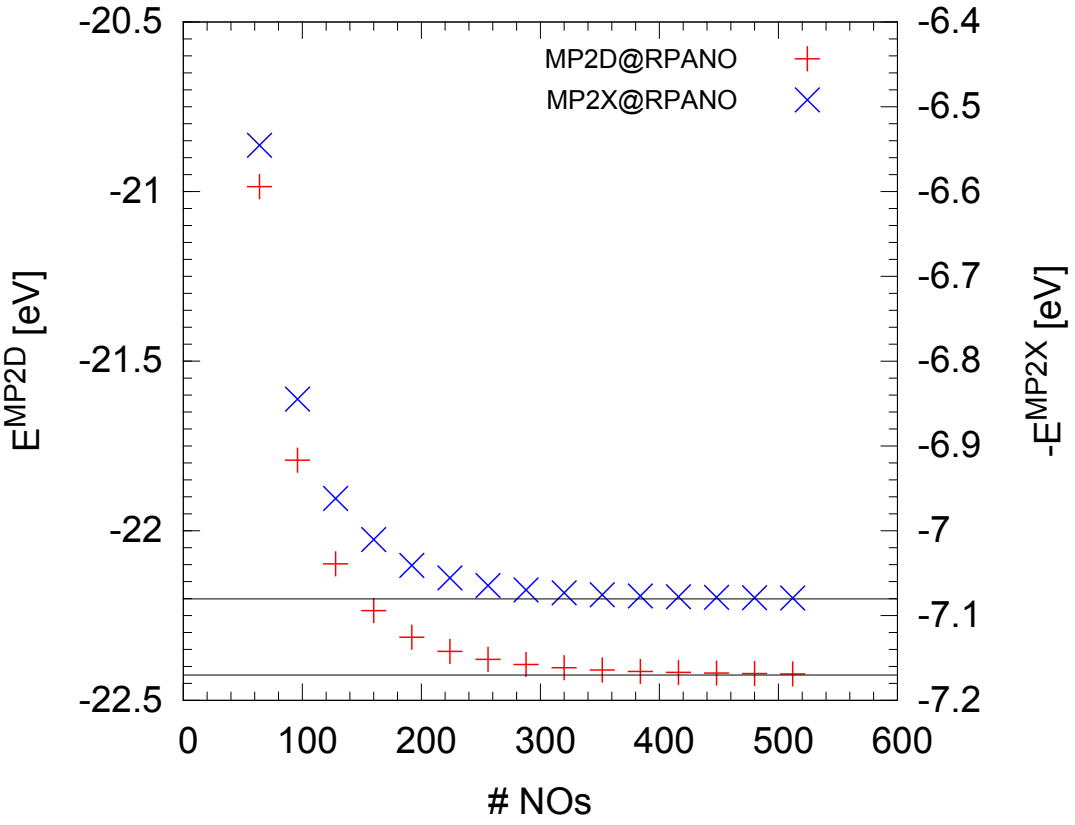

Figure 11.17: Convergence behavior of the direct and the exchange contribution to the MP2 correlation energy for the F_2 molecule. The convergence with respect to the number of RPANOs is shown. The black lines indicate the converged result for the full basis set. Note the different scales.

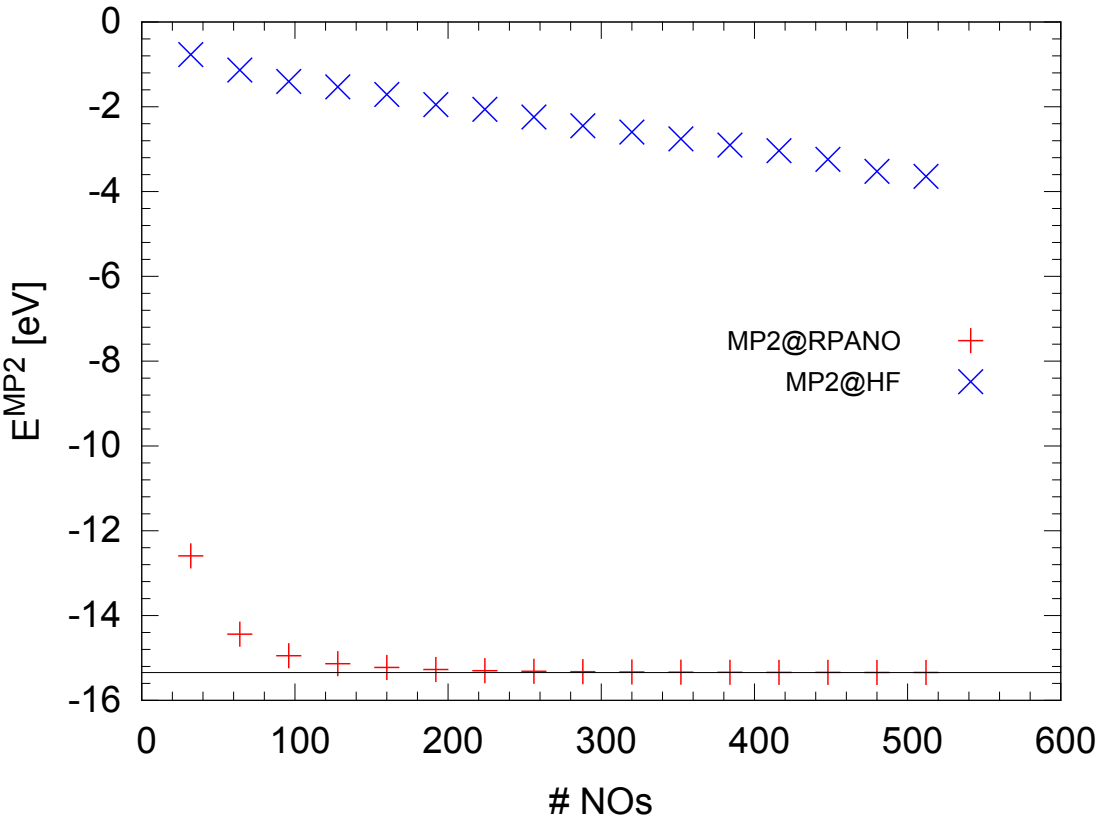

Figure 11.18: Convergence behavior of the total MP2 correlation energy for the F_2 molecule. The convergence with respect to the number of RPANOs and HF orbitals is compared. The black line indicates the converged result for the full basis set.

11.4.4 Diamond

The fourth benchmark system, diamond, was chosen to demonstrate the method on a simple periodic multi electron system. Fig. 11.19 shows that the convergence behavior of the MP2 energy is slightly improved by the use of RPANOs, but the effect is much smaller than in the molecular systems. Since we use the primitive cell, the number of plane waves in the full basis set is much smaller than it was for the molecules with large vacuum regions between the periodic images - in this case ≈ 400 for diamond vs. ≈ 47000 for H_2. In this case, between 200-300 RPANOs were sufficient to reach convergence, similar to the numbers for the hydrogen molecule. Thus the improvement being small is not caused by an under-performance of RPANOs, but rather due to a comparatively small number of orbitals in the full basis set.

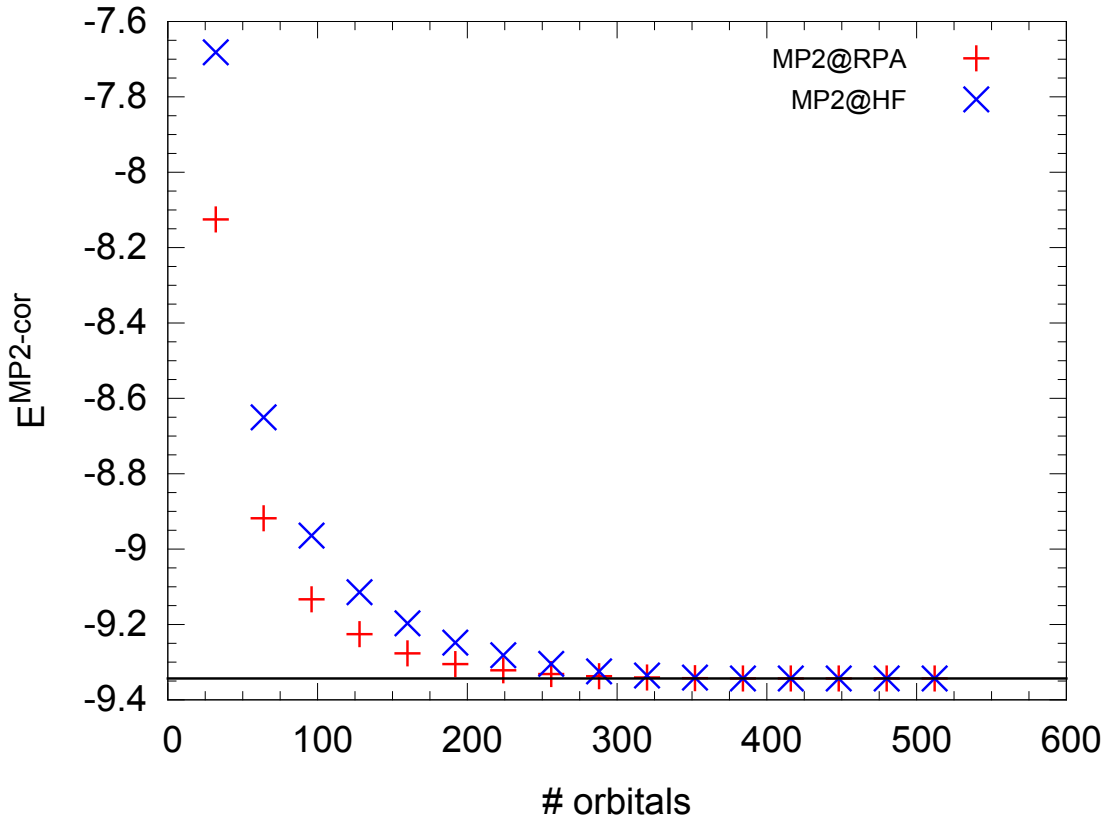

Figure 11.19: Convergence behavior of the MP2 correlation energy for diamond. The convergence with respect to the number of RPANOs and HF-orbitals is compared. The black line shows the result for the full basis set. The calculation was performed in the primitive cell with experimental lattice parameter $d = 3.567$ Å. We used the PAW method [182, 105] with a $4 \times 4 \times 4$ k-mesh and a plane wave cut-off of 600 eV.

11.5 Conclusion

We have tested the efficiency of RPANOs for MP2 and FCI calculations and found that for atoms and molecules they can drastically reduce the number of orbitals that are necessary to reach converged correlation energies in comparison to canonical HF or PBE orbitals. In the present implementation, the calculation of RPANOs scales only cubically with system size. This favorable scaling affords the proposed method an advantage over a similar method using MP2 natural orbitals, which scale with the fifth order of the system size in the canonical implementation (and with fourth order if an approximation is used) [156]. In general, the compute cost of correlated methods increases steeply with respect to the number of orbitals, even exponentially for CI. Thus the compute cost for the preceding compression of the space of orbitals will generally be small compared to the savings gained in the final accurate correlated calculations.

An important finding of the present work is that RPANOs yield a set of orbitals which allows to converge the correlation energy rapidly, even in cases, where the RPA itself is most likely not very accurate. Typical examples for such situations are bond breaking and bond making, in this study exemplified for the case of bond dissociation of H_2. Specifically, upon dissociation, we found cases where the first few RPANOs deviate significantly from the natural orbitals determined from the FCI correlated density matrix. Regardless of this difficulty, when the correlation energy is expanded in an increasing set of RPANOs, rapid convergence with the number of RPANOs is observed even for these "difficult" cases.

The present method is especially useful for systems comprised of large vacuum regions where the basis set size becomes unmanageable when plane waves are used (we are talking of ten thousands of plane wave orbitals). In fact, some of us have already applied a preliminary implementation of the algorithm presented here to calculate RPA natural orbitals and subsequently solve the BSE equations in this smaller basis. In this way, we were able to determine accurate quasiparticle energies in the GWΓ approximation for molecules [183]. Apart from molecular systems, open structures (zeolites) and surface science studies with large vacuum regions are likely to be an interesting and promising field of application for the RPANO method. Recall that coupled cluster methods scale at least with the fourth order of the number of virtual orbitals. If one is capable to compress the number of virtual orbitals by say a factor 2-3, speed ups of one to two orders of magnitude can be expected. We also note that the RPA is expected to be already fairly accurate for the prediction of adsorption energies [6, 86], however, close to transition states we expect that methods beyond the RPA will be required. Our results for the bond dissociation in H_2 gives hope that the RPANOs will work also well in such challenging situations. Overall, the present implementation will greatly boost the applicability of plane wave basis sets allowing them to compete with the now omnipresent local Gaussian basis sets used in quantum chemistry.

Last not least, natural orbitals in periodic systems can be used as a stepping stone for "strongly" correlated calculations, such as dynamical mean-field theory (DMFT)

or density matrix renormalization group (DMRG) theory. There are already examples in literature indicating that such an approach might be at least competitive with the usual approach of maximally localized Wannier functions [184, 185, 186], since natural orbitals with an occupancy far from zero or one, are likely to contribute most to the correlation energy. Thus, combining perturbative methods for weakly correlated orbitals with an accurate correlation method for the strongly correlated orbitals is an important future development to be pursued.

Chapter 12

Conclusion and outlook

The first part of this thesis provided a reference to the theoretical concepts underlying the application of the RPA in electronic structure methods. Starting with a one-dimensional single particle Hamiltonian, step by step the fundamental concepts that finally lead to the RPA@PBE method – using PAWs – are introduced.

To underline the capabilities of the RPA as a state-of-the-art electronic structure method, it was applied to several difficult problems from the exciting field of surface science [4, 5, 6]. The agreement with experimental data and other advanced electronic structure methods was remarkable in the investigated materials problems, providing further evidence that the RPA achieves a good compromise between performance and accuracy.

For every electronic structure method, it is desirable, that forces between the atoms are readily computable, so that relaxed ground state structures, vibrational properties, as well as finite temperature properties of any material are straightforwardly accessible. In the course of this thesis, a novel method for the efficient calculation of non-Hellmann-Feynman forces for the RPA in solids was developed [1]. This represents a completely new feature that was not available in any electronic structure code before. Conveniently, this method should in principle be transferable to other correlated, perturbative methods, for example MP2. However, as it is, the current implementation is unfortunately only applicable to gapped systems. The underlying problem is that for metals, the RPA should be applied with a finite temperature approach. This task is work in progress, but significant advances in the calculation of finite temperature RPA correlation energies were recently made by Kaltak and Kresse [187]. Although it is a very difficult challenge, we expect that the forces algorithm can be transferred to this new frame work in the foreseeable future and that the current limitations to gapped systems can be overcome.

Despite its current limitations, a very promising application of the RPA forces algorithm was presented with reference to a method developed by Bokdam *et al.* [2]. With RPA forces at hand, one can create finite temperature ensembles with MD simulations and use them to benchmark different density functionals. This allows to systematically select the best functional for large scale structure predictions

of a given material, providing a huge advantage over the common trial and error approach.

Finally, the RPA 1-RDM – which is an intermediate quantity in the calculation of RPA forces – was examined. It was shown that approximate natural orbitals from the RPA provide an excellent basis for more involved correlated methods, as for example FCI [3]. This is another promising development based on the RPA, proving once again its versatility.

We conclude that the RPA has an enormous potential for electronic structure methods. On the one hand, various RPA related methods already provide extremely useful tools for elaborate applications. On the other hand, open problems like the implementation of RPA forces at finite temperatures offer an exciting basis for further theoretical research and method development.

Part IV

Appendices

Appendix A

Formulary

Fourier transformations:

$$f(\nu) = \mathcal{F}[f(\tau)](\nu) = \int e^{\mathrm{i}\,\tau\nu} f(\tau)\mathrm{d}\tau \tag{A.1}$$

$$f(\tau) = \mathcal{F}^{-1}[f(\nu)](\tau) = \frac{1}{2\pi}\int e^{-\mathrm{i}\,\tau\nu} f(\tau)\mathrm{d}\nu \tag{A.2}$$

$$\mathcal{F}[\mathrm{i}\,\partial_t f(t)](\omega) = \omega\mathcal{F}[f(t)](\omega) \tag{A.3}$$

Green's function (imaginary time):

$$\underline{G}(\boldsymbol{r},\boldsymbol{r}',\tau) = \ \Theta(-\tau)\sum_n \psi_n(\boldsymbol{r})\psi_n^*(\boldsymbol{r}')e^{-\epsilon_n\tau} f(\epsilon_n) \tag{A.4}$$

$$\overline{G}(\boldsymbol{r},\boldsymbol{r}',\tau) = -\,\Theta(\tau)\sum_n \psi_n(\boldsymbol{r})\psi_n^*(\boldsymbol{r}')e^{-\epsilon_n\tau}(1-f(\epsilon_n)) \tag{A.5}$$

$$G(\boldsymbol{r},\boldsymbol{r}',\tau) = \overline{G}(\boldsymbol{r},\boldsymbol{r}',\tau) + \underline{G}(\boldsymbol{r},\boldsymbol{r}',\tau) \tag{A.6}$$

Polarizability:

$$\chi(\boldsymbol{r},\boldsymbol{r}',\tau) = G(\boldsymbol{r},\boldsymbol{r}',\tau)G(\boldsymbol{r},\boldsymbol{r}',-\tau)^* \tag{A.7}$$

Useful identities for Green's function and polarizability:

$$G(\boldsymbol{r},\boldsymbol{r}',\tau) = G(\boldsymbol{r}',\boldsymbol{r},\tau)^* \tag{A.8}$$

$$\chi(\boldsymbol{r},\boldsymbol{r}',\tau) = \chi(\boldsymbol{r},\boldsymbol{r}',-\tau)^* = \chi(\boldsymbol{r}',\boldsymbol{r},-\tau) = \chi(\boldsymbol{r}',\boldsymbol{r},\tau)^* \tag{A.9}$$

$$\chi(\boldsymbol{r},\boldsymbol{r}',\nu) = \chi(\boldsymbol{r},\boldsymbol{r}',\nu)^* = \chi(\boldsymbol{r}',\boldsymbol{r},-\nu) = \chi(\boldsymbol{r}',\boldsymbol{r},-\nu)^* \tag{A.10}$$

$$\frac{\delta F}{\delta\phi(\tau)} = 2\pi\mathcal{F}^{-1}[\frac{\delta F}{\delta\phi(\nu)}](-\tau) \tag{A.11}$$

and since

$$\frac{\delta E^{\text{c-RPA}}}{\delta \chi(\boldsymbol{r}, \boldsymbol{r}', \nu)} = -\frac{1}{4\pi} W^{\text{c-RPA}}(\boldsymbol{r}', \boldsymbol{r}, \nu) \tag{A.12}$$

$$\Rightarrow \frac{\delta E^{\text{c-RPA}}}{\delta \chi(\boldsymbol{r}, \boldsymbol{r}', \tau)} = -\frac{1}{2} W^{\text{c-RPA}}(\boldsymbol{r}', \boldsymbol{r}, -\tau) \tag{A.13}$$

Proof of Eq. (A.11): Let F be a functional $F = F[\phi(\nu)]$ and let $\phi(\nu)$ be the Fourier transformed function $\phi(\nu) = \mathcal{F}[\phi(\tau)](\nu)$, then

$$\delta F = \int \frac{\delta F}{\delta \phi(\nu)} \delta\phi(\nu) \, \mathrm{d}\nu \tag{A.14}$$

$$= \int \frac{\delta F}{\delta \phi(\nu)} \int e^{\mathrm{i}\,\tau\nu} \delta\phi(\tau) \, \mathrm{d}\tau \mathrm{d}\nu \tag{A.15}$$

$$= \iint \frac{\delta F}{\delta \phi(\nu)} e^{\mathrm{i}\,\tau\nu} d\nu \; \delta\phi(\tau) \, \mathrm{d}\tau \tag{A.16}$$

$$\Rightarrow \frac{\delta F}{\delta \phi(\tau)} = \int \frac{\delta F}{\delta \phi(\nu)} e^{\mathrm{i}\,\tau\nu} \mathrm{d}\nu = 2\pi \mathcal{F}^{-1}[\frac{\delta F}{\delta \phi(\nu)}](-\tau) \tag{A.17}$$

Plane wave basis notation

$$|\phi_{n,\boldsymbol{k}}\rangle = \sum_{\boldsymbol{G}} C_{\boldsymbol{G}n\boldsymbol{k}} \, |\boldsymbol{G} + \boldsymbol{k}\rangle \tag{A.18}$$

$$\langle \boldsymbol{k} + \boldsymbol{G} | \boldsymbol{k} + \boldsymbol{G}' \rangle = \delta_{\boldsymbol{G},\boldsymbol{G}'} \tag{A.19}$$

$$\langle \boldsymbol{r} | \boldsymbol{k} + \boldsymbol{G} \rangle = \frac{1}{\Omega} e^{\mathrm{i}(\boldsymbol{k}+\boldsymbol{G})\boldsymbol{r}} \tag{A.20}$$

Two electron integrals:

$$\langle ij|kl\rangle = \int \mathrm{d}^3\mathbf{r}_1 \mathrm{d}^3\mathbf{r}_2 \phi_i^*(\mathbf{r}_1)\phi_j^*(\mathbf{r}_2) \frac{1}{r_{12}} \phi_k^*(\mathbf{r}_1)\phi_l^*(\mathbf{r}_2) \tag{A.21}$$

Appendix B

Abbreviations

1-RDM	one particle reduced density matrix
AC	adiabatic connection
BOA	Born-Oppenheimer approximation
BZ	(first) Brillouin zone
C	Coulomb
c	correlation
cc	complex conjugate
CC	coupled cluster
CI	configuration interaction
p-CCSD(T)	periodic CC including singles, doubles and perturbative triples
DF	density functional
DFT	density functional theory
DMC	diffusion Monte Carlo
ee	electron-electron
ext	external
EXX	exact exchange
fcc	face centered cubic
FCI	full configuration interaction
FDT	fluctuation dissipation theorem
FFT	fast Fourier transform
FNQMC	fixed-node quantum Monte Carlo
GGA	generalized gradient approximation
GW	see section 4.4
GWSE	GW single excitations
H	Hartree
hBN	hexagonal boron nitride
hcp	hexagonal close-packed
HF	Hartree-Fock
kin	kinetic

KS	Kohn-Sham
l.h.s	left hand side
LDA	local density approximation
LAPW	linearized augmented-plane-wave (method)
MBD	many body dispersion (correction)
MBPT	many body perturbation theory
MD	molecular dynamics
MF	mean-field
MP	MøllerPlesset (perturbation theory)
MP2	second order MP
MP2D	direct contribution to MP2 correlation energy
MP2X	exchange contribution to MP2 correlation energy
occ	occupied
PAW	projector augmented wave (method)
PBE	Perdew-Burke-Ernzerhof (functional)
r.h.s	right hand side
RDM	reduced density matrix
Ref.	reference(s)
RPA	random phase approximation
RPA@PBE	applied RPA calculation using PBE orbitals
TD-DFT	time-dependent DFT
TS	Tkatchenko and Scheffler
uocc	unoccupied
USP	ultra soft pseudo potential(s)
`VASP`	Vienna ab-initio simulation package
vdW	van der Waals
vdW-DF	non-local van der Waals density functional
w.r.t.	with respect to
xc	exchange correlation

Appendix C

List of publications and presentations

C.1 Peer reviewed articles

- Benjamin Ramberger, Zoran Sukurma, Tobias Schäfer, and Georg Kresse. "RPA natural orbitals and their application to post-Hartree-Fock electronic structure methods". In: *The Journal of Chemical Physics* 151.21 (Dec. 2019), p. 214106. DOI: 10.1063/1.5128415.

- Jan Gerit Brandenburg, Andrea Zen, Martin Fitzner, Benjamin Ramberger, Georg Kresse, Theodoros Tsatsoulis, Andreas Grüneis, Angelos Michaelides, and Dario Alfè. "Physisorption of Water on Graphene: Subchemical Accuracy from Many-Body Electronic Structure Methods". In: *The Journal of Physical Chemistry Letters* 10.3 (Feb. 2019), pp. 358–368. DOI: 10.1021/acs.jpclett.8b03679.

- Tobias Schäfer, Benjamin Ramberger, and Georg Kresse. "Laplace transformed MP2 for three dimensional periodic materials using stochastic orbitals in the plane wave basis and correlated sampling". In: *The Journal of Chemical Physics* 148.6 (Feb. 2018), p. 064103. DOI: 10.1063/1.5016100.

- José A. Garrido Torres, Benjamin Ramberger, Herbert A. Früchtl, Renald Schaub, and Georg Kresse. "Adsorption energies of benzene on close packed transition metal surfaces using the random phase approximation". In: *Physical Review Materials* 1.6 (Nov. 2017), p. 060803. DOI: 10.1103/PhysRevMaterials.1.060803.

- Menno Bokdam, Jonathan Lahnsteiner, Benjamin Ramberger, Tobias Schäfer, and Georg Kresse. "Assessing Density Functionals Using Many Body Theory for Hybrid Perovskites". In: *Physical Review Letters* 119.14 (Oct. 2017), pp. 1–5. DOI: 10.1103/PhysRevLett.119.145501.

- Yasmine S. Al-Hamdani, Mariana Rossi, Dario Alfè, Theodoros Tsatsoulis, Benjamin Ramberger, Jan Gerit Brandenburg, Andrea Zen, Georg Kresse, Andreas Grüneis, Alexandre Tkatchenko, and Angelos Michaelides. "Properties of the water to boron nitride interaction: From zero to two dimensions with benchmark accuracy". In: *The Journal of Chemical Physics* 147.4 (July 2017), p. 044710. DOI: 10.1063/1.4985878.

- Tobias Schäfer, Benjamin Ramberger, and Georg Kresse. "Quartic scaling MP2 for solids: A highly parallelized algorithm in the plane wave basis". In: *Journal of Chemical Physics* 146.10 (Mar. 2017), p. 104101. DOI: 10.1063/1.4976937.

- Benjamin Ramberger, Tobias Schäfer, and Georg Kresse. "Analytic Interatomic Forces in the Random Phase Approximation". In: *Physical Review Letters* 118.10 (Mar. 2017), pp. 1–5. DOI: 10.1103/PhysRevLett.118.106403.

C.2 Contributed talks

- Benjamin Ramberger. *RPA natural orbitals and their application to higher hierarchy methods*. 15th ViCoM Workshop. Vienna, Austria. Apr. 2019.

- Benjamin Ramberger. *Analytic Interatomic Forces in the Random Phase Approximation*. Seminar talk at SUNCAT @ Stanford. Stanford, United States. Mar. 2018.

- Benjamin Ramberger. *Analytic Interatomic Forces in the Random Phase Approximation*. American Physical Society: APS March Meeting. Los Angeles, United States. Mar. 2018.

- Benjamin Ramberger. *Analytic Interatomic Forces in the Random Phase Approximation*. ETSF Young Researchers' Meeting. Tarragona, Spain. 2017.

- Benjamin Ramberger. *Analytic Interatomic Forces in the Random Phase Approximation*. CECAM workshop: Theoretical Chemistry for Extended Systems: systematically improvable electronic structure methods. Toulouse, France. May 2017.

- Benjamin Ramberger. *Calculation of first derivatives in the random phase approximation for solids*. 66. OePG Jahrestagung. Vienna, Austria. Sept. 2016.

- Benjamin Ramberger. *Forces in the random phase approximation for solids*. 10th ViCoM Workshop. Stadtschlaining, Austria. Mar. 2016.

- Benjamin Ramberger. *Calculating forces in the random phase approximation (RPA)*. 65. OePG Jahrestagung. Vienna, Austria. Sept. 2015.

C.3 Poster presentations

- Benjamin Ramberger. *Calculating forces in the random phase approximation in solids*. 14th ViCoM Workshop. Krumbach, Austria. Oct. 2018.
- Benjamin Ramberger. *Calculating forces in the random phase approximation in solids*. From Electrons to Phase Transitions 2018: A ViCoM Conference. Vienna, Austria. Apr. 2018.
- Benjamin Ramberger. *Calculating forces in the random phase approximation in solids*. Total Energy and Force Methods. Cambridge, United Kingdom. Jan. 2018.
- Benjamin Ramberger and Menno Bokdam. *Assessing density functionals using many body theory for hybrid perovskites*. 13th ViCoM Workshop. Stadtschlaining, Austria. Oct. 2017.
- Benjamin Ramberger. *Calculating forces in the random phase approximation for solids*. 2nd ViCoM Young Researchers Meeting. Vienna, Austria. Sept. 2016.
- Benjamin Ramberger. *Calculating forces in the random phase approximation for solids*. Total Energy and Force Methods. Luxemburg, Luxemburg. Jan. 2016.

Note that the similar poster titles “Calculating forces in the random phase approximation **for** solids” and “Calculating forces in the random phase approximation **in** solids” describe to different posters. While the first contained mainly the theoretical foundations, the later presented various applications along with a very brief overview of the method.

Bibliography

[1] Benjamin Ramberger, Tobias Schäfer, and Georg Kresse. "Analytic Interatomic Forces in the Random Phase Approximation". In: *Physical Review Letters* 118.10 (Mar. 2017), pp. 1–5. DOI: 10.1103/PhysRevLett.118.106403.

[2] Menno Bokdam et al. "Assessing Density Functionals Using Many Body Theory for Hybrid Perovskites". In: *Physical Review Letters* 119.14 (Oct. 2017), pp. 1–5. DOI: 10.1103/PhysRevLett.119.145501.

[3] Benjamin Ramberger et al. "RPA natural orbitals and their application to post-Hartree-Fock electronic structure methods". In: *The Journal of Chemical Physics* 151.21 (Dec. 2019), p. 214106. DOI: 10.1063/1.5128415.

[4] Yasmine S. Al-Hamdani et al. "Properties of the water to boron nitride interaction: From zero to two dimensions with benchmark accuracy". In: *The Journal of Chemical Physics* 147.4 (July 2017), p. 044710. DOI: 10.1063/1.4985878.

[5] Jan Gerit Brandenburg et al. "Physisorption of Water on Graphene: Subchemical Accuracy from Many-Body Electronic Structure Methods". In: *The Journal of Physical Chemistry Letters* 10.3 (Feb. 2019), pp. 358–368. DOI: 10.1021/acs.jpclett.8b03679.

[6] José A. Garrido Torres et al. "Adsorption energies of benzene on close packed transition metal surfaces using the random phase approximation". In: *Physical Review Materials* 1.6 (Nov. 2017), p. 060803. DOI: 10.1103/PhysRevMaterials.1.060803.

[7] P. Hohenberg and W. Kohn. "Inhomogeneous Electron Gas". In: *Physical Review* 136.3B (Nov. 1964), B864–B871. DOI: 10.1103/PhysRev.136.B864.

[8] W. Kohn and L. J. Sham. "Self-Consistent Equations Including Exchange and Correlation Effects". In: *Physical Review* 140.4A (Nov. 1965), A1133–A1138. DOI: 10.1103/PhysRev.140.A1133.

[9] John P. Perdew, Kieron Burke, and Matthias Ernzerhof. *Generalized Gradient Approximation Made Simple*. 1996. DOI: 10.1103/PhysRevLett.77.3865.

[10] John P. Perdew et al. “Erratum: Atoms, molecules, solids, and surfaces: Applications of the generalized gradient approximation for exchange and correlation”. In: *Physical Review B* 48.7 (Aug. 1993), pp. 4978–4978. DOI: 10.1103/PhysRevB.48.4978.2.

[11] A. D. Becke. “Density-functional exchange-energy approximation with correct asymptotic behavior”. In: *Physical Review A* 38.6 (1988), pp. 3098–3100. DOI: 10.1103/PhysRevA.38.3098.

[12] Aron J. Cohen, Paula Mori-Sánchez, and Weitao Yang. “Insights into current limitations of density functional theory”. In: *Science* 321.5890 (2008), pp. 792–794. DOI: 10.1126/science.1158722.

[13] Stefan Grimme. “Semiempirical GGA-type density functional constructed with a long-range dispersion correction”. In: *Journal of Computational Chemistry* 27.15 (2006), pp. 1787–1799. DOI: 10.1002/jcc.20495.

[14] Alexandre Tkatchenko and Matthias Scheffler. “Accurate molecular van der Waals interactions from ground-state electron density and free-atom reference data”. In: *Physical Review Letters* 102.7 (2009), pp. 6–9. DOI: 10.1103/PhysRevLett.102.073005.

[15] John P Perdew, Matthias Ernzerhof, and Kieron Burke. “Rationale for mixing exact exchange with density functional approximations”. In: *J. Chem. Phys.* 105.May 2016 (1996), p. 9982. DOI: 10.1063/1.472933.

[16] Axel D Becke. “A new mixing of Hartree-Fock and local-density-functional theories”. In: *J. Chem. Phys.* 98.2 (1993), pp. 1372–1377. DOI: 10.1063/1.464304.

[17] Chengteh Lee, Weitao Yang, and Robert G. Parr. “Development of the Colle-Salvetti correlation-energy formula into a functional of the electron density”. In: *Physical Review B* 37.2 (1988), pp. 785–789. DOI: 10.1103/PhysRevB.37.785.

[18] F. J. Devlin et al. “Ab Initio Calculation of Vibrational Absorption and Circular Dichroism Spectra Using Density Functional Force Fields: A Comparison of Local, Nonlocal, and Hybrid Density Functionals”. In: *The Journal of Physical Chemistry* 99.46 (1995), pp. 16883–16902. DOI: 10.1021/j100046a014.

[19] Jochen Heyd, Gustavo E. Scuseria, and Matthias Ernzerhof. “Hybrid functionals based on a screened Coulomb potential”. In: *Journal of Chemical Physics* 118.18 (2003), pp. 8207–8215. DOI: 10.1063/1.1564060.

[20] A. Stroppa and G. Kresse. “The shortcomings of semi-local and hybrid functionals: What we can learn from surface science studies”. In: *New Journal of Physics* 10 (2008). DOI: 10.1088/1367-2630/10/6/063020.

[21] David Bohm and David Pines. “A collective description of electron interactions. I. magnetic interactions”. In: *Physical Review* 82.5 (1951), pp. 625–634. DOI: 10.1103/PhysRev.82.625.

[22] David Pines and David Bohm. "A collective description of electron interactions: II. Collective vs individual particle aspects of the interactions". In: *Physical Review* 85.2 (1952), pp. 338–353. DOI: 10.1103/PhysRev.85.338.

[23] David Bohm and David Pines. "A collective description of electron interactions: III. Coulomb interactions in a degenerate electron gas". In: *Physical Review* 92.3 (1953), pp. 609–625. DOI: 10.1103/PhysRev.92.609.

[24] David Pines. "A Collective Description of Electron Interactions: IV. Electron Interaction in Metals". In: *Physical Review* 92.3 (1953), p. 626. DOI: 10.1103/PhysRev.92.626.

[25] Alexander L Fetter and John D Walecka. *Quantum theory of many-particle systems*. eng. Dover ed., 1. publ. 2003. ISBN: 9780486428277.

[26] Richard D Mattuck. *A Guide to Feynman Diagrams in the Many-Body Problem*. 2. Aufl. Courier Corporation, 1992. ISBN: 0-486-67047-3.

[27] David C. Langreth and John P. Perdew. "Exchange-correlation energy of a metallic surface: Wave-vector analysis". In: *Physical Review B* 15.6 (Mar. 1977), pp. 2884–2901. DOI: 10.1103/PhysRevB.15.2884.

[28] Xinguo Ren et al. "Random-phase approximation and its applications in computational chemistry and materials science". In: *Journal of Materials Science* 47.21 (Mar. 2012), pp. 7447–7471. DOI: 10.1007/s10853-012-6570-4.

[29] Judith Harl and Georg Kresse. "Cohesive energy curves for noble gas solids calculated by adiabatic connection fluctuation-dissipation theory". In: *Physical Review B* 77.4 (Jan. 2008), p. 045136. DOI: 10.1103/PhysRevB.77.045136.

[30] Judith Harl, Georg Kresse, and Judith Harl. "Accurate bulk properties from approximate many-body techniques". In: *Physical Review Letters* 103.5 (July 2009), p. 056401. DOI: 10.1103/PhysRevLett.103.056401.

[31] Judith Harl, Laurids Schimka, and Georg Kresse. "Assessing the quality of the random phase approximation for lattice constants and atomization energies of solids". In: *Physical Review B* 81.11 (Mar. 2010), p. 115126. DOI: 10.1103/PhysRevB.81.115126.

[32] John F. Dobson, Angela White, and Angel Rubio. "Asymptotics of the dispersion interaction: Analytic benchmarks for van der Waals energy functionals". In: *Physical Review Letters* 96.7 (2006), pp. 4–7. DOI: 10.1103/PhysRevLett.96.073201.

[33] S. Lebègue et al. "Cohesive properties and asymptotics of the dispersion interaction in graphite by the random phase approximation". In: *Physical Review Letters* 105.19 (2010), pp. 1–4. DOI: 10.1103/PhysRevLett.105.196401.

[34] Peter J Feibelman et al. “The CO/Pt(111) Puzzle ”. In: *The Journal of Physical Chemistry B* 105.18 (May 2001), pp. 4018–4025. DOI: 10.1021/jp002302t.

[35] Merzuk Kaltak, Jiri Klimes, and Georg Kresse. “Low scaling algorithms for the random phase approximation: Imaginary time and laplace transformations”. In: *Journal of Chemical Theory and Computation* 10.6 (June 2014), pp. 2498–2507. DOI: 10.1021/ct5001268.

[36] Johannes Rekkedal et al. “Communication: Analytic gradients in the random-phase approximation”. In: *Journal of Chemical Physics* 139.8 (Aug. 2013), p. 081101. DOI: 10.1063/1.4819399.

[37] Asbjörn M. Burow et al. “Analytical first-order molecular properties and forces within the adiabatic connection random phase approximation”. In: *Journal of Chemical Theory and Computation* 10.1 (2014), pp. 180–194. DOI: 10.1021/ct4008553.

[38] Benjamin Ramberger. *Calculating forces in the Random Phase Approximation*. June 2015. URL: http://othes.univie.ac.at/37990/.

[39] Wolfgang Pauli. “Exclusion Principle and Quantum Mechanics”. In: *Writings on Physics and Philosophy*. 8. Berlin, Heidelberg: Springer Berlin Heidelberg, 1994, pp. 165–181. DOI: 10.1007/978-3-662-02994-7_20.

[40] Julian Schwinger. “The theory of quantized fields. I”. In: *Physical Review* 82.6 (1951), pp. 914–927. DOI: 10.1103/PhysRev.82.914.

[41] P. A. M. Dirac. *The Principles of Quantum Mechanics*. 3rd Editio. Cambridge: Cambridge University Press, 1947.

[42] M. Born and R. Oppenheimer. “Zur Quantentheorie der Molekeln”. In: *Annalen der Physik* 389.20 (1927), pp. 457–484. DOI: 10.1002/andp.19273892002.

[43] J. Patterson and B. Bailey. *Solid-State Physics: Introduction to the Theory*. Springer Berlin Heidelberg, 2010. ISBN: 9783642025891.

[44] Stephan-Enzo Ungersböck. “Advanced Modeling of Strained CMOS Technology”. PhD thesis. Technical University of Vienna, 2007.

[45] Felix Bloch. “Über die Quantenmechanik der Elektronen in Kristallgittern”. In: *Zeitschrift für Physik* 52.7-8 (1929), pp. 555–600. DOI: 10.1007/BF01339455.

[46] Neil W Ashcroft and N David Mermin. *Solid state physics*. eng. HRW international editions : Science, physics. Philadelphia: Saunders College [u.a.], 1988. ISBN: 0030839939.

[47] Alexandrina Stoyanova. “Delocalized and Correlated Wave Functions for Excited States in Extended Systems”. PhD thesis. University of Groningen, 2006. ISBN: 903672788X.

[48] P. A. M. Dirac. "The Quantum Theory of the Electron". In: *Proceedings of the Royal Society A: Mathematical, Physical and Engineering Sciences* 117.778 (Feb. 1928), pp. 610–624. DOI: 10.1098/rspa.1928.0023.

[49] Eduard Matito, Miquel Duran, and Miquel Solà. "A novel exploration of the hartree-fock homolytic bond dissociation problem in the hydrogen molecule by means of electron localization measures". In: *Journal of Chemical Education* 83.8 (2006), pp. 1243–1248. DOI: 10.1021/ed083p1243.

[50] D. R. Hartree. "The Wave Mechanics of an Atom with a Non-Coulomb Central Field. Part I. Theory and Methods". In: *Mathematical Proceedings of the Cambridge Philosophical Society* 24.1 (Jan. 1928), pp. 89–110. DOI: 10.1017/S0305004100011919.

[51] V. Fock. "Näherungsmethode zur Lösung des quantenmechanischen Mehrkörperproblems". In: *Zeitschrift für Physik* 61.1-2 (1930), pp. 126–148. DOI: 10.1007/BF01340294.

[52] J. A. Pople and R. K. Nesbet. "Self-consistent orbitals for radicals [13]". In: *The Journal of Chemical Physics* 22.3 (1954), pp. 571–572. DOI: 10.1063/1.1740120.

[53] Attila Szabo and Neil S. Ostlund. *Modern Quantum Chemistry - Introduction to Advanced Electronic Structure Theory*. New ed. New York: Courier Corporation, 1996. ISBN: 978-0-486-69186-2.

[54] Robert G. Parr et al. "Electronegativity: The density functional viewpoint". In: *The Journal of Chemical Physics* 68.8 (1978), pp. 3801–3807. DOI: 10.1063/1.436185.

[55] M. Levy. "Universal variational functionals of electron densities, first-order density matrices, and natural spin-orbitals and solution of the v-representability problem". In: *Proceedings of the National Academy of Sciences of the United States of America* 76.12 (1979), pp. 6062–6065. DOI: 10.1073/pnas.76.12.6062.

[56] H. Englisch and R. Englisch. "Hohenberg-Kohn theorem and non-V-representable densities". In: *Physica A: Statistical Mechanics and its Applications* 121.1-2 (Aug. 1983), pp. 253–268. DOI: 10.1016/0378-4371(83)90254-6.

[57] Weitao Yang, Yingkai Zhang, and Paul W. Ayers. "Degenerate ground states and a fractional number of electrons in density and reduced density matrix functional theory". In: *Physical Review Letters* 84.22 (2000), pp. 5172–5175. DOI: 10.1103/PhysRevLett.84.5172.

[58] D. M. Ceperley and B. J. Alder. "Ground state of the electron gas by a stochastic method". In: *Physical Review Letters* 45.7 (1980), pp. 566–569. DOI: 10.1103/PhysRevLett.45.566.

[59] John P. Perdew and Yue Wang. "Accurate and simple analytic representation of the electron-gas correlation energy". In: *Physical Review B* 45.23 (1992), pp. 13244–13249. DOI: 10.1103/PhysRevB.45.13244.

[60] H. N. Rojas, R. W. Godby, and R. J. Needs. "Space-time method for ab initio calculations of self-energies and dielectric response functions of solids". In: *Physical Review Letters* 74.10 (Mar. 1995), pp. 1827–1830. DOI: 10.1103/PhysRevLett.74.1827.

[61] L. Steinbeck et al. "Enhancements to the GW space-time method". In: *Computer Physics Communications* 125.1-3 (Mar. 2000), pp. 105–118. DOI: 10.1016/S0010-4655(99)00466-X.

[62] Merzuk Kaltak, Jiri Klimes, and Georg Kresse. "Cubic scaling algorithm for the random phase approximation: Self-interstitials and vacancies in Si". In: *Physical Review B - Condensed Matter and Materials Physics* 90.5 (2014), p. 054115. DOI: 10.1103/PhysRevB.90.054115.

[63] Peitao Liu et al. "Cubic scaling GW: Towards fast quasiparticle calculations". In: *Physical Review B* 94.16 (Oct. 2016), p. 165109. DOI: 10.1103/PhysRevB.94.165109.

[64] G. C. Wick. "Properties of Bethe-Salpeter wave functions". In: *Physical Review* 96.4 (1954), pp. 1124–1134. DOI: 10.1103/PhysRev.96.1124.

[65] F. Bloch. "Zur Theorie des Austauschproblems und der Remanenzerscheinung der Ferromagnetika". In: *Zeitschrift für Physik* 74.5-6 (1932), pp. 295–335. DOI: 10.1007/BF01337791.

[66] Lars Hedin. "New Method for Calculating the One-Particle Green's Function with Application to the Electron-Gas Problem". In: *Physical Review* 139.3A (Aug. 1965), A796–A823. DOI: 10.1103/PhysRev.139.A796.

[67] D.C. Langreth and J.P. Perdew. "The exchange-correlation energy of a metallic surface". In: *Solid State Communications* 17.11 (Dec. 1975), pp. 1425–1429. DOI: 10.1016/0038-1098(75)90618-3.

[68] O. Gunnarsson and B. I. Lundqvist. "Exchange and correlation in atoms, molecules, and solids by the spin-density-functional formalism". In: *Physical Review B* 13.10 (1976), pp. 4274–4298. DOI: 10.1103/PhysRevB.13.4274.

[69] R. P. Feynman. "Forces in molecules". In: *Physical Review* 56.4 (1939), pp. 340–343. DOI: 10.1103/PhysRev.56.340.

[70] K. Held et al. "Hedin Equations, GW, GW+DMFT, and All That". In: (2011).

[71] Andrew J. Morris et al. "Vertex corrections in localized and extended systems". In: *Physical Review B - Condensed Matter and Materials Physics* 76.15 (2007), pp. 1–9. DOI: 10.1103/PhysRevB.76.155106.

[72] A. Görling and A. HeSSelmann. “Random-phase approximation correlation methods for molecules and solids”. In: *Molecular Physics* (2011). DOI: 10.1080/00268976.2011.614282.

[73] A. HeSSelmann and A. Görling. “Random-phase approximation correlation methods for molecules and solids”. In: *Molecular Physics* 109.21 (2011), pp. 2473–2500. DOI: 10.1080/00268976.2011.614282.

[74] J Lindhard. “On the properites of a gas of charged particles”. In: *Kgl. Danske Videnskab. Selskab, Mat-fys. Medd.* 28 (1954), p. 8.

[75] L. D. Landau. “The Theory of a Fermi Liquid”. In: *Soviet Phys. JETP* 3.6 (1957), p. 920.

[76] Murray Gell-Mann and Keith A. Brueckner. “Correlation energy of an electron gas at high density”. In: *Physical Review* 106.2 (1957), pp. 364–368. DOI: 10.1103/PhysRev.106.364.

[77] J Goldstone. “Derivation of the Brueckner many-body theory”. In: *Proceedings of the Royal Society of London. Series A. Mathematical and Physical Sciences* 239.1217 (Feb. 1957), pp. 267–279. DOI: 10.1098/rspa.1957.0037.

[78] P. Nozières and D. Pines. “A dielectric formulation of the many body problem: Application to the free electron gas”. In: *Il Nuovo Cimento Series 10* 9.3 (1958), pp. 470–490. DOI: 10.1007/BF02725103.

[79] P. Nozières and D. Pines. “Correlation Energy of a Free Electron Gas”. In: *Physical Review* 111.2 (July 1958), pp. 442–454. DOI: 10.1103/PhysRev.111.442.

[80] Attila Szabo and Neil S. Ostlund. “The correlation energy in the random phase approximation: Intermolecular forces between closed-shell systems”. In: *The Journal of Chemical Physics* 67.August 2008 (1977), pp. 4351–4360. DOI: 10.1063/1.434580.

[81] Filipp Furche. “Molecular tests of the random phase approximation to the exchange-correlation energy functional”. In: *Physical Review B* 64.19 (2001), pp. 1–8. DOI: 10.1103/PhysRevB.64.195120.

[82] Martin Fuchs and Xavier Gonze. “Accurate density functionals: Approaches using the adiabatic-connection fluctuation-dissipation theorem”. In: *Physical Review B - Condensed Matter and Materials Physics* 65.23 (2002), pp. 1–4. DOI: 10.1103/PhysRevB.65.235109.

[83] Y. M. Niquet, M. Fuchs, and X. Gonze. “Exchange-correlation potentials in the adiabatic connection fluctuation-dissipation framework”. In: *Physical Review A - Atomic, Molecular, and Optical Physics* 68.3 (2003), p. 13. DOI: 10.1103/PhysRevA.68.032507.

[84] Michael Rohlfing and Thomas Bredow. “Binding energy of adsorbates on a noble-metal surface: Exchange and correlation effects”. In: *Physical Review Letters* 101.26 (2008), pp. 1–4. DOI: 10.1103/PhysRevLett.101.266106.

[85] Xinguo Ren, Patrick Rinke, and Matthias Scheffler. "Exploring the random phase approximation: Application to CO adsorbed on Cu(111)". In: *Physical Review B - Condensed Matter and Materials Physics* 80.4 (2009), pp. 1–8. DOI: 10.1103/PhysRevB.80.045402.

[86] L. Schimka et al. "Accurate surface and adsorption energies from many-body perturbation theory". In: *Nature Materials* 9.9 (Sept. 2010), pp. 741–744. DOI: 10.1038/nmat2806.

[87] Florian Göltl and Jürgen Hafner. "Alkane adsorption in Na-exchanged chabazite: The influence of dispersion forces". In: *Journal of Chemical Physics* 134.6 (2011). DOI: 10.1063/1.3549815.

[88] Jie Ma et al. "Adsorption and diffusion of water on graphene from first principles". In: *Physical Review B - Condensed Matter and Materials Physics* 84.3 (2011), pp. 1–4. DOI: 10.1103/PhysRevB.84.033402.

[89] Hyun Jung Kim et al. "Benzene adsorbed on Si(001): The role of electron correlation and finite temperature". In: *Physical Review B - Condensed Matter and Materials Physics* 85.4 (2012), pp. 1–5. DOI: 10.1103/PhysRevB.85.041403.

[90] K. S. Singwi et al. "Electron Correlations at Metallic Densities". In: *Physical Review* 176.2 (Dec. 1968), pp. 589–599. DOI: 10.1103/PhysRev.176.589.

[91] Lars Hedin and Stig O. Lundqvist. "Effects of Electron-Electron and Electron-Phonon Interactions on the One-Electron States of Solids". English. In: *Solid State Physics*. Ed. by Frederick Seitz, David Turnbull, and Henry Ehrenreich. Vol. 23. doi:10.1016/S0081-1947(08)60615-3. United States: Academic Press, 1969, pp. 1–181. ISBN: 978-0-12-607723-0. DOI: 10.1016/S0081-1947(08)60615-3.

[92] Stefan Kurth and J. Perdew. "Density-functional correction of random-phase-approximation correlation with results for jellium surface energies". In: *Physical Review B - Condensed Matter and Materials Physics* 59.16 (1999), pp. 10461–10468. DOI: 10.1103/PhysRevB.59.10461.

[93] Zidan Yan, John P. Perdew, and Stefan Kurth. "Density functional for short-range correlation: Accuracy of the random-phase approximation for isoelectronic energy changes". In: *Physical Review B - Condensed Matter and Materials Physics* 61.24 (2000), pp. 16430–16439. DOI: 10.1103/PhysRevB.61.16430.

[94] Andreas Grüneis et al. "Making the random phase approximation to electronic correlation accurate". In: *Journal of Chemical Physics* 131.15 (2009). DOI: 10.1063/1.3250347.

[95] Jefferson E. Bates and Filipp Furche. "Communication: Random phase approximation renormalized many-body perturbation theory". In: *Journal of Chemical Physics* 139.17 (2013). DOI: 10.1063/1.4827254.

[96] Xinguo Ren et al. “Beyond the random-phase approximation for the electron correlation energy: The importance of single excitations”. In: *Physical Review Letters* 106.15 (2011), pp. 16–19. DOI: 10.1103/PhysRevLett.106.153003.

[97] Joachim Paier et al. “Assessment of correlation energies based on the random-phase approximation”. In: *New Journal of Physics* 14 (2012). DOI: 10.1088/1367-2630/14/4/043002.

[98] Xinguo Ren et al. “Resolution-of-identity approach to Hartree-Fock, hybrid density functionals, RPA, MP2 and GW with numeric atom-centered orbital basis functions”. In: *New Journal of Physics* 14 (2012). DOI: 10.1088/1367-2630/14/5/053020.

[99] Thomas Olsen and Kristian S. Thygesen. “Extending the random-phase approximation for electronic correlation energies: The renormalized adiabatic local density approximation”. In: *Physical Review B - Condensed Matter and Materials Physics* 86.8 (2012), pp. 1–4. DOI: 10.1103/PhysRevB.86.081103.

[100] Patrick Bleiziffer, Andreas HeSSelmann, and Andreas Görling. “Efficient self-consistent treatment of electron correlation within the random phase approximation”. In: *Journal of Chemical Physics* 139.8 (2013). DOI: 10.1063/1.4818984.

[101] Jiri Klimes and Georg Kresse. “Kohn-Sham band gaps and potentials of solids from the optimised effective potential method within the random phase approximation”. In: *Journal of Chemical Physics* 140.5 (2014). DOI: 10.1063/1.4863502.

[102] David Vanderbilt. “Soft self-consistent pseudopotentials in a generalized eigenvalue formalism”. In: *Physical Review B* 41.11 (Apr. 1990), pp. 7892–7895. DOI: 10.1103/PhysRevB.41.7892.

[103] O. Krogh Andersen. “Linear methods in band theory”. In: *Physical Review B* 12.8 (Oct. 1975), pp. 3060–3083. DOI: 10.1103/PhysRevB.12.3060.

[104] P. E. Blöchl. “Projector augmented-wave method”. In: *Phys. Rev. B* 50.24 (1994), p. 17953. DOI: 10.1103/PhysRevB.50.17953.

[105] G. Kresse and D. Joubert. “From ultrasoft pseudopotentials to the projector augmented-wave method”. In: *Physical Review B* 59.3 (Jan. 1999), pp. 1758–1775. DOI: 10.1103/PhysRevB.59.1758.

[106] J A Pople et al. “Derivative studies in hartree-fock and møller-plesset theories”. In: *International Journal of Quantum Chemistry* 16.S13 (June 2009), pp. 225–241. DOI: 10.1002/qua.560160825.

[107] Trygve Helgaker, Poul Jørgensen, and Nicholas C Handy. “A numerically stable procedure for calculating Møller-Plesset energy derivatives, derived using the theory of Lagrangians”. In: *Theoretica Chimica Acta* 76.4 (1989), pp. 227–245. DOI: 10.1007/BF00532006.

[108] Mauro Del Ben, Jürg Hutter, and Joost VandeVondele. "Forces and stress in second order Møller-Plesset perturbation theory for condensed phase systems within the resolution-of-identity Gaussian and plane waves approach". In: *The Journal of Chemical Physics* 143.10 (2015). DOI: http://dx.doi.org/10.1063/1.4919238.

[109] Martin M. Rieger et al. "GW space-time method for the self-energy of large systems". In: *Computer Physics Communications* 117.3 (1999), pp. 211–228. DOI: 10.1016/S0010-4655(98)00174-X.

[110] M. Städele et al. "Exact exchange Kohn-Sham formalism applied to semiconductors". In: *Physical Review B* 59.15 (Apr. 1999), pp. 10031–10043. DOI: 10.1103/PhysRevB.59.10031.

[111] T Miyake et al. "Total energy of solids: An exchange and random-phase approximation correlation study". In: *Physical Review B* 66.24 (Dec. 2002), p. 245103. DOI: 10.1103/PhysRevB.66.245103.

[112] M Fuchs et al. "Describing static correlation in bond dissociation by KohnSham density functional theory". In: *The Journal of Chemical Physics* 122.9 (Mar. 2005), p. 094116. DOI: 10.1063/1.1858371.

[113] Filipp Furche. "Developing the random phase approximation into a practical post-KohnSham correlation model". In: *The Journal of Chemical Physics* 129.11 (Sept. 2008), p. 114105. DOI: 10.1063/1.2977789.

[114] Nils Erik Dahlen, Robert Van Leeuwen, and Ulf Von Barth. "Variational energy functionals of the Green function and of the density tested on molecules". In: *Physical Review A - Atomic, Molecular, and Optical Physics* 73.1 (2006), pp. 1–13. DOI: 10.1103/PhysRevA.73.012511.

[115] Yasmine S. Al-Hamdani et al. "Communication: Water on hexagonal boron nitride from diffusion Monte Carlo". In: *The Journal of Chemical Physics* 142.18 (May 2015), p. 181101. DOI: 10.1063/1.4921106.

[116] Yanbin Wu, Lucas K. Wagner, and Narayana R. Aluru. "Hexagonal boron nitride and water interaction parameters". In: *The Journal of Chemical Physics* 144.16 (Apr. 2016), p. 164118. DOI: 10.1063/1.4947094.

[117] Stefan Grimme et al. "A consistent and accurate ab initio parametrization of density functional dispersion correction (DFT-D) for the 94 elements H-Pu". In: *The Journal of Chemical Physics* 132.15 (2010). DOI: http://dx.doi.org/10.1063/1.3382344.

[118] Alexandre Tkatchenko et al. "Accurate and efficient method for many-body van der Waals interactions". In: *Physical Review Letters* 108.23 (2012), pp. 1–5. DOI: 10.1103/PhysRevLett.108.236402.

[119] Jiri Klimes and Angelos Michaelides. "Perspective: Advances and challenges in treating van der Waals dispersion forces in density functional theory". In: *The Journal of Chemical Physics* 137.12 (Sept. 2012), p. 120901. DOI: 10.1063/1.4754130.

[120] Jiri Klimes et al. "Singles correlation energy contributions in solids". In: *The Journal of Chemical Physics* 143.10 (Sept. 2015), p. 102816. DOI: 10.1063/1.4929346.

[121] J. L. Warren et al. "Lattice dynamics of diamond". In: *Physical Review* 158.3 (1967), pp. 805–808. DOI: 10.1103/PhysRev.158.805.

[122] J. Kulda et al. "Overbending of the longitudinal optical phonon branch in diamond as evidenced by inelastic neutron and x-ray scattering". In: *Physical Review B* 66.24 (2002), p. 241202. DOI: 10.1103/PhysRevB.66.241202.

[123] R. Nicklow, N. Wakabayashi, and H. G. Smith. "Lattice dynamics of pyrolytic graphite". In: *Physical Review B* 5.12 (1972), pp. 4951–4962. DOI: 10.1103/PhysRevB.5.4951.

[124] J Maultzsch et al. "Phonon dispersion in graphite". In: *Physical review letters* 92.7 (2004), p. 075501. DOI: 10.1103/PhysRevLett.92.075501.

[125] M. Mohr et al. "Phonon dispersion of graphite by inelastic x-ray scattering". In: *Physical Review B* 76.3 (July 2007), p. 035439. DOI: 10.1103/PhysRevB.76.035439.

[126] G Kresse, J Furthmüller, and J Hafner. "Ab initio Force Constant Approach to Phonon Dispersion Relations of Diamond and Graphite". In: *EPL (Europhysics Letters)* 32.9 (1995), p. 729.

[127] Kerstin Hummer, Judith Harl, and Georg Kresse. "Heyd-Scuseria-Ernzerhof hybrid functional for calculating the lattice dynamics of semiconductors". In: *Physical Review B - Condensed Matter and Materials Physics* 80.11 (2009). DOI: 10.1103/PhysRevB.80.115205.

[128] Martin Schütz et al. "Analytical energy gradients for local second-order Moøller-Plesset perturbation theory using density fitting approximations". In: *Journal of Chemical Physics* 121.2 (2004), pp. 737–750. DOI: 10.1063/1.1760747.

[129] Georg Kresse. "Ab-initio Molekular Dynamik für flüssige Metalle". PhD thesis. Technical University of Vienna, 1993.

[130] Stefan Grimme, Stephan Ehrlich, and Lars Goerigk. "Effect of the damping function in dispersion corrected density functional theory". In: *Journal of Computational Chemistry* 32.7 (May 2011), pp. 1456–1465. DOI: 10.1002/jcc.21759.

[131] M. Dion et al. "Van der Waals Density Functional for General Geometries". In: *Physical Review Letters* 92.24 (June 2004), p. 246401. DOI: 10.1103/PhysRevLett.92.246401.

[132] Éamonn D. Murray, Kyuho Lee, and David C. Langreth. "Investigation of exchange energy density functional accuracy for interacting molecules". In: *Journal of Chemical Theory and Computation* 5.10 (2009), pp. 2754–2762. DOI: 10.1021/ct900365q.

[133] Jiri Klimes, David R. Bowler, and Angelos Michaelides. "Chemical accuracy for the van der Waals density functional". In: *Journal of Physics Condensed Matter* 22.2 (2010). DOI: 10.1088/0953-8984/22/2/022201.

[134] Wei Liu et al. "Quantitative Prediction of Molecular Adsorption: Structure and Binding of Benzene on Coinage Metals". In: *Physical Review Letters* 115.3 (July 2015), p. 036104. DOI: 10.1103/PhysRevLett.115.036104.

[135] David A. King. "Thermal desorption from metal surfaces: A review". In: *Surface Science* 47.1 (Jan. 1975), pp. 384–402. DOI: 10.1016/0039-6028(75)90302-7.

[136] Handan Yildirim, Thomas Greber, and Abdelkader Kara. "Trends in Adsorption Characteristics of Benzene on Transition Metal Surfaces: Role of Surface Chemistry and van der Waals Interactions". In: *The Journal of Physical Chemistry C* 117.40 (Oct. 2013), pp. 20572–20583. DOI: 10.1021/jp404487z.

[137] P.A. Redhead. "Thermal desorption of gases". In: *Vacuum* 12.4 (July 1962), pp. 203–211. DOI: 10.1016/0042-207X(62)90978-8.

[138] Hyeran Ihm et al. "Calorimetric Measurement of the Heat of Adsorption of Benzene on Pt(111) ". In: *The Journal of Physical Chemistry B* 108.38 (Sept. 2004), pp. 14627–14633. DOI: 10.1021/jp040159o.

[139] Jianwei Sun, Adrienn Ruzsinszky, and John P Perdew. "Strongly Constrained and Appropriately Normed Semilocal Density Functional". In: *Phys. Rev. Lett.* 115.3 (July 2015), p. 36402. DOI: 10.1103/PhysRevLett.115.036402.

[140] Aliaksandr V Krukau et al. "Influence of the exchange screening parameter on the performance of screened hybrid functionals". In: *The Journal of Chemical Physics* 125.22 (Dec. 2006), p. 224106. DOI: 10.1063/1.2404663.

[141] Jií Klime, David R. Bowler, and Angelos Michaelides. "Van der Waals density functionals applied to solids". In: *Physical Review B* 83.19 (May 2011), p. 195131. DOI: 10.1103/PhysRevB.83.195131.

[142] John P Perdew et al. "Restoring the Density-Gradient Expansion for Exchange in Solids and Surfaces". In: *Phys. Rev. Lett.* 100.13 (Apr. 2008), p. 136406. DOI: 10.1103/PhysRevLett.100.136406.

[143] J. C. Slater. "A Simplification of the Hartree-Fock Method". In: *Physical Review* 81.3 (Feb. 1951), pp. 385–390. DOI: 10.1103/PhysRev.81.385.

[144] Chr Møller and M. S. Plesset. "Note on an approximation treatment for many-electron systems". In: *Physical Review* 46.7 (Oct. 1934), pp. 618–622. DOI: 10.1103/PhysRev.46.618.

[145] Jiri Cizek. "On the Correlation Problem in Atomic and Molecular Systems. Calculation of Wavefunction Components in UrsellType Expansion Using QuantumField Theoretical Methods". In: *The Journal of Chemical Physics* 45.11 (Dec. 1966), pp. 4256–4266. DOI: 10.1063/1.1727484.

[146] Oktay Sinanolu. "Many-electron theory of atoms and molecules. I. Shells, electron pairs vs many-electron correlations". In: *The Journal of Chemical Physics* 36.3 (Feb. 1962), pp. 706–717. DOI: 10.1063/1.1732596.

[147] Rodney J. Bartlett and Monika Musia. "Coupled-cluster theory in quantum chemistry". In: *Reviews of Modern Physics* 79.1 (2007), pp. 291–352. DOI: 10.1103/RevModPhys.79.291.

[148] Jeppe Olsen et al. "Determinant based configuration interaction algorithms for complete and restricted configuration interaction spaces". In: *The Journal of Chemical Physics* 89.4 (1988), pp. 2185–2192. DOI: 10.1063/1.455063.

[149] Peter J. Knowles and Nicholas C. Handy. "A determinant based full configuration interaction program". In: *Computer Physics Communications* 54.1 (Apr. 1989), pp. 75–83. DOI: 10.1016/0010-4655(89)90033-7.

[150] George H. Booth, Alex J. W. Thom, and Ali Alavi. "Fermion Monte Carlo without fixed nodes: A game of life, death, and annihilation in Slater determinant space". In: *The Journal of Chemical Physics* 131.5 (2009), p. 054106. DOI: 10.1063/1.3193710.

[151] Deidre Cleland, George H. Booth, and Ali Alavi. "Communications: Survival of the fittest: Accelerating convergence in full configuration-interaction quantum Monte Carlo". In: *The Journal of Chemical Physics* 132.4 (Jan. 2010), p. 041103. DOI: 10.1063/1.3302277.

[152] Norm M. Tubman et al. "A deterministic alternative to the full configuration interaction quantum Monte Carlo method". In: *Journal of Chemical Physics* 145.4 (2016). DOI: 10.1063/1.4955109.

[153] Norm M. Tubman et al. "Modern Approaches to Exact Diagonalization and Selected Configuration Interaction with the Adaptive Sampling CI Method". In: (July 2018), pp. 1–22.

[154] Yann Garniron et al. "Selected configuration interaction dressed by perturbation". In: *The Journal of Chemical Physics* 149.6 (Aug. 2018), p. 064103. DOI: 10.1063/1.5044503.

[155] Ernest R. Davidson. "Properties and Uses of Natural Orbitals". In: *Reviews of Modern Physics* 44.3 (July 1972), pp. 451–464. DOI: 10.1103/RevModPhys.44.451.

[156] Andreas Grüneis et al. "Natural orbitals for wave function based correlated calculations using a plane wave basis set". In: *Journal of Chemical Theory and Computation* 7.9 (Sept. 2011), pp. 2780–2785. DOI: 10.1021/ct200263g.

[157] Fabien Bruneval. "Improved density matrices for accurate molecular ionization potentials". In: *Physical Review B* 99.4 (Jan. 2019), p. 041118. DOI: 10.1103/PhysRevB.99.041118.

[158] Fabien Bruneval. "Assessment of the Linearized GW Density Matrix for Molecules". In: *Journal of Chemical Theory and Computation* 15.7 (July 2019), pp. 4069–4078. DOI: 10.1021/acs.jctc.9b00333.

[159] Maria Hellgren et al. "Static correlation and electron localization in molecular dimers from the self-consistent RPA and GW approximation". In: *Physical Review B* 91.16 (Apr. 2015), p. 165110. DOI: 10.1103/PhysRevB.91.165110.

[160] Henk Eshuis, Jefferson E. Bates, and Filipp Furche. "Electron correlation methods based on the random phase approximation". In: *Theoretical Chemistry Accounts* 131.1 (Jan. 2012), p. 1084. DOI: 10.1007/s00214-011-1084-8.

[161] Jan Wilhelm et al. "Large-Scale Cubic-Scaling Random Phase Approximation Correlation Energy Calculations Using a Gaussian Basis". In: *Journal of Chemical Theory and Computation* 12.12 (2016), pp. 5851–5859. DOI: 10.1021/acs.jctc.6b00840.

[162] T. L. Gilbert. "Hohenberg-Kohn theorem for nonlocal external potentials". In: *Physical Review B* 12.6 (Sept. 1975), pp. 2111–2120. DOI: 10.1103/PhysRevB.12.2111.

[163] Iris Theophilou et al. "Orbitals from local RDMFT: Are they Kohn-Sham or natural orbitals?" In: *The Journal of Chemical Physics* 143.5 (Aug. 2015), p. 054106. DOI: 10.1063/1.4927784.

[164] L. J. Sham and M. Schlter. "Density-functional theory of the energy gap". In: *Physical Review Letters* 51.20 (1983), pp. 1888–1891. DOI: 10.1103/PhysRevLett.51.1888.

[165] R. W. Godby, M. Schlüter, and L. J. Sham. "Accurate exchange-correlation potential for silicon and its discontinuity on addition of an electron". In: *Physical Review Letters* 56.22 (1986), pp. 2415–2418. DOI: 10.1103/PhysRevLett.56.2415.

[166] D. S. Kosov. "Restoring the Pauli principle in the random phase approximation ground state". In: *Chemical Physics Letters* 690 (2017), pp. 20–24. DOI: 10.1016/j.cplett.2017.10.032.

[167] Felix Hummel et al. "Screened Exchange Corrections to the Random Phase Approximation from Many-Body Perturbation Theory". In: *Journal of Chemical Theory and Computation* 15.5 (2019), pp. 3223–3236. DOI: 10.1021/acs.jctc.8b01247.

[168] Ernest R. Davidson. "The iterative calculation of a few of the lowest eigenvalues and corresponding eigenvectors of large real-symmetric matrices". In: *Journal of Computational Physics* 17.1 (Jan. 1975), pp. 87–94. DOI: 10.1016/0021-9991(75)90065-0.

[169] G. Kresse and J. Hafner. "Ab initio molecular dynamics for liquid metals". In: *Physical Review B* 47.1 (Jan. 1993), pp. 558–561. DOI: 10.1103/PhysRevB.47.558.

[170] G. Kresse and J. Furthmüller. "Efficiency of ab-initio total energy calculations for metals and semiconductors using a plane-wave basis set". In: *Computational Materials Science* 6.1 (July 1996), pp. 15–50. DOI: 10.1016/0927-0256(96)00008-0.

[171] G. Kresse and J. Furthmüller. "Efficient iterative schemes for ab initio total-energy calculations using a plane-wave basis set". In: *Physical Review B - Condensed Matter and Materials Physics* 54.16 (Oct. 1996), pp. 11169–11186. DOI: 10.1103/PhysRevB.54.11169.

[172] M. Marsman et al. "Second-order MollerPlesset perturbation theory applied to extended systems. I. Within the projector-augmented-wave formalism using a plane wave basis set". In: *The Journal of Chemical Physics* 130.18 (2009), p. 184103. DOI: 10.1063/1.3126249.

[173] Tobias Schäfer, Benjamin Ramberger, and Georg Kresse. "Quartic scaling MP2 for solids: A highly parallelized algorithm in the plane wave basis". In: *Journal of Chemical Physics* 146.10 (Mar. 2017), p. 104101. DOI: 10.1063/1.4976937.

[174] Zoran Sukurma. "The implementation of the full configuration interaction method." available at http://othes.univie.ac.at/56624/. MA thesis. University of Vienna, Aug. 2019.

[175] Jing Li et al. "Comparing many-body approaches against the helium atom exact solution". In: *SciPost Physics* 6.4 (Apr. 2019), p. 040. DOI: 10.21468/scipostphys.6.4.040.

[176] James J. Shepherd et al. "Convergence of many-body wave-function expansions using a plane-wave basis: From homogeneous electron gas to solid state systems". In: *Physical Review B* 86.3 (July 2012), p. 035111. DOI: 10.1103/PhysRevB.86.035111.

[177] Jiri Klimes, Merzuk Kaltak, and Georg Kresse. "Predictive GW calculations using plane waves and pseudopotentials". In: *Physical Review B* 90.7 (Aug. 2014), p. 075125. DOI: 10.1103/PhysRevB.90.075125.

[178] Vladimir I. Korobov. "Nonrelativistic ionization energy for the helium ground state". In: *Physical Review A* 66.2 (Aug. 2002), p. 024501. DOI: 10.1103/PhysRevA.66.024501.

[179] P. E M Siegbahn and M. R A Blomberg. "Bond-dissociation using hybrid DFT". In: *International Journal of Quantum Chemistry* 110.2 (Feb. 2010), pp. 317–322. DOI: 10.1002/qua.22204.

[180] Karl K. Irikura. "Experimental vibrational zero-point energies: Diatomic molecules". In: *Journal of Physical and Chemical Reference Data* 36.2 (2007), pp. 389–397. DOI: 10.1063/1.2436891.

[181] Y. P. Zhang et al. "Dissociation Energies of Molecular Hydrogen and the Hydrogen Molecular Ion". In: *Physical Review Letters* 92.20 (May 2004), p. 203003. DOI: 10.1103/PhysRevLett.92.203003.

[182] G. Kresse and J. Hafner. "Norm-conserving and ultrasoft pseudopotentials for first-row and transition elements". In: *Journal of Physics: Condensed Matter* 6.40 (Oct. 1994), pp. 8245–8257. DOI: 10.1088/0953-8984/6/40/015.

[183] Emanuele Maggio and Georg Kresse. "GW Vertex Corrected Calculations for Molecular Systems". In: *Journal of Chemical Theory and Computation* 13.10 (Oct. 2017), pp. 4765–4778. DOI: 10.1021/acs.jctc.7b00586.

[184] Alexander A. Rusakov et al. "Self-Energy Embedding Theory (SEET) for Periodic Systems". In: *Journal of Chemical Theory and Computation* 15.1 (Jan. 2019), pp. 229–240. DOI: 10.1021/acs.jctc.8b00927.

[185] Tran Nguyen Lan, Alexei A. Kananenka, and Dominika Zgid. "Communication: Towards ab initio self-energy embedding theory in quantum chemistry". In: *Journal of Chemical Physics* 143.24 (Dec. 2015), p. 241102. DOI: 10.1063/1.4938562.

[186] Alexander A. Rusakov and Dominika Zgid. "Self-consistent second-order Green's function perturbation theory for periodic systems". In: *Journal of Chemical Physics* 144.5 (Feb. 2016), p. 054106. DOI: 10.1063/1.4940900.

[187] Merzuk Kaltak and Georg Kresse. "Minimax Isometry Method: A compressive sensing approach for Matsubara summation in many-body perturbation theory". In: *pre-print arXiv:1909.01740* (Sept. 2019). *Accepted in PRB.*

Curriculum Vitae

Jul. 2015	Start of this dissertation University of Vienna Austria
Oct. 2013 - Jun. 2015	Master of Science *graduated with distinction* • Physics University of Vienna Austria
Oct. 2011 - Sep. 2013	Bachelor of Science *graduated with distinction* • Physics University of Vienna Austria
Sep. 2010 - Jun. 2011	Bachelor of Science *graduated with distinction* • Medicinal Chemistry and Pharmaceutical Sciences Dublin Institute of Technology Ireland
Sep. 2004 - Jun. 2009	VET Diploma *graduated with distinction* • Biochemistry, Biotechnology and Genetic Engineering Höhere Bundes-Lehr- und Versuchsanstalt für chemische Industrie Austria
Honours and Rewards	• Austrian National Award from the Austrian Federal Ministry of Education, Science and Research for the 50 best Master graduates 2015 • Deans list University of Vienna - Faculty of Physics 2014/15 • best overall performance and best bachelor thesis in final year of the BSc Medicinal Chemistry and Pharmaceutical Sciences 2011 at Dublin Institute of Technology